Blood Compatibility and Hydration States of Polymers with Tertiary Amide Frameworks: Poly(2-oxazoline)s and Their Poly(tertiary amido acrylate) Derivatives

刘, 诗晨

Doctoral Dissertation 2021

Blood Compatibility and Hydration States of Polymers with Tertiary Amide Frameworks: Poly(2-oxazoline)s and Their Poly(tertiary amido acrylate) Derivatives

Kyushu University
Graduate School of Engineering
Department of Applied Chemistry
Tanaka Masaru Lab
Shichen Liu

Contents

Abstract

Blood compatibility is the prerequisite for blood-contacting medical devices to serve patients. Once foreign materials come into contact with blood, a series of blood responses such as hemostasis, inflammation, and thrombus formation are evoked, which may further lead to serious complications as well. These adverse reactions not only impair patients' health but also increase their financial burden. With the extensive application of various blood-contacting medical devices in clinical practice nowadays, it is instant to improve the blood compatibility of the devices. The most widely adopted method is to modify the devices' surfaces with blood-compatible polymers. Understanding the blood compatibility mechanism of these polymers can effectively guide the advance of blood-compatible polymers. Among existing mechanisms, the hydration theory has aroused the wide interest of researchers. Based on the studies on various well-known biopolymers and synthetic polymers, our lab proposed the "intermediate water" (IW) concept. It is believed the IW formed on polymers can prevent cells and proteins from directly contacting polymers, thus avoiding subsequent blood reactions. Furthermore, the content of IW is related to the polymer structure and blood compatibility, so the IW concept can also work as a guiding principle for the development of novel blood-compatible polymers. Based on these two points, this thesis focuses on the blood compatibility mechanism of poly(2-oxazoline)s (POXs). Inspired by POXs' tertiary amide frameworks, the corresponding poly(tertiary amido acrylate) derivatives are also developed.

In **Chapter 1**, the research background of this thesis is overviewed, including the problems of

blood-contacting medical devices, the blood reactions on blood-contacting medical devices, and surface modification strategy. Additionally, the characteristics of POXs, as well as a detailed description of the IW concept, are also presented.

As a promising polymer emerging in recent years, the physicochemical properties, chemical modification, and biomedical application of POXs have been widely studied, yet their blood compatibility mechanism is few reported. In **Chapter 2**, poly(2-methyl-2-oxazoline) (PMeOx), poly(2-ethyl-2-oxazoline) (PEtOx), poly(2-*n*-butyl-2-oxazoline) (PBuOx), and poly(2-phenyl-2-oxazoline) (PPhOx) were selected as POX models for the comparative study of their blood compatibility and hydration states. The four POXs were grafted onto glass substrates through photo-grafting, and their blood compatibility was estimated via platelet adhesion and the degree of denaturation of the adsorbed fibrinogen. The hydration states of the POXs were investigated using differential scanning calorimetry (DSC) and attenuated total reflection infrared spectroscopy (ATR-IR). The predominant population of IW was present in the hydrated PMeOx and PEtOx but was scarce in the hydrated PBuOx and PPhOx. This could be the reason for the blood compatibility of PMeOx and PEtOx. The carbonyl groups in PMeOx and PEtOx could be fully hydrated. However, in PBuOx and PPhOx, water mainly existed as bulk water. The hydration of the carbonyl groups is hindered by the bulky side chain, and IW cannot be generated. This knowledge provides a perspective for understanding the blood compatibility of PMeOx and PEtOx from the water–polymer interactions and may inspire the development of novel blood-compatible POX derivatives.

Despite the outstanding advantages of PMeOx and PEtOx, their polymerization requires a

rather rigorous environment, and their water solubility complicates the surface immobilization. According to the conclusions in **Chapter 2**, for POXs, when the number of carbon atoms linked to the carbonyl of an tertiary amide is less than two, the tertiary amide framework is not sterically hindered, and they can interact with water and form IW. Inspired by such conclusions and the construction of poly(2-methacryloyloxyethyl phosphorylcholine) (PMPC) and poly(2-methoxyethyl acrylate) (PMEA), in **Chapter 3**, four poly(tertiary amido acrylate) analogs, which are composed of (meth)acrylate backbones and tertiary amide frameworks in the side chains, i.e., poly[2-(*N*-methylacetamido)ethyl acrylate] (PAEA), poly[2-(*N*-methylacetamido)ethyl methacrylate] (PAEM), poly[2-(*N*-methylpropionamido)ethyl acrylate] (PPEA), and poly[2-(*N*-ethylacetamido)ethyl acrylate] (PEAE) are designed. The monomers are synthesized through a two-step strategy, by which the steric hindrance around the tertiary amide can be precisely controlled. The monomers can be easily polymerized by convenient free radical polymerization. Since the prepared homopolymers are water-soluble, the water-insoluble copolymers were also synthesized by copolymerizing with their monomers with hydrophobic *n*-butyl (meth)acrylate to further coat on substrates directly.

In **Chapter 4**, the blood compatibility and hydration states of poly(tertiary amidoacylate)s and corresponding copolymers were investigated. All the poly(tertiary amidoacylate) analogs showed compatibility with red blood cells and cytocompatibility against HeLa and NHDF cell lines as PMeOx or PEtOx. PPEA and PEAE were thermosensitive in water solutions, and the lower critical solution temperature of the PPEA solution (10 mg mL^{-1}) was 37 °C. Among the four copolymers,

poly[*n*-butyl methacrylate$_{70}$-*co*-2-(*N*-methylacetamido)ethyl methacrylate$_{30}$] showed the best blood compatibility to suppress the adsorption of plasma proteins, denaturation of adsorbed fibrinogen, and platelet adhesion. The IW was found in all homopolymers and copolymers by DSC. The present work demonstrated that the tertiary amide moiety in the sidechain of poly(meth)acrylate was an effective contributor to blood compatibility and IW. Furthermore, changing the vicinal groups linked to the tertiary amide moiety may widen the scope of blood-compatible polymers with different physicochemical properties in hydrated conditions.

In **Chapter 5**, the conclusions of the whole thesis are presented.

CHAPTER 1

Introduction

1.1 Thrombogenicity of blood-contacting medical devices

1.1.1 Problems on blood-contacting medical devices

Blood-contacting medical devices are extensively used in modern medicine (some commonly used devices are listed in **Figure 1.1**). Generally, they can be classified into three categories according to the placement, (i) indwelling devices, like intravenous cannulas or peripherally inserted central venous catheters (CVCs), (ii) implantable devices, such as coronary stents, prosthetic heart valves, and ventricular assist, (iii) extracorporeal artificial organs, such as hemodialyzer, cardiopulmonary bypass (CPB) circuits and extracorporeal membrane oxygenator (ECMO).[1] They are envisioned to serve the recipients well, not disturb the blood flow and prompt the blood response. However, adverse reactions induced by the devices such as clot formation, thrombosis, embolization, and thromboembolic complications,[2] remain inevitable in current clinical practice. For example, the CVCs, which are perhaps the most widely used blood-contacting devices, are used for venous access or drug delivery, and the duration of their use can range from days to months. Meanwhile, the use of CVCs accompanies a high risk of symptomatic venous thrombosis. The deep-vein thrombosis (DVT) which often occurs at the insertion sites of CVCs, as well as the pulmonary embolism (PE) that the detached clots from the CVCs travel through the superior vena cava to lodge in the lunges, can lead to the venous-access failure and

cause harm to or death of patients. In particular, the cancer patients who need to receive long-term drug therapy through CVCs are relevant to the aforementioned problems. Furthermore, thromboembolic complications are a major cause of mortality and morbidity with cardiovascular devices. For instance, the thrombosis formed on prosthetic valves can put patients at risk of stroke. The failure of artificial vascular grafts caused by thrombosis can result in ischemia and the death of downstream tissue beds.[2] To alleviate possible thromboembolic complications, patients usually need to take continuous antiplatelet or anticoagulation therapy after implantation. Extracorporeal circuits are used to assist the function of organs for those patients who suffer organ failure. Especially during the current devasting global COVID-19 pandemic, the ECMO plays a crucial role in life-saving. Yet, to prevent clotting in the extracorporeal circuit, high concentrations of heparin are indispensable during the procedures. The concentrations of heparin are over 10-fold higher than those used to treat patients with established thrombosis. Such high concentrations may lead to the patients' bleeding.[1]

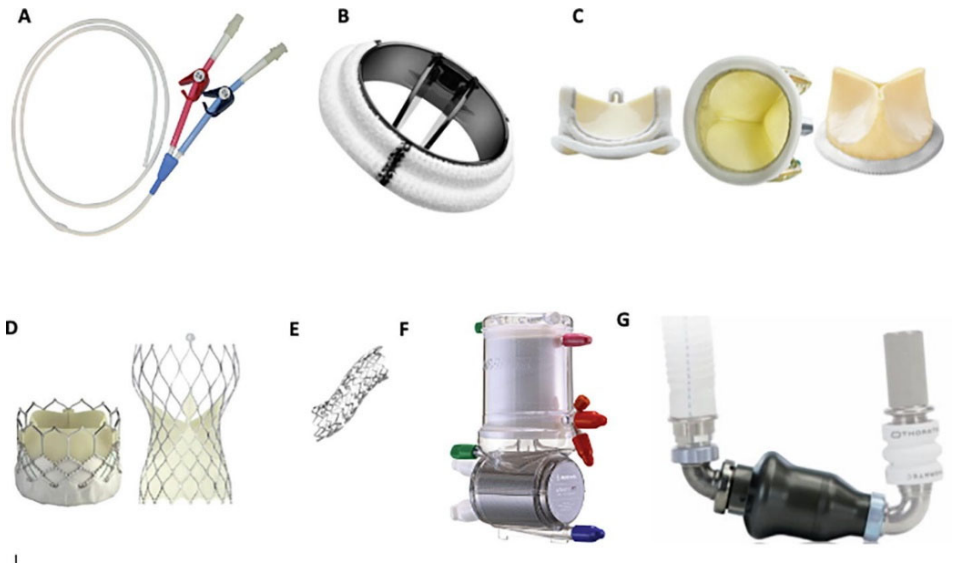

Figure 1.1. Examples of blood-contacting medical devices. (A) double-lumen central venous catheter, (B) bileaflet mechanical heart valve with Dacron sewing ring, (C) bioprosthetic heart valves by Edwards, St. Jude Medical, and LivaNova (from left to right), (D) transcatheter aortic valves by Edwards and Medtronic, (E) coronary stent by Boston Scientific, (F) oxygenator and heat exchanger used in cardiopulmonary bypass circuits, and (G) a left ventricular assist device, Heartmate 2, by Thoratec. Copyrights belong to the respective manufacturers.[1]

It is worth noting that the various adverse reactions caused by a blood-contacting device are always concomitant in clinic practice. Thus, the term “thrombogenicity” is used to broadly define the extent to which a blood-contacting device induces adverse reactions.[2] Mitigating or even eliminating the thrombogenicity is an essential and challenging subject for blood-contacting devices. As outlined above, patients need to take anticoagulants to reduce the incidence of complications and ensure the function of medical devices, but they meanwhile bear the

accompanying risk of side effects, such as blood coagulation disorders. More than that, the treatment of complications can be expensive. Once severe thrombosis forms and device failure occurs, the replacement of devices is also costly to the patients. For extracorporeal circuits, which are subjected to repeated blood exposure in individual patients, preventing the thrombosis can improve the reusability, and thus reduce the financial burden for patients.[2]

Thus, a question naturally comes to us, how to mitigate the thrombogenicity of blood-contacting devices? Before answering this question, it is necessary to be aware of the generation of thrombogenicity.

1.1.2 Blood reaction on blood-contacting devices

Thrombogenicity is the consequence of blood responses to foreign materials. Following the same procedures as the hemostatic mechanism, the blood responses involve a series of interdependent reactions such as protein adsorption, blood cell (platelet in particular) adhesion and activation, coagulation and complement activation.

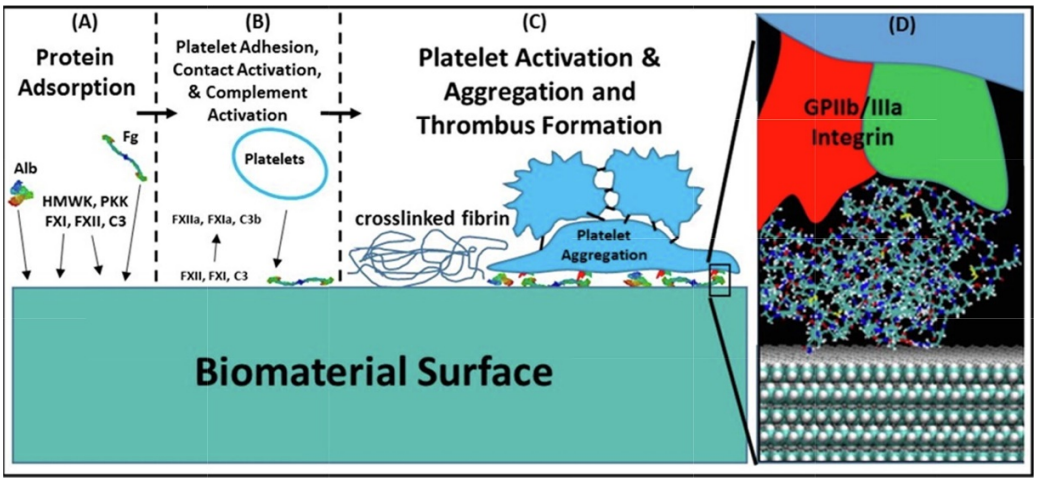

Figure 1.2. Overview of protein adsorption and subsequent events occurring on biomaterial surfaces. (A) Adsorption of proteins to biomaterial surface as an initial event (Alb: albumin, Fg: Fibrinogen, HMWK: high-molecular-weight kininogen, PKK: prekallikrein, FXI & FXII: factor XI and factor XII intrinsic blood coagulation cascade proteins, C3: complement protein 3). (B) Non-activated platelets adhere to layers of adsorbed proteins, adsorbed FXI and FXII initiate contact activation processes, and C3 is activated to C3b. (C) Activated platelets, contact activation proteins, and complement activation synergistically interact to induce thrombus formation. (D) Platelet interaction with an adsorbed protein via a GPIIb/IIIa integrin receptor; protein is illustrated as adsorbed on a polyethylene surface. Refereed to *Acta Biomater.* **2019**, *94*, 11–24. Copyrights 2013 Acta Biomater.

The adsorption of plasma proteins is the initial event amongst the procedures occurring upon blood contact with foreign materials. It has been reported the cover of protein layers on surfaces can be completed in times of the order of seconds. Protein adsorption is the basis of subsequent blood reactions. Cellular reactions, such as adhesion, activation, and the generation and release of enzymes are established on the recognization of integrin receptors on the cell membranes to the proteins absorbed on the foreign materials. The protein adsorption and subsequent events occurring on surfaces are illustrated in **Figure 1.2**.[3]

Adsorbed fibrinogen, fibronectin, vitronectin, and von Willebrand factor (vWF) are strongly associated with platelet adhesion. The interactions between these adhesive proteins and platelets

are mediated by the platelet glycoprotein IIb/IIIa (GP IIb/IIIa, integrin $\alpha_{IIb}\beta_3$) and platelet glycoprotein Ib (GP Ib, mainly interacting with vWF). Upon the activation of platelets (responses of platelets caused by stimulation), the GP IIb/IIIa undergoes a conformational change, and the binding between the platelets and adhesive proteins occurs. In addition, the GP IIb/IIIa at resting state can also react with deformed adhesive proteins. Following platelet adhesion, a series of platelet release reactions are initiated, and the adenosine diphosphate (ADP), thrombin, and thromboxane A_2 are thus released. These secrets synergetically contribute to the platelet recruitment into the growing platelet aggregate. Simultaneously, some resting platelets are activated by the secrets; the GP IIb/IIIa undergoes a conformational change, the subsequent process takes place as aforementioned. Moreover, the thrombin directly binds with the platelets, activating platelets to produce more thrombin, release more ADP and thromboxane A_2, and form fibrin. Consequently, the platelet aggregate is enhanced. The adhered, activated, and aggregated platelets compose the platelet thrombus. The platelet thrombus is further stabilized by fibrin.[2]

The surface contact mediating coagulation (intrinsic pathway) together with the tissue factors mediated coagulation (extrinsic pathway) constitute the coagulation. Herein, the intrinsic pathway is briefly introduced. Following surface contact, inactive factor XII is automatically activated to become enzyme factor XIIa. The adsorbed high molecular weight kininogen also facilitates the formation of factor XIIa via acting as a cofactor in the factor XII activation. The factor XIIa then activates prekallikrein and factor XI. The activated prekallikrein prompts the generation of kallikrein which further activates factor XII, while the activated factor XI results in the generation

of thrombin. Besides promoting platelet aggregation as aforesaid, the thrombin plays a role in the transformation of fibrinogen to fibrin. In the above contact activation, the factor XII which initiates the "cascade" of reactions can be repeatedly activated. Thereby, the reactions are quickly amplified and significant amounts of thrombin are formed in a short time.[1,2] Complement activation tends to occur on the surfaces of blood-contacting devices as well. Briefly, surfaces activate the complement system via the classical pathway and alternative pathway, which finally mediate the adhesion of both leukocytes and platelets on the surfaces.[2]

Since it is the artificial surfaces that induce the above reactions, it is natural to consider modifying the surface properties to regulate thrombogenicity. In fact, extensive research has been conducted on the surface modification of blood-contacting devices.[4-7]

1.2 Surface modification of blood-contacting medical devices

According to the anti-thrombogenicity mechanism, the surface modification of blood-contacting medical devices can be categorized as bioactive modification, passive modification, and endothelialization.[8]

1.2.1 Bioactive surface modification

The bioactive method is to incorporate bioactive molecules such as anticoagulants and fibrinolytic agents (promote the removal of fibrin deposits) on the surfaces.[4] In contrast to systemic anticoagulation therapy, the in-situ supply of anticoagulation can decrease the total drug load for

the patients. Among kinds of bioactive molecules, heparin is the most extensively investigated and the only one applying in surface treatment on the market currently. Heparin is a naturally occurring glycosaminoglycan, which works as a catalyst to accelerate the inhibitory effect of antithrombin III on thrombin and other coagulation factors (e.g., factor Xa, IXa, XIa, XIIa).[9,10] Although without the drawbacks of saturation and consumptions as some direct coagulation inhibitors, the heparin, as well as other indirect inhibitors such as thrombomodulin and tissue plasminogen activator, still suffer some general challenges of bioactive molecules. Firstly, animal-derived bioactive molecules are restricted in large-scale production and have risks in product contamination.[11-13] Though recent advances in synthetic production, it still requires multi-step and costly preparation and intensive purification.[10] Secondly, some bioactive molecules with peptide or polysaccharide structures are prone to degradation in vivo, and thus the long-term activity is reduced.[8] Thirdly, to reduce the loss of bioactive molecules on the surface and extend their continued bioactivity, covalent immobilization is used. Yet, the absence of suitable conjugation sites on some bioactive molecules may make the covalent immobilization difficult to establish.[8] Additionally, with the surface rearrangement over time, bioactive molecules may not be accessible to the target biomolecules in the human body.[14]

1.2.2 Passive surface modification

As mentioned before, the adsorbed proteins on surfaces dominate subsequent blood reactions, and it has been revealed that the protein adsorption behaviors strongly depend on the surface

properties.[15-17] The idea of passive modification is to cut off the blood reactions from the source, i.e., to prevent the proteins from interacting with surfaces. The other understanding of passive surface is that protein adsorption still occurs on the surface, but the adsorbed proteins are inert to arouse the cell reactions. These characteristics of the passive surface are usually associated with the terms “non-fouling,” “antifouling,” or “stealth.” In terms of platelet adhesion, the adsorption of albumin and fibrinogen are mainly considered. Albumin is the most abundant protein in plasma and tends to be preferentially adsorbed onto surfaces.[18] It has been generally accepted that the adsorption of albumin causes no platelet adhesion as it lacks amino acid sequences to bind with platelets.[19] What is more, some studies have shown that adsorbed albumin blocks platelet adhesion.[20,21] However, Sivaraman et al. reported that the adsorption induces the unfolding of albumin and exposes or forms binding sites to platelet receptors. Once the unfolding exceeds a critical degree, platelets can adhere to the albumin via a receptor-mediated process.[19] Fibrinogen is the most important protein supporting platelet adhesion among the adhesive proteins.[2] The platelet adhesion is strongly correlated with the conformational change of adsorbed fibrinogen as the adsorption can stimulate the exposure of platelet activation site, i.e. the dodecapeptide sequence $HHLGGAKQAGDV^{400-411}$ at the carboxyl terminus of fibrinogen γ' chains.[22] Hence, as the evaluation of the efficiency of the passive surface modification, the investigation of protein adsorption behaviors usually focuses on the quantities and conformational changes of albumin or fibrinogen.

The most widely adopted method to construct a passive surface is to incorporate non-fouling

polymer on the surface. It is mainly related to two interdependent aspects: the surface construction techniques and the selection of non-fouling polymers. The surface construction technique determines the stability of polymer on the surface, as well as surface parameters such as polymer chain density, polymer layer thickness, and roughness, all of which are related to the surface's blood compatibility.[23,24] For example, surface construction techniques that can achieve high polymer chain density are usually favorable. At high density, polymer chains repel from each other, stretch away from the substrate, and reach a fully extended conformation, which is called the "brush" configuration. While at a very low density, the polymer chains adopt a "mushroom" configuration that polymer chains coil randomly. The "brush" configuration is more effective to prevent protein adsorption.[4] For the selection of non-fouling polymers, there are two available types, i.e., hydrophilic types and zwitterionic types. The hydrophilic polymers are usually electrically neutral and contain polar groups which act as proton donors or acceptors to form hydrogen bonds with water.[23] Some typical examples of this kind of polymers include ethylene glycol-based polymers, poly(2-oxazoline)s (POXs), polysaccharides (e.g., dextran, cellulose), polyacrylamide, and polypeptides (chemical structures are shown in **Figure 1.3**).[25,26] Zwitterionic polymers refer to polymers that possess an equal number of cations and anions in their chains. Thus, the zwitterionic polymers remain overall electrically neutral. Furthermore, the zwitterionic polymer exhibits super hydrophilicity due to a thick hydration layer formed through the strong electrostatic interaction between the abundant ions and water.[27] Poly(2-methacryloyloxyethyl phosphorylcholine) (PMPC), poly(carboxybetaine methacrylate) (PCBMA), poly(sulfobetaine

methacrylate) (PSBMA) and poly(serine methacrylate) (PSrMA) are the representatives of zwitterionic polymers (chemical structures are shown in **Figure 1.3**).[28,29] It is worth mentioning that the anti-thrombogenicity decrease is not only confined to the bioactive surface. Oxidative degradation of non-fouling polymers in the physiological environment can lead to a limited lifetime for the passive surface. Likewise, the so-called "non-adhesive encounters" trick of low protein adsorption should be specially noticed. In other words, the passive surface prevents the significant formation of clotting as well as activates platelets. As evidenced for poly(hydroxyethyl methacrylate) (PHEMA) based hydrogels, activated cells, and thrombotic substances peeled off from the surface and cause damages to the downstream organs.[8] More research into the development of non-fouling polymers and understanding polymer-protein interaction in vivo is thus needed.

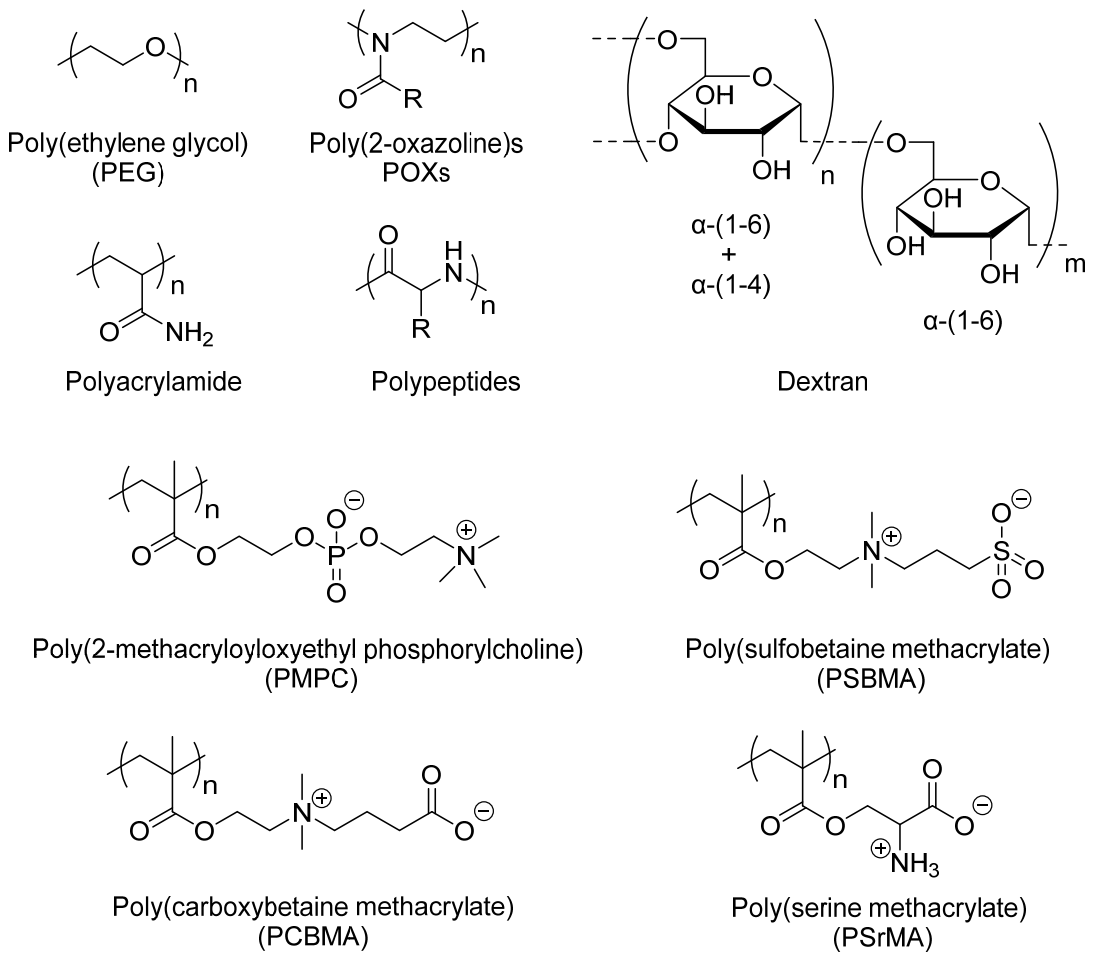

Figure 1.3. Chemical structures of representative non-fouling hydrophilic polymers and zwitterionic polymers.

1.2.3 Surface endothelialization

The vascular endothelium is the only know surface with ideal blood compatibility.[4] To some extent, either the bioactive or passive surface modification can be regarded to approach some characteristics of the vascular endothelium.[8] The confluent layer of endothelial cells attached to a basement membrane constitutes the endothelium and is the foundation of endothelium's blood

compatibility, e.g., providing natural anticoagulant. Surface endothelialization is to modify surfaces via physical, chemical, or biological methods to promote early endothelial cells' adhesion, migration, proliferation, and finally, to form an endothelial layer on the surface.[30] A promising strategy is to immobilize cell adhesion proteins or active peptides on surfaces, such as collagen type I, fibronectin, Arg-Gly-Asp (RGD), Arg-Glu-Asp-Val (REDV), and Tyr-Lle-Gly-Ser-Arg (YIGSR) peptide.[31] To immobilize these biomolecules, the non-fouling poly(ethylene glycol) (PEG) with a suitable chain length is usually used as a spacer. It is expected to enhance the specific adhesion by reducing the nonspecific protein adsorption and increasing the accessibility of biomolecules to cells.[17,31,32] Recently, our lab found that a surface that was modified by the silsesquioxane/poly(2-methoxyethyl acrylate) (PMEA) hybrid material not only prevented platelets adhesion but also significantly improved the adhesion and extension of human umbilical vein endothelial cells.[33] This opens up new avenues for the development of novel blood-compatible polymers with specific adsorption properties independent of biomolecules, albeit it would be a challenge.

Before moving onto the next section, it would be beneficial to clarify some terms that are widely encountered in literature but easily confused. According to Ratner et al.,[2] the aforementioned blood compatibility refers to the property of a material or device that allows it to function in contact with blood without inducing adverse reactions. This definition is quite close to that of non-thrombogenicity in terms of causing adverse reactions. However, combined with the characteristic of vascular endothelium, real blood compatibility should include the property that

the artificial surfaces can adapt to the blood environment and eventually integrate with the blood environment. Given that the current evaluations of blood reactions on artificial surfaces primarily focus on short-term, in-vitro, and thrombosis-related tests,[2] the mutual substitution between blood compatibility and non-thrombogenicity is generally accepted. In the following sections, the term blood compatibility is used instead of non-thrombogenicity.

Biocompatibility can be defined as the ability of a material to perform with an appropriate host response in a specific application.[2] In other words, the material is intended to be functional as well as non-toxic to the human body. The nontoxicity encompasses tissue compatibility and blood compatibility. Thus, blood compatibility and biocompatibility should be distinguished.

1.3 Mechanism of blood-compatible polymers

1.3.1 Steric repulsion theory and hydration theory

Although using non-fouling polymers to modify the device surfaces is relatively widely adopted to improve the blood compatibility of the surfaces, when polymers are used in clinical practice, they gradually tend to expose some unanticipated intrinsic flaws. We always expect outperformed polymers to overcome the problems. On the other hand, with the growing interest in precision medicines tailored to the individual needs of the patients, the emergence of gene and immune therapies, and advances in three-dimensional (3D) printing technologies, there is an increasing demand for smart biocompatible polymers which can respond to changes in physiological parameters and exogenous stimuli.[34] Therefore, our pursuit of novel biocompatible

polymers never ceased. Since blood compatibility is a premise for biocompatibility, we naturally turn our attention to the blood compatibility of polymers first. To develop novel blood-compatible polymers, the common characteristics of existing blood-compatible polymers were generalized and intended to act as a guiding principle. Whitesides et al.[35] summarized four molecular-level features of chemical groups that incorporated on the protein adsorption-resistant surfaces: (i) hydrophilic, (ii) including hydrogen-bond acceptors, (iii) without hydrogen-bond donors, (iv) overall electrically neutral. Yet, exceptions to these rules have been reported.[36] For example, according to Luk et al.,[37] self-assembled monolayers (SAMs) presenting mannitol groups are inert to protein adsorption, despite the mannitol being rich in hydrogen-bond donors. Whereupon, some researchers attempted to analyze the cause of polymers' blood compatibility to establish the guiding principle. Currently, the steric repulsion theory and hydration theory are relatively popular.

The steric repulsion theory is often used to explain the blood compatibility of polymers with high chain mobility, PEG representatively.[24,38-40] The steric repulsion can be described as follows (a schematic diagram is shown in **Figure 1.4**). The flexible polymer chains generate a large number of chain conformations or excluded volumes. When protein molecules approach polymer chains, polymer chains are significantly compressed, resulting in a loss of conformational freedom, which contributes to the loss of the entropic component of free energy and thus a free energy penalty. In other words, the displacement of excluded volumes by proteins is thermodynamically unfavorable.[4,41,42]

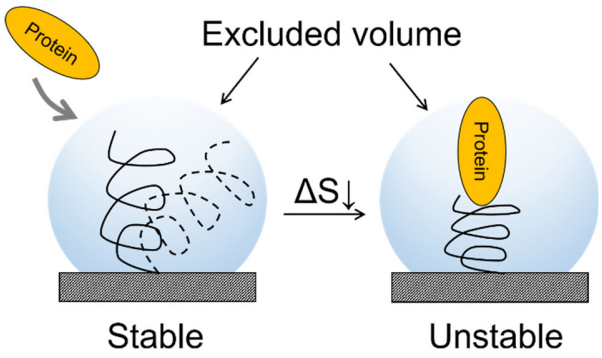

Figure 1.4. Schematic diagram of steric repulsion theory.[43]

Compared to the steric repulsion theory, the hydration theory appears to be more compelling these years. It makes sense to consider water as a key role in blood compatibility since water is the first blood component to interact with foreign surfaces. Water molecules' expulsion from the foreign surface and the protein surface is the initial and most important step in facilitating protein adsorption by lowering the free energy barrier due to dehydration entropic effects.[44] The hydration theory can be generally explained as follows: polymer's polar groups interact with water, forming hydration layers that prevent proteins from penetrating the polymer layer.[4] However, the hydration layer concept is insufficient to explain the blood compatibility of polymers, since some polymers such as poly(2-hydroxyethyl methacrylate) and poly(2-hydroxyethyl acrylate), can form hydration layers but are not blood-compatible.[45] In recent years, an increasing number of experimental and theoretical studies have looked further into the composition of hydration layers.[44,46,47]

1.3.2 Intermediate water concept

By keeping a foothold in the study of PMEA, our lab has been committed to investigating the relationship between polymers' hydration states and their blood compatibility. Through a variety of thermal and spectroscopic measurements on PMEA, consistency is established that the hydration layers of the PMEA comprise three types of water. According to their crystallization behaviors, they are named non-freezing water (NFW), freezing-bound water, and freezing water or free water (FW). In the differential scanning calorimetry (DSC) measurement, (i) the NFW does not crystallize even at −100 °C and is thus nondetectable in the DCS thermogram, (ii) freezing-bound water crystallizes at ca. −40 °C (cold crystallization) and melts below 0 °C, (iii) FW melts at ca. 0 °C (a representative DSC thermogram of hydrated PMEA is shown **Figure 1.5a**).[48] The existence of the three types of water is also reflected in their different dynamic behaviors. According to the ^{2}H-NMR and ^{13}C-NMR spectra of hydrated PMEA: (i) NFW exhibits low mobility due to a strong interaction with the PMEA chain, (ii) the mobility of freezing-bound water is higher than that of NFW, (iii) FW has the highest mobility due to its location far from the PMEA chain.[49] By investigating the process of water sorption into the PMEA film with time-resolved, in situ, attenuated total reflection infrared (ATR-IR) spectroscopy, Morita et al. revealed three different O–H stretching vibration [ν(O–H)] bands in the process, which can be assigned to the three hydrated water (shown in **Figure 1.5b**).[50,51] The ν(O–H) band of NFW is at approximately 3600 cm^{-1}, which usually appears at the wavenumber of water molecules isolated from hydrogen-bonds or hydrogen-bonded to carbonyl groups. The ν(O–H) band of freezing-bound is at around

3400 cm^{-1} and FW has a broad vibration band ranged from 3400 to 3200 cm^{-1} which resembles that of bulk water.[48,50]

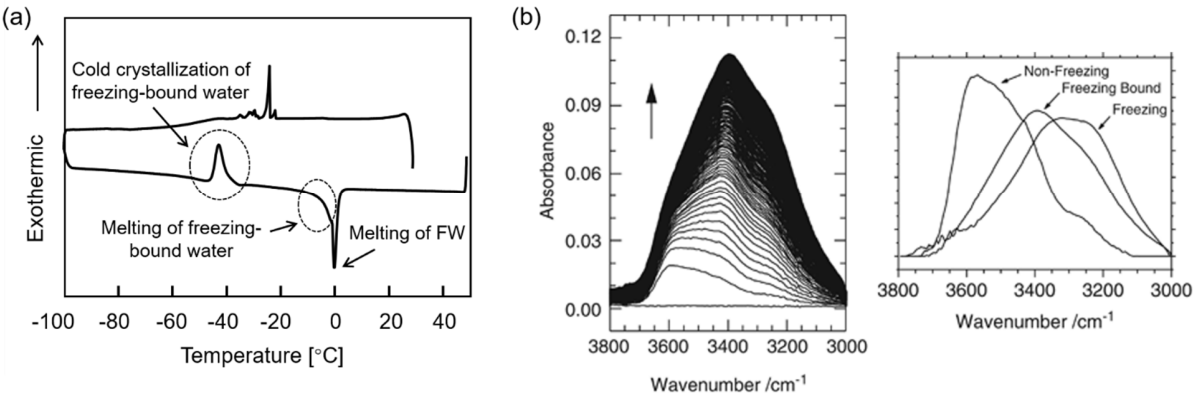

Figure 1.5. (a) A representative DSC thermogram of hydrated PMEA. (b) Time-resolved ATR-IR spectra of the sorption process for liquid water into a PMEA film (left) and pure spectra and of NFW, freezing-bound water, and FW (right) calculated using alternating least squares from the left of (b). The left and right of (b) referred to literature.[50,51]

Compared to the ^{2}H-NMR, ^{13}C-NMR, and ATR-IR measurement, DSC measurement is easy to operate, sample preparation is simple, and results are pretty straightforward. Therefore, we chose DSC measurement to analyze the composition of hydration layers, or hydration states, of a number of well-known blood-compatible and non-blood-compatible polymers. By comparing the obtained and reported DSC results, it is found that the freezing bound water is present in blood compatible polymers, such as synthetic type: PEG, PMPC, polyvinylpyrrolidone, poly(methylvinyl ether), poly(tetrahydrofurfuryl acrylate), and natural type: gelatin, albumin, cytochrome *c*, and hyaluronan, alginate, DNA, RNA, while barely in non-blood-compatible

polymers.[45,48,29] Thus, we proposed that freezing-bound water plays a key role in the blood compatibility of polymers.

Furthermore, according to the computer simulations by Jiang et al on the water-induced repulsion between lysozymes and some oligo(ethylene glycol) (OEG), zwitterionic and sugar-based protein resistant SAMs, the interfacial water molecules in the vicinity of these SAMs act as a physical barrier preventing the adsorption of lysozymes.[52-55] The repulsion barrier is consist of tight binding water molecules with the functional groups of the SAMs and the adjacent water molecules (2-3 nm of thickness and around 6-10 layers of water molecules) around the SAMs. Meanwhile, the results revealed by frequency modulation non-contact AFM technique also demonstrated that a stable layer of structured water molecules which has thickness of 2-3 nm locates around the OEG-SAM. While for other protein adhesive SAMs, such stable layer is absent.[56]

Table 1.1. Characteristics of FW, Freezing-bound Water and NFW

Hydrated water	Freezability[a]	Stretching vibration band [cm^{-1}][b]	Correlation time [s][c]	Surface force[d]
FW	Melting at 0 °C	3400-3200	10^{-12}-10^{-11}	No interaction
Freezing-bound water	Freezing and melting below 0 °C	3400	10^{-10}-10^{-9}	Repulsion at a long range (2-4 nm)
NFW	Non-freezing below 0°C	3600	10^{-8}-10^{-6}	Repulsion at a long range (< 1 nm)

[a]Characterized by DSC. [b]Characterized by time-resolved ATR-IR. [c]Characterized by solid state NMR. [d]Characterized by AFM.

Based on the characteristics of each water shown in the DSC, NMR, IR and AFM results (summarized in **Table 1.1**), it is reasonable to assume that water deposits on the blood compatible polymer surface in the following order: NFW comes first, followed by freezing-bound water, and FW comes last. NFW interacts strongly with polymer chains, while freezing-bound water is loosely bound to the polymer or NFW. FW is slightly affected by polymers and is freely exchanged with bulk water and results in a structure that resembles bulk water. The freezing-bound water can prevent the cells or proteins from directly contacting the polymer surface or NFW. Because freezing-bound water is so intermediated in terms of location and interaction strength with polymer when compared with NFW and FW, we refer to it as intermediate water (IW) instead.[48]

Looking back to the beginning of this chapter, it is natural to wonder whether the IW concept can support the development of novel blood-compatible polymers. According to the IR spectrum and quantum chemical calculations on PMEA, NFW mainly (85.6%) interacts with two carbonyl groups while IW interacts with the methoxy moiety in the side chain.[50] The chemical structure of a polymer can affect how water interacts with it, and as a result, blood compatibility may suffer. In fact, this inference has been demonstrated in studies of the hydration states and blood compatibility of a series of PMEA derivatives (the graphic conclusion is shown in **Figure 1.6**). To put it another way, generally, the higher the IW content, the better the blood compatibility of the polymer is. Hence, when designing the structure of a novel polymer, aiming at increasing the IW content to improve blood compatibility would be effective.

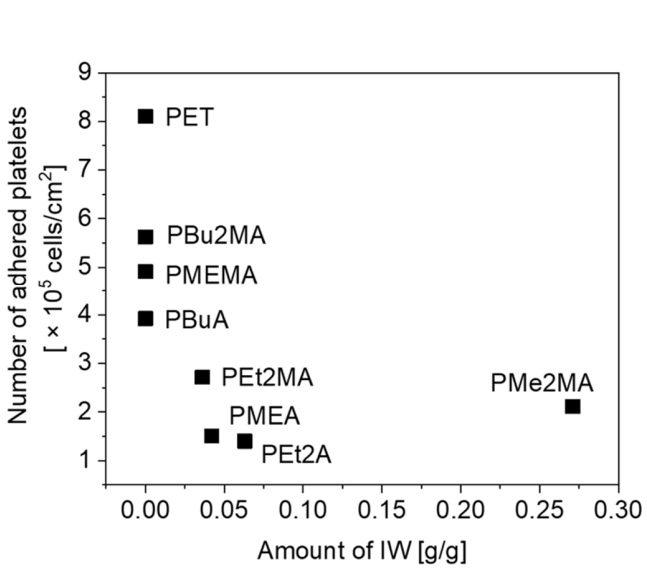

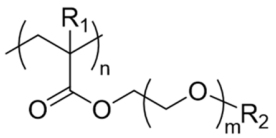

R_1	R_2	m	polymer
CH_3	C_4H_9	2	PBu2MA
CH_3	CH_3	1	PMEMA
H	C_4H_9	0	PBuA
CH_3	C_2H_5	2	PEt2MA
H	CH_3	1	PMEA
H	C_2H_5	2	PEt2A
CH_3	CH_3	2	PMe2MA

Chemical structures of PMEA derivatives

Figure 1.6. The correlation between IW water content (the gram of IW per gram of polymer) and the number of adhered platelets of PMEA derivatives. The chemical structures of PMEA derivatives are shown in the left part of the figure.

In conclusion, a thick IW layer can prevent the direct contact of bio-components on the surface of polymers or NFW, which plays a key role in the excellent blood compatibility of polymers. The presence of IW can also be regarded as an intrinsically common feature of blood-compatible polymers. Since DSC measurement can facilely and straightly detect the IW, it can be used to preliminarily judge polymers' blood compatibility. The content of IW is related to the polymer's blood compatibility. In general, the higher the content of IW, the better the blood compatibility. Therefore, IW can be employed to guide the development of novel blood-compatible polymers.

1.4 Poly(2-oxazoline)s

As the most representative hydrophilic non-fouling polymer, PEG has been extensively studied in e.g., drug delivery, tissue engineering, antifouling surfaces, and biosensors. It has been regarded as the gold standard of biocompatible polymer.[57] However, the drawbacks that have recently been revealed on PEG motivate researchers to seek alternative polymers. One problem is that PEG can arouse the immune system to generate specific anti-PEG antibodies. For some peptide or protein drugs that are easily degraded or eliminated by the human body, conjugating them with PEG (PEGylated) can increase their circulation time and concentration in the target tissue, thereby improving the therapeutic efficacy. The anti-PEG antibodies can accelerate the clearance of the PEGylated drugs from blood, resulting in a loss of therapeutic efficacy.[41,58] What is more, as anti-PEG antibodies were discovered in individuals who had never received PEGylated therapeutics, it is considered that using PEG-containing hygiene and cosmetic products could cause the generation of anti-PEG antibodies.[59] The other issue is the degradation of PEG in physical conditions. It has been reported that the metabolism of PEG, which involves sequential oxidations by alcohol dehydrogenase and aldehyde dehydrogenase, can generate toxic organic acids in patients.[60]

POXs, especially poly(2-methyl-2-oxazoline) (PMeOx) and poly(2-ethyl-2-oxazoline) (PEtOx) have been considered as promising candidates for PEG. POXs have comparable biocompatibility and well-defined chain structure to PEG.[61-62] With regards to chemical stability, POXs are theoretically less prone to oxidation than PEG, because the adjacent C-H bond to nitrogen is less polarized than to oxygen. Pidhatika et al.[63] compared the stability of PEG and PMeOx coatings on

substrates in physiological and oxidative media, respectively, and found that PMeOx showed higher stability and thus prolonged anti-protein resistance. Yet, Ulbricht et al. reported that in the presence of reactive oxygen species, the stability of PEtOx is not significantly higher than that of PEG.[64] Since these studies were conducted in vitro and polymers' stability is strongly dependent on the environment, more research into the stability of POXs in vivo is needed.

The outstanding advantage of POXs is the ease of functionalization, which comes from their cationic ring-opening polymerization (CROP). The CROP of 2-oxazoline monomers follows a typical chain-growth polymerization process, including initiation, propagation, and termination (**Figure 1.7**). Generally, a nucleophilic attack from the lone pair on the nitrogen of the 2-oxazoline monomer to an electrophilic initiator forms a cationic oxazolinium species. Subsequently, the lone pair on the nitrogen attacks the electropositive 5-position of the oxazolinium species, resulting in the cleavage of the O(1)-C(5) bond and isomerization to a tertiary amide while forming a new oxazolinium species. The chain grows as the monomer continues to attack the new oxazolinium species. The chain propagation is terminated by a nucleophilic attack of a nucleophile (terminator) to the 5-position of the oxazolinium species. Under ideal polymerization conditions of fast initiation, no chain transfer, and no chain termination, the CROP is living polymerization. Namely, the molecular weight of POXs can be well controlled by the molar ratio of monomer to the initiator, and the molar mass distribution can be very narrow. Thus, except for selecting an initiator with a rapid initiation rate, the synthesis of POXs requires all regents to be highly purified to avoid interference from nucleophilic impurities such as moisture and oxygen.[65]

By introducing functional groups to the initiators or terminators, it is easy to realize the functionalization of the α-chain-ends or ω-chain-ends. The third way to functionalize is to incorporate the functional groups into the side chains of the oxazoline monomers, provided that those groups do not interfere with the polymerization. For example, the successful polymerization of oxazoline monomers with alkenes, alkynes, and azides has been reported. Concerning some nucleophilic groups which would interfere with the CROP, such as amines, alcohols, thiols, and carboxylic acids, introducing them into the side chain needs protection and deprotection before and after CROP.[66] Recently, a hydrolysis-reacylation method was successfully exploited to introduce nucleophilic groups into the side chains. Sedlacek et al synthesized a class of superhydrophilic POXs derivatives bearing various pendant ether groups by acylating the acidic hydrolyzed PEtOx, i.e., polyethyleneimine (PEI) with different carboxylic acids.[67] Subsequently, by using the same strategy, the authors introduced a series of tertiary amines into POX side chains.[68] Some of the functional groups that have been successfully introduced into the POXs chains are listed in **Figure 1.7**.

Another characteristic of POXs is that their physicochemical properties are influenced by the hydrocarbon side chains. In terms of biochemical application, the hydrophilicity of POXs is usually discussed. Generally, as the side chain length increase, the POX becomes more hydrophobic. For example, PMeOx is completely water-soluble, whilst PEtOx has a lower critical solution temperature (LCST) in the range of 61-69 ℃, and the LCST of poly(2-isopropyl-2-oxazoline) (P*i*PrOx) decreases to 36-39 ℃. When the number of carbon atoms exceeds three, the

POXs become water-insoluble.[65] Moreover, the hydrophilicity of POXs can be precisely controlled by manipulating the copolymerization of different 2-oxazoline monomers which includes the composition and the chain structure of the copolymer.[69] It should be noted that the copolymer chain structure, namely, statistical or block distribution, is determined by the 2-oxazoline monomers involved in the copolymerization as well as the monomer addition sequence. This knowledge is important for the construction of self-assembled amphiphilic POX copolymers or micelle.[70]

The characteristics of POXs endow their numerous potential in various biomedical applications, polymer therapeutics, tissue engineering, and non-fouling surface modification. Therein polymer therapeutics encompass polymer-drug conjugates, polymer-protein conjugates, polymer micelles, gene delivery.[71] For those drugs with poor water solubility, conjugating the drugs with biocompatible polymers can effectively improve the solubility of the drugs and prolong the circulation time in the body.[72] The easy functionalization of POXs allows for multiple approaches to drug conjugation, as well as to protein conjugation. Drugs can also be trapped in the hydrophobic core of an amphiphilic micelle to improve the drug delivery efficacy because the micelle size can be controlled to exceed the renal threshold to extend the blood circulation. The variation of hydrophilicity of POXs with the side chain provides easy access to construct micelle.[62] If thermoresponsive POX chain segments are incorporated into an amphiphilic block POX copolymer, it is expected to achieve the temperature-induced self-assembled micelle.[73,74] In terms of gene delivery application, it is mainly related to the hydrolyzed product of POXs, i.e., linear PEI which acts as a cationic polymer vector to complex and condense the anionically charged

nucleic acids.[74] Furthermore, because the functional groups at the chain ends or side chains of POXs are devisable, it is facial to obtain POX hydrogels by introducing some cross-linkable groups, such as oxazoline and unsaturated groups. Another way to prepare POX hydrogels is to cross-link the PEI repeating units obtained from the partially hydrolyzed POXs using isocyanates, aldehydes, acids, and their derivatives.[75] As for the non-fouling surface modification using POXs, it involves the surface construction techniques as mentioned in the previous section and will be elaborated on in **Chapter 2**.

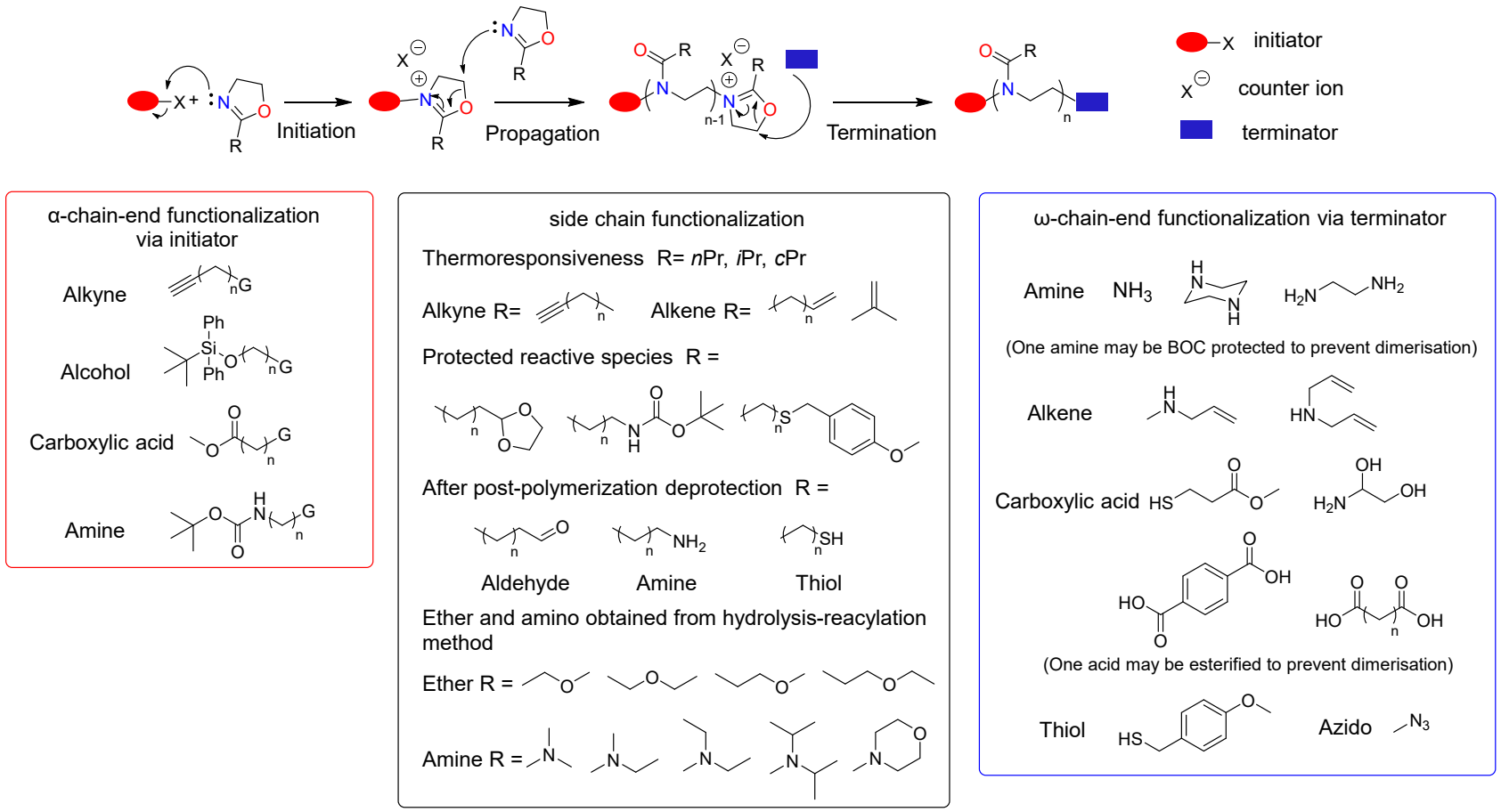

Figure 1.7. General steps of CROP of 2-oxazolines, and examples of some functional groups introduced into the α-chain end, side chain, and ω-chain end.[62, 67-70]

1.5 Objectives of the thesis

The previous section describes the characteristics and some biomedical applications of POXs. Albeit there is currently much research on the physicochemical properties of POX homologs and the development of novel POX derivatives, few studies are on the hydration states of POXs. In addition, PMeOx and PEtOx, like PEG, are water-soluble polymers that are advantageous in drug delivery but less convenient for blood-compatible surface modification, which may usually require tedious surface immobilization. Thirdly, the CROP of POXs can be problematic. In fact, the CROP of POXs was first reported in 1966, but it did not arouse extensive interest at the time, owing to the limitations of long polymerization times and high costs that could not compete with commodity polymers.[62,76] Although microwave irradiation was found can accelerate the CROP, a rigorous reaction environment is still necessary.

Aiming at the above problems, the research objectives of this thesis includes the following aspects.

(i) The blood compatibility and hydration states of POXs. Since the physicochemical properties of POXs are affected by side chains, four POX homologs, i.e. PMeOx, PEtOx, poly(2-*n*-butyl-2-oxazoline) (PBuOx), and poly(2-phenyl-2-oxazoline) (PPhOx), are selected as models to study the relationship between side chain chemical sturctures, hydration state, and blood compatibility. A comprehension of this can contribute to the understanding of the biocompatibility mechanism of PMeOx and PEtOx and may inspire the development of novel blood-compatible

POX derivatives.

(ii) The development of POX derivatives. Inspired by biocompatible PMeOx and PEtOx and combined the conclusion from (i), the poly(meth)acrylates containing tertiary amide frameworks on the side chains, i.e., poly[2-(*N*-methylacetamido)ethyl acrylate] (PAEA), poly[2-(*N*-methylacetamido)ethyl methacrylate] (PAEM), poly[2-(*N*-methylpropionamido)ethyl acrylate] (PPEA), and poly[2-(*N*-ethylacetamido)ethyl acrylate] (PEAE), are designed (**Figure 1.8**). These POX derivatives can be easily prepared through free-radical polymerization and have the potential to living polymerization, i.e., reversible addition-fragmentation chain transfer (RAFT) polymerization. By copolymerization with hydrophobic (meth)acrylate monomers, the water solubility of POX derivatives can be controlled and can be conveniently immobilized on surfaces via physical interaction.

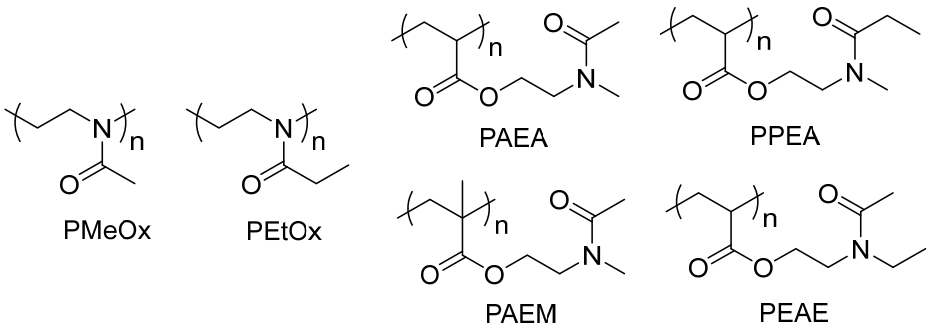

Figure 1.8. Chemical structures of PMeOx and PEtOx and four poly(tertiary amido acrylate) analogs denoted as PAEA, PPEA, PAEM, and PEAE.

(iii) The blood compatibility and hydration states of POX derivatives. The blood compatibility and hydration states of poly(tertiary amido acrylate) derivatives are compared to investigate the

effect of the vicinal groups linked to the tertiary amide moiety on them, which could pave the way for further advancement of poly(tertiary amido acrylate) derivatives.

This thesis includes five chapters.

In **Chapter 1**, background information is provided, including the thrombogenicity of blood-contacting medical devices, their generation, and their solution, as well as the characteristics of POXs and the IW concept.

Chapter 2 presents the synthesis and surface immobilization of POXs. The blood compatibility of POXs is compared by the platelet adhesion test and denaturation degree of adsorbed fibrinogen. The hydration states of POXs are investigated by the DSC and IR measurements.

In **Chapter 3**, the synthesis and molecular characterization of four poly (tertiary amido acrylate) analogs and corresponding water-insoluble copolymers are presented.

In **Chapter 4**, the blood compatibility of hydration states of poly (tertiary amido acrylate) analogs and corresponding water-insoluble copolymers are investigated. Since the poly (tertiary amido acrylate) analogs are water-soluble, their blood compatibility is evaluated by the hemolysis test as well as PMeOx and PEtOx. Furthermore, the cell viability and thermosensitivity of the poly (tertiary amido acrylate) analogs are also investigated. The blood compatibility of poly (tertiary amido acrylate) copolymers is investigated by plasma protein adsorption, denaturation degree of adsorbed fibrinogen, and platelet adhesion. The hydration states of poly (tertiary amido acrylate) analogs and corresponding water-insoluble copolymers are estimated by DSC measurements.

The conclusions of the thesis are summarized, and some recommendations are made for future research in **Chapter 5**.

1.6 Reference

(1) Jaffer, I. H.; Weitz, J. I. The Blood Compatibility Challenge. Part 1: Blood-Contacting Medical Devices: The Scope of the Problem. *Acta Biomater.* **2019**, *94*, 2–10.

(2) Ratner, B. D.; Hoffman, A. S.; Schoen, F. J.; Lemons, J. E. *Biomaterials Science*, 3rd ed.; Academic Press, 2013.

(3) Brash, J. L.; Horbett, T. A.; Latour, R. A.; Tengvall, P. The Blood Compatibility Challenge. Part 2: Protein Adsorption Phenomena Governing Blood Reactivity. *Acta Biomater.* **2019**, *94*, 11–24.

(4) Liu, X.; Yuan, L.; Li, D.; Tang, Z.; Wang, Y.; Chen, G.; Chen, H.; Brash, J. L. Blood Compatible Materials: State of the Art. *J Mater Chem B* **2014**, *2* (35), 5718–5738.

(5) Qi, P.; Maitz, M. F.; Huang, N. Surface Modification of Cardiovascular Materials and Implants. *Surf. Coatings Technol.* **2013**, *233*, 80–90.

(6) Biran, R.; Pond, D. Heparin Coatings for Improving Blood Compatibility of Medical Devices. *Adv. Drug Deliv. Rev.* **2017**, *112*, 12–23.

(7) Zhang, K.; Liu, T.; Li, J. A.; Chen, J. Y.; Wang, J.; Huang, N. Surface Modification of Implanted Cardiovascular Metal Stents: From Antithrombosis and Antirestenosis to Endothelialization. *J Biomed Mater Res A* **2014**, *102* (2), 588–609.

(8) Maitz, M. F.; Martins, M. C. L.; Grabow, N.; Matschegewski, C.; Huang, N.; Chaikof, E. L.; Barbosa, M. A.; Werner, C.; Sperling, C. The Blood Compatibility Challenge. Part 4: Surface Modification for Hemocompatible Materials: Passive and Active Approaches to Guide Blood-Material Interactions. *Acta Biomater.* **2019**, *94*, 33–43.

(9) Bussey, H.; Francis, J. L. Heparin Overview and Issues. *Pharmacotherapy* **2004**, *24* (8 II), 103S-107S.

(10) Baytas, S. N.; Linhardt, R. J. Advances in the Preparation and Synthesis of Heparin and Related Products. *Drug Discov. Today* **2020**, *25* (12), 2095–2109.

(11) Liu, H.; Zhang, Z.; Linhardt, R. J. Lessons Learned from the Contamination of Heparin. *Nat. Prod. Rep.* **2009**, *26* (3), 313–321.

(12) Huntington, J. A. Natural Inhibitors of Thrombin. *Thromb. Haemost.* **2014**, *111* (4), 583–589.

(13) Alban, S. From Heparins to Factor Xa Inhibitors and Beyond. *Eur. J. Clin. Invest.* **2005**, *35* (1), 12–20.

(14) Goddard, J. M.; Hotchkiss, J. H. Polymer Surface Modification for the Attachment of Bioactive Compounds. *Prog. Polym. Sci.* **2007**, *32* (7), 698–725.

(15) Wahlgren, M.; Arnebrant, T. Protein Adsorption to Solid Surfaces. *Trends Biotechnol.* **1991**, *9* (1), 201–208.

(16) Faulón Marruecos, D.; Schwartz, D. K.; Kaar, J. L. Impact of Surface Interactions on Protein Conformation. *Curr. Opin. Colloid Interface Sci.* **2018**, *38*, 45–55.

(17) Yuan, L.; Yu, Q.; Li, D.; Chen, H. Surface Modification to Control Protein/Surface Interactions. *Macromol. Biosci.* **2011**, *11* (8), 1031–1040.

(18) Sivaraman, B.; Latour, R. A. Time-Dependent Conformational Changes in Adsorbed Albumin and Its Effect on Platelet Adhesion. *Langmuir* **2012**, *28* (5), 2745–2752.

(19) Sivaraman, B.; Latour, R. A. The Adherence of Platelets to Adsorbed Albumin by Receptor-Mediated Recognition of Binding Sites Exposed by Adsorption-Induced Unfolding. *Biomaterials* **2010**, *31* (6), 1036–1044.

(20) Lambrecht, L. K.; Young, B. R.; Stafford, R. E.; Park, K.; Albrecht, R. M.; Mosher, D. F.; Cooper, S. L. The Influence of Preadsorbed Canine von Willebrand Factor, Fibronectin and Fibrinogen on Ex Vivo Artificial Surface-Induced Thrombosis. *Thromb. Res.* **1986**, *41* (1), 99–117.

(21) Tsai, W. B.; Grunkemeier, J. M.; McFarland, C. D.; Horbett, T. A. Platelet Adhesion to Polystyrene-Based Surfaces Preadsorbed with Plasmas Selectively Depleted in Fibrinogen, Fibronectin, Vitronectin, or von Willebrand's Factor. *J. Biomed. Mater. Res.* **2002**, *60* (3), 348–359.

(22) Kobayashi, S.; Wakui, M.; Iwata, Y.; Tanaka, M. Poly(ω-Methoxyalkyl Acrylate)s: Nonthrombogenic Polymer Family with Tunable Protein Adsorption. *Biomacromolecules* **2017**, *18* (12), 4214–4223.

(23) Wang, F.; Zhang, H.; Yu, B.; Wang, S.; Shen, Y.; Cong, H. Review of the Research on Anti-Protein Fouling Coatings Materials. *Prog. Org. Coatings* **2020**, *147*, 105860.

(24) Svoboda, J.; Sedláček, O.; Riedel, T.; Hrubý, M.; Pop-Georgievski, O. Poly(2-Oxazoline)s One-Pot Polymerization and Surface Coating: From Synthesis to Antifouling Properties Out-Performing Poly(Ethylene Oxide). *Biomacromolecules* **2019**, *20* (9), 3453–3463.

(25) Liu, L.; Li, W.; Liu, Q. Recent Development of Antifouling Polymers: Structure, Evaluation, and Biomedical Applications in Nano/Micro-Structures. *Wiley Interdiscip. Rev. Nanomedicine Nanobiotechnology* **2014**, *6* (6), 599–614.

(26) Damodaran, V. B.; Murthy, S. N. Bio-Inspired Strategies for Designing Antifouling Biomaterials. *Biomater. Res.* **2016**, *20* (1), 1–11.

(27) Zheng, L.; Sundaram, H. S.; Wei, Z.; Li, C.; Yuan, Z. Applications of Zwitterionic Polymers. *React. Funct. Polym.* **2017**, *118*, 51–61.

(28) Blaszykowski, C.; Sheikh, S.; Thompson, M. Surface Chemistry to Minimize Fouling from Blood-Based Fluids. *Chem. Soc. Rev.* **2012**, *41* (17), 5599–5612.

(29) Tanaka, M.; Sato, K.; Kitakami, E.; Kobayashi, S.; Hoshiba, T.; Fukushima, K. Design of Biocompatible and Biodegradable Polymers Based on Intermediate Water Concept. *Polym. J.* **2015**, *47* (2), 114–121.

(30) Jana, S. Endothelialization of Cardiovascular Devices. *Acta Biomater.* **2019**, *99*, 53–71.

(31) Ren, X.; Feng, Y.; Guo, J.; Wang, H.; Li, Q.; Yang, J.; Hao, X.; Lv, J.; Ma, N.; Li, W. Surface Modification and Endothelialization of Biomaterials as Potential Scaffolds for Vascular Tissue Engineering Applications. *Chem. Soc. Rev.* **2015**, *44* (15), 5680–5742.

(32) Yin, M.; Yuan, Y.; Liu, C.; Wang, J. Development of Mussel Adhesive Polypeptide

Mimics Coating for In-Situ Inducing Re-Endothelialization of Intravascular Stent Devices. *Biomaterials* **2009**, *30* (14), 2764–2773.

(33) Nishimura, S. N.; Ueda, T.; Kobayashi, S.; Tanaka, M. Silsesquioxane/Poly(2-Methoxyethyl Acrylate) Hybrid with Both Antithrombotic and Endothelial Cell Adhesive Properties. *ACS Appl. Polym. Mater.* **2020**, *2* (11), 4790–4801.

(34) Kowalski, P. S.; Bhattacharya, C.; Afewerki, S.; Langer, R. Smart Biomaterials: Recent Advances and Future Directions. *ACS Biomater. Sci. Eng.* **2018**, *4* (11), 3809–3817.

(35) Ostuni, E.; Chapman, R. G.; Holmlin, R. E.; Takayama, S.; Whitesides, G. M. A Survey of Structure-Property Relationships of Surfaces That Resist the Adsorption of Protein. *Langmuir* **2001**, *17* (18), 5605–5620.

(36) Dalsin, J. L.; Messersmith, P. B. Bioinspired Antifouling Polymers. *Mater. Today* **2005**, *8* (9), 38–46.

(37) Luk, Y. Y.; Kato, M.; Mrksich, M. Self-Assembled Monolayers of Alkanethiolates Presenting Mannitol Groups Are Inert to Protein Adsorption and Cell Attachment. *Langmuir* **2000**, *16* (24), 9604–9608.

(38) Yang, Z.; Galloway, J. A.; Yu, H. Protein Interactions with Poly(Ethylene Glycol) Self-Assembled Monolayers on Glass Substrates: Diffusion and Adsorption. *Langmuir* **1999**, *15* (24), 8405–8411.

(39) Wang, H.; Li, L.; Tong, Q.; Yan, M. Evaluation of Photochemically Immobilized Poly(2-Ethyl-2-Oxazoline) Thin Films as Protein-Resistant Surfaces. *ACS Appl. Mater.*

Interfaces **2011**, *3* (9), 3463–3471.

(40) Ngo, B. K. D.; Grunlan, M. A. Protein Resistant Polymeric Biomaterials. *ACS Macro Letters*. 2017, pp 992–1000.

(41) Yang, Q.; Lai, S. K. Anti-PEG Immunity: Emergence, Characteristics, and Unaddressed Questions. *Wiley Interdiscip. Rev. Nanomed. Nanobiotechnol.* **2015**, *7* (5), 655–677.

(42) Sonoda, T.; Kobayashi, S.; Herai, K.; Tanaka, M. Side-Chain Spacing Control of Derivatives of Poly(2-Methoxyethyl Acrylate): Impact on Hydration States and Antithrombogenicity. *Macromolecules* **2020**, *53* (19), 8570–8580.

(43) Lee, J. H.; Lee, H. B.; Andrade, J. D. Blood Compatibility of Polyethylene Oxide Surfaces. *Prog. Polym. Sci.* 1995, pp 1043–1079.

(44) Chen, S.; Li, L.; Zhao, C.; Zheng, J. Surface Hydration: Principles and Applications toward Low-Fouling/Nonfouling Biomaterials. *Polymer (Guildf).* **2010**, *51* (23), 5283–5293.

(45) Tanaka, M.; Mochizuki, A. Effect of Water Structure on Blood Compatibility - Thermal Analysis of Water in Poly(Meth)Acrylate. *J. Biomed. Mater. Res.* **2004**, *68* (4), 684–695.

(46) Kitano, H.; Mori, T.; Takeuchi, Y.; Tada, S.; Gemmei-Ide, M.; Yokoyama, Y.; Tanaka, M. Structure of Water Incorporated in Sulfobetaine Polymer Films as Studied by ATR-FTIR. *Macromol. Biosci.* **2005**, *5* (4), 314–321.

(47) Leng, C.; Sun, S.; Zhang, K.; Jiang, S.; Chen, Z. Molecular Level Studies on Interfacial Hydration of Zwitterionic and Other Antifouling Polymers in Situ. *Acta Biomater.* **2016**, *40*, 6–15.

(48) Tanaka, M.; Hayashi, T.; Morita, S. The Roles of Water Molecules at the Biointerface of Medical Polymers. *Polym. J.* **2013**, *45*, 701–710.

(49) Miwa, Y.; Ishida, H.; Saitô, H.; Tanaka, M.; Mochizuki, A. Network Structures and Dynamics of Dry and Swollen Poly(Acrylate)s. Characterization of High- and Low-Frequency Motions as Revealed by Suppressed or Recovered Intensities (SRI) Analysis of 13C NMR. *Polymer (Guildf).* **2009**, *50* (25), 6091–6099.

(50) Morita, S.; Tanaka, M.; Ozaki, Y. Time-Resolved in Situ ATR-IR Observations of the Process of Sorption of Water into a Poly(2-Methoxyethyl Acrylate) Film. *Langmuir* **2007**, *23* (7), 3750–3761.

(51) Tanabe, A.; Tanaka, M.; Morita, S.; Ozaki, Y. Multivariate Curve Resolution Analysis on the Multi-Component Water Sorption Process into a Poly(2-Methoxyethyl Acrylate) Film. *Appl. Spectrosc.* **2008**, *62* (1), 46–50.

(52) Zheng, J.; Li, L.; Tsao, H. K.; Sheng, Y. J.; Chen, S.; Jiang, S. Strong Repulsive Forces between Protein and Oligo (Ethylene Glycol) Self-Assembled Monolayers: A Molecular Simulation Study. *Biophys. J.* **2005**, *89* (1), 158–166.

(53) Zheng, J.; Li, L.; Chen, S.; Jiang, S. Molecular Simulation Study of Water Interactions with Oligo (Ethylene Glycol)-Terminated Alkanethiol Self-Assembled Monolayers. *Langmuir* **2004**, *20* (20), 8931–8938.

(54) Hower, J. C.; He, Y.; Bernards, M. T.; Jiang, S. Understanding the Nonfouling Mechanism of Surfaces through Molecular Simulations of Sugar-Based Self-Assembled

Monolayers. *J. Chem. Phys.* **2006**, *125* (21), 214704.

(55) He, Y.; Chen, S.; Hower, J. C.; Bernards, M. T.; Jiang, S. Molecular Simulation Studies of Nanoscale Friction between Phosphorylcholine Self-Assembled Monolayer Surfaces: Correlation between Surface Hydration and Friction. *J. Chem. Phys.* **2007**, *127* (8), 084708.

(56) Hayashi, T.; Tanaka, Y.; Koide, Y.; Tanaka, M.; Hara, M. Mechanism Underlying Bioinertness of Self-Assembled Monolayers of Oligo(Ethyleneglycol)-Terminated Alkanethiols on Gold: Protein Adsorption, Platelet Adhesion, and Surface Forces. *Phys. Chem. Chem. Phys.* **2012**, *14* (29), 10196–10206.

(57) Konradi, R.; Acikgoz, C.; Textor, M. Polyoxazolines for Nonfouling Surface Coatings — A Direct Comparison to the Gold Standard PEG. *Macromol. Rapid Commun.* **2012**, *33* (19), 1663–1676.

(58) Ishida, T.; Kiwada, H. Accelerated Blood Clearance (ABC) Phenomenon upon Repeated Injection of PEGylated Liposomes. *Int. J. Pharm.* **2008**, *354* (1–2), 56–62.

(59) Zhang, P.; Sun, F.; Liu, S.; Jiang, S. Anti-PEG Antibodies in the Clinic: Current Issues and beyond PEGylation. *J. Control. Release* **2016**, *244*, 184–193.

(60) Herold, D. A.; Keil, K.; Bruns, D. E. Oxidation of Polyethylene Glycols by Alcohol Dehydrogenase. *Biochem. Pharmacol.* **1989**, *38* (1), 73–76.

(61) Mero, A.; Pasut, G.; Via, L. D.; Fijten, M. W. M.; Schubert, U. S.; Hoogenboom, R.; Veronese, F. M. Synthesis and Characterization of Poly(2-Ethyl 2-Oxazoline)-Conjugates with Proteins and Drugs: Suitable Alternatives to PEG-Conjugates? *J. Control. Release* **2008**, *125* (2),

87–95.

(62) Sedlacek, O.; Monnery, B. D.; Filippov, S. K.; Hoogenboom, R.; Hruby, M. Poly(2-Oxazoline)s - Are They More Advantageous for Biomedical Applications Than Other Polymers? *Macromol. Rapid Commun.* **2012**, *33* (19), 1648–1662.

(63) Pidhatika, B.; Rodenstein, M.; Chen, Y.; Rakhmatullina, E.; Mühlebach, A.; Acikgöz, C.; Textor, M.; Konradi, R. Comparative Stability Studies of Poly(2-Methyl-2-Oxazoline) and Poly(Ethylene Glycol) Brush Coatings. *Biointerphases* **2012**, *7* (1–4), 1.

(64) Ulbricht, J.; Jordan, R.; Luxenhofer, R. On the Biodegradability of Polyethylene Glycol, Polypeptoids and Poly(2-Oxazoline)S. *Biomaterials* **2014**, *35* (17), 4848–4861.

(65) Glassner, M.; Vergaelen, M.; Hoogenboom, R. Poly(2-Oxazoline)s: A Comprehensive Overview of Polymer Structures and Their Physical Properties. *Polym. Int.* **2018**, *67* (1), 32–45.

(66) Guillerm, B.; Monge, S.; Lapinte, V.; Robin, J. J. How to Modulate the Chemical Structure of Polyoxazolines by Appropriate Functionalization. *Macromol. Rapid Commun.* **2012**, *33* (19), 1600–1612.

(67) Sedlacek, O.; Janouskova, O.; Verbraeken, B.; Hoogenboom, R. Straightforward Route to Superhydrophilic Poly(2-Oxazoline)s via Acylation of Well-Defined Polyethylenimine. *Biomacromolecules* **2019**, *20* (1), 222–230.

(68) Sedlacek, O.; Bera, D.; Hoogenboom, R. Poly(2-Amino-2-Oxazoline)s: A New Class of Thermoresponsive Polymers. *Polym. Chem.* **2019**, *10* (34), 4683–4689.

(69) Hoogenboom, R.; Thijs, H. M. L.; Jochems, M. J. H. C.; Van Lankvelt, B. M.; Fijten,

M. W. M.; Schubert, U. S. Tuning the LCST of Poly(2-Oxazoline)s by Varying Composition and Molecular Weight: Alternatives to Poly(N-Isopropylacrylamide)? *Chem. Commun.* **2008**, 5758–5760.

(70) Verbraeken, B.; Monnery, B. D.; Lava, K.; Hoogenboom, R. The Chemistry of Poly(2-Oxazoline)S. *Eur. Polym. J.* **2017**, *88*, 451–469.

(71) De La Rosa, V. R. Poly(2-Oxazoline)s as Materials for Biomedical Applications. *J. Mater. Sci. Mater. Med.* **2014**, *25* (5), 1211–1225.

(72) Hoogenboom, R. Poly(2-Oxazoline)s: A Polymer Class with Numerous Potential Applications. *Angew. Chem. Int. Ed.* **2009**, *48* (43), 7978–7994.

(73) Hoogenboom, R.; Schlaad, H. Thermoresponsive Poly(2-Oxazoline)s, Polypeptoids, and Polypeptides Polymer. *Polym. Chem* **2017**, *8*, 24.

(74) Adams, N.; Schubert, U. S. Poly(2-Oxazolines) in Biological and Biomedical Application Contexts. *Adv. Drug Deliv. Rev.* **2007**, *59* (15), 1504–1520.

(75) Kelly, A. M.; Wiesbrock, F. Strategies for the Synthesis of Poly(2-Oxazoline)-Based Hydrogels. *Macromol. Rapid Commun.* **2012**, *33* (19), 1632–1647.

(76) Kempe, K. Chain and Step Growth Polymerizations of Cyclic Imino Ethers: From Poly(2-Oxazoline)s to Poly(Ester Amide)S. *Macromol. Chem. Phys.* **2017**, *218* (11), 1700021.

CHAPTER 2

Effect of Pendant Groups on the Blood Compatibility and Hydration States of POXs

2.1 Introduction

The side chains play a key role in varying the physicochemical properties of POXs.[1] Recently, copolymerization and the introduction of functional groups into side chains have been used to modify the composition of side chains for various applications.[1-5] Despite the prosperity in the chemical modification and application of POXs, there are few reports on the effect of the side chains on the blood compatibility of POXs. Hence, four POX homologs, PMeOx, PEtOx, poly(2-*n*-butyl-2-oxazoline) (PBuOx), and poly(2-phenyl-2-oxazoline) (PPhOx), are chosen as models in this chapter to investigate the effect of pendant groups on their blood compatibility. Based on the IW concept, the effect of pendant groups on the hydration states of the four POXs is also analyzed to establish the relationship between the pendant groups, hydration states, and blood compatibility. The knowledge of the effect can help us understand the blood compatibility mechanism of PMeOx and PEtOx and may effectively guide the development of novel POX derivatives.

The blood compatibility of the four POXs is estimated on their immobilized surfaces. It is worth noting that the characteristics of CROP endow various strategies for the surface immobilization of POXs. Here is a short overview of the POXs immobilization. Generally, surface immobilization or surface construction can be classified into physical immobilization and chemical grafting. Physical immobilization mainly relies on hydrogen bonding, hydrophobic or electrostatic

interactions between polymers and substrates.[6,7] Representative physical immobilization includes drop-casting, dip-coating, spin-coating. These methods are simple, rapid, and inexpensive.[6] However, for water-soluble polymers, like PMeOx and PEtOx, these methods are less suitable than chemical grafting which can provide better stability. Chemical grafting can be divided into "grafting from" and "grafting to." In the former case, appropriate initiator molecules are preliminarily immobilized on the substrate and initiate the polymer chain propagation.[8] In terms of POXs, initiating moieties such as tosylate, triflate, bromine, and iodine have been incorporated on silica surfaces or gold surfaces to initiate the polymerization of POXs.[9] "Grafting to" means the polymer chains bear groups that can react with the substrate or vice versa, and with these groups, the immobilization of the polymer can be achieved. Compared with "grafting from," the "grafting to" of POXs allows for a wider variety of functional groups to anchor to substrates. For instance, silane groups for attaching to silica substrates can be introduced by directly quenching the living oxazolinium species with silane coupling agents such as (3-aminopropyl)triethoxysilane (APTES), (3-aminopropyl)triethoxysilane (APTMS), sodium (3-mercaptopropyl)trimethoxysilane (MPTMS), and (4-aminobutyl)dimethylmethoxy silane (ABDMMS).[9] With the advancement of "click chemistry" in the biomedical field, POXs have been found to be a good platform for applying click reactions, such as Cu-catalyzed Azide Alkyne Cycloaddition (CuAAC), Diels-Alder, and thiol-ene, because the clickable groups, including alkyne, azide, alkene, and thiol, can be easily introduced into the chain-end or side chain.[10,11] Furthermore, Pidhatika et al. prepared a bottle brush-like poly(L-lysine)-graft-P(MeOx) (PLL-g-PMeOx) copolymer through the reaction

between the amine on the PLL side chain and the chain-end glutaric anhydride or ethyl piperidine-4-carboxylate of the PMeOx.[12,13] The copolymer can be spontaneously immobilized on the negatively charged Nb_2O_5-coated silicon wafer, relying on the multiple electrostatic interactions with the polycationic PLL. What's more, there is a photoimmobilization method that does not necessitate the introduction of specific anchoring groups into POXs. Photoreactive moieties are preliminarily incorporated onto the substrates, and polymers are immobilized on the substrates via light-induced reactions with the photoreactive moieties. The benzophenone and perfluorophenyl azide are two typical photoreactive moieties.[14,15] Under UV irradiation, the benzophenone generates radical that attacks the C-H bonds in the backbones or side chains of POXs. While the perfluorophenyl azide forms a singlet perfluorophenyl nitrene and releases N_2, the C-H bonds of POXs react with the nitrene and achieve immobilization.[9] Because of these reaction characteristics, photoimmobilization is versatile for a wide range of polymers, regardless of their water solubility. In this chapter, the four POX analogs are immobilized on the glass substrates using benzophenone.

The hydration states of the POXs were analyzed based on the contents of NFW, IW, and FW obtained from the DSC measurements. Furthermore, to understand the water–polymer interaction at the molecular level, attenuated total reflection infrared spectroscopy (ATR-IR) was used to analyze the ν(O–H) of water and ν(C=O) of POXs.

2.2 Materials and methods

2.2.1 Materials

2-Methyl-2-oxazoline (MeOx), 2-*n*-butyl-2-oxazoline (BuOx), 2-phenyl-2-oxazoline (PhOx), triethoxysilane, and platinum on activated charcoal were purchased from Sigma-Aldrich Co., USA. 2-Ethyl-2-oxazoline (EtOx), methyl *p*-toluenesulfonate (MeOTs), 4-hydroxybenzophenone, and allyl bromide were purchased from Tokyo Chemical Industry Co. Ltd., Japan. Potassium hydroxide and potassium carbonate were purchased from Fujifilm Wako Pure Chemical Co., Japan. Dehydrated acetonitrile, dehydrated *N*, *N*-dimethylacetamide (DMAc), and other solvents for synthesis were purchased from Kanto Chemical Co. Inc., Japan. MeOx, EtOx, BuOx, PhOx, and MeOTs were vacuum distilled over CaH_2 before used. Poly(*n*-butyl acrylate) (PBuA, M_n = 99 kg mol^{-1}, M_w/M_n = 1.5) was synthesized according to a previously reported procedure.[16] Poly(*n*-butyl methacrylate$_{70}$-*co*-2-methacryloyloxyethyl phosphorylcholine$_{30}$) (PMPC, M_n = 250 kg mol^{-1}, M_w/M_n = 2.4) was obtained from the NOF Corporation, Japan. Micro cover glass (ϕ = 14 mm, thickness = 0.13–0.17 mm) was purchased from Matsunami Glass Ind., Ltd., Japan. Silicon wafers (resistivity 0.012–0.015 Ω cm) were purchased from AS ONE Co., Japan. Poly(ethylene terephthalate) film (Diafoil) was obtained from Mitsubishi Plastics, Inc., Japan. Human whole blood for the platelet adhesion test was purchased from Tennessee Blood Services, USA. Anti-fibrinogen γ′ antibody was purchased from Merck Millipore, Germany. Peroxidase-conjugated antimouse IgG Ab was purchased from Bio-Rad Laboratories, USA. Blocking-One was purchased from Nacalai Tesque, Japan. 2,2'-Azinobis(3-ethyl-benzothiazoline-6-sulfonic acid ammonium

salt) (ABTS) substrate was purchased from Roche Diagnostics K. K., Japan. Other commercially available reagents were used as received unless otherwise specified.

2.2.2 Synthesis and characterization of POXs

The polymerization of all the POXs followed the same procedures in a nitrogen-filled glove box. Twenty milliliters of 2-oxazoline monomer solution and 5 mL of MeOTs solution were successively added into a previously flame-dried Schlenk flask. The flask was then removed from the glove box, and the polymerization solution was stirred continuously at an elevated temperature. The reaction was subsequently terminated by methanolic KOH (1 M) at room temperature overnight. In the case of PMeOx and PEtOx, the reaction mixture was precipitated in excess diethyl ether. The precipitate was dissolved in and dialyzed (MWCO = 6–8 kg mol^{-1}) against deionized water for 2 days. The aqueous polymer solution was dried by lyophilization to yield white powders. In the case of PBuOx, after termination, the crude polymer solution was precipitated in an excess amount of water. The precipitate was dissolved in methanol and dialyzed (MWCO = 6–8 kg mol^{-1}) against deionized water for 2 days. The mixture in the dialysis tubing was collected and filtered. The white powder was then dried under reduced pressure at 60 °C for 2 days. In the case of PPhOx, the raw polymer solution was poured into excess diethyl ether to precipitate the product. The precipitate was then dissolved in DMAc and precipitated in diethyl ether. After repeating the dissolution/precipitation process twice more, the precipitate was soaked in deionized water while stirring for 2 days to remove the DMAc and water-soluble impurities. The precipitate was then

collected and dried under reduced pressure at 60 °C for 2 days. The detailed synthesis parameters for each POX are listed in **Table 2.1**.

Table 2.1. Synthesis Parameters of POXs

Polymer	Amount of monomer [g]	Amount of initiator [mg]	M/I [mol/mol][a]	Solvent	Temp [°C]	Reaction time [h]	Conv. [%][b]
PMeOx	6.40	61.5	228	ACN	80	46	96.7
PEtOx	7.44	55.4	252	ACN	80	59	100
PBuOx	12.3	45.0	238	ACN	80	65	99.8
PPhOx	11.0	53.5	261	DMAc	130	46	98.2

[a]The molar ratio of monomer to the initiator; [b]The molar conversion of monomer determined by NMR.

Nuclear magnetic resonance (NMR) spectra were recorded using a 600 MHz NMR spectrometer (Bruker AVANCE III, USA) at room temperature. All the chemical shifts are presented in ppm. The proton chemical shifts were referenced to the TMS (0.00 ppm).

The molecular weight (M_n) and molecular weight distribution (M_w/M_n) of the POXs were measured via gel permeation chromatography (GPC) using an HPLC system (Prominence, Shimadzu, Japan) equipped with four columns (guard, α-m, α-m, and α-3000) (TSKgel, Tosoh, Japan) and a refractive index detector at 40 °C. The eluent was dimethylformamide containing 10 mM LiBr at a flow rate of 1.0 mL min^{-1}. M_n and M_w/M_n were calculated against narrow dispersity poly(methyl methacrylate) standards. The analytes of the POX solutions were filtered through 0.2 μm polytetrafluoroethylene filters before injection.

2.2.3 Surface immobilization of POXs

The POXs were immobilized on the glass substrates using the photo-immobilized method.[14] The glass substrates were cleaned according to a previously reported method.[17] The cover glasses were immersed in SC1 solution (NH_4OH:H_2O_2:H_2O = 1:1:5 in v/v) at 70 °C for 30 min and then rinsed with water and methanol successively. The glasses were dried under a N_2 stream and immersed in a 4-(3-triethoxysilyl)propoxybenzophenone/toluene solution (10 mg mL^{-1}) at 70 °C for 1 h. The surface coupling reagent 4-(3-triethoxysilyl)propoxybenzophenone was prepared according to the method used in a previous study.[18] After removing the solution, the glasses were warmed at 90 °C for another 30 min, cooled to room temperature, rinsed with toluene and methanol, and dried under a stream of N_2.

Following the above pretreatment, 40 μL of the POX solution (10 mg mL^{-1}) was spin-coated onto the substrate using a spin coater (MS-A100, Mikasa, Japan) with a protocol of 500 rpm for 1 s, 0 rpm for 5 s, ramp up for 2 s, 3000 rpm for 30 s, and ramp down for 2 s. PMeOx, PEtOx, and PBuOx were dissolved in methanol, and PPhOx was dissolved in chloroform. After drying the substrate under reduced pressure at room temperature overnight, it was illuminated by a UV lamp at λ = 254 nm (6 W, illumination distance of 26 mm) for 30 min. The PMeOx, PEtOx, and PBuOx grafted substrates were obtained after washing them with methanol, and the PPhOx grafted substrates were washed with chloroform. To obtain the POX grafted silicon substrate, the same grafting procedure was conducted on a 1 cm × 1 cm cut silicon plate. The procedures to prepare the POXs modified substrates are illustrated in **Figure 2.1**. Besides, for the human platelet

adhesion test and denaturation degree evaluation of adsorbed fibrinogen, the PBuA and PMPC coated PET substrates were set as positive and negative controls, respectively. The PET film was cut into a disk with a diameter of 14 mm by a GCC C180II laser engraving machine. Then the bare PET substrates were cleaned by toluene and dried in a vacuum oven at rt overnight. Forty microliters of PBuA solution (10 mg mL^{-1}, dissolved in THF) and PMPC solutions (10 mg mL^{-1}, dissolved in methanol) were spin-coated onto the PET substrates with the same spin-coating protocol as POXs, respectively.

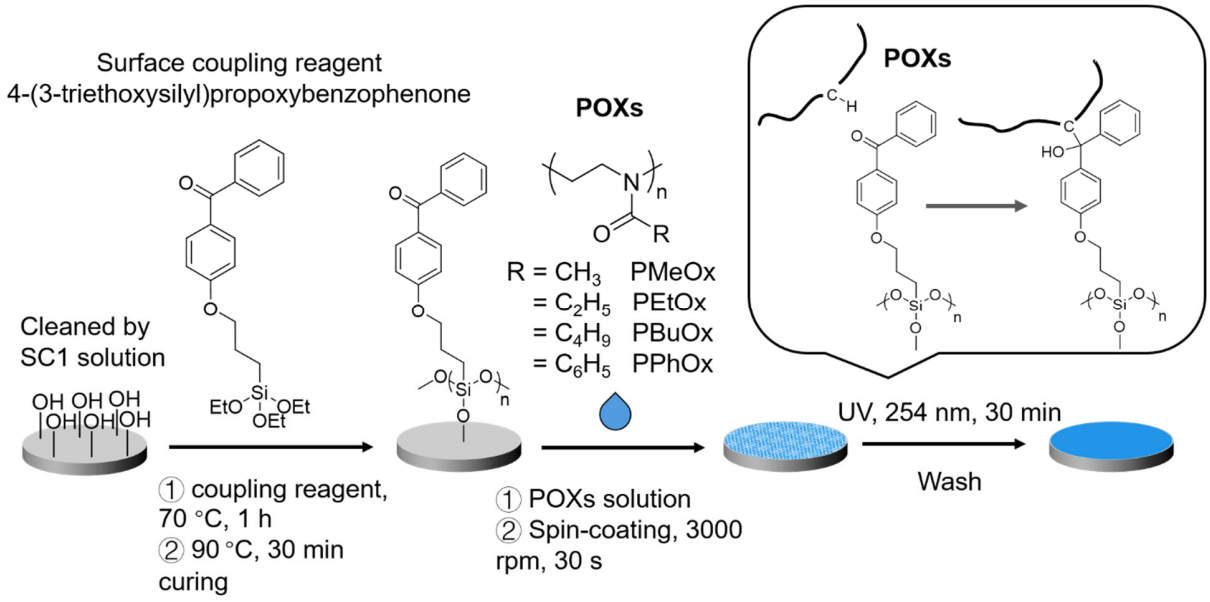

Figure 2.1. The procedures to prepare the POXs modified substrates.

2.2.4 Surface characterization

The chemical composition of the POX grafted glasses was characterized by X-ray photoelectron spectroscopy (XPS) (APEX ESCA, ULVAC-PHI, Japan) at 2.0×10^{-7} Pa using a monochromatic Al-Kα X-ray source at 150 W with an incident angle of 15°. The thicknesses of

the dry POX layers were measured using an ellipsometer (AutoSE, Horiba, Japan) on the POX grafted silicon substrates. Except for the ellipsometry measurement, the other experiments on the POX surfaces were conducted on the POX grafted glasses. The static water contact angle of the sessile water droplet (2.0 μL) on the POX surfaces was measured using a contact angle goniometer (DropMaster DMo-501SA, Kyowa, Japan).

2.2.5 Human platelet adhesion test

The human platelet adhesion test was conducted according to a reported procedure.[19] 480 μL of plasma solution in which the platelet concentration was adjusted to a seeding density of 4×10^7 cells cm^{-2} was placed on each polymer substrate. The substrates were incubated at 37 °C for 1 h and then rinsed with phosphate-buffered saline (PBS) (−). The platelets adhered to the substrates were fixed by immersion in 1% (v/v) glutaraldehyde in PBS (−) at 37 °C for 2 h. The substrates were rinsed with PBS (−) and Milli-Q water and dried at room temperature. The number of adhered platelets was counted on scanning electron micrographs obtained by scanning electron microscopy (VE-9800, Keyence, Japan). The procedures are illustrated in **Figure 2.2**.

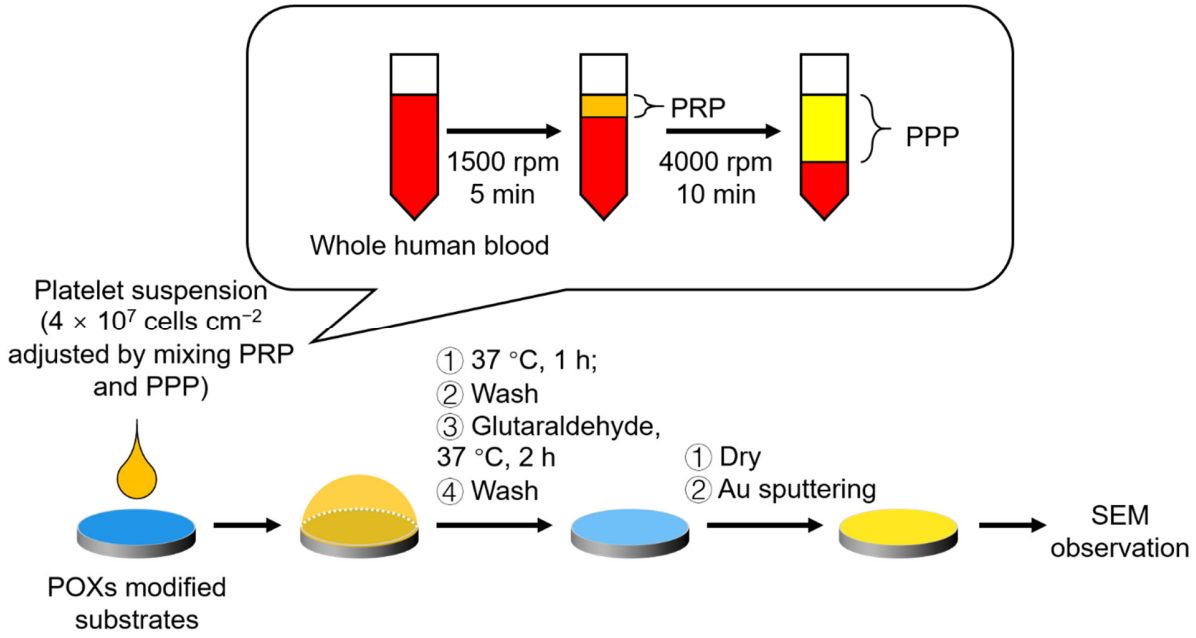

Figure 2.2. Procedures of platelet adhesion test.

2.2.6 Denaturation degree evaluation of fibrinogen

The conformational alteration of fibrinogen adsorbed on the POX surface was evaluated via an enzyme-linked immunosorbent assay (ELISA). All the procedures were conducted at 37 °C unless otherwise specified. The substrates were covered with PBS (−) and incubated for 1 h. After removing the PBS (−), 200 μL of platelet-poor plasma (PPP)[20] was placed onto each substrate and incubated for 1 h. The PPP solution was then outwelled, and the substrate was rinsed with PBS (−). After draining the PBS (−), each substrate was covered with 200 μL of Blocking One solution [20% v/v in PBS (−)] for 1 h. The substrate was then incubated with 150 μL of 1% v/v anti-fibrinogen γ′ antibody solution/diluted Bocking One solution [2% v/v in PBS (−)] for 2 h, 150 μL of 0.2‰ v/v peroxidase-conjugated antimouse IgG antibody/diluted Blocking One solution [2% v/v in PBS (−)]

for 1.5 h, and 200 μL of 1 mg mL^{-1} ABTS solution for 30 min at room temperature successively. Before the addition of a new reagent, the substrate was rinsed with PBS (−) and drained well. The solution on the surface colored by ABTS was pipetted well, and 100 μL of the solution was then transferred to a 96-well plate. The absorbance of the solution was measured at a wavelength of 405 nm using a microtiter plate reader (Infinite M Plex, Tecan, Switzerland). The general procedures of ELISA are illustrated in **Figure 2.3**.

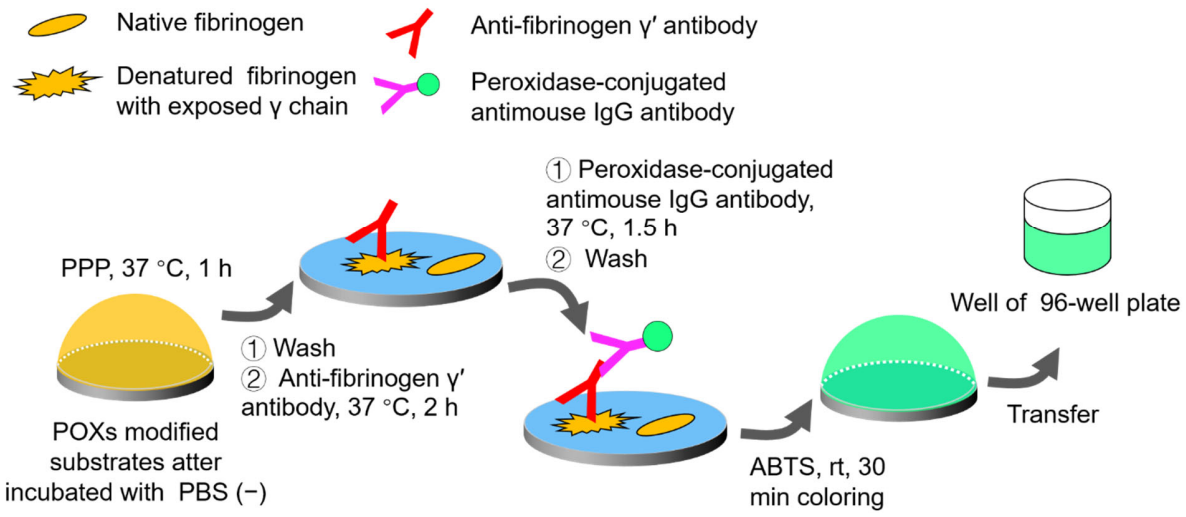

Figure 2.3. General procedures of ELISA.

2.2.7 Quantification of hydrated water by DSC

The quantification of hydrated water in the POX/water systems was performed using a differential scanning calorimeter (X-DSC7000, Seiko, Japan). PMeOx and PEtOx were dissolved in pure water at ca. 10% w/v and filtered through 0.2 μm cellulose acetate filters. Polymer solutions were placed in aluminum pans and left at room temperature for minutes to hours until a

predetermined mass of water was evaporated. The weights of the POX/water samples were controlled to 3–5 mg. The sample pans were sealed using an auto sealer. For PBuOx and PPhOx, fully hydrated polymer samples were prepared by immersion in pure water for more than 2 weeks. After removing the water and wiping the excess moisture from the surface, the samples were left at room temperature for different times. Then, 3–5 mg of each sample was placed in aluminum pans and sealed using an auto sealer. Before conducting the DSC measurements, the sealed POX samples were left overnight at room temperature to ensure homogeneity.

The hydrated samples were cooled to −100 °C at a rate of 5.0 °C min^{-1}, held at −100 °C for 5 min, and then heated to 50 °C at the same rate under a nitrogen purge flow. After the measurements, the pans were pierced and dried under reduced pressure at 110 °C to obtain the weights of the dry polymers.

In this work, IW was defined as the hydrated water that shows crystal formation around −40 °C during the heating scan (cold crystallization) and/or during the cooling scan (crystallization). The crystallized IW was melted below 0 ℃. FW was defined as water that shows a melting point at 0 ℃ in the heating scan like bulk water. It is noteworthy that at a higher water content, it becomes difficult to determine the amount of IW, as the cold crystallization peak does not clearly appear as well as some of the IW crystallizes at the cooling scan with FW. In this case, we referred to the melting peak at 0 ℃ was caused by the sum of IW and FW. Then, NFW was calculated as follows: (the total amount of water) – (the amount of IW + FW).

Thus, the weight contents of the total water, IW, FW, and NFW in the hydrated polymers were

calculated using the following equations:

$$W_{total} = (W_1 - W_0)/W_0$$

$$W_{IW} = \Delta H_c/\Delta H^o_{fus}/W_0$$

$$W_{FW} = \Delta H_m/\Delta H^o_{fus}/W_0 - W_{IW}$$

$$W_{NFW} = W_{total} - W_{IW} - W_{FW}$$

The molar contents of total water, IW, FW, and NFW in the polymers/water systems were calculated as the molar ratios of water molecules to repeating units of polymers in this work by the following equations:

$$N_{total} = [(W_1 - W_0)/M_{water}]/[W_0/M_{mono}]$$

$$N_{IW} = [(\Delta H_c/\Delta H^o_{fus})/M_{water}]/[W_0/M_{mono}]$$

$$N_{FW} = [(\Delta H_m/\Delta H^o_{fus})/M_{water}]/[W_0/M_{mono}] - N_{IW}$$

$$N_{NFW} = N_{total} - N_{IW} - N_{FW}$$

where W_0 and W_1 are the weights (g) of the dried and hydrated samples, respectively. W_{total}, W_{IW}, W_{FW}, and W_{NFW} are the weight contents (g/g) of the total water, IW, FW, and NFW, respectively; N_{total}, N_{NFW}, $N_{IW,}$ and N_{FW} are the molar contents (mol/mol) of total water, NFW, IW, and FW, respectively. ΔH_c is the sum of enthalpy change (J g^{-1}**)** of cold crystallization in the heating scan and crystallization in the cooling scan; ΔH_m is the enthalpy change (J g^{-1}) of ice melting; ΔH^o_{fus} is the heat of fusion of water, and its value is assumed to be equal to the heat of fusion of pure water (334 J g^{-1});[21,22] M_{water} and M_{mono} are the molar masses (g mol^{-1}) of H_2O or D_2O and oxazoline monomers, respectively.

2.2.8 Evaluation of hydrated POXs by ATR-IR

The infrared (IR) spectra of hydrated POXs comprising different water contents were measured using an IR spectrometer (FT/IR-6600, Jasco, Japan) equipped with an ATR accessory and a diamond element. For water-soluble PMeOx and PEtOx, the POX/water mixture with a predetermined water content was put or dropped on the diamond. For water-insoluble PBuOx and PPhOx, they were immersed in water for more than 2 weeks to be fully hydrated. Then the POX was taken out from water, wiped the surficial water, and left at room temperature for different periods. After measurement, the POX was timely recollected in an aluminum pan. The calculation of the water content was the same as the DSC measurement. The spectra were measured at a resolution of 4 cm^{-1}, and the 32 scans thus obtained were averaged. The baseline adjustment, normalization, and second-order differential were processed using the analysis software matched with the spectrometer.

2.3 Results and discussion

2.3.1 Synthesis and surface immobilization of POXs

The POXs were prepared via CROP. The NMR spectra of four POXs (**Figure 2.4**), as well as the chemical shift of each signal in the spectra, are shown below.

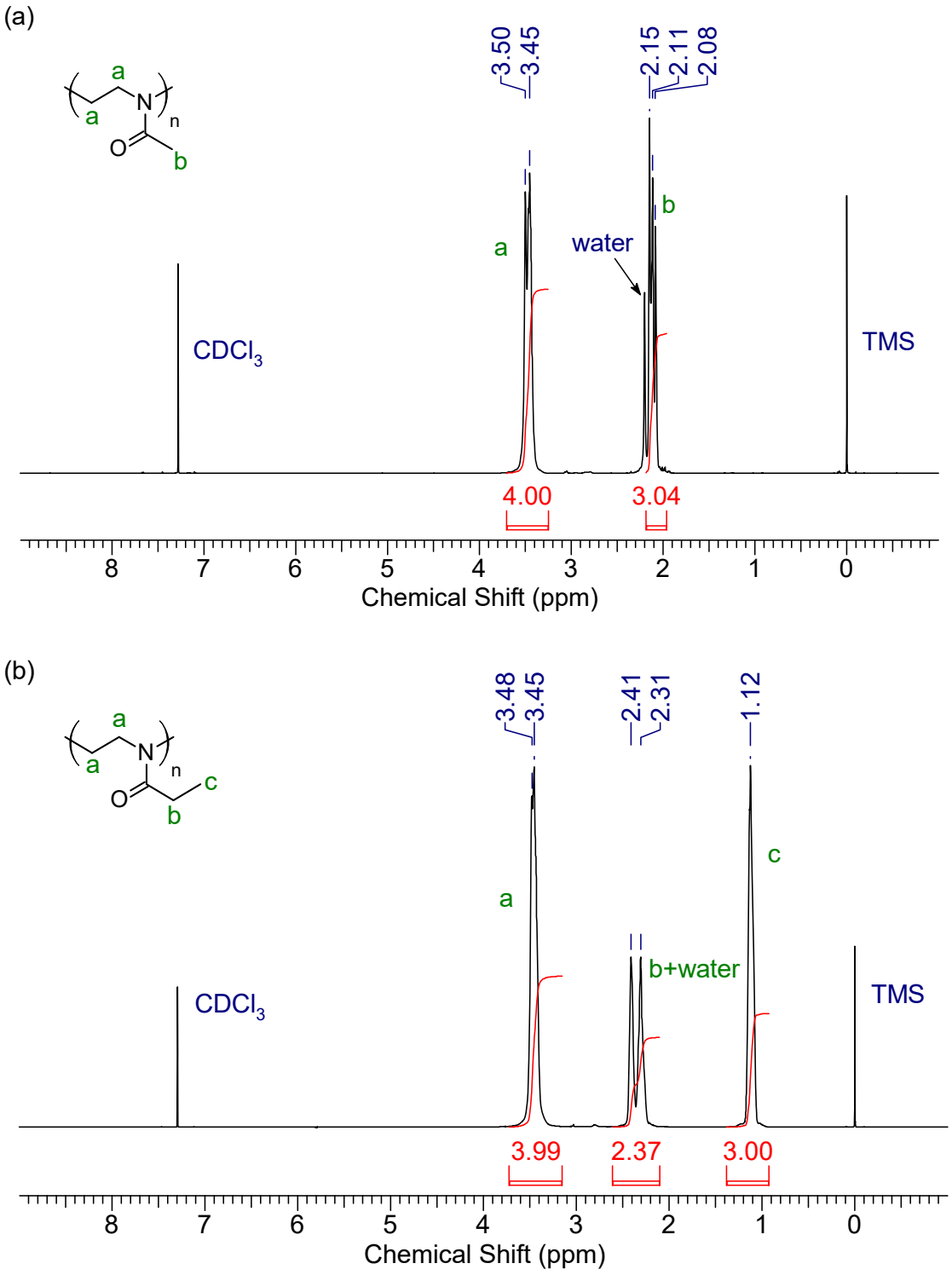
(a)
3.50
3.45
2.15
2.11
2.08
a
b
water
CDCl3
TMS
4.00
3.04
8
7
6
5
4
3
2
1
0
Chemical Shift (ppm)
(b)
3.48
3.45
2.41
2.31
1.12
a
c
b+water
CDCl3
TMS
3.99
2.37
3.00
8
7
6
5
4
3
2
1
0
Chemical Shift (ppm)

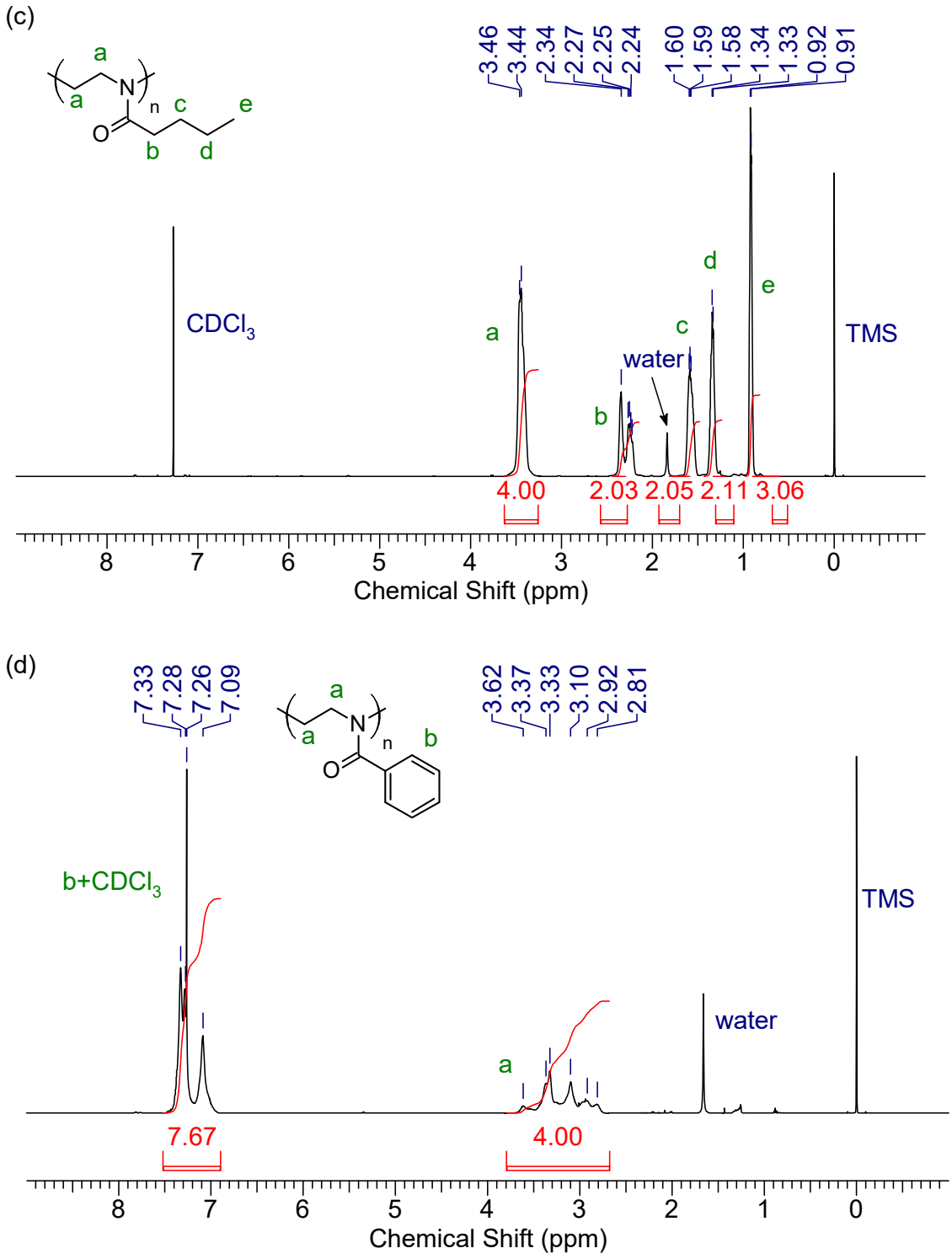

Figure 2.4. ^{1}H spectra (600 MHz, in $CDCl_3$) of (a) PMeOx, (b) PEtOx, (c) PBuOx and (d)

PPhOx.

PMeOx, ^{1}H NMR (600 MHz, $CDCl_3$) δppm: 2.08–2.15 (m, 3H, -C*H*$_3$), 3.45–3.50 (m, 4H, -C*H*$_2$C*H*$_2$N-).

PEtOx, ^{1}H NMR (600 MHz, $CDCl_3$) δppm: 1.12 (s, 3H, -CH$_2$C*H*$_3$), 2.31–2.41 (m, 2H, -C*H*$_2$CH$_3$), 3.45–3.48 (m, 4H, -C*H*$_2$C*H*$_2$N-).

PBuOx, ^{1}H NMR (600 MHz, $CDCl_3$) δppm: 0.91–0.92 (m, 3H, -(CH$_2$)$_3$C*H*$_3$), 1.33–1.34 (m, 2H, -(CH$_2$)$_2$C*H*$_2$CH$_3$), 1.58–1.60 (m, 2H, -CH$_2$C*H*$_2$CH$_2$CH$_3$), 2.24–2.34 (m, 2H, -C*H*$_2$(CH$_2$)$_2$CH$_3$), 3.44–3.46 (m, 4H, -C*H*$_2$C*H*$_2$N-).

PPhOx, ^{1}H NMR (600 MHz, $CDCl_3$) δppm: 2.81–3.62 (m, 4H, -C*H*$_2$C*H*$_2$N-), 7.09–7.32 (m, 5H, -C$_6$*H*$_5$).

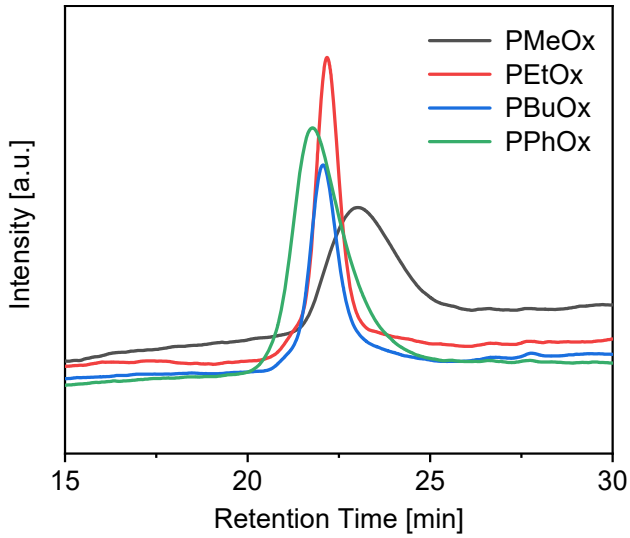

Figure 2.5. GPC traces of POXs using DMF containing 10 mM LiBr as eluent.

For each POX, the ratio of the monomer to initiator was controlled to ca. 250 (mol/mol) (**Table 2.1**) to obtain a similar degree of polymerization (DP). Although the long reaction time allowed almost complete monomer conversion for all the POXs, the experimental DP of PMeOx and PPhOx was much smaller than those of the other two polymers (**Table 2.2**). This was likely caused by the chain transfer reaction, which is verified by the higher M_w/M_n value (**Table 2.2**) and broader peaks in the GPC traces (**Figure 2.5**). It has been reported that the higher chain transfer rate of MeOx might be due to the lower steric hindrance of its 2-methyl-2-oxazolinium α-proton.[23] According to the chain transfer mechanism of CROP (shown in **Figure 2.6**) proposed by Litt et al.,[24] the 2-oxazoline monomer, which acts as a base rather than a nucleophile, initiates the chain transfer by abstracting a proton from the α-position of the oxazolinium side chain. This hydrogen abstraction generates an enamine end-functionalized polymer chain and a protonated monomer. The protonated monomer can continue the chain propagation. Owing to the weak nucleophilicity, the enamine end-functionalized chains can further attack another living propagating chain, especially at higher monomer conversion, and thus lead to branching.[25] Compared to the oxazolinium of EtOx and BuOx, the α-position in the 2-methyl-2-oxazolinium exhibits lower steric hindrance. The hydrogen abstraction of MeOx may occur faster because of its higher accessibility to the α-position, resulting in a higher chain transfer degree.[23] For PPhOx, a higher reaction temperature can increase the chain transfer rate, although 130 °C was reported as an optimal polymerization temperature when using MeOTs as an initiator.[26]

After obtaining the POXs, they were photo-immobilized on the glass or silica substrates. The

surface parameters of the POX grafted substrates are listed in **Table 2.2**. The PMeOx and PEtOx grafted surfaces exhibited higher hydrophilicity as compared with their counterparts, but the thickness of PMeOx and PEtOx layers was thinner than the others. Especially the homogeneousness of the PMeOx layers is suspectable which can be inferred from the largest deviation of the thickness. In the side chains of PMeOx and PPhOx, the aliphatic C–H bonds are less than those in PEtOx and PBuOx, which would lower their immobilization availability or grafting density. Moreover, the significant surface free energy difference between the benzophenone modified surface and hydrophilic PMeOx and PEtOx makes it difficult for the two polymers to wet the surface as easily as the other hydrophobic POXs. Furthermore, the PMeOx had the smallest M_n, and thus, its smallest bulk radius of gyration restricted the polymer coils from contacting the benzophenone sites.[14] Given all this, the PMeOx formed the thinnest and uneven layers on the substrates. The immobilization of the POXs was further verified by elemental composition analysis using XPS (XPS spectra in **Figure 2.7**). After the POXs grafting, the C and N contents increased, and the Si and O contents decreased. In summary, the POXs grafted substrates were successfully prepared, although the PMeOx layers were not homogeneous. The platelet adhesion test and ELISA were conducted on these

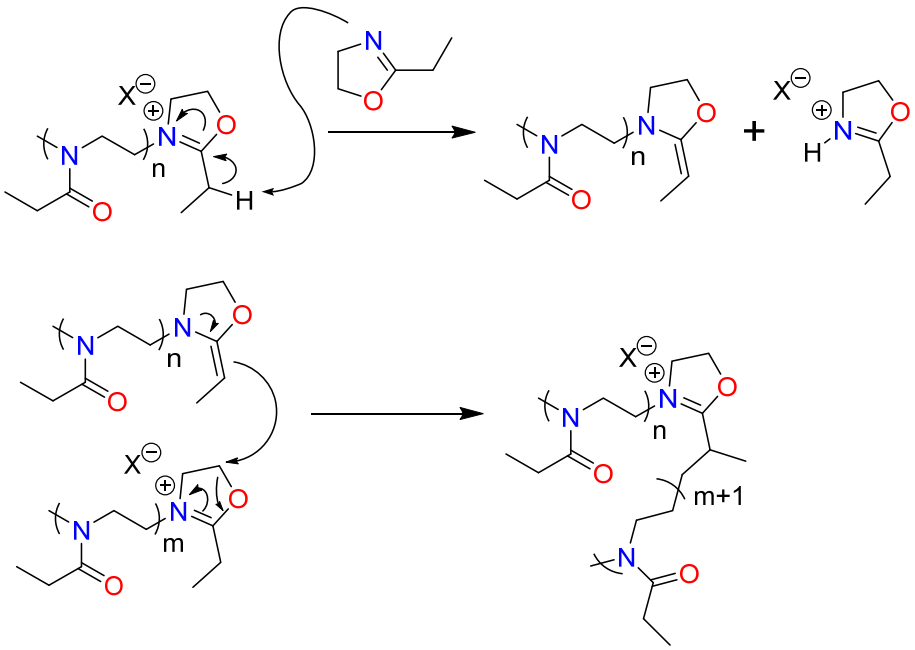

Figure 2.6. Chain transfer mechanism of CROP of POXs proposed by Litt et al.[25] PEtOx is schematic as a model of POXs.

Table 2.2. Surface Parameters of POX Layers

	M_n [kg mol^{-1}][b]	M_w/M_n[b]	DP	Water contact angle [deg][c]	Thickness [nm][d]	Element composition [atom %][e]			
						Si	O	C	N
Glass[a)]	-	-	-	-	-	11.5	82.8	5.2	-
Benzoph-enone	-	-	-	82.0 ± 3.0	-	19.6	58.8	21.5	-
PMeOx	10.8	1.56	127	25.7 ± 4.5	3.00 ± 1.3	6.1	30.8	50.5	12.0
PEtOx	24.8	1.30	250	39.5 ± 2.9	3.96 ± 0.46	4.9	30.2	49.9	15.0
PBuOx	26.5	1.28	208	87.2 ± 1.4	9.79 ± 0.86	2.2	12.5	75.2	10.1
PPhOx	26.2	1.53	178	71.8 ± 2.3	4.24 ± 0.69	11.4	39.6	43.1	6.0

[a]The glass was washed with SC1 solution. [b]Determined by GPC. [c]The data were measured at 30 s after the water droplet contacted with the surface and represents the mean ± standard deviation (SD) (n = 9, 3 substrates × 3 points). [d)]The data represent the mean ± SD (n = 9, 3 substrates × 3 points). [e)]Determined using XPS.

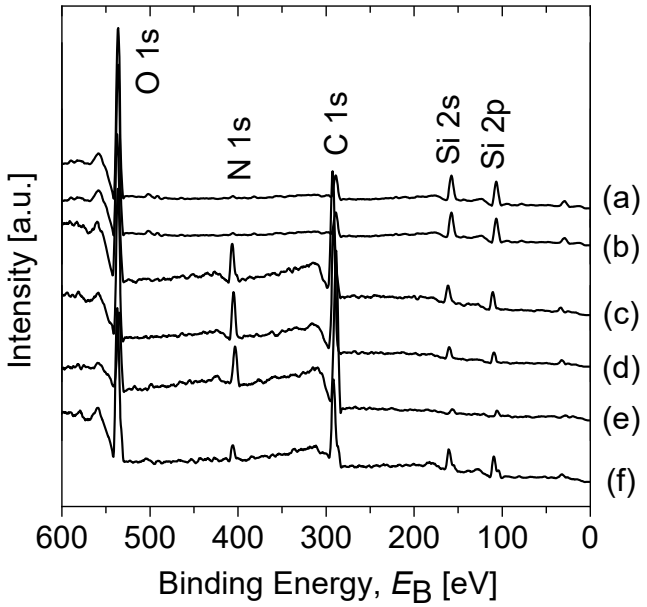

Figure 2.7. XPS spectra of (a) bare glass, (b) benzophenone modified glass, (c) PMeOx grafted glass, (d) PEtOx grafted glass, (e) PBuOx grafted glass and (f) PPhOx grafted glass.

2.3.2 Blood compatibility of POX grafted surface

The results of the in vitro platelet adhesion on the POX grafted glasses are presented in **Figure 2.8a**. The platelet adhesion on the surface is strongly related to the adsorption of plasma proteins, especially the conformational alteration of the adsorbed fibrinogen.[27] Herein, the degree of

denaturation of the adsorbed fibrinogen was evaluated based on the exposure degree of the gamma chain (**Figure 2.8b**). The as-expected results of the platelet adhesion test and ELISA on the PBuA and PMPC coated surfaces verified the reliability of the experiments.[28] The PEtOx grafted surfaces significantly inhibited the platelet adhesion as compared with PBuOx and PPhOx grafted surfaces, and a similar situation was observed in the exposure degree of the fibrinogen γ' chains. This indicates that on these surfaces the conformational alteration of the adsorbed fibrinogen dominated the platelet adhesion. Unexpectedly, the well-known antifouling PMeOx did not inhibit platelet adhesion in this work.[29] This can be attributed to the thin and uneven layers of PMeOx, as mentioned previously. Moreover, the exposure degree of the fibrinogen γ' chains on PMeOx was comparatively low. This may suggest that there existed a more complex platelet adhesion mechanism on the PMeOx grafted surface, and the glass as well.[27,30,31] However, it can be ascertained that the blood compatibility of hydrophobic PBuOx and PPhOx was worse than that of the hydrophilic PEtOx. The hydration states of the POXs were analyzed via DSC and ATR-IR to establish their relationship with blood compatibility.

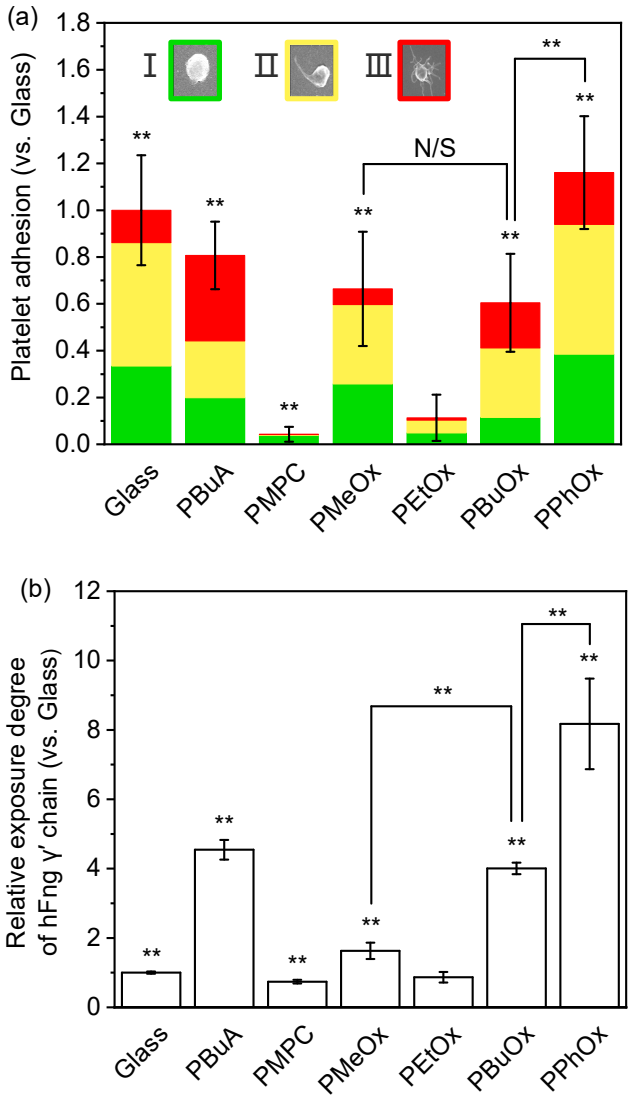

Figure 2.8. (a) Number of platelets adhered onto POX grafted glasses. The number was normalized relative to that on the glasses. The data represent the mean ± SD (n = 9, 3 donors × 3 substrates). The green, yellow, and red bars in each column indicate the percentages of resting (I), moderately activated (II), and advanced activated platelets (III), respectively. A representative illustration of each activation state of the platelet is listed at the top of the columns and indicated by the same color corresponding to that in the column. (b) Exposure degree of the γ′ chains in

fibrinogen that adsorbed on POX grafted glasses obtained via ELISA. The exposure degree was relative to that on the glasses. The data represent the mean ± SD (n = 5). In all the figures, **: P < 0.01 versus PEtOx grafted glass.

2.3.3 Hydration states of POXs evaluated using DSC

The DSC thermograms of each POX comprising different water contents are presented in **Figure 2.9–2.12**. In the thermograms of PMeOx and PEtOx, when the water contents were low, no peaks were observed. It can be inferred that adsorbed water initially occupied the polar sites, and the interaction was sufficiently strong to prevent the water molecules from forming clusters for crystallization. As the water content increased, the exothermic peak started to appear in the heating scans and gradually shifted into the cooling scans. While in the thermograms of PBuOx and PPhOx, the positions of the small IW peaks barely shifted after they appeared. The peak shifting in PMeOx and PEtOx with water content variation has also been reported in the DSC measurements of PEG and xanthan water systems.[32,33] The peak at the different positions was likely due to the transformation of the dominant water structure. It has been reported that polymer hydration is a multistep process.[34] In the study of the hydration process of poly[2-(2-methoxyethoxy)ethyl methacrylate] (PMEO$_2$MA) hydrogel by ATR-FTIR, Piechocki et al.[35] found that with water content increasing, the initial “polymer-water-polymer” and “polymer-water” interactions (hydrogen bonds) were gradually replaced by the “polymer-water-water” interaction and finally the “water-water” hydrogen bonds dominated in the system. An interesting trend in the

DSC thermogram was that the exothermic peak's onset temperature gradually approached and finally merged with the crystallization peak of bulk water, which may reflect the similar evolution of the water interaction as in the $PMEO_2MA$ hydrogel. This trend meanwhile brought difficulty to the quantitative analysis of the IW since the deconvolution of the DSC thermogram is not theoretically available herein.[36] Because the FW characteristically resembled the bulk water, the crystallization of the FW during DSC measurement was regarded as approximately equal to bulk water. Hence, we measured the DSC of a series of pure water samples, and the mass of the sample was set close to the FW mass in the polymer/water system. To exclude the effect of the heating/cooling rate on the crystallization shape, the measurements were conducted under the same conditions as the polymer/water samples. The endpoint of the crystallization peak of water showed a low deviation (1 °C) and averaged at −32.3 °C. We decided that when the onset temperature of the exothermic peak was lower than −32.3 °C, the peak was regarded as mainly contributed by IW. When the onset temperature of the exothermic peak was over −32.3 °C, the FW mainly increased. The maximum contents of IW before their peaks merged with FW on the DSC thermograms of PMeOx and PEtOx were calculated, as well as the corresponding NFW, FW. In **Figure 2.13**, the contents of IW and FW presented are the contents before they merged.

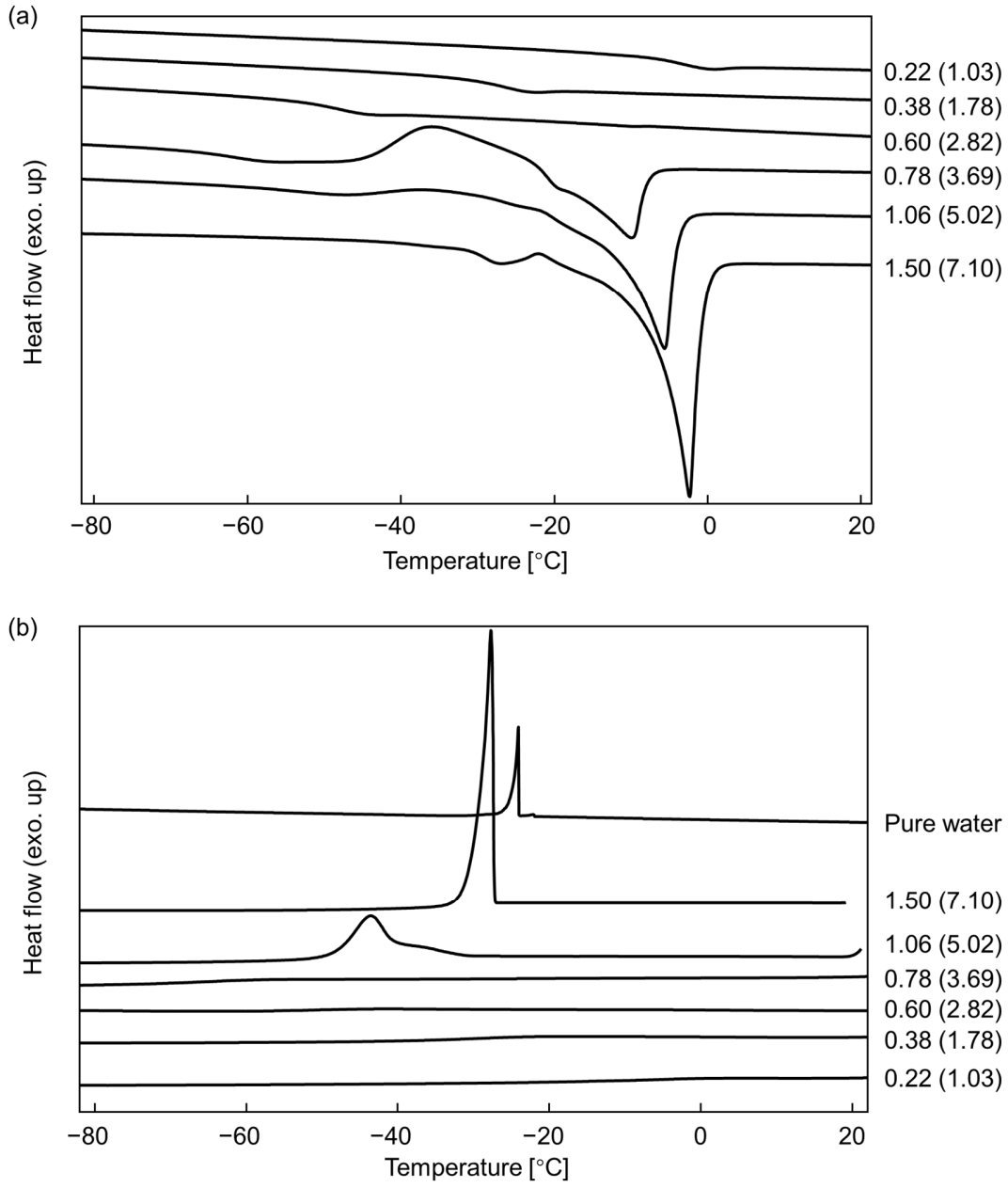

Figure 2.9. DSC thermograms of PMeOx/water system: (a) heating scan and (b) cooling scan. The values marked on the right side of each curve represent the total water contents, and the values outside and in the bracket represent the weight content (g/g) and corresponding molar content (mol/mol), respectively.

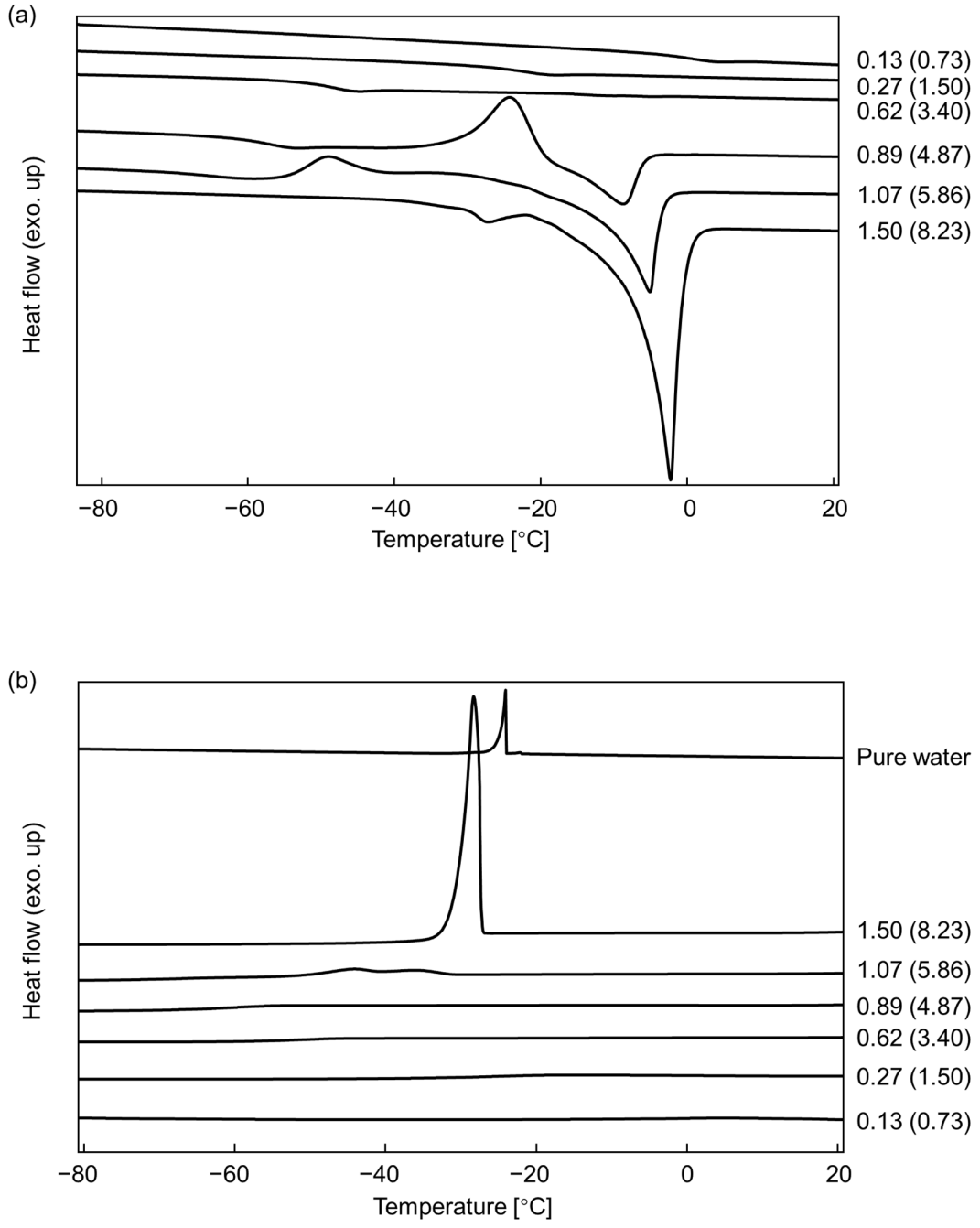

Figure 2.10. DSC thermograms of PEtOx/water system: (a) heating scan and (b) cooling scan.

The values marked on the right side of each curve represent the total water contents, and the values

outside and in the bracket represent the weight content (g/g) and corresponding molar content (mol/mol), respectively.

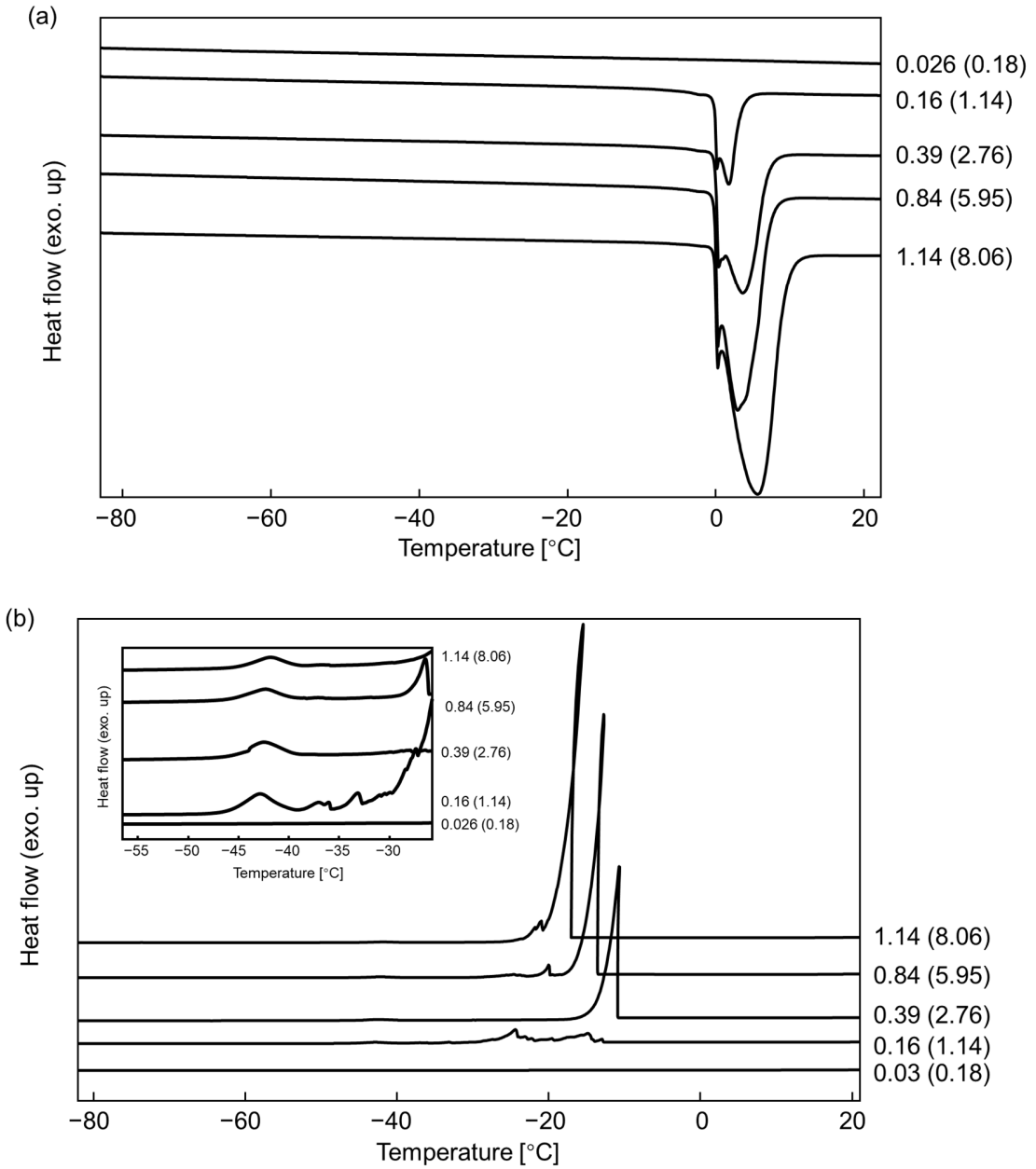

Figure 2.11. DSC thermograms of PBuOx/water system: (a) heating scan and (b) cooling scan. The values marked on the right side of each curve represent the total water contents, and the values

outside and in the bracket represent the weight content (g/g) and corresponding molar content (mol/mol), respectively. The inset in (b) is the enlargement of the peaks at the temperature of −30–−55 °C.

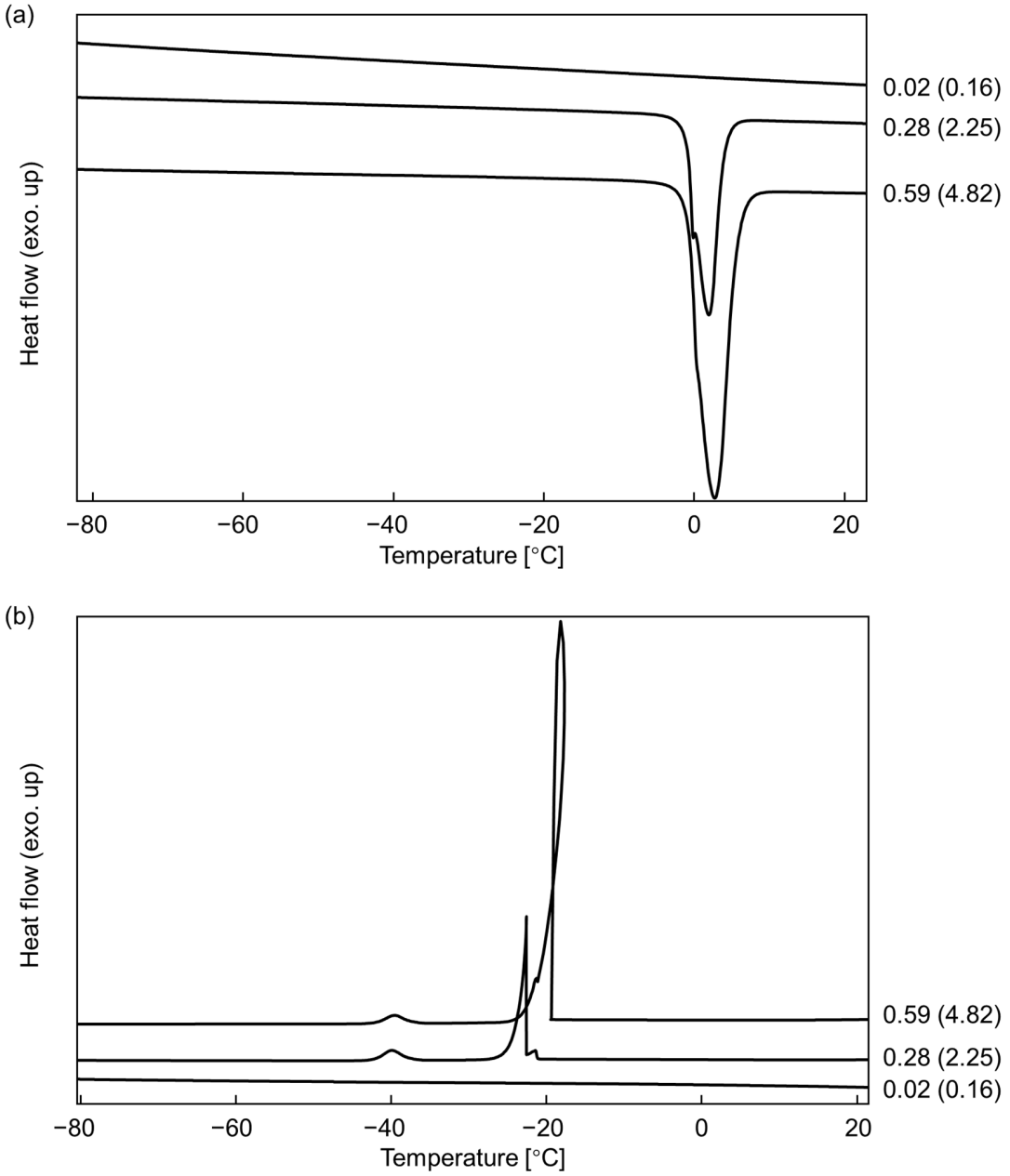

Figure 2.12. DSC thermograms of PPhOx/water system: (a) heating scan and (b) cooling scan.

The values marked on the right side of each curve represent the total water contents, and the values outside and in the bracket represent the weight content (g/g) and corresponding molar content (mol/mol), respectively.

It can be observed that, for PMeOx and PEtOx, the variation trend of their hydration water contents along with the total water contents is almost identical, except that the maximum IW content (2.1 mol/mol) in PEtOx is greater than that (1.28 mol/mol) in PMeOx. Theoretically, one C=O group in a tertiary amide can interact with 0.5–2 water molecules on average directly via hydrogen bonds (the hydrogen bonding forms are illustrated in **Figure 2.14**). The protonation of N is not considered here. According to the computation of Szostak et al.,[37] in a non-planarity amide which can be achieved from steric repulsion around the nitrogen atom, the sum of twist angles and nitrogen pyramidalizaton value of the barrier between N- *vs*. O-protonation of an amide appears approximately 50-60°. While it is much lower than that of distortion of a fully perpendicular amide bond (150.0°), which has been proposed to be necessary for efficient N-protonation. Before the appearance of IW, the average number of interacting water molecules per repeating unit of PMeOx and PEtOx was more than 2 (**Figure 2.13a** and **2.13b**). This suggests that the carbonyl groups can be completely hydrated by the NFW. Moreover, it can be inferred that some water molecules indirectly interacted with the carbonyl through “water bridges” that comprised water molecules that had interacted directly with the carbonyl. With the increase in the IW content, the NFW content tends to become constant. More water molecules are expected to be directly or indirectly linked to

water bridges. It can be predicted that the restriction of the carbonyl over the outer water layers becomes weaker. The dominant molecular interactions in the PMeOx and PEtOx aqueous systems may gradually change from an initial polymer–water interaction toward a water-water interaction, as indicated by the IW peaks merging into the FW peaks in the DSC thermograms. In **Figure 2.13c** and **2.13d**, the variation trends of the water content in the PBuOx and PPhOx water systems differ from those in the hydrophilic POX systems. The NFW and IW contents remained constant at approximately 0, which indicates that a very small amount of water interacted with the PBuOx and PPhOx. The water primarily existing in the systems comprised bulk water but not FW. Therefore, the bulky side chains might effectively prevent water from interacting with C=O.

According to the quantitative analysis of water, we inferred how the water interacted differently with the polymer in each POX system. However, to observe the difference directly, we used ATR-IR to evaluate the water structure through *ν*(O–H) and the hydration of carbonyl via *ν*(C=O).

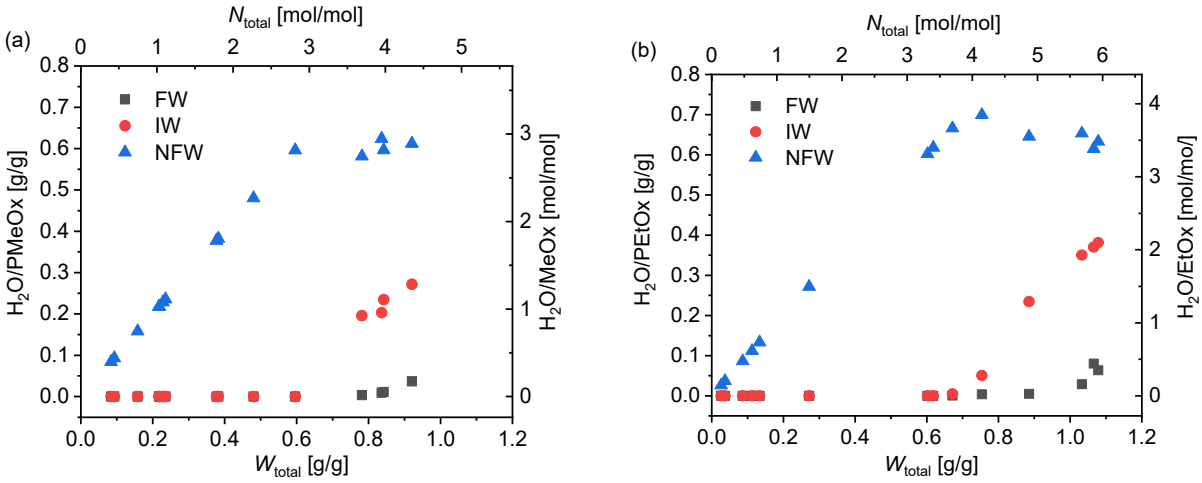

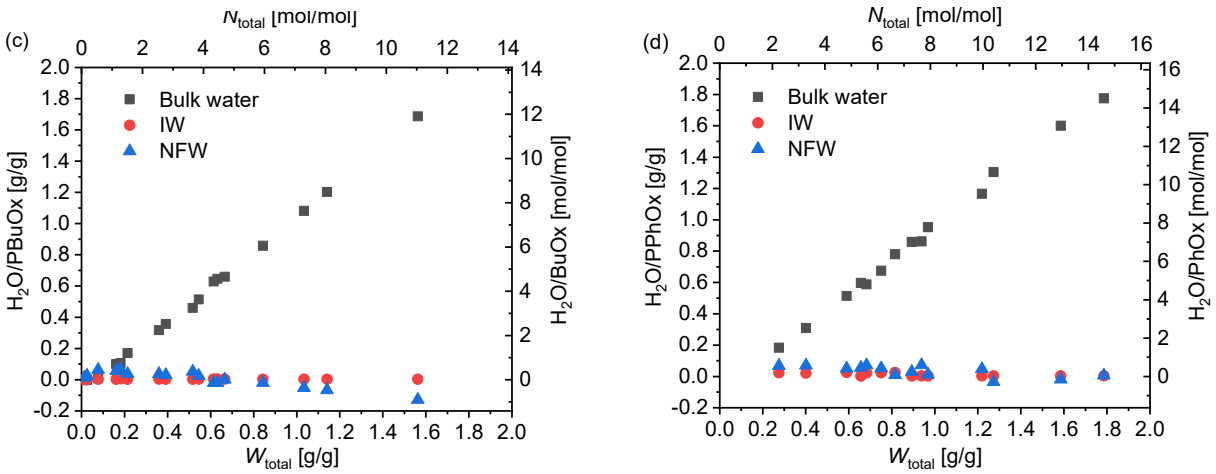

Figure 2.13. Weight contents (g/g) and molar contents (mol/mol) of total water, FW (or bulk water), IW, and NFW in (a) PMeOx and (b) PEtOx aqueous systems and (c) PBuOx and (d) PPhOx water systems.

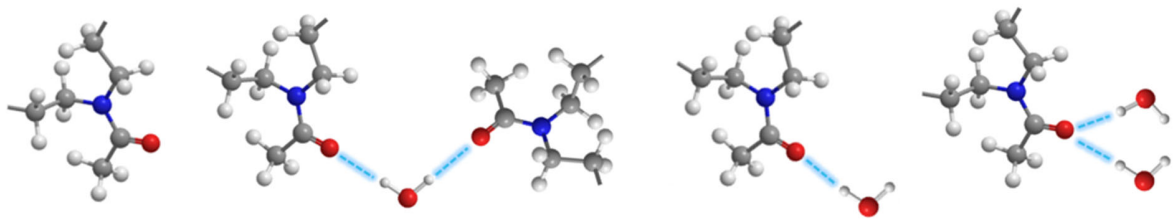

Figure 2.14. Possible direct hydrogen bonding forms between water and POXs (taking PMeOx as an example).

2.3.4 Hydration states of POXs evaluated using ATR-IR

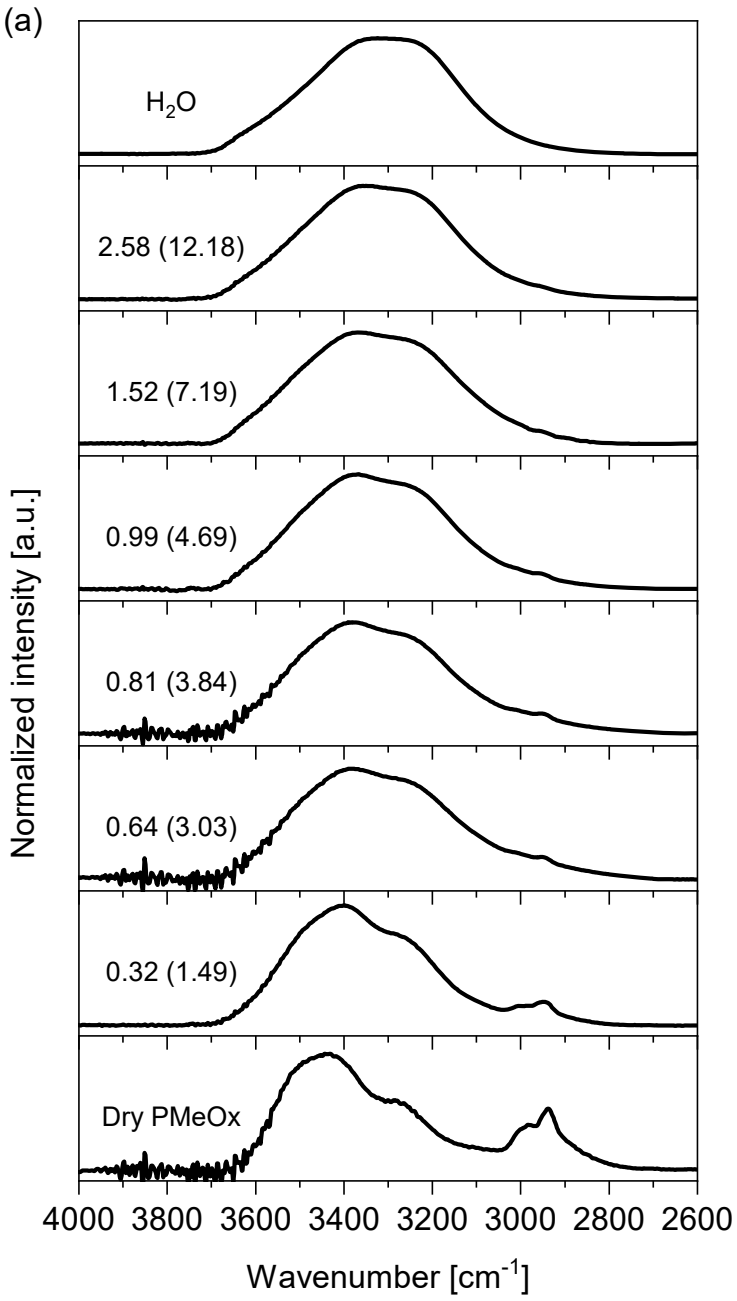

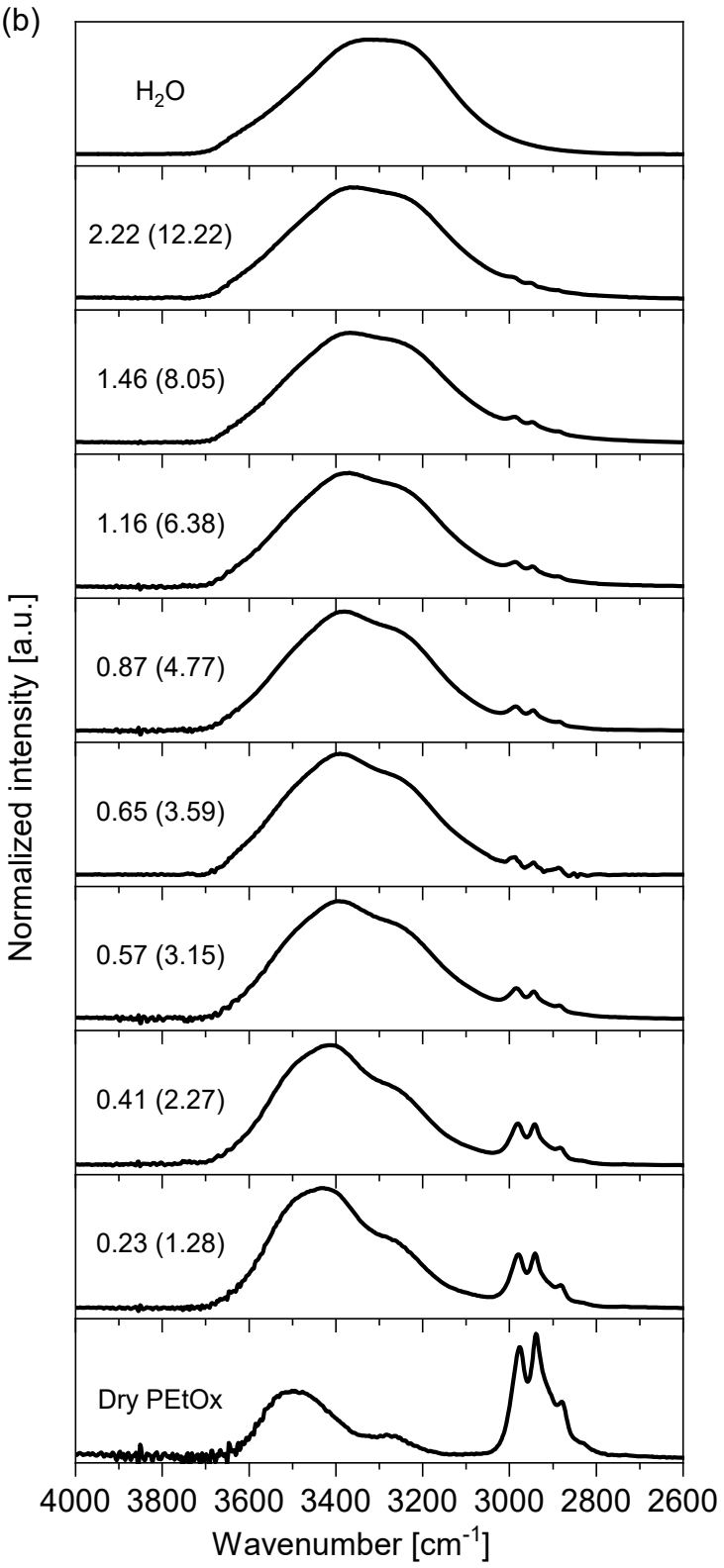
(b)
H2O
2.22 (12.22)
1.46 (8.05)
1.16 (6.38)
0.87 (4.77)
0.65 (3.59)
0.57 (3.15)
0.41 (2.27)
0.23 (1.28)
Dry PEtOx
Normalized intensity [a.u.]
4000 3800 3600 3400 3200 3000 2800 2600
Wavenumber [cm-1]

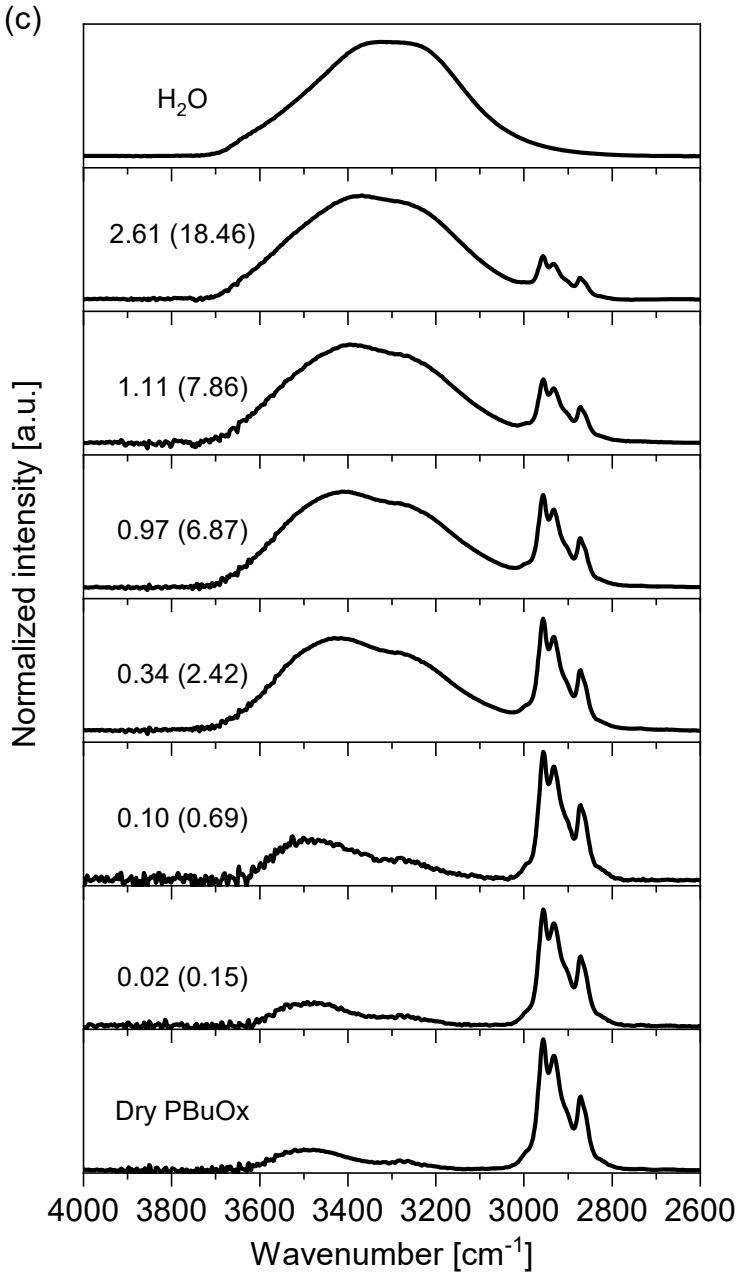
(c)
H2O
2.61 (18.46)
1.11 (7.86)
0.97 (6.87)
0.34 (2.42)
0.10 (0.69)
0.02 (0.15)
Dry PBuOx
Normalized intensity [a.u.]
4000 3800 3600 3400 3200 3000 2800 2600
Wavenumber [cm-1]

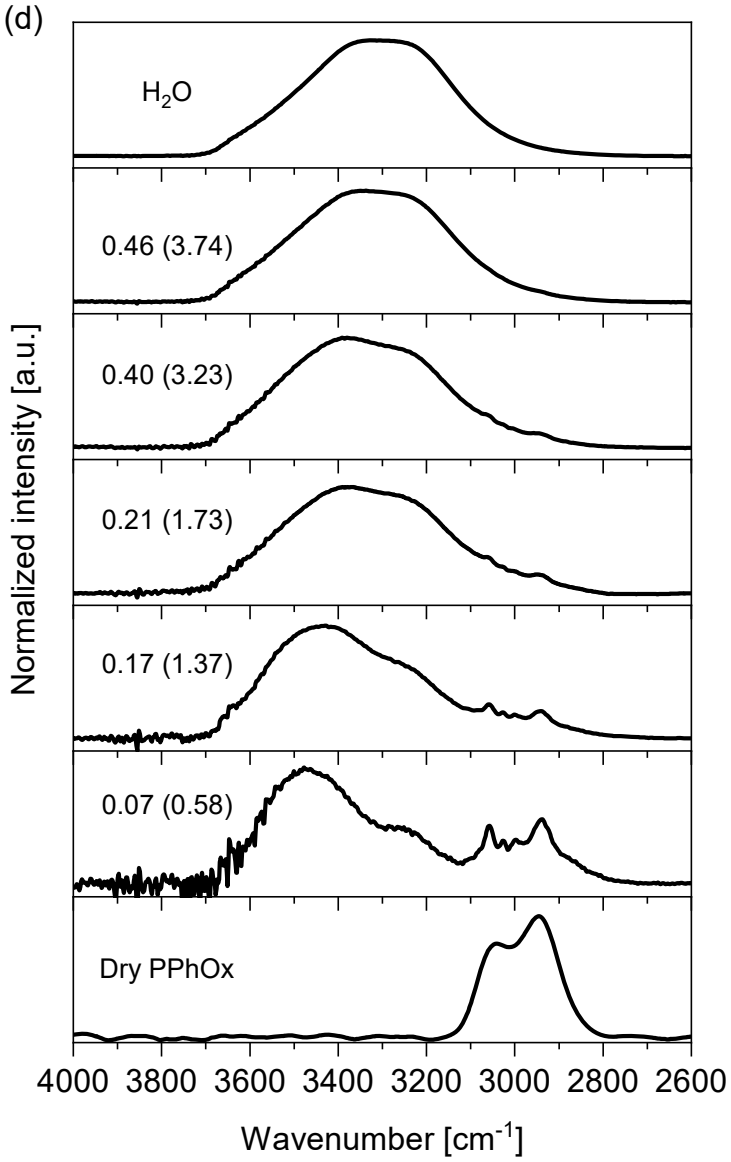

Figure 2.15. Normalized spectra of (a) PMeOx, (b) PEtOx, (c) PBuOx, (d) PPhOx H_2O systems with different total water contents at the range of 4000–2600 cm^{-1}. The values outside and in the brackets represent the weight contents (g/g) and molar contents (mol/mol) of the total water contents. The normalization was performed in relation to the total integral intensity in the spectra range 4000–2600 cm^{-1}.

In the IR spectrum, the *ν*(O–H) of water, which is sensitive to hydrogen bonds, is usually used to study the water structure in various systems.[35,38] The normalized IR spectra of POX/water systems with different water contents are presented in **Figure 2.15**. In the spectra of the dry POXs, the bands assigned to the C–H vibration in the side chains or the backbones of the polymers are located at 3700–2700 cm^{-1} and overlap with the *ν*(O–H) of water. Thus, the second derivative method was used to decompose the IR spectra.[39,40]

In **Figure 2.16**, the second derivative spectrum of pure water shows four bands at 3626, 3506, 3375, and 3219 cm^{-1}, respectively, which are similar to the data reported in the literature.[35] In comparison, the bands in the second derivative spectra of dry POXs are located differently and are separate from those of pure water. According to Piechocki's work,[35] in the poly[2-(2-methoxyethoxy)ethyl methacrylate] hydrogel/water system, the more hydrogen bonds a water molecule formed with polymer chains or other water molecules, the lower the wavenumber of the *ν*(O–H) band that was observed. They assigned the band at 3650 cm^{-1} to the free O–H and that at 3250 cm^{-1} to the *ν*(O–H) of a water molecule that is hydrogen-bonded with four water molecules. The *ν*(O–H) of water involved in the water-polymer interaction is located in the range of 3650–3250 cm^{-1}. Correspondingly, in this work, we assigned the band at around 3626 cm^{-1} and 3219 cm^{-1} to the free O–H and the *ν*(O–H) of a water molecule that forms hydrogen bonds with four water molecules, respectively. In **Figure 2.16a**, the intensity of the characteristic band of free O–H increases as the water content increases, while the intensity of the characteristic band of PMeOx at approximately 3500 cm^{-1} decreases. The two bands at approximately 3400 cm^{-1} and 3250 cm^{-1}

of the PMeOx/water systems exhibit a clear red shift as compared to those of dry PMeOx. This may reflect the shift in the polymer chains' vibration caused by hydration, or the evolution of the water structure. The evolution becomes clearer from the bands at approximately 3400 cm^{-1} in **Figure 2.16b**, because of the absence of the PEtOx chains' vibration in the neighboring wavenumber range. We proposed that the band at 3375 cm^{-1} of pure water corresponds to the *ν*(O–H) of water molecules that formed three hydrogen bonds.[41] At the water molar contents of 1.28 and 2.27, the carbonyl group approximately interacts with one or two water molecules. In both cases, one water molecule forms one hydrogen bond. At water contents greater than 3.15 mol/mol, water–water hydrogen bonds are primarily developed, and water molecules are formed with more than two hydrogen bonds. Therefore, the *ν*(O–H) red-shifted further to the 3375 cm^{-1}. In **Figure 2.15d**, there is no absorbance in the range of 3700–3200 cm^{-1} of the dry PPhOx; thus, the intensity in its second derivative spectrum in this range should be 0 (not shown in **Figure 2.16d**). At high water contents, the second derivative spectra of the PBuOx and PPhOx water systems resemble that of pure water. At low water contents (0.69 mol/mol for PBuOx and ≤ 1.37 mol/mol for PPhOx), the intensive bands located in 3550–3400 cm^{-1} can be mainly ascribed to the weak water–water interaction at the interface between the hydrophobic polymer and water rather than the water-polymer interaction.[38] Besides, unlike the PMeOx and PEtOx water systems, the bands at around 3219 cm^{-1} in PBuOx and PPhOx systems barely shift, which demonstrates even at low water contents, water can hydrogen-bond with the other four water molecules. In other words, at low water contents, water-water interaction still dominates in the systems, and this corresponds to the

DSC results.

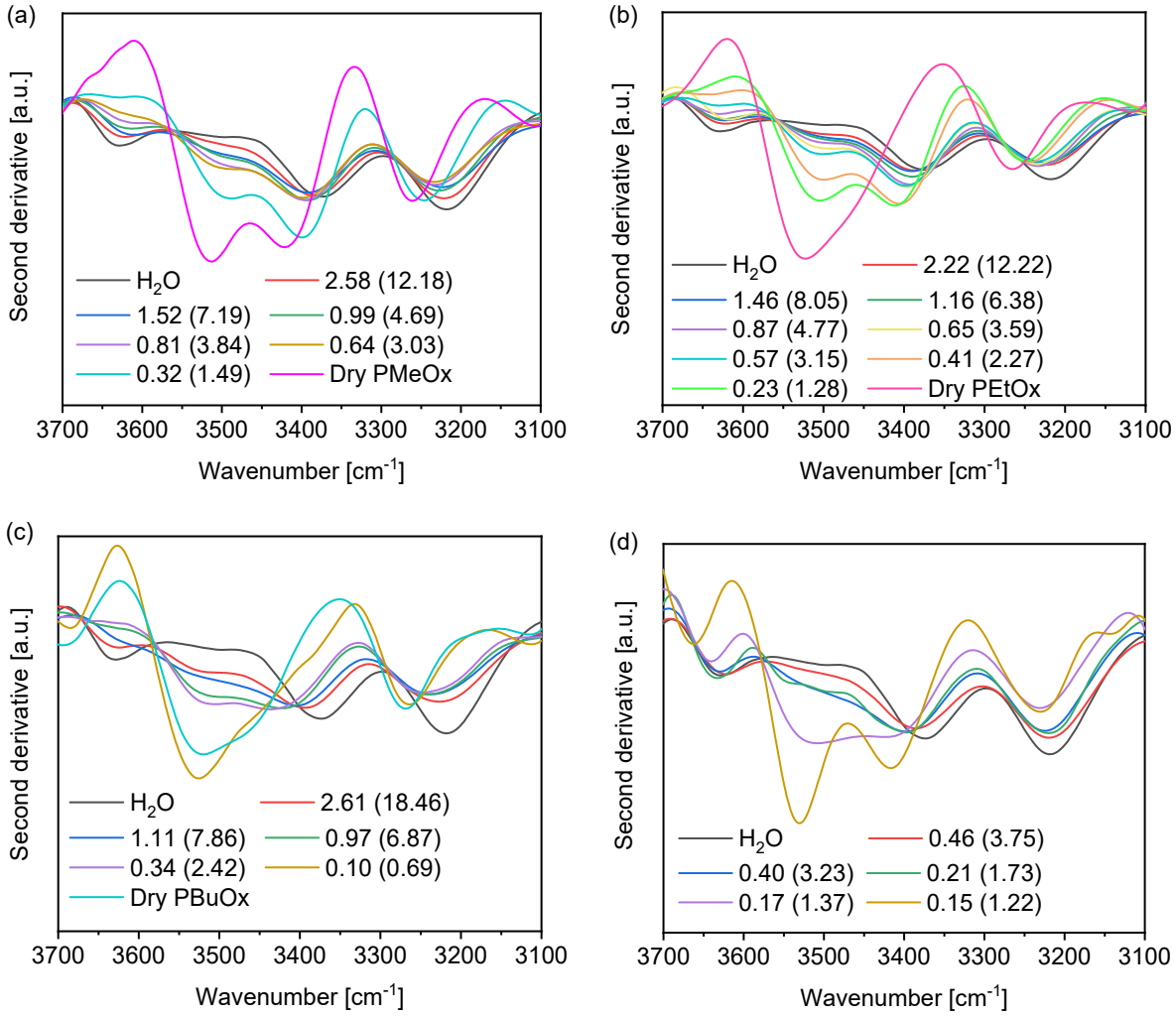

Figure 2.16. Second derivative spectra of (a) PMeOx, (b) PEtOx, (c) PBuOx, and (d) PPhOx water systems with different total water contents in the range of 3700–3100 cm^{-1}. The values outside and inside the brackets represent the weight contents (g/g) and molar contents (mol/mol), respectively.

In addition to the water structure, we also studied the ν(C=O) to evaluate the hydration state of

carbonyl. To eliminate the interference of the δ(O−H) band of water on the ν(C=O), IR measurements were conducted using POXs/D_2O systems. The IR spectra are shown in **Figure 2.17**. They are normalized in relation to the total integral intensity in the spectra range of 4500–500 cm^{-1}. In **Figure 2.17a**, the hydration induced an apparent red shift of the ν(C=O) compared with the free C=O (1620 cm^{-1}) in the dry PMeOx. The ν(C=O) did not vary significantly with the increase in water content and remained constant at approximately 1608 cm^{-1}. This suggests that there is no difference in the stretching vibration of the carbonyl interacting with different numbers of water molecules directly or indirectly. In the PEtOx systems (**Figure 2.17b**), a similar situation was observed. The hydration caused a red shift of approximately 20 cm^{-1} compared to the ν(C=O) in dry PEtOx (1628 cm^{-1}). In the PBuOx and PPhOx systems, hydration did not significantly affect the ν(C=O). The red shifts were less than 3 cm^{-1} for both hydrophobic POXs. It should be noted that the multiple peaks in the PPhOx system were caused by the overlap of the stretching vibration of the aromatic ring. Consequently, the hydration of the carbonyl groups in PBuOx and PPhOx was hindered.

From the DSC results, IW was observed in the hydrated PMeOx and PEtOx. However, only a small amount of IW was present in the hydrated PBuOx and PPhOx. It should be highlighted that the blood compatibility of PMeOx was not confirmed in this study possibly owing to the thin and uneven grafting layers on the substrates. However, the antifouling property of PMeOx has been proven in the literature.[42,29] According to the IW concept we proposed, the IW can indicate the blood compatibility of polymers because it can prevent the proteins and blood cells from directly

contacting the polymer surface. Therefore, the relationship between the IW and blood compatibility of PMeOx and PEtOx agrees with the theory that we proposed previously. From the analysis of the water structure and the hydration of carbonyl, we found that the carbonyl groups in PMeOx and PEtOx could be fully hydrated. The polymer–water interactions in the hydrated PMeOx and PEtOx were also similar, i.e., approximately more than two directly or indirectly interacting water molecules per carbonyl mainly contributed to the NFW, and the IW mostly interacted with the carbonyl through the NFW bridges. In the hydrophobic PBuOx and PPhOx systems, the carbonyl groups were scarcely hydrated. The polymer–water interaction was small, and water mainly existed as bulk water. The bulky butyl group and aromatic ring impede the water from accessing the carbonyl. Thus, proteins and blood cells can directly interact with PBuOx and PPhOx. Based on these results, the effect of pendant groups on the blood compatibility and hydration states of POXs is graphicly shown in **Figure 2.18**.

The findings in this chapter may provide some ideas for the development of novel blood-compatible POX derivatives. For example, the surface immobilization of PMeOx and PEtOx can sometimes be challenging because of their water solubility. The hydrophobic PBuOx is not blood-compatible but can be easily immobilized through physical interactions. Introducing new hydrophilic sites on the side chain of PBuOx or increasing the exposure of carbonyl groups to water is a promising method for improving the IW amount, and a balance between hydrophobicity and blood compatibility may be realized.

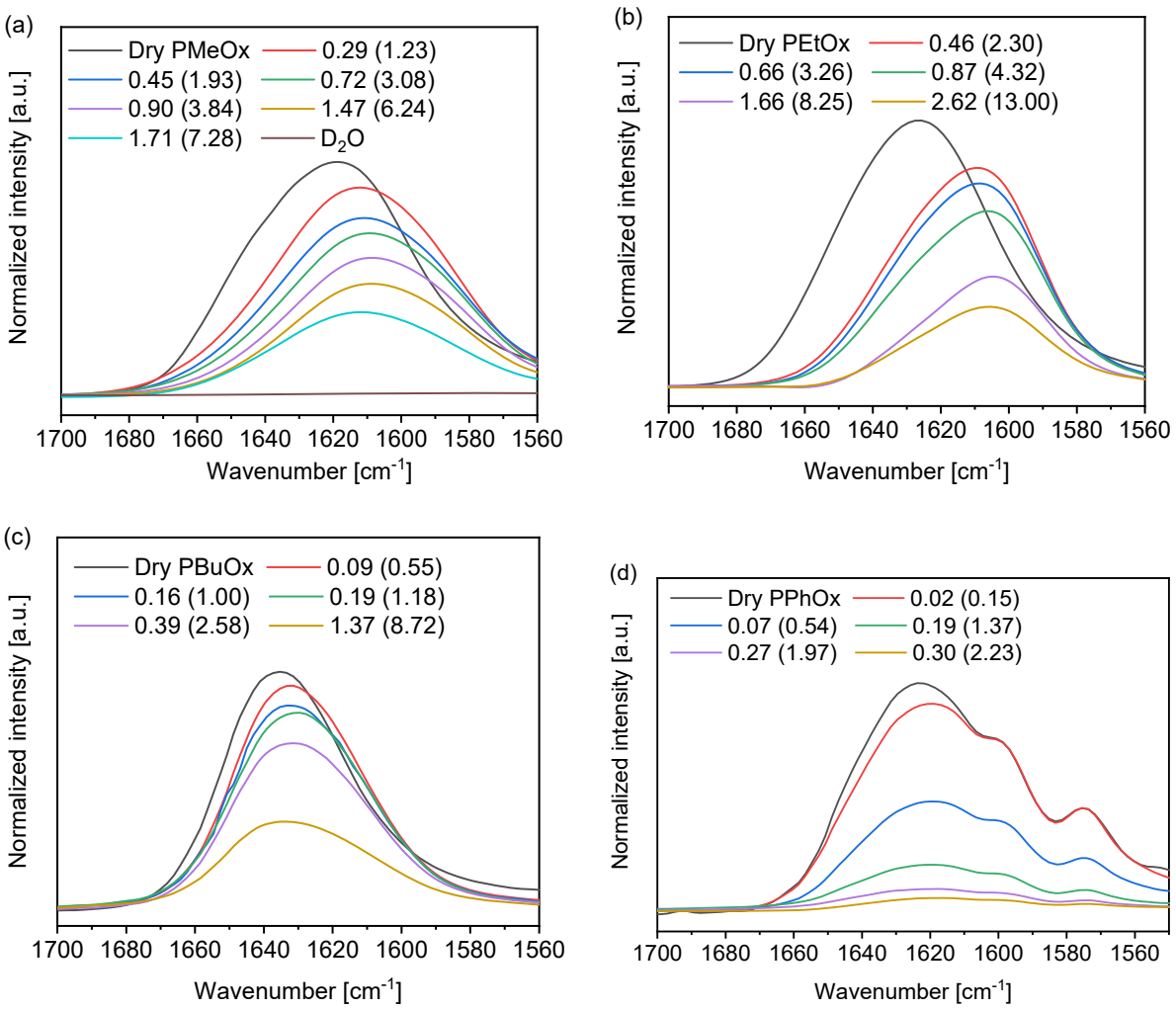

Figure 2.17 Normalized spectra of (a) PMeOx, (b) PEtOx, (c) PBuOx, and (d) PPhOx D_2O systems with different total water contents in the range of 1700–1550 cm^{-1}. The values outside and inside the brackets represent the weight contents (g/g) and molar contents (mol/mol), respectively.

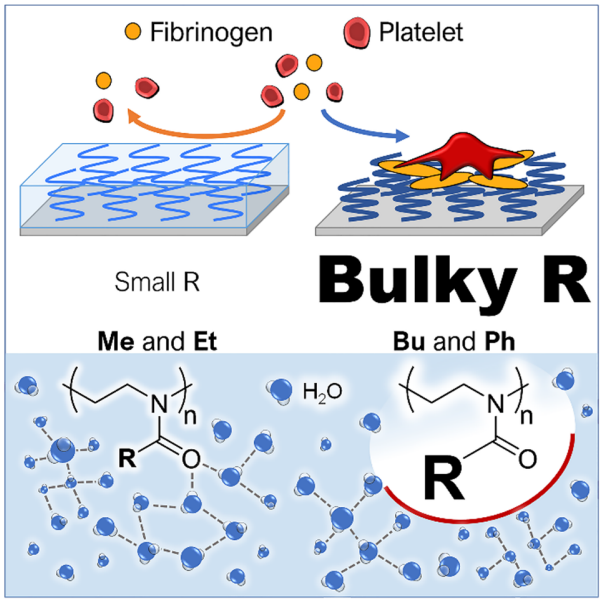

Figure 2.18. A graphic conclusion of the effect of pendant groups on the blood compatibility and hydration states of POXs.

2.4 Conclusions

In this study, PMeOx, PEtOx, PBuOx, and PPhOx were selected as POX models for the comparison of their blood compatibility and hydration states. The four POXs were grafted onto glass substrates through photo-grafting, and their blood compatibility was estimated via platelet adhesion and the degree of denaturation of the adsorbed fibrinogen. The hydration states of the POXs were investigated using DSC and ATR-IR. The IW was present in the hydrated PMeOx and PEtOx, but was scarce in the hydrated PBuOx and PPhOx. This could be the reason for the blood compatibility of PMeOx and PEtOx. The carbonyl groups in PMeOx and PEtOx could be fully hydrated. However, in PBuOx and PPhOx, water mainly existed as bulk water. The hydration of the carbonyl groups is hindered by the bulky side chain, and IW cannot be generated. This

knowledge provides a perspective for understanding the blood compatibility of PMeOx and PEtOx from the water–polymer interactions and may inspire the development of novel blood-compatible POX derivatives.

2.5 Reference

(1) Glassner, M.; Vergaelen, M.; Hoogenboom, R. Poly(2-Oxazoline)s: A Comprehensive Overview of Polymer Structures and Their Physical Properties. *Polym. Int.* **2018**, *67* (1), 32–45.

(2) Hoogenboom, R. Poly(2-Oxazoline)s Based on Fatty Acids. *Eur. J. Lipid Sci. Technol.* **2011**, *113* (1), 59–71.

(3) De La Rosa, V. R. Poly(2-Oxazoline)s as Materials for Biomedical Applications. *J. Mater. Sci. Mater. Med.* **2014**, *25* (5), 1211–1225.

(4) Sedlacek, O.; Bera, D.; Hoogenboom, R. Poly(2-Amino-2-Oxazoline)s: A New Class of Thermoresponsive Polymers. *Polym. Chem.* **2019**, *10* (34), 4683–4689.

(5) Sedlacek, O.; Janouskova, O.; Verbraeken, B.; Hoogenboom, R. Straightforward Route to Superhydrophilic Poly(2-Oxazoline)s via Acylation of Well-Defined Polyethylenimine. *Biomacromolecules* **2019**, *20* (1), 222–230.

(6) Wang, F.; Zhang, H.; Yu, B.; Wang, S.; Shen, Y.; Cong, H. Review of the Research on Anti-Protein Fouling Coatings Materials. *Prog. Org. Coatings* **2020**, *147*, 105860.

(7) Konradi, R.; Acikgoz, C.; Textor, M. Polyoxazolines for Nonfouling Surface Coatings — A Direct Comparison to the Gold Standard PEG. *Macromol. Rapid Commun.* **2012**, *33* (19), 1663–

1676.

(8) Morgese, G.; Benetti, E. M. Polyoxazoline Biointerfaces by Surface Grafting. *Eur. Polym. J.* **2017**, *88*, 470–485.

(9) Tauhardt, L.; Kempe, K.; Gottschaldt, M.; Schubert, U. S. Poly(2-Oxazoline) Functionalized Surfaces: From Modification to Application. *Chem. Soc. Rev.* **2013**, *42* (20), 7998–8011.

(10) Binder, W. H.; Sachsenhofer, R. "Click" Chemistry in Polymer and Materials Science. *Macromol. Rapid Commun.* **2007**, *28* (1), 15–54.

(11) Lava, K.; Verbraeken, B.; Hoogenboom, R. Poly(2-Oxazoline)s and Click Chemistry: A Versatile Toolbox toward Multi-Functional Polymers. *Eur. Polym. J.* **2015**, *65*, 98–111.

(12) Pidhatika, B.; Möller, J.; Benetti, E. M.; Konradi, R.; Rakhmatullina, E.; Mühlebach, A.; Zimmermann, R.; Werner, C.; Vogel, V.; Textor, M. The Role of the Interplay between Polymer Architecture and Bacterial Surface Properties on the Microbial Adhesion to Polyoxazoline-Based Ultrathin Films. *Biomaterials* **2010**, *31* (36), 9462–9472.

(13) Konradi, R.; Pidhatika, B.; Mühlebach, A.; Textor, M. Poly-2-Methyl-2-Oxazoline: A Peptide-like Polymer for Protein-Repellent Surfaces. *Langmuir* **2008**, *24* (3), 613–616.

(14) Prucker, O.; Naumann, C. A.; Ru, R.; Knoll, W.; Frank, C. W. Photochemical Attachment of Polymer Films to Solid Surfaces via Monolayers of Benzophenone Derivatives. *J. Am. Chem. Soc* **1999**, *121*, 8766–8770.

(15) Yan, M.; Ren, J. Covalent Immobilization of Ultrathin Polymer Films by Thermal Activation of Perfluorophenyl Azide. *Chem. Mater.* **2004**, *16* (9), 1627–1632.

(16) Tanaka, M.; Mochizuki, A. Effect of Water Structure on Blood Compatibility - Thermal Analysis of Water in Poly(Meth)Acrylate. *J. Biomed. Mater. Res.* **2004**, *68* (4), 684–695.

(17) Higashi, N.; Hirata, A.; Nishimura, S.; Koga, T. Thermo-Responsive Polymer Brushes on Glass Plate Prepared from a New Class of Amino Acid-Derived Vinyl Monomers and Their Applications in Cell-Sheet Engineering. *Colloids Surf. B* **2017**, *159*, 39–46.

(18) Gianneli, M.; Roskamp, R. F.; Jonas, U.; Loppinet, B.; Fytas, G.; Knoll, W. Dynamics of Swollen Gel Layers Anchored to Solid Surfaces. *Soft Matter* **2008**, *4* (7), 1443–1447.

(19) Kobayashi, S.; Wakui, M.; Iwata, Y.; Tanaka, M. Poly(ω-Methoxyalkyl Acrylate)s: Nonthrombogenic Polymer Family with Tunable Protein Adsorption. *Biomacromolecules* **2017**, *18* (12), 4214–4223.

(20) Sato, K.; Kobayashi, S.; Kusakari, M.; Watahiki, S.; Oikawa, M.; Hoshiba, T.; Tanaka, M. The Relationship Between Water Structure and Blood Compatibility in Poly(2-Methoxyethyl Acrylate) (PMEA) Analogues. *Macromol. Biosci.* **2015**, *15* (9), 1296–1303.

(21) Hatakeyama, H.; Hatakeyama, T. Interaction between Water and Hydrophilic Polymers. *Thermochim. Acta* **1998**, *308* (1–2), 3–22.

(22) Tanaka, M.; Motomura, T.; Ishii, N.; Shimura, K.; Onishi, M.; Mochizuki, A.; Hatakeyama, T. Cold Crystallization of Water in Hydrated Poly(2-Methoxyethyl Acrylate) (PMEA). *Polym Int* **2000**, *49*, 1709–1713.

(23) Sedlacek, O.; Monnery, B. D.; Hoogenboom, R. Synthesis of Defined High Molar Mass Poly(2-Methyl-2-Oxazoline). *Polym. Chem.* **2019**, *10* (11), 1286–1290.

(24) Litt, M.; Levy, A.; Herz, J. Polymerization of Cyclic Imino Ethers. X. Kinetics, Chain Transfer, and Repolymerization. *J Macromol. Sci. A* **1975**, *9* (5), 703–727.

(25) Monnery, B. D.; Jerca, V. V.; Sedlacek, O.; Verbraeken, B.; Cavill, R.; Hoogenboom, R. Defined High Molar Mass Poly(2-Oxazoline)s. *Angew. Chem. Int. Ed.* **2018**, *57* (47), 15400–15404.

(26) Hoogenboom, R.; Fijten, M. W. M.; Schubert, U. S. The Effect of Temperature on the Living Cationic Polymerization of 2-Phenyl-2-Oxazoline Explored Utilizing an Automated Synthesizer. *Macromol. Rapid Commun.* **2004**, *25* (1), 339–343.

(27) Sivaraman, B.; Latour, R. A. The Relationship between Platelet Adhesion on Surfaces and the Structure versus the Amount of Adsorbed Fibrinogen. *Biomaterials* **2010**, *31* (5), 832–839.

(28) Sato, K.; Kobayashi, S.; Sekishita, A.; Wakui, M.; Tanaka, M. Synthesis and Thrombogenicity Evaluation of Poly(3-Methoxypropionic Acid Vinyl Ester): A Candidate for Blood-Compatible Polymers. *Biomacromolecules* **2017**, *18* (5), 1609–1616.

(29) Svoboda, J.; Sedláček, O.; Riedel, T.; Hrubý, M.; Pop-Georgievski, O. Poly(2-Oxazoline)s One-Pot Polymerization and Surface Coating: From Synthesis to Antifouling Properties Out-Performing Poly(Ethylene Oxide). *Biomacromolecules* **2019**, *20* (9), 3453–3463.

(30) Sivaraman, B.; Latour, R. A. The Adherence of Platelets to Adsorbed Albumin by Receptor-Mediated Recognition of Binding Sites Exposed by Adsorption-Induced Unfolding. *Biomaterials* **2010**, *31* (6), 1036–1044.

(31) Zhang, L.; Casey, B.; Galanakis, D. K.; Marmorat, C.; Skoog, S.; Vorvolakos, K.; Simon, M.; Rafailovich, M. H. The Influence of Surface Chemistry on Adsorbed Fibrinogen Conformation, Orientation, Fiber Formation and Platelet Adhesion. *Acta Biomater.* **2017**, *54*, 164–174.

(32) Huang, L.; Nishinari, K. Interaction Between Poly(Ethylene Glycol) and Water as Studied by Differential Scanning Calorimetry. *J Polym Sci B Polym Phys* **2001**, *39*, 496–506.

(33) Yoshida, H.; Hatakeyama, T.; Hatakeyama, H. Phase Transitions of the Water-Xanthan System. *Polymer* **1990**, *31* (4), 693–698.

(34) Morita, S.; Tanaka, M.; Ozaki, Y. Time-Resolved in Situ ATR-IR Observations of the Process of Sorption of Water into a Poly(2-Methoxyethyl Acrylate) Film. *Langmuir* **2007**, *23* (7), 3750–3761.

(35) Piechocki, K.; Kozanecki, M.; Saramak, J. Water Structure and Hydration of Polymer Network in PMEO2MA Hydrogels. *Polymer* **2020**, *210*, 122974.

(36) Hatakeyama, T.; Tanaka, M.; Hatakeyama, H. Studies on Bound Water Restrained by Poly(2-Methacryloyloxyethyl Phosphorylcholine): Comparison with Polysaccharide-Water Systems. *Acta Biomater.* **2010**, *6* (6), 2077–2082.

(37) Szostak, R.; Aubé, J.; Szostak, M. An Efficient Computational Model to Predict Protonation at the Amide Nitrogen and Reactivity along the C-N Rotational Pathway. *Chem. Commun.* **2015**, *51* (29), 6395–6398.

(38) Scatena, L. F.; Brown, M. G.; Richmond, G. L. Water at Hydrophobic Surfaces: Weak

Hydrogen Bonding and Strong Orientation Effects. *Science* **2001**, *292* (5518), 908–912.

(39) Kroning, A.; Furchner, A.; Adam, S.; Uhlmann, P.; Hinrichs, K. Probing Carbonyl–Water Hydrogen-Bond Interactions in Thin Polyoxazoline Brushes. *Biointerphases* **2016**, *11* (1), 019005.

(40) Li, T.; Tang, H.; Wu, P. Molecular Evolution of Poly(2-Isopropyl-2-Oxazoline) Aqueous Solution during the Liquid–Liquid Phase Separation and Phase Transition Process. *Langmuir* **2015**, *31* (24), 6870–6878.

(41) Ohno, K.; Okimura, M.; Akai, N.; Katsumoto, Y. The Effect of Cooperative Hydrogen Bonding on the OH Stretching-Band Shift for Water Clusters Studied by Matrix-Isolation Infrared Spectroscopy and Density Functional Theory. *Phys. Chem. Chem. Phys.* **2005**, *7* (16), 3005–3014.

(42) Morgese, G.; Verbraeken, B.; Ramakrishna, S. N.; Gombert, Y.; Cavalli, E.; Rosenboom, J. G.; Zenobi-Wong, M.; Spencer, N. D.; Hoogenboom, R.; Benetti, E. M. Chemical Design of Non-Ionic Polymer Brushes as Biointerfaces: Poly(2-Oxazine)s Outperform Both Poly(2-Oxazoline)s and PEG. *Angew. Chem. Int. Ed.* **2018**, *57* (36), 11667–11672.

CHAPTER 3

Synthesis of Poly(tertiary amido acrylate) Analogs and Their (Co)polymers

3.1 Introduction

As mentioned in the previous two chapters, although PMeOx and PEtOx exhibit excellent blood compatibility, they mainly suffer from two challenges. The first one is that they are water-soluble. Usually, a tedious chemical effort is needed for the functionalization of polymers or substrates. Secondly, the CROP of POXs requires a strict reaction environment to avoid interference by extrinsic nucleophilic impurities, such as moisture, oxygen, or solvents. Additionally, the unavoidable intrinsic chain transfer becomes obvious at high temperatures or high monomer-to-initiator ratios. Both aspects lead to the "compromised" living polymerization of oxazoline monomers.[1] Conversely, vinyl monomers can easily achieve polymerization by non-living free radical polymerization or living RAFT radical polymerization. Either of the two methods shows higher tolerability to impurities.[2] Moreover, the water solubility of vinyl polymers is easy to adjust by copolymerization with hydrophobic components.

Modifying vinyl monomer side chains with functional groups that mimic natural biomolecules is a compelling strategy to develop blood-compatible polymers. PMPC prepared by Nakabayashi and Chapman is the most successful representative.[3,4] The sidechain of PMPC mimics the phosphorylcholine group of phosphatidylcholines and sphingomyelin, mainly constituting the cell

membrane. Although PMPC is water-soluble, by suitably copolymerizing with hydrophobic monomers, the water-resistance of PMPC copolymers can be improved while maintaining blood compatibility. For example, the commercially available poly(*n*-butyl methacrylate$_{70}$-*co*-2-methacryloyloxyethyl phosphorylcholine$_{30}$) exhibited excellent nonthrombogenicity. Analogously, poly(phosphobetaine methacrylate), poly(carboxybetaine methacrylate), poly(sulfobetaine methacrylate), the sidechains of these polymers, imitated natural biomolecules and showed blood compatibility.[5] Furthermore, the sidechain can also be constructed by the unit of synthesized polymers. Poly(2-methoxyethyl acrylate) (PMEA), whose sidechain is constituted by one repeating unit of PEG, is a blood-compatible material approved by the Food and Drug Administration (FDA).[6]

According to **Chapter 2**, for PMeOx and PEtOx, the tertiary amide frameworks can be fully hydrated to generate IW. While in PBuOx and PPhOx, the tertiary amide frameworks are sterically hindered to form IW. Thus, combining these conclusions as well as the construction strategy of PMPC and PMEA, three poly(tertiary amido acrylate) analogs, PAEA, PAEM, PPEA, each of which bears a tertiary amide framework in the side chain, were designed and prepared by convenient free radical polymerization. Notably, we only investigated the steric hindrance effect from the carbonyl side of an amide on the interaction between water and the tertiary amide framework in the previous chapter. Yet, the steric hindrance from the nitrogen side may also affect the water interaction. Therefore, the PEAE, which has an ethyl group linked to the nitrogen in the side chain, was also prepared. Besides, for POXs, their thermosensitivity is affected by the steric

hindrance around the tertiary amide framework. The four poly(tertiary amido acrylate) analogs might show different thermosensitivity. The chemical structures of all the poly(tertiary amido acrylate) analogs are shown in **Figure 3.1**. Because all the prepared poly(tertiary amido acrylate) analogs are water-soluble. To easily immobilize them on substrates by physical interaction, their water-insoluble copolymers were also prepared by copolymerizing with their monomers with hydrophobic *n*-butyl (meth)acrylates.

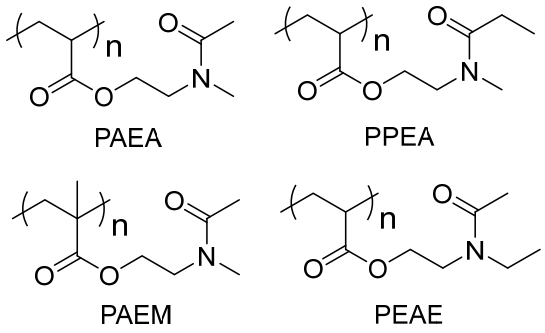

Figure 3.1. Chemical structures of PAEA, PPEA, PAEM, and PEAE.

3.2 Materials

Acetic anhydride, acryloyl chloride, 2-(ethylamino)ethanol, *n*-butyl acrylate (BuA), and *n*-butyl methacrylate (BMA) were purchased from Tokyo Chemical Industry Co. Ltd., Japan. Neutral aluminum oxide, 2-(methylamino)ethanol and propionic anhydride were purchased from Sigma-Aldrich Co., USA. Triethylamine and 2,2’-azobis(isobutyronitrile) were purchased from Kanto Chemical Co. Inc., Japan. 2,2'-Azobis(isobutyronitrile) was recrystallized before use. Anhydrous potassium carbonate was purchased from Fujifilm Wako Pure Chemical Co., Japan. BMH was purchased from Seiko Chemical Co. Ltd., Japan. Solvents for synthesizing monomers and

polymers were purchased from Kanto Chemical Co. Inc., Japan.

3.3 Molecular characterization methods

NMR spectra were recorded on a Bruker AVANCE III 600 MHz or a Bruker AVANCE III 400 MHz at rt unless otherwise specified. All chemical shifts are given in ppm. Proton chemical shifts were referenced to solvent residual signals or the TMS (0.00 ppm) if it was contained in the NMR solvent. Carbon chemical shifts were referenced to $CDCl_3$ (77.2 ppm) or DMSO (39.5 ppm). In the case of D_2O as the NMR solvent, the carbon chemical shifts were referenced according to the correspondence to the proton chemical shifts in the ^{1}H-^{13}C HMQC spectrum. The molecular weight of the amide alcohols and monomers was characterized by a JEOL JMS-700 fast atom bombardment mass spectrometer (FAB-MS). The molecular weight (M_n) and molecular weight distribution (M_w/M_n) of the homopolymers of poly(tertiary amido acrylate) analogs were measured by a gel permeation chromatography (GPC) instrument on an HPLC system equipped with a Shimadzu Prominence system and four Tosoh TSKgel columns (guard, α-m, α-m, and α-3000) and a refractive index detector at 40 °C. The eluent was DMF containing 10 mM LiBr at a flow rate of 1.0 mL min^{-1}. The M_n and M_w/M_n were calculated against narrow dispersity poly(methyl methacrylate) standards. The M_n and M_w/M_n of copolymers were measured through a size exclusion chromatography (SEC) instrument on a Malvern Viscotek system equipped with a refractive index and ultraviolet detectors at 40 °C and four Tosoh TSKgel columns (guard, G5000, G4000, and G3000). The system was eluted by tetrahydrofuran (THF) at a flow rate of 1.0 mL

min^{-1}. The M_n and M_w/M_n were calculated against narrow dispersity polystyrene standards. The analytes of polymer solutions were filtered through 0.2 μm polytetrafluoroethylene filters before injection.

3.4 Preparation of monomers

The procedures to prepare tertiary amide (meth)acrylate monomers are illustrated in **Figure 3.2**. Monomer preparation was accomplished by two steps: (i) preparation of amide alcohol,[7] (ii) coupling reaction between amide alcohol and acryloyl chloride or methacryloyl chloride. The same strategy was employed to synthesize secondary amide acrylate in recent work by Mahmud et al.[8] Since the tertiary amide moiety is deemed the repeating unit of POXs, functionalization from 2-oxazolines seems feasible by combining the chemical properties of 2-oxazolines. Weber[9] reported three routes to functionalize (meth)acrylate with POX units by 2-oxazolines. The first route is to initiate the ring-opening polymerization of 2-oxazolines by (meth)acryloyl chloride, the second is to terminate the oligomerized oxazolines' active species with (meth)acrylate anion directly, and the third is to esterify the hydroxy-terminated oxazoline chains with (meth)acryloyl chloride. However, none of them can realize the precise control of the number of POX units, while the two-step method assures only one unit. The synthesis and experimental details are described in the following sections.

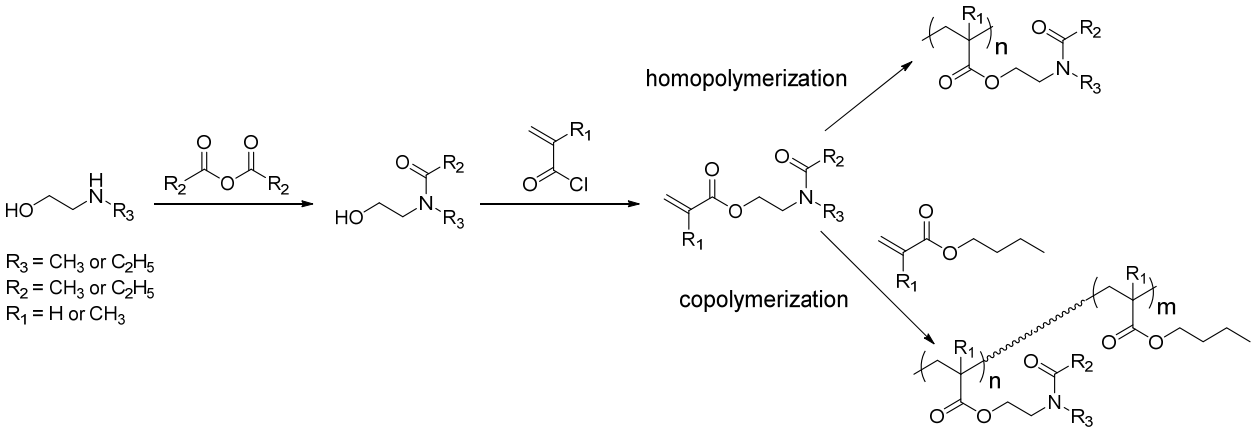

Figure 3.2. Synthesis of tertiary amide (meth)acrylate monomers and corresponding homopolymers and copolymers.

3.4.1 Preparation of 2-(*N*-methylacetamido)ethyl acrylate (NMAEA)

3.4.1.1 Preparation of *N*-(2-hydroxyethyl)-*N*-methylacetamide (NHEMA)

Acetic anhydride (22.45 g, 220 mmol, 1.1 equiv.) was added dropwise to a suspension of neutral aluminum oxide (30.59 g, 300 mmol, 1.5 equiv.) and 2-(methylamino)ethanol (15.02 g, 200 mmol, 1 equiv.) in an ice-water bath. The reaction mixture was stirred at rt for 20 min. The Al_2O_3 was filtered off by suction filtration and further rinsed by DCM (500 mL). Ca. 6 mL water, as well as 4.5 g anhydrous K_2CO_3 were added to the filtrate.

The mixture was stirred for another 15 min until the water layer became neutralized. Then, a large excess of anhydrous K_2CO_3 was added and stirred to remove the water. After filtering the solid and removing the DCM in the filtrate by a rotary evaporator, the crude product was further purified by flash column chromatography (mobile phase: ether/MeOH = 9:1). Unless otherwise specified, the vanillin/concentrated sulfuric acid/ethanol solution (3 g/0.5 mL/50 mL) was used as

the dye in a previous TLC for all the column chromatography in this work. After removing the eluent, the NHEMA was finally achieved as a yellowish liquid. (13.12 g, yield: 56%).

HR-FAB-MS ($C_5H_{11}NO_2$): m/z^{exp} = 118.0876 (M + H), m/z^{theo} =118.0868 (M + H).

Because of the lone pair electrons in nitrogen, the rotation of the amide bond is hindered in the tertiary-chiral amide, leading to the formation of rotamers. Thus, in the NMR spectra of tertiary amide alcohols and tertiary amide monomers in this work, all of the signals split into two proportionable groups at rt.

^{1}H NMR (600 MHz, D_2O) δ_{ppm}: 2.15 & 2.18 (s, 3H, OCC*H*$_3$), 2.96 & 3.14 (s, 3H, NC*H*$_3$), 3.53 & 3.58 (t, 2H, *J* = 5.5 Hz, NC*H*$_2$CH$_2$), 3.75 & 3.80 (t, 2H, *J* = 5.5 Hz, OC*H*$_2$).

^{13}C NMR (151 MHz, D_2O) δ_{ppm}: 20.6 & 21.0 (OC*C*H$_3$), 33.5 & 37.2 (N*C*H$_3$), 49.7 & 52.7 (N*C*H$_2$CH$_2$), 58.7 & 58.9 (O*C*H$_2$), 174.4 (O=*C*).

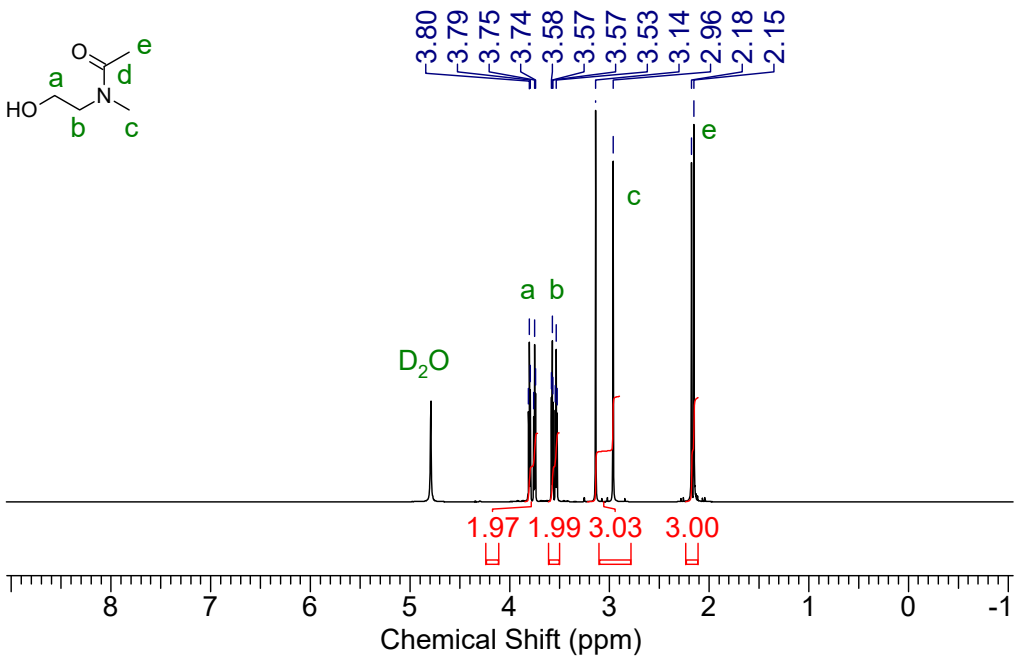

Figure 3.3. ^{1}H NMR spectrum of *N*-(2-hydroxyethyl)-*N*-methylacetamide (NHEMA, in D_2O, 600 MHz).

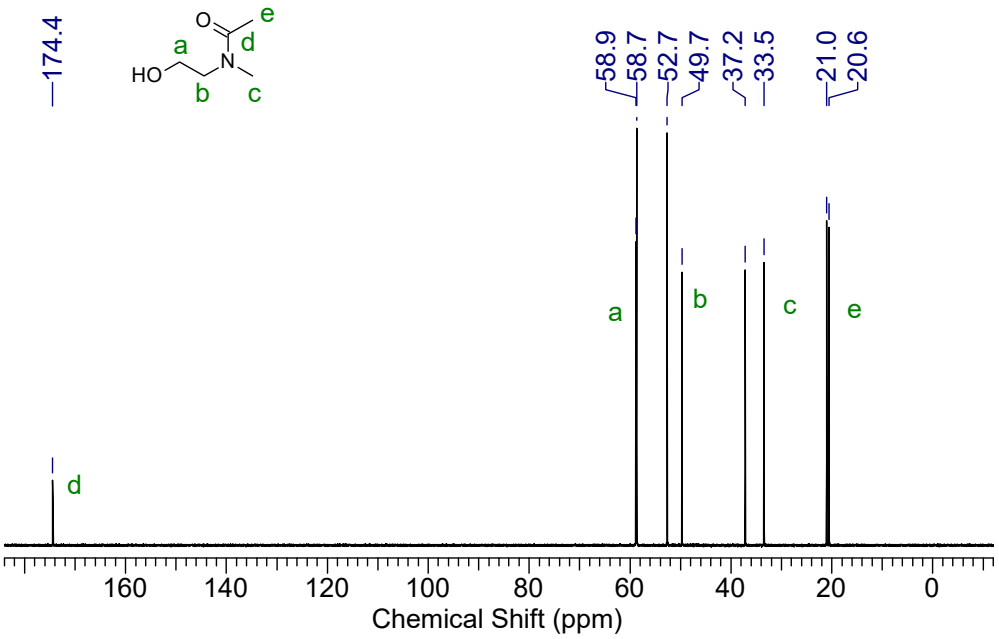

Figure 3.4. ^{13}C NMR spectrum of *N*-(2-hydroxyethyl)-*N*-methylacetamide (NHEMA, in D_2O,

151 MHz).

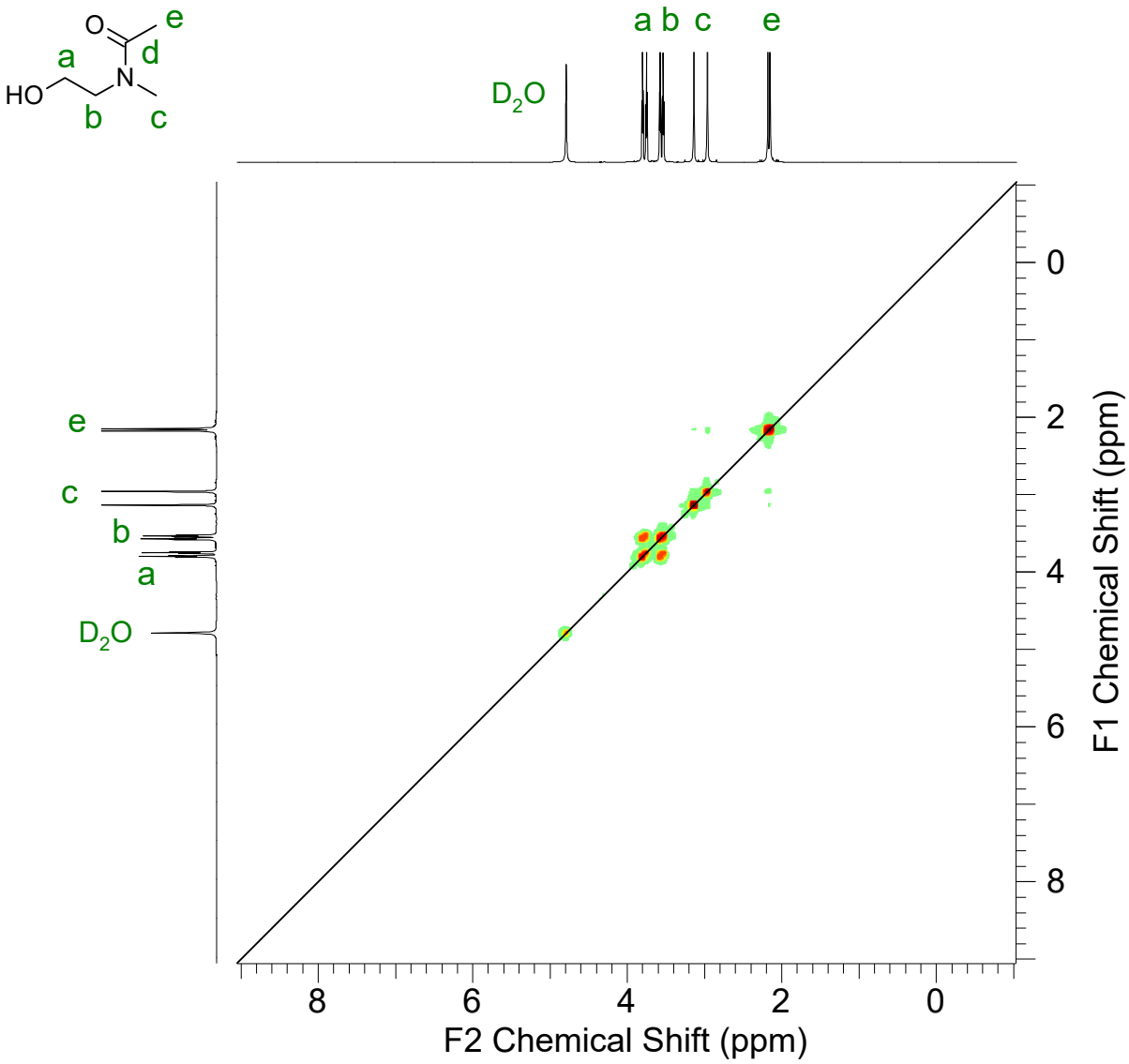

Figure 3.5. ^{1}H-^{1}H COSY spectrum of *N*-(2-hydroxyethyl)-*N*-methylacetamide (NHEMA, in D_2O, 600 MHz).

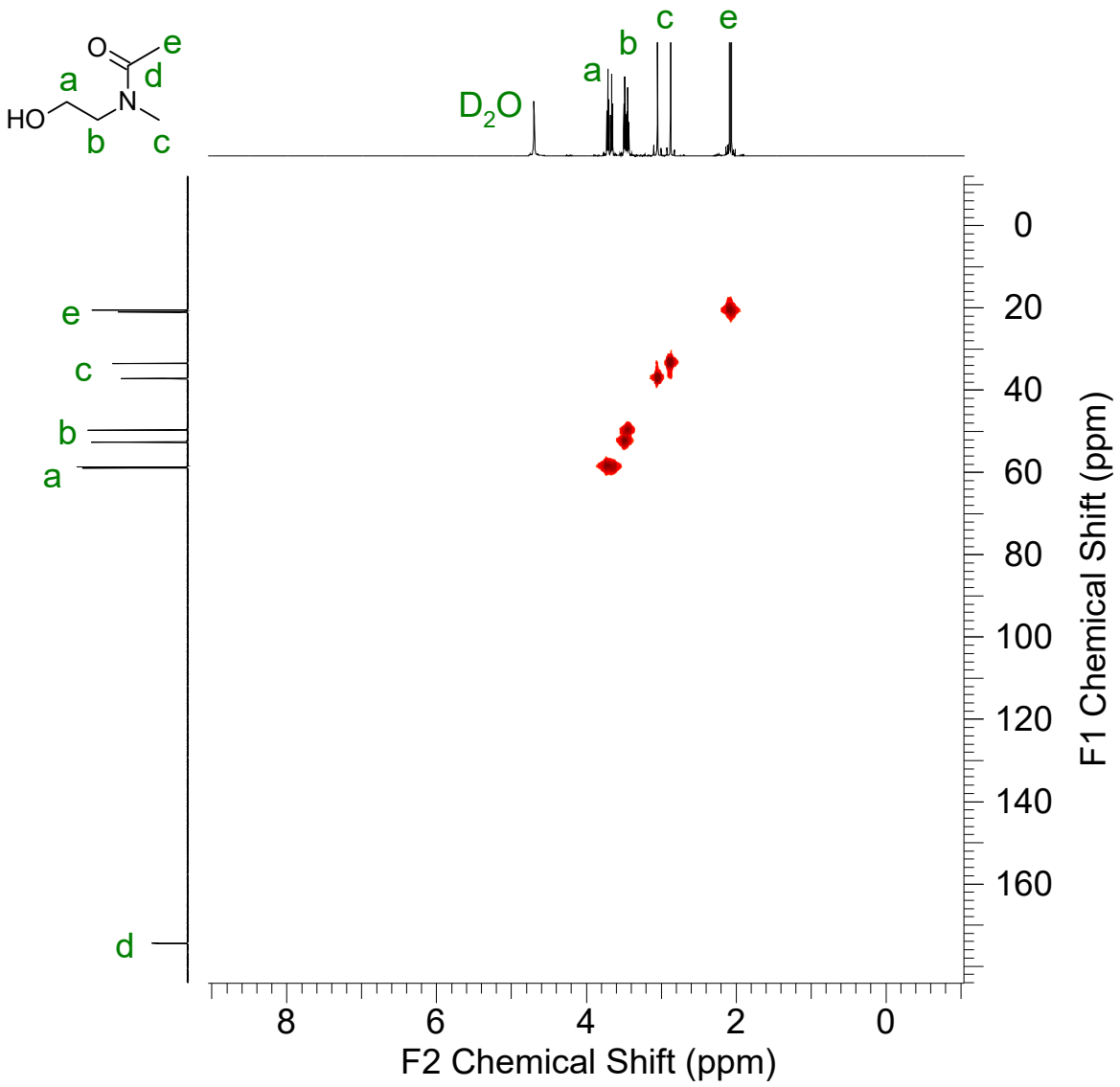

Figure 3.6. ^{1}H-^{13}C HMQC spectrum of *N*-(2-hydroxyethyl)-*N*-methylacetamide (NHEMA, in D_2O, 400 MHz for ^{1}H, 101 MHz for ^{13}C).

3.4.1.2 Preparation of NMAEA

To a mixture of NHEMA (12.30 g, 105 mmol, 1 equiv.), triethylamine (11.69 g, 115.5 mmol, 1.1 equiv.), and 140 mL of anhydrous DCM immersed in an ice-water bath, acryloyl chloride (10.45 g, 115.5 mmol, 1.1 equiv.) was added dropwise over 15 min. The esterification reaction was stirred overnight at rt. Then the white precipitate in the reaction mixture was filtered off by suction filtration and rinsed by a small amount of DCM. After evaporating the DCM in the filtrate, the oily crude product was then purified by fractional vacuum distillation. The main fraction (bp = 63 °C at 0.08 Torr) was eluted by DCM through a short basic Al_2O_3 column to remove the residual acrylic acid. The NMAEA was finally obtained as a colorless liquid after the evaporation of DCM (10.21 g, yield: 57%).

HR-FAB-MS ($C_8H_{13}NO_3$): m/z^{exp} = 172.0979 (M + H), m/z^{theo} =172.0974 (M + H).

At 90 °C, the paired signals in the NMR spectrum of NMAEA tend to merge into ones, proving the paired signals are caused by the rotamers but not impurities.

^{1}H NMR (600 MHz, DMSO) δ_{ppm}: 1.97 & 1.99 (s, 3H, OCC*H*$_3$), 2.81 & 2.99 (s, 3H, NC*H*$_3$), 3.54 & 3.59 (t, 2H, *J* = 5.6 Hz, NC*H*$_2$CH$_2$), 4.19 & 4.27 (t, 2H, *J* = 5.5 Hz, OC*H*$_2$), 5.95 & 5.98 (dd, H, *J* = 10.2, 1.5 Hz and 10.5, 1.5 Hz, C*H*$_2$=), 6.15 (m, H, OCC*H*=), 6.31 & 6.34 (dd, H, *J* = 4.9, 1.5 Hz, C*H*$_2$=)

^{13}C NMR (151 MHz, DMSO) δ_{ppm}: 21.0 & 21.5 (OC*C*H$_3$), 32.7 & 36.5 (N*C*H$_3$), 45.7 & 48.5 (N*C*H$_2$CH$_2$), 61.5 & 61.7 (O*C*H$_2$), 128.0 & 128.2 (OC*C*H=), 131.5 & 131.8 (*C*H$_2$=), 165.2 & 165.3 (*C*OO), 169.6 & 170.0 (*C*ON).

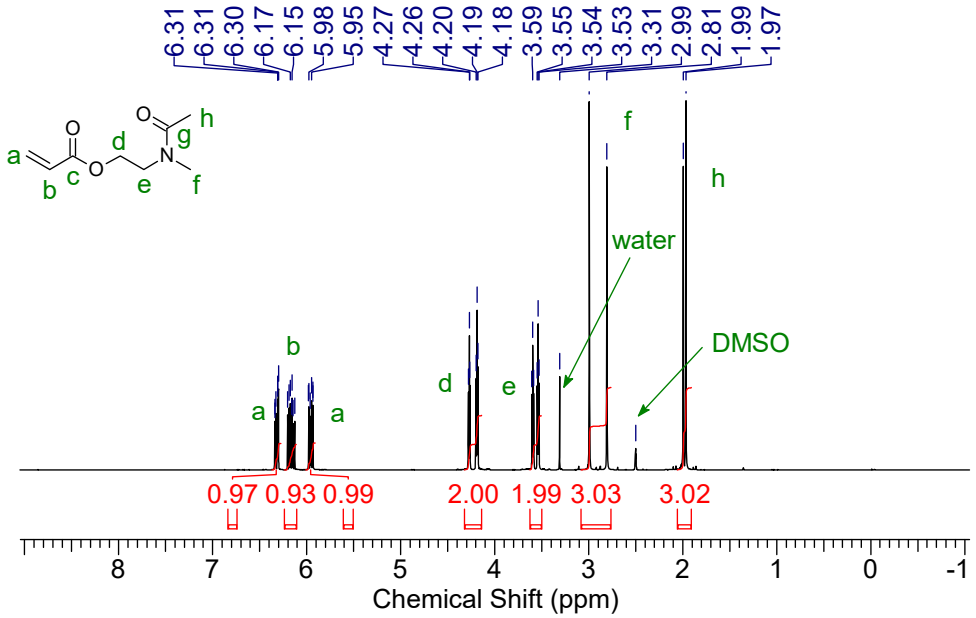

Figure 3.7. ^{1}H NMR spectrum of 2-(*N*-methylacetamido)ethyl acrylate (NMAEA, in DMSO, 600 MHz).

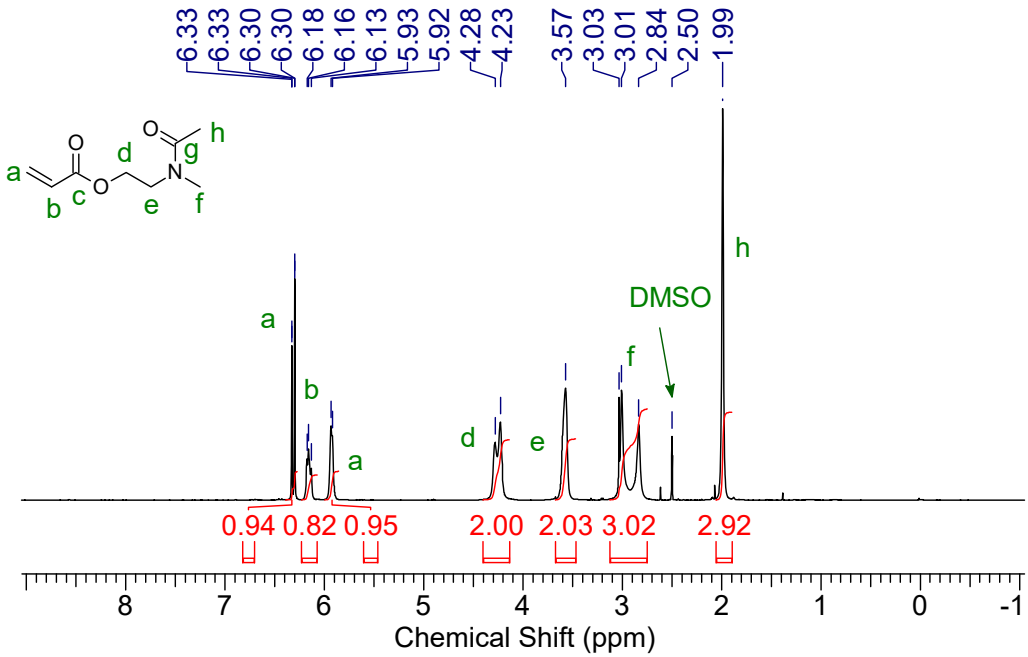

Figure 3.8. ^{1}H NMR spectrum of 2-(*N*-methylacetamido)ethyl acrylate at 90 °C (NMAEA, in

DMSO, 600 MHz).

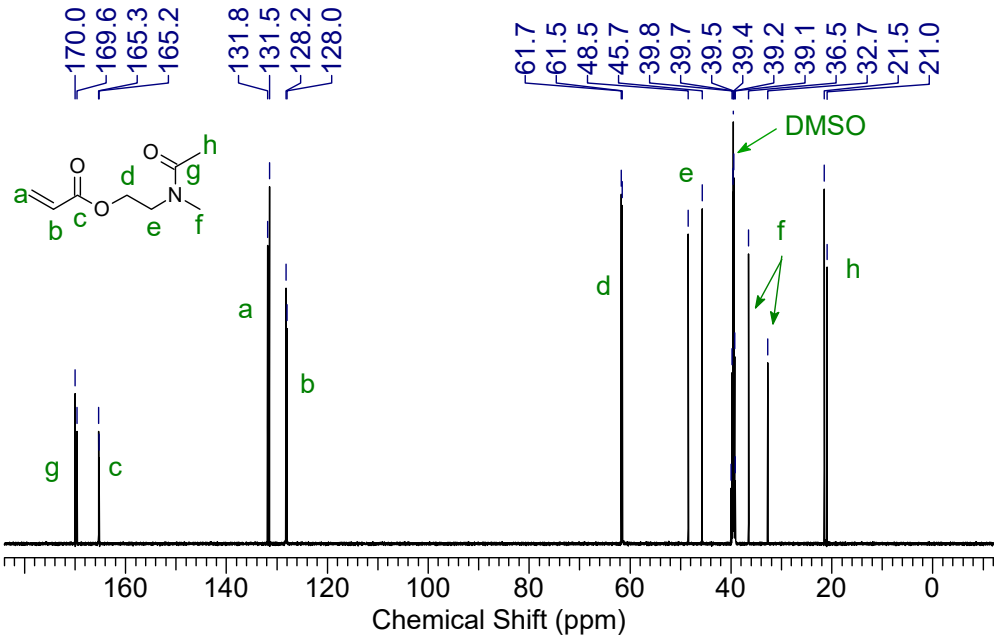

Figure 3.9. ^{13}C NMR spectrum of 2-(*N*-methylacetamido)ethyl acrylate (NMAEA, in DMSO, 151 MHz).

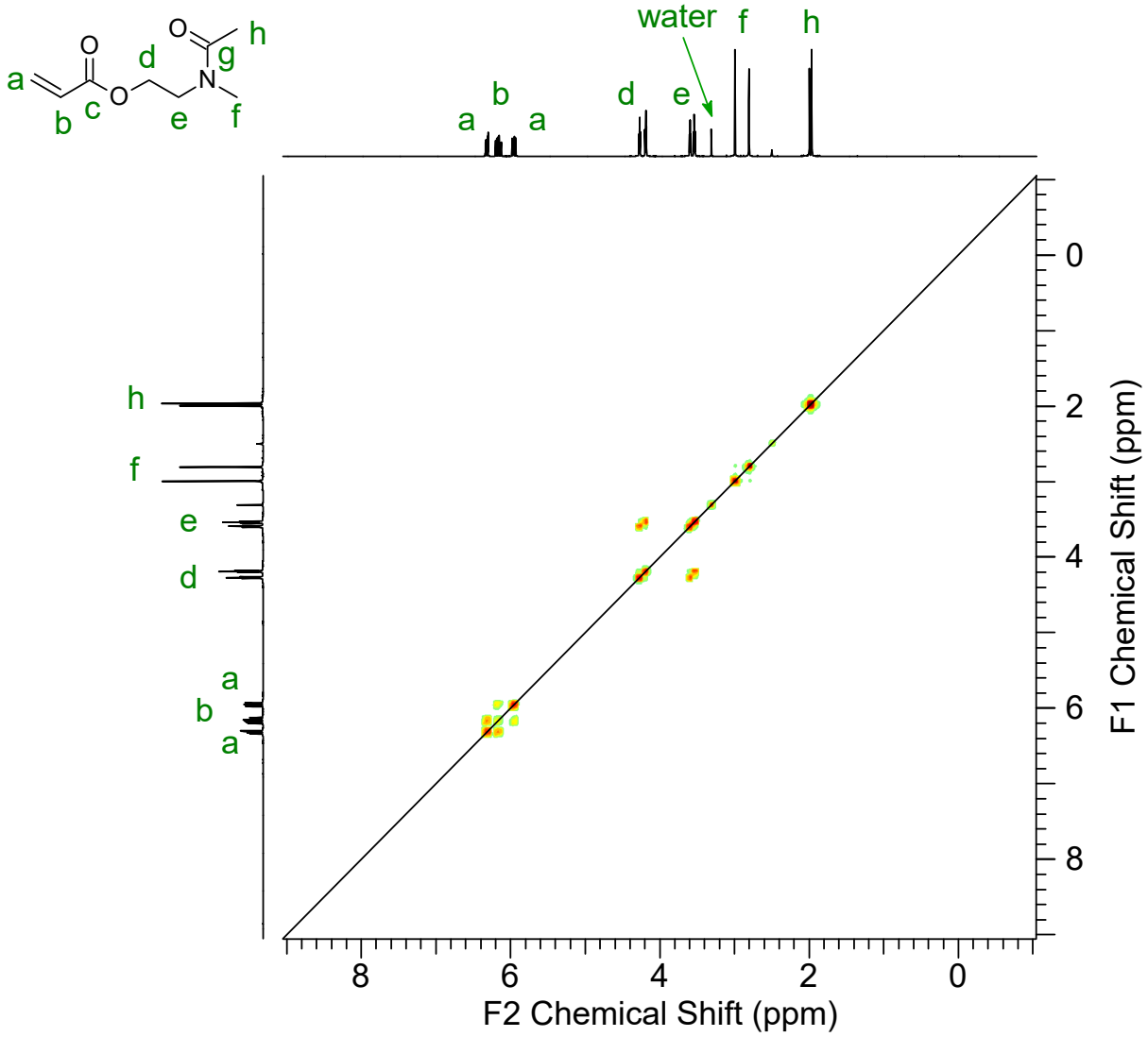

Figure 3.10. ^{1}H-^{1}H COSY spectrum of 2-(*N*-methylacetamido)ethyl acrylate (NMAEA, in DMSO, 600 MHz).

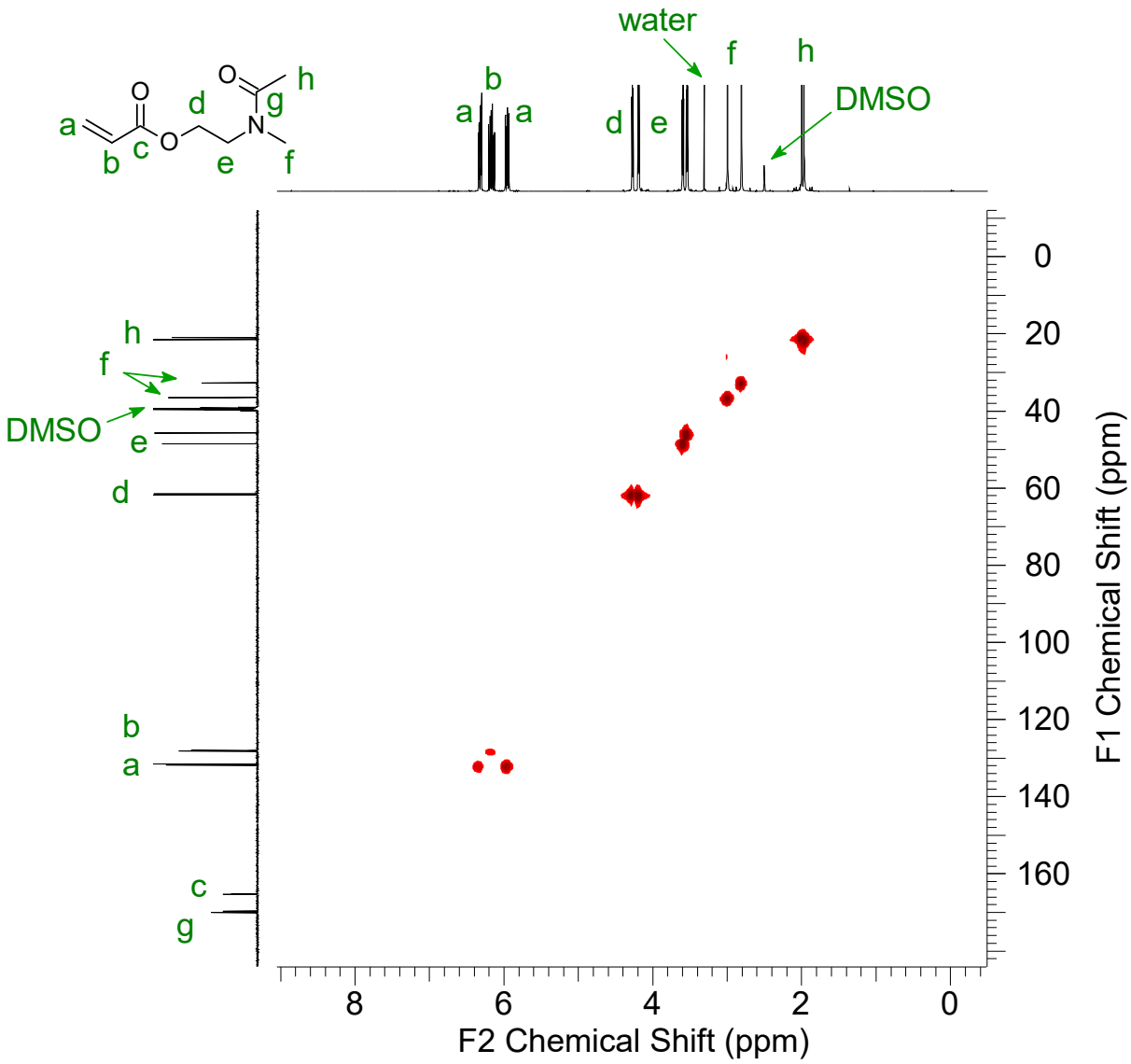

Figure 3.11. ^{1}H-^{13}C HMQC spectrum of 2-(*N*-methylacetamido)ethyl acrylate (NMAEA, in DMSO, 600 MHz for ^{1}H, 151 MHz for ^{13}C).

3.4.2 Preparation of 2-(*N*-methylacetamido)ethyl methacrylate (NMAEM)

To a mixture of NHEMA (22.12 g, ca. 189 mmol, 1 equiv., roughly purified before the flash column chromatography), triethylamine (21.04 g, 208 mmol, 1.1 equiv.), and 200 mL of anhydrous

DCM immersed in an ice-water bath, methacryloyl chloride (21.74 g, 208 mmol, 1.1 equiv.) was added dropwise over 15 min. After stirring overnight at rt, the white precipitate in the reaction mixture was filtered off by suction filtration and rinsed by diethyl ether. After removing the diethyl ether by an evaporator, 1.5 ‰ w/w high-temperature polymerization inhibitor BMH was added to the oily crude product, and then the crude product was purified by fractional vacuum distillation to obtain colorless NMAEM (bp = 65-69 °C at 0.08 Torr, 8.47g, yield: 24%).

HR-FAB-MS ($C_9H_{15}NO_3$): m/z^{exp} = 186.1144 (M + H), m/z^{theo} =186.1130 (M + H).

Because the preparation of the NMAEM was carried out with the raw NHEMA, there was a small fraction of impurity in the NMAEM. The impurity was the byproduct from the synthesis of NHEMA, which can be confirmed from the ^{1}H NMR spectrum (**Fig. 3.13**) of the byproduct isolated by the flash column chromatography purification of NHEMA.

^{1}H NMR (600 MHz, $CDCl_3$) δ_{ppm}: 1.95 (m, 3H, CH_2=CC*H*$_3$), 2.09 & 2.13 (s, 3H, COC*H*$_3$), 2.97 & 3.09 (s, 3H, NC*H*$_3$), 3.63 & 3.67 (t, 2H, *J* = 5.6 Hz, NC*H*$_2$CH$_2$), 4.29 (overlapped, 2H, OC*H*$_2$), 5.59 & 5.62 (quint, H, *J* = 1.5 Hz, C*H*$_2$=), 6.10 (m, H, C*H*$_2$=).

^{13}C NMR (151 MHz, $CDCl_3$) δ_{ppm}: 18.20 & 18.22 (CH_2=C*C*H$_3$), 21.2 & 21.7 (CO*C*H$_3$), 33.4 & 37.4 (N*C*H$_3$), 46.7 & 49.2 (N*C*H$_2$CH$_2$), 61.5 & 62.6 (O*C*H$_2$), 125.8 & 126.3 (*C*H$_2$=), 135.7 & 136.0 (CH_2=*C*CH$_3$), 167.0 & 167.1 (*C*OO), 170.7 & 170.9 (*C*ON).

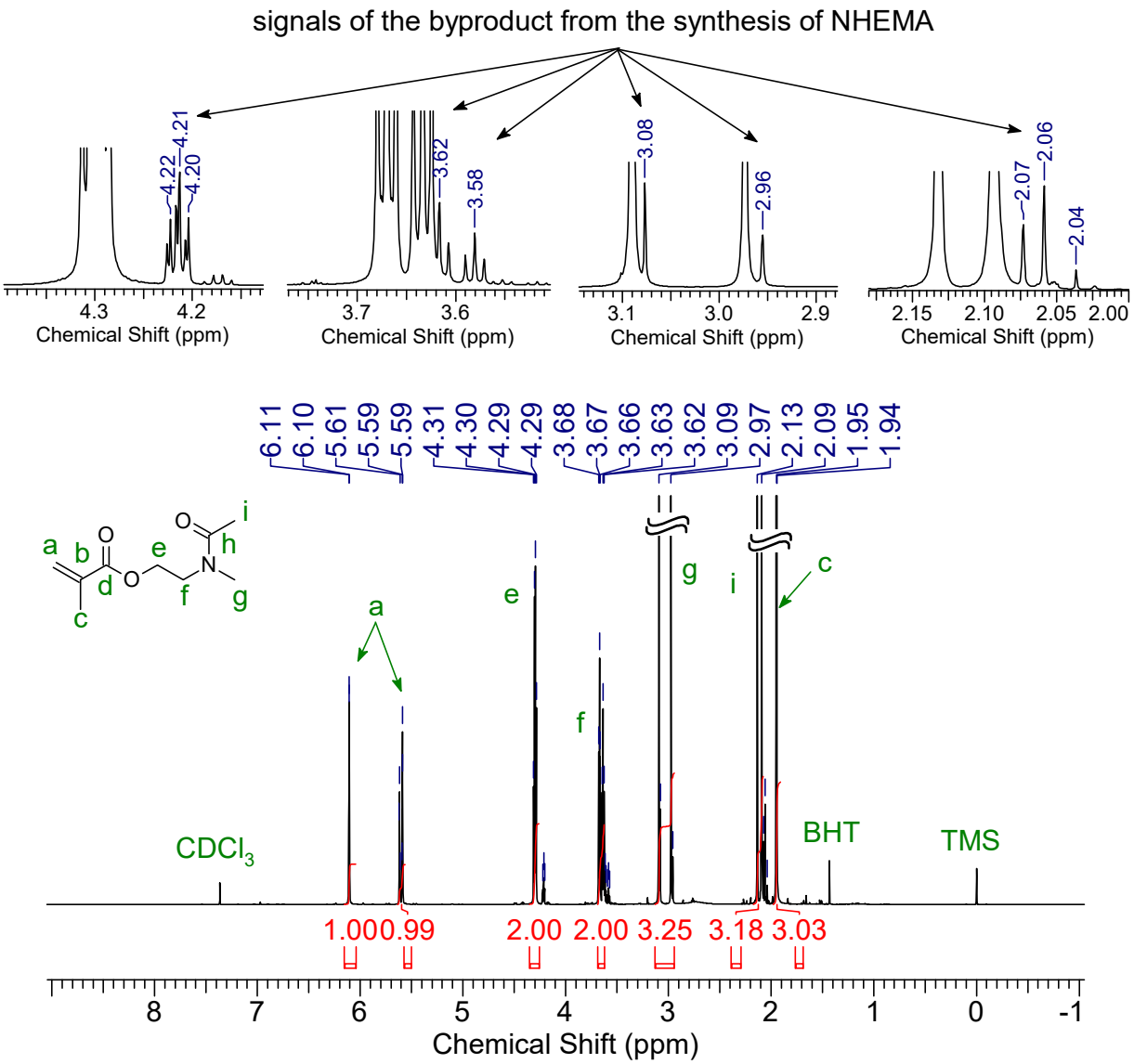

Figure 3.12. ^{1}H NMR spectrum of 2-(*N*-methylacetamido)ethyl methacrylate (NMAEM, in $CDCl_3$, 600 MHz).

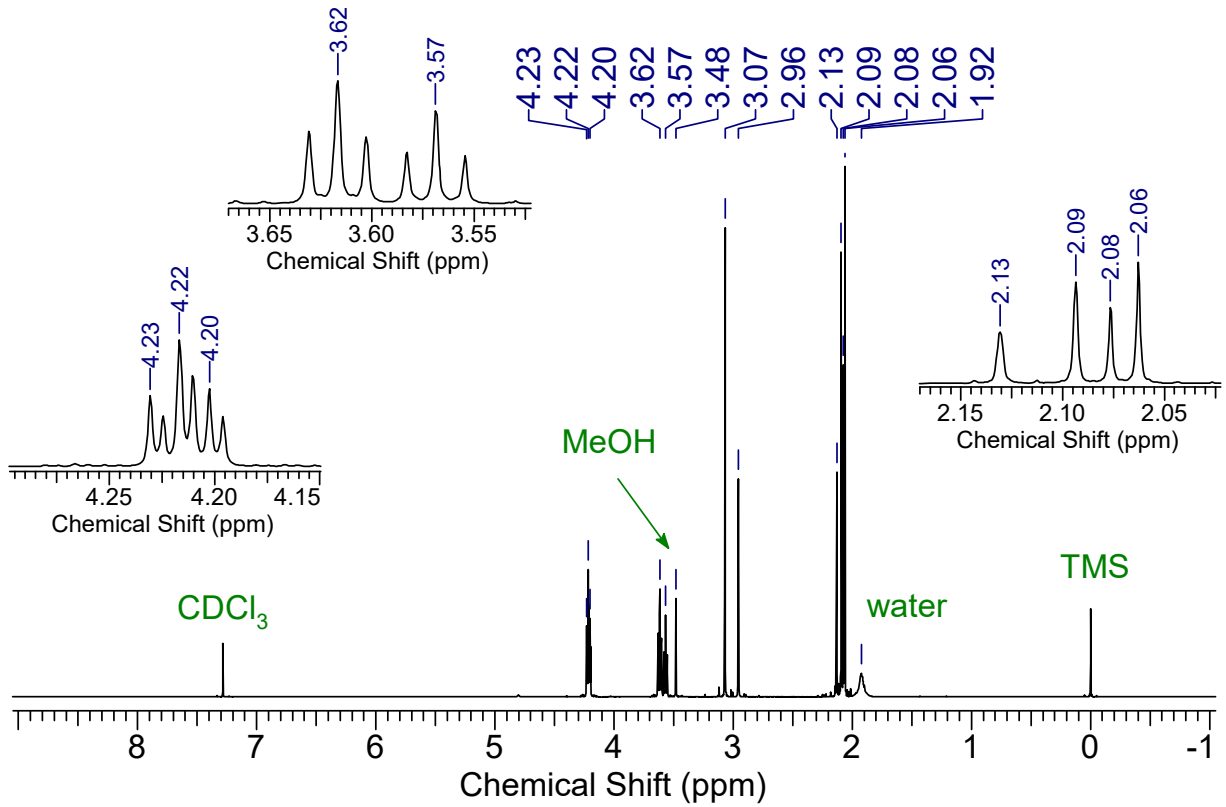

Figure 3.13. ^{1}H NMR spectrum of the byproduct separated from the synthesis of NHEMA (in $CDCl_3$, 400 MHz).

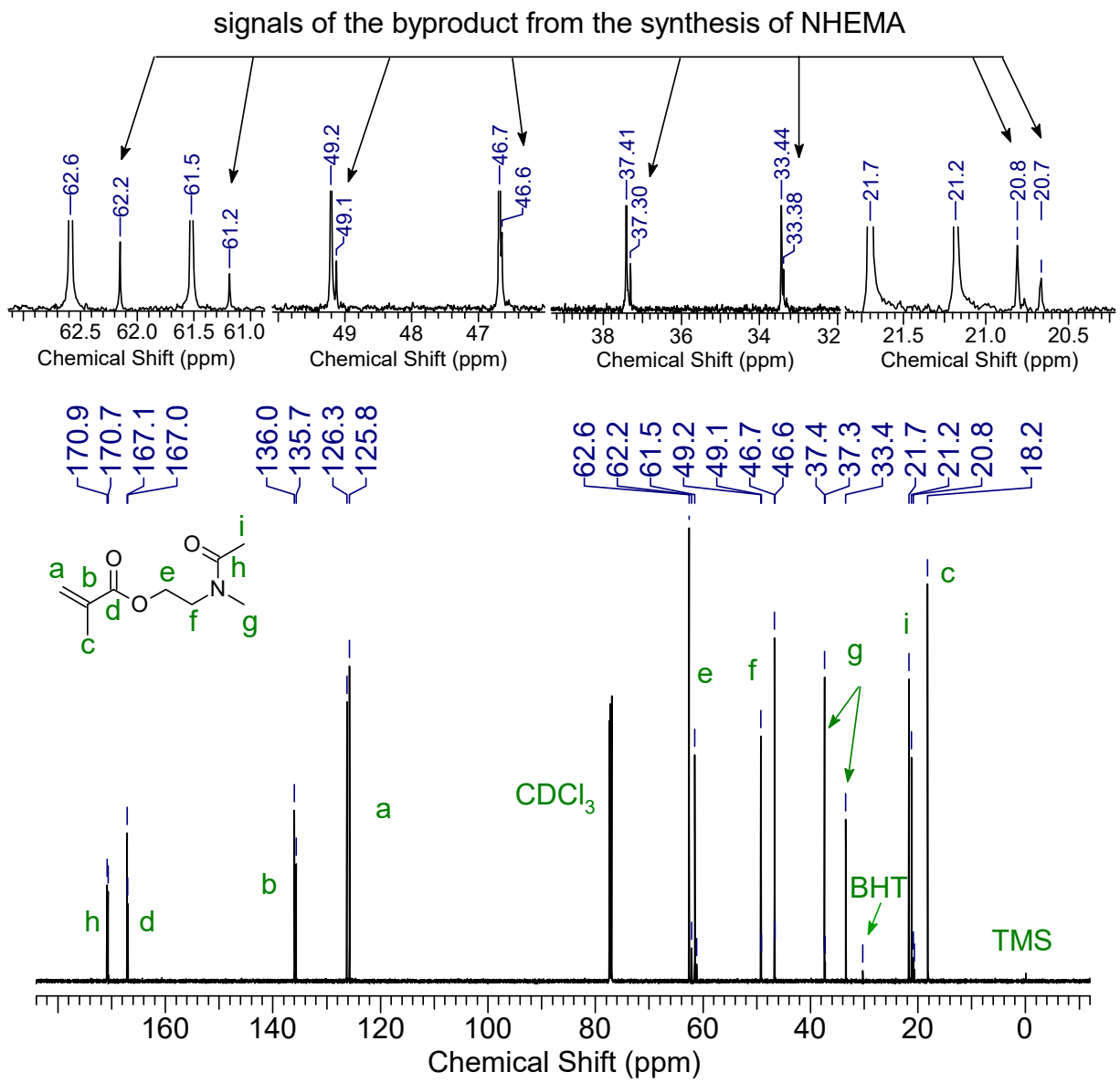

Figure 3.14. ^{13}C NMR spectrum of 2-(*N*-methylacetamido)ethyl methacrylate (NMAEM, in $CDCl_3$, 151 MHz).

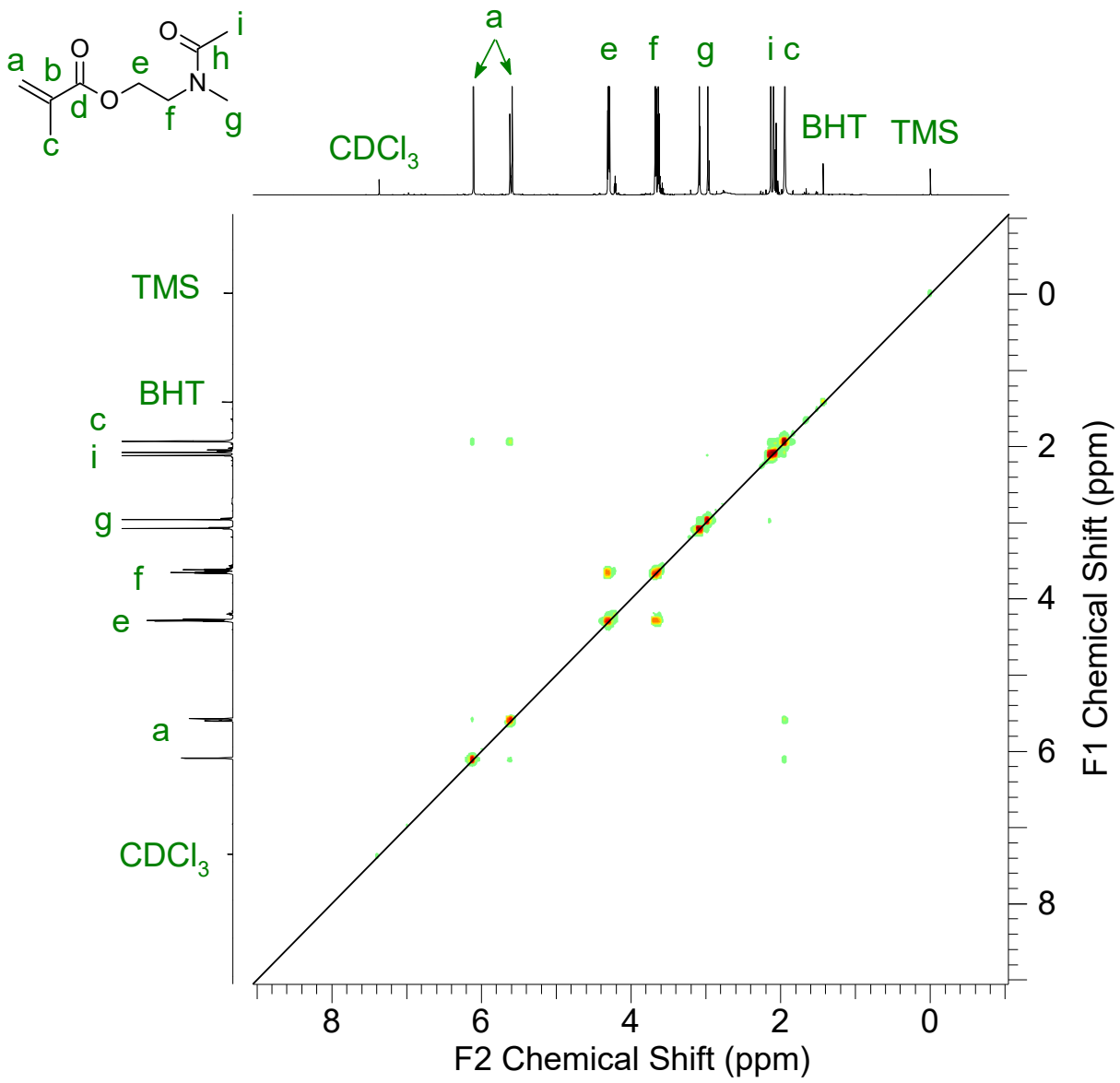

Figure 3.15. ^{1}H-^{1}H COSY spectrum of 2-(*N*-methylacetamido)ethyl methacrylate (NMAEM, in $CDCl_3$, 600 MHz).

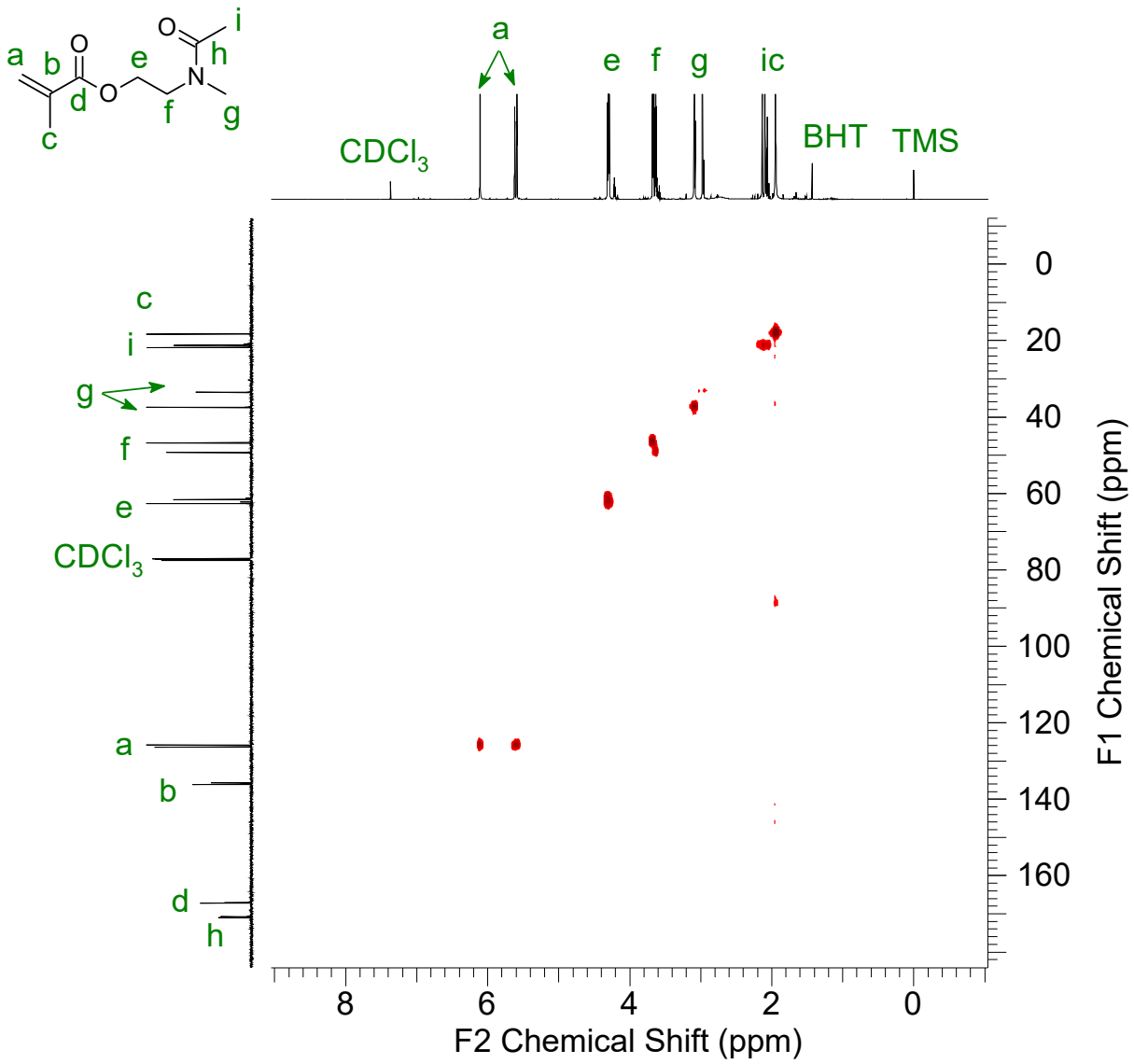

Figure 3.16. ^{1}H-^{13}C HMQC spectrum of 2-(*N*-methylacetamido)ethyl methacrylate (NMAEM, in $CDCl_3$, 600 MHz for ^{1}H, 151 MHz for ^{13}C).

3.4.3 Preparation of 2-(*N*-methylpropionamido)ethyl acrylate (NMPEA)

3.4.3.1 Preparation of *N*-(2-hydroxyethyl)-*N*-methylpropionamide (NHEMP)

Propionic anhydride (28.63 g, 220 mmol, 1.1 equiv.) was added dropwise to a suspension of neutral Al_2O_3 (30.59 g, 300 mmol, 1.5 equiv.) and 2-(methylamino)ethanol (15.02 g, 200 mmol, 1 equiv.) in an ice-water bath. The reaction mixture was stirred at rt. for 20 min. The Al_2O_3 was filtered off by suction filtration and further rinsed by DCM (500 mL). Ca. 6 mL water, as well as 4.5 g anhydrous K_2CO_3 were added to the filtrate. The mixture was stirred for another 15 min until the water layer became neutralized. Then, a large excess of anhydrous K_2CO_3 was added and stirred to remove the water. After filtering the solid and removing the DCM in the filtrate by rotary evaporator, the crude product was further purified by flash column chromatography (mobile phase: DCM/MeOH = 9.3:0.7). After removing the eluent, the NHEMP was obtained as a colorless liquid (17.02 g, yield: 65%).

HR-FAB-MS ($C_6H_{13}NO_2$): m/z^{exp} = 132.1041 (M + H), m/z^{theo} =132.1025 (M + H).

^{1}H NMR (600 MHz, D_2O) δ_{ppm}: 1.22 (overlapped, 3H, $COCH_2CH_3$), 2.58 (overlapped, 3H, $COCH_2CH_3$), 3.07 & 3.24 (s, 3H, NCH_3), 3.65 & 3.69 (t, 2H, J = 5.8 Hz, NCH_2CH_2), 3.85 & 3.90 (t, 2H, J = 5.6 Hz, OCH_2).

^{13}C NMR (151 MHz, D_2O) δ_{ppm}: 9.0 & 9.5 ($COCH_2CH_3$), 26.3 & 26.9 ($COCH_2CH_3$), 33.9 & 36.7 (NCH_3), 50.1 & 52.1 (NCH_2CH_2), 59.0 & 59.3 (OCH_2), 177.9 & 178.1 (CON).

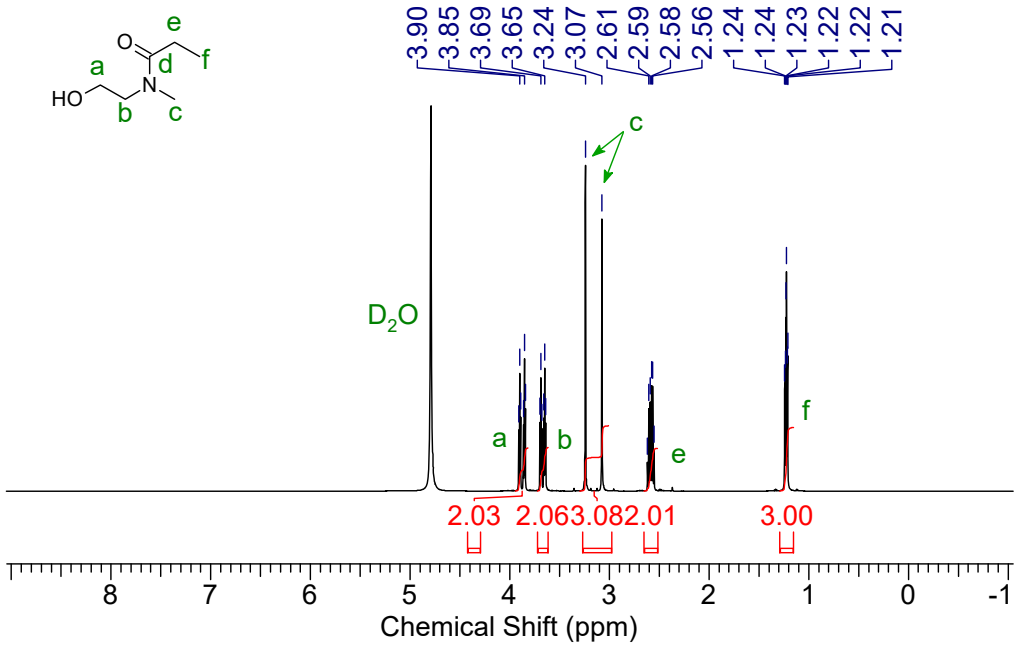

Figure 3.17. ^{1}H NMR spectrum of *N*-(2-hydroxyethyl)-*N*-methylpropionamide (NHEMP, in D_2O, 600 MHz).

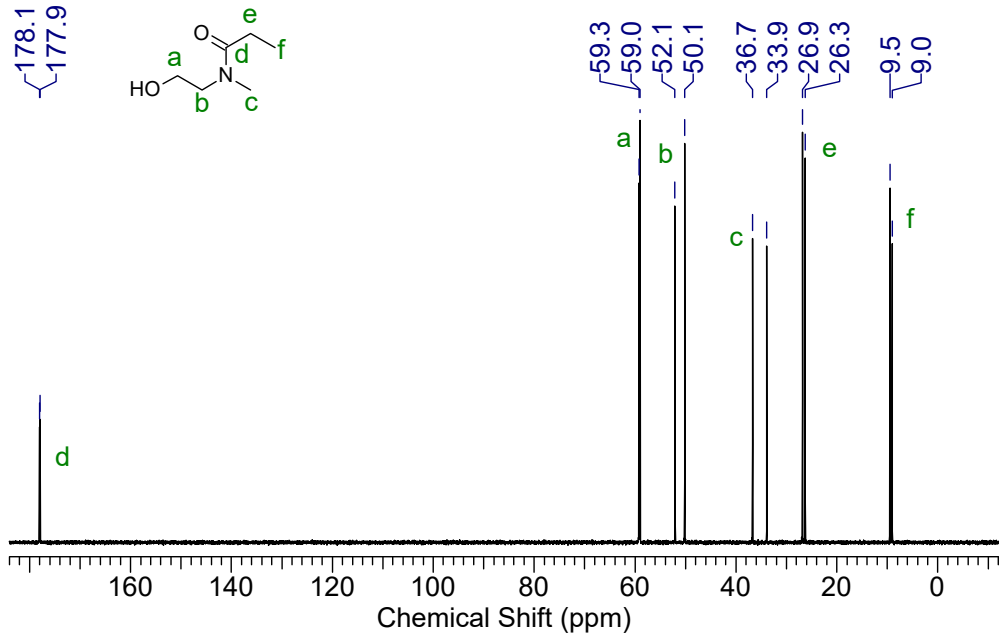

Figure 3.18. ^{13}C NMR spectrum of *N*-(2-hydroxyethyl)-*N*-methylpropionamide (NHEMP, in

D_2O, 151 MHz).

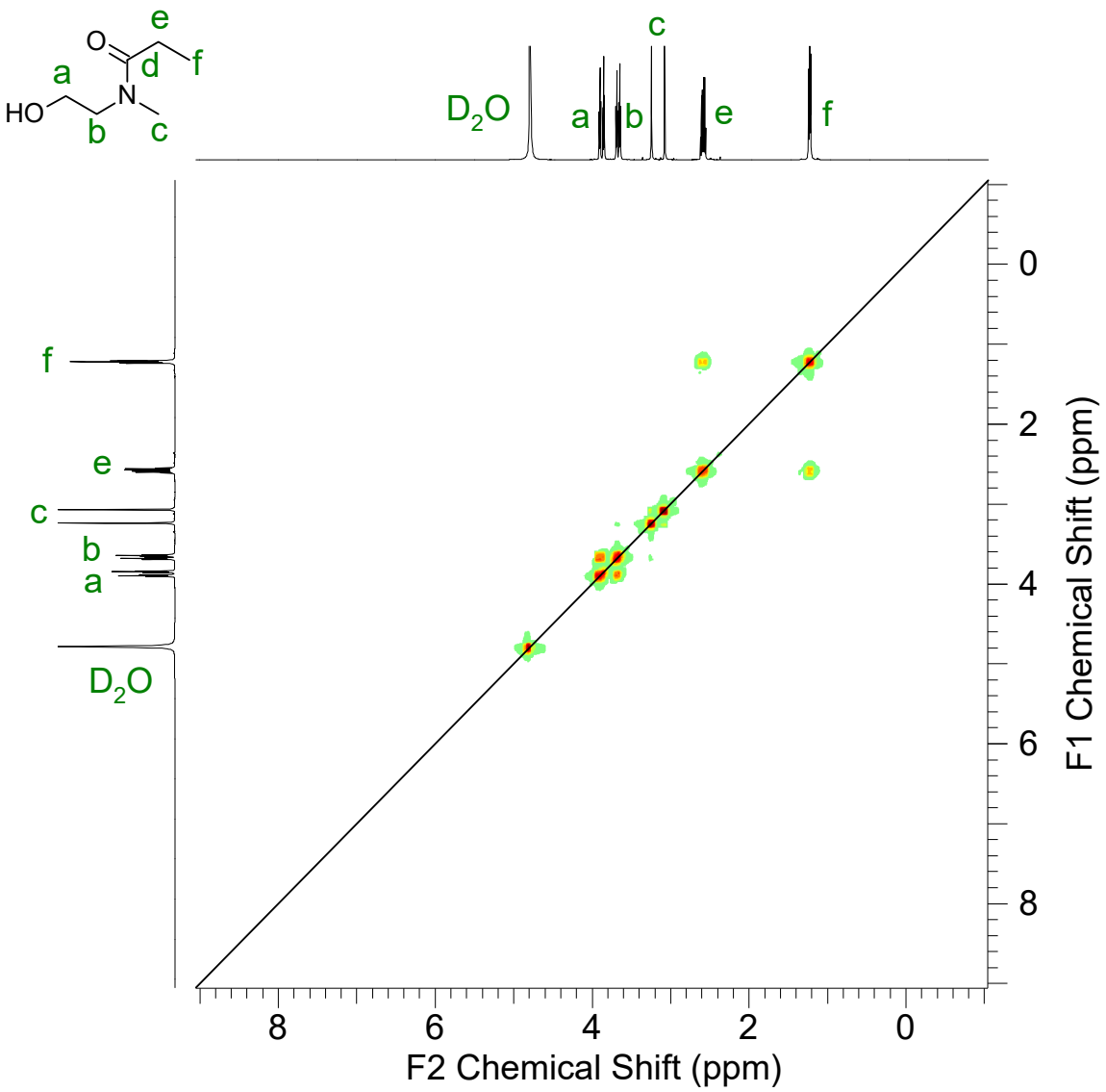

Figure 3.19. ^1H-^1H COSY spectrum of *N*-(2-hydroxyethyl)-*N*-methylpropionamide (NHEMP, in D_2O, 600 MHz).

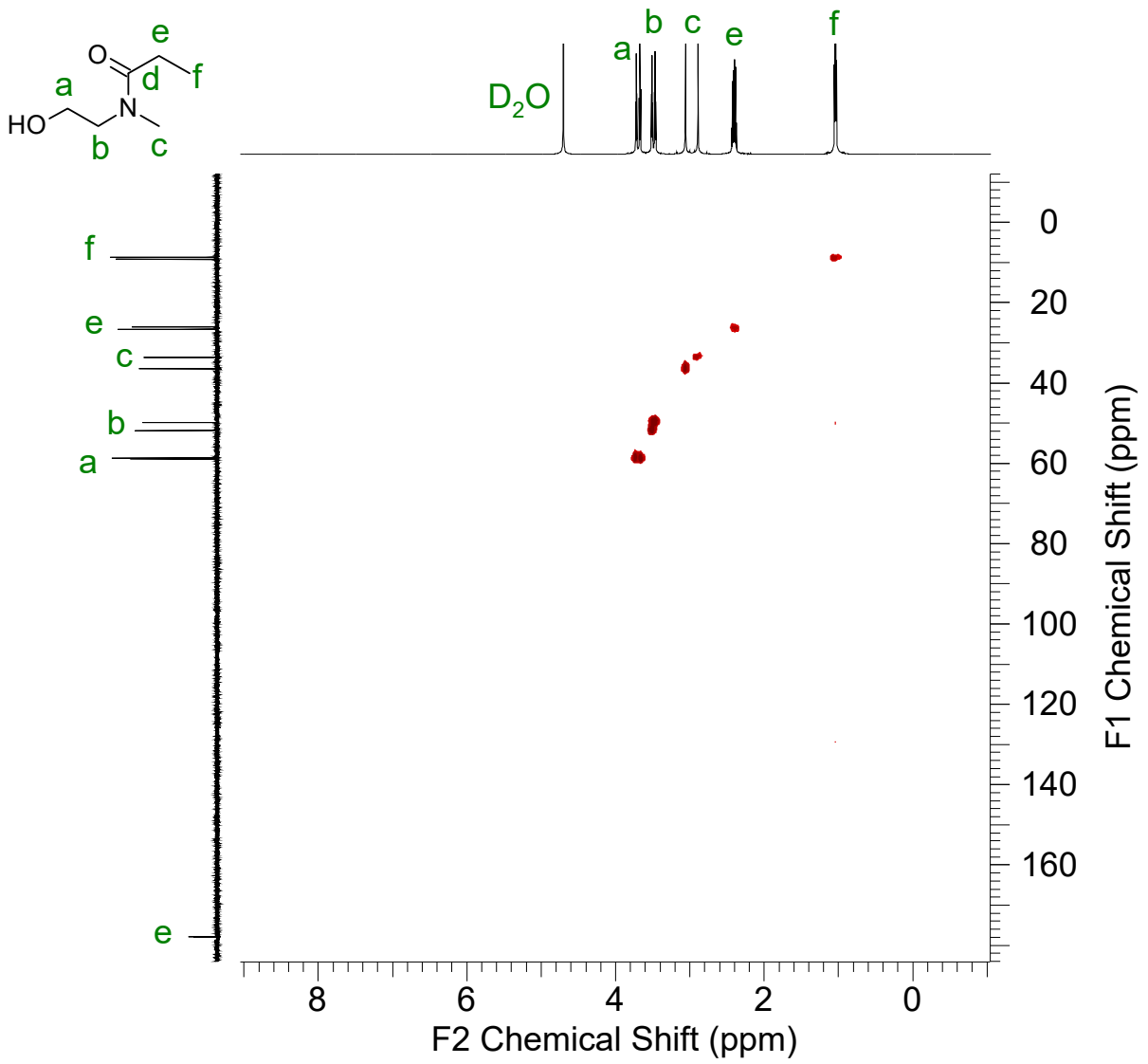

Figure 3.20. ^{1}H-^{13}C HMQC spectrum of *N*-(2-hydroxyethyl)-*N*-methylpropionamide (NHEMP, in D_2O, 600 MHz for ^{1}H, 151 MHz for ^{13}C).

3.4.3.2 Preparation of NMPEA

To a mixture of NHEMP (13.34 g, 102 mmol, 1 equiv.), triethylamine (11.33 g, 112 mmol, 1.1 equiv.), and 120 mL of anhydrous DCM immersed in an ice-water bath, acryloyl chloride (10.14 g, 112 mmol, 1.1 equiv.) was added dropwise over 15 min. The esterification reaction was stirred overnight at rt. Then the white precipitate in the reaction mixture was filtered off by suction filtration and rinsed by diethyl ether. After evaporating the diethyl ether in the filtrate, the oily crude product was then purified by fractional vacuum distillation. The main fraction (bp = 70 °C at 0.08Torr) was eluted by DCM through a short basic Al_2O_3 column to remove the residual acrylic acid. The NMPEA was finally obtained as a colorless liquid after the evaporation of DCM (8.3 g, yield: 44%).

HR-FAB-MS ($C_9H_{15}NO_3$): m/z^{exp} = 186.1156 (M + H), m/z^{theo} =186.1130 (M + H).

^{1}H NMR (600 MHz, $CDCl_3$) δ_{ppm}: 1.03 (m, 3H, $COCH_2CH_3$), 2.25 & 2.30 (q, 2H, *J* = 7.3 Hz, $COCH_2CH_3$), 2.89 & 2.99 (s, 3H, NCH_3), 3.58 (overlapped, 2H, NCH_2CH_2), 4.21 (overlapped, 2H, NCH_2CH_2), 5.76 & 5.79 (dd, H, *J* = 10.5, 1.5 Hz and 10.5, 1.1 Hz, CH_2=CH), 6.03 (m, H, CH_2=CH), 6.29 (dd, H, *J* = 17.3, 1.5 Hz, CH_2=CH).

^{13}C NMR (151 MHz, $CDCl_3$) δ_{ppm}: 8.7 & 9.1 ($COCH_2CH_3$), 25.6 & 26.2 ($COCH_2CH_3$), 33.2 & 36.1 (NCH_3), 46.5 & 47.8 (NCH_2CH_2), 61.0 & 62.0 (NCH_2CH_2), 127.4 & 127.9 (CH_2=CH), 130.8 & 131.1 (CH_2=CH), 165.2 & 165.4 (COO), 173.49 & 173.54 (CON).

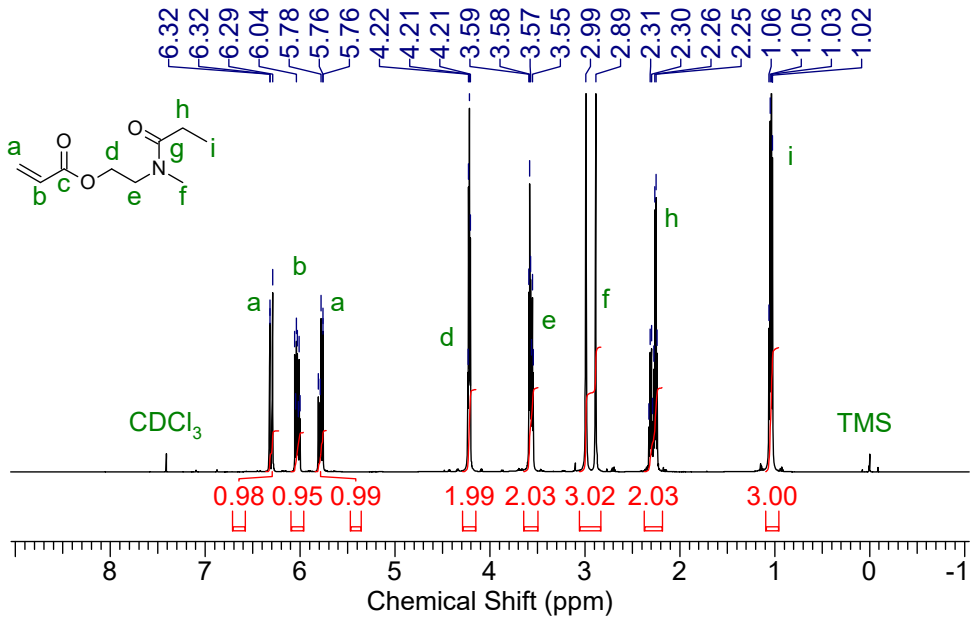

Figure 3.21. ^{1}H NMR spectrum of 2-(*N*-methylpropionamido)ethyl acrylate (NMPEA, in $CDCl_3$, 600 MHz).

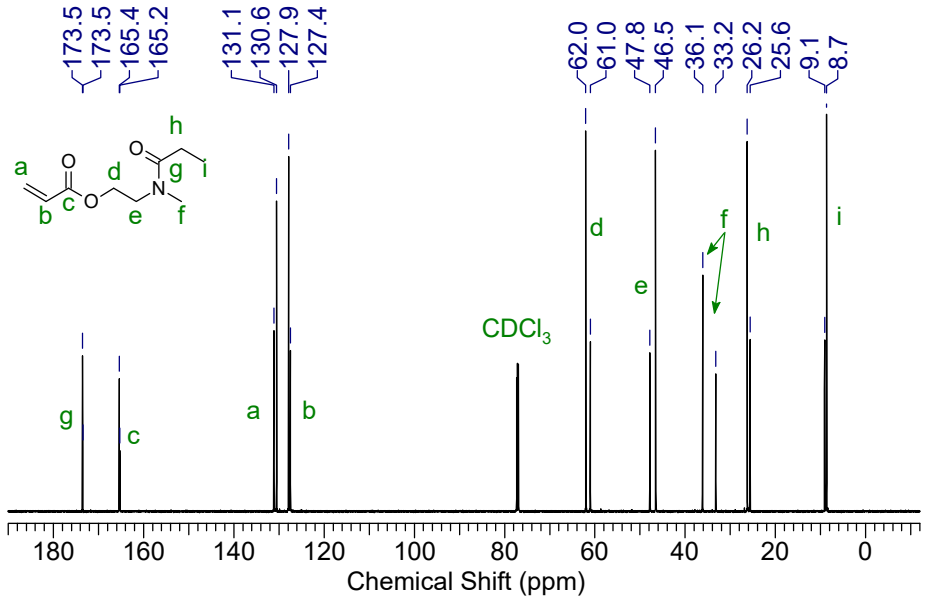

Figure 3.22. ^{13}C NMR spectrum of 2-(*N*-methylpropionamido)ethyl acrylate (NMPEA, in $CDCl_3$, 151 MHz).

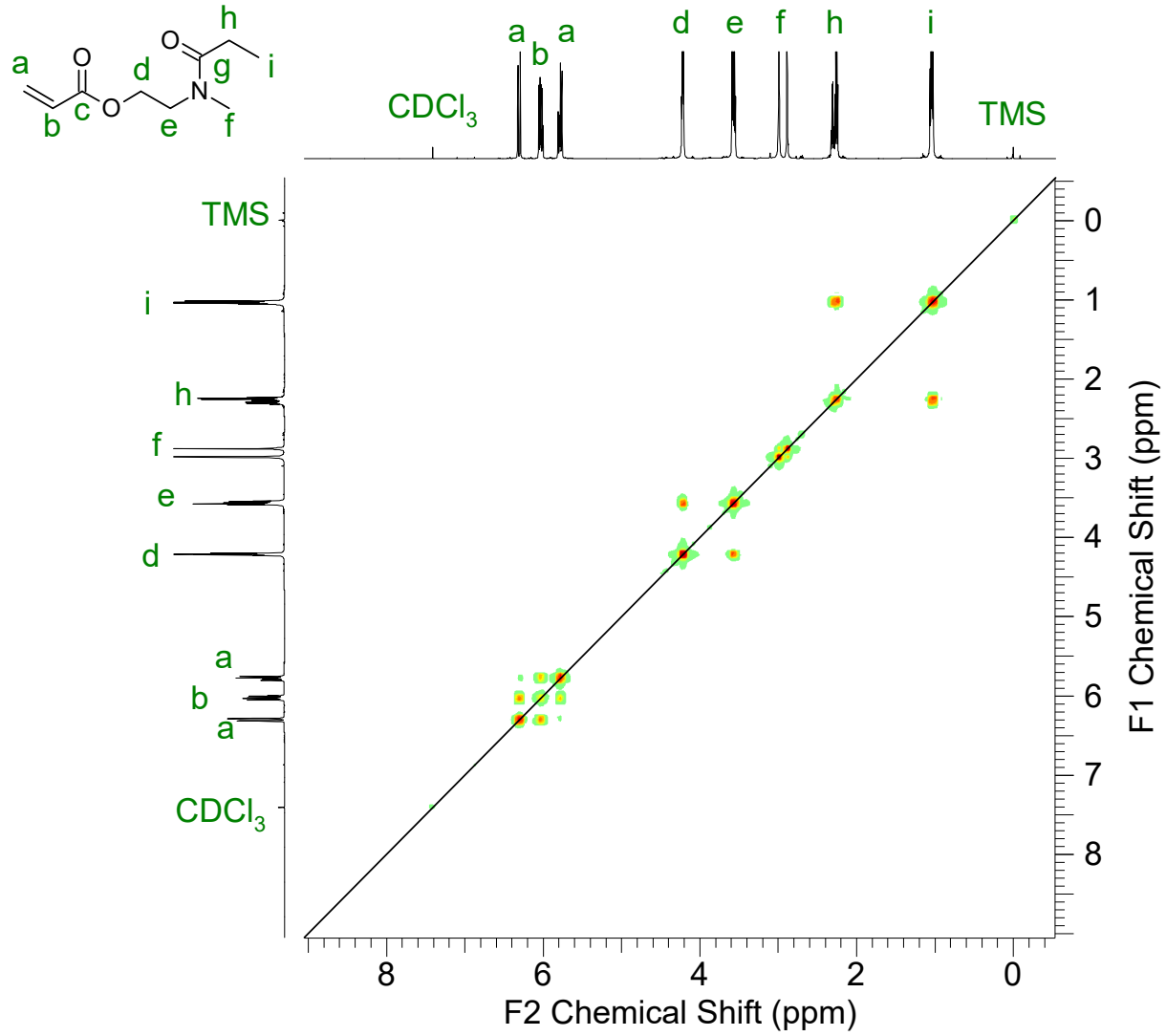

Figure 3.23. ^{1}H-^{1}H COSY spectrum of 2-(*N*-methylpropionamido)ethyl acrylate (NMPEA, in $CDCl_3$, 600 MHz).

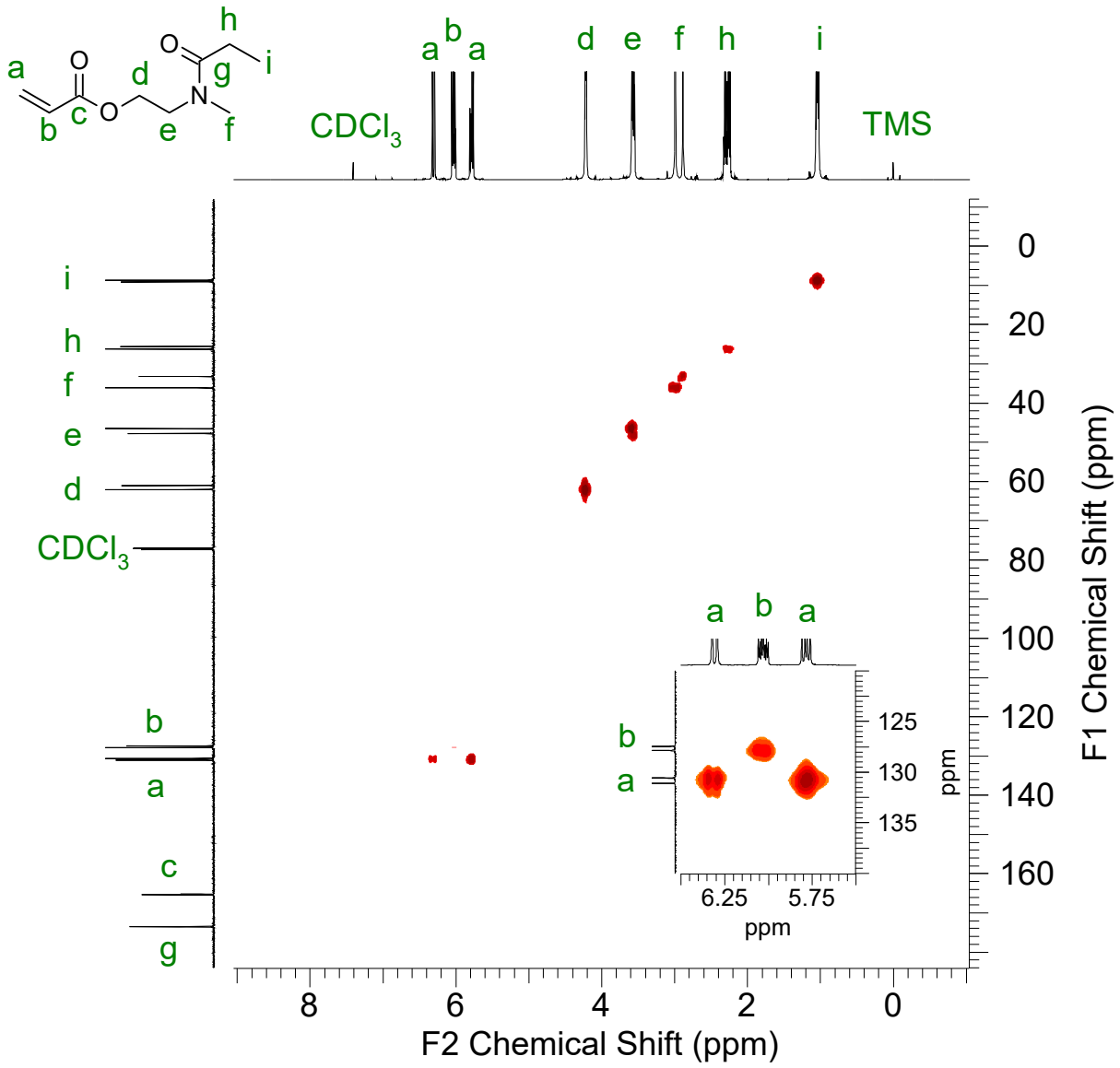

Figure 3.24. ^{1}H-^{13}C HMQC spectrum of 2-(*N*-methylpropionamido)ethyl acrylate (NMPEA in $CDCl_3$, 600 MHz for ^{1}H, 151 MHz for ^{13}C).

3.4.4 Preparation of 2-(*N*-ethylacetamido)ethyl acrylate (NEAEA)

3.4.4.1 *N*-ethyl-*N*-(2-hydroxyethyl)acetamide (NEHEA)

Acetic anhydride (33.69 g, 330 mmol, 1.1 equiv.) was added dropwise to a suspension of neutral Al_2O_3 (45.89 g, 450 mmol, 1.5 equiv.) and 2-(ethylamino)ethanol (26.74 g, 300 mmol, 1 equiv.) in an ice-water bath. The reaction mixture was stirred at rt for 20 min. The Al_2O_3 was filtered off by suction filtration and further rinsed by 500 mL DCM. Ca. 6 mL water, as well as 4.5 g anhydrous K_2CO_3 were added to the filtrate. The mixture was stirred for another 15 min until the water layer became neutralized. Then, a large excess of anhydrous K_2CO_3 was added and stirred to remove the water. After filtering the solid and removing the DCM in the filtrate by rotary evaporator, the crude product was further purified by flash column chromatography (mobile phase: DCM/MeOH = 9:1). After removing the eluent, the NEHEA was obtained as a colorless liquid (29.5 g, yield: 75%).

HR-FAB-MS ($C_6H_{13}NO_2$): m/z^{exp} = 132.0998 (M + H), m/z^{theo} = 132.1025 (M + H).

^{1}H NMR (600 MHz, D_2O) δ_{ppm}: 1.14 & 1.23 (t, 3H, *J* = 7.3 Hz, NCH_2CH_3), 2.17 & 2.18 (s, 3H, $COCH_3$), 3.40-3.57 (overlapped, 4H, CH_2NCH_2), 3.75 & 3.80 (t, 2H, *J* = 5.8 Hz and 6 Hz, NCH_2CH_2).

^{13}C NMR (600 MHz, D_2O) δ_{ppm}: 11.3 & 12.2 (NCH_2CH_3), 19.9 & 20.4 ($COCH_3$), 40.6 & 44.3 (NCH_2CH_3), 47.0 & 49.7 (NCH_2CH_2), 58.5 & 58.6 (NCH_2CH_2), 173.4 & 173.5 (*C*OO).

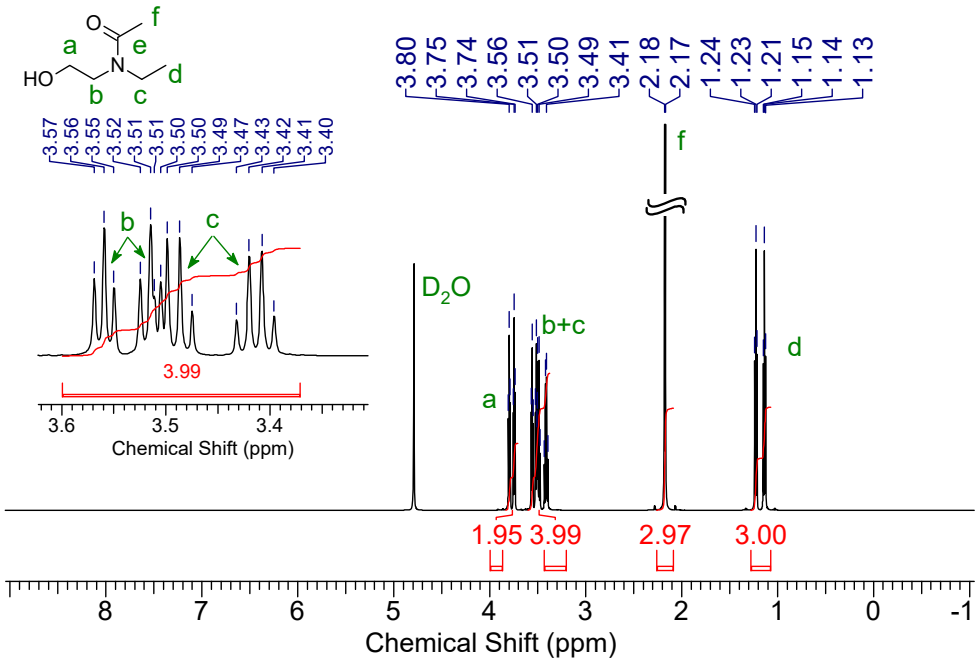

Figure 3.25. ^{1}H NMR spectrum of *N*-ethyl-*N*-(2-hydroxyethyl)acetamide (NEHEA, in D_2O, 600 MHz).

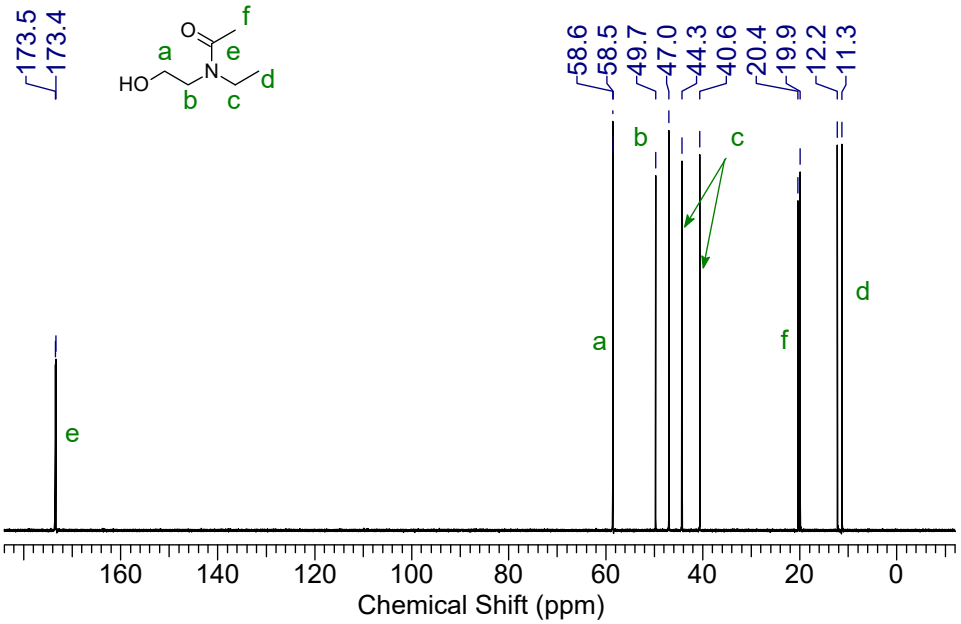

Figure 3.26. ^{13}C NMR spectrum of *N*-ethyl-*N*-(2-hydroxyethyl)acetamide (NEHEA, in D_2O, 600 MHz).

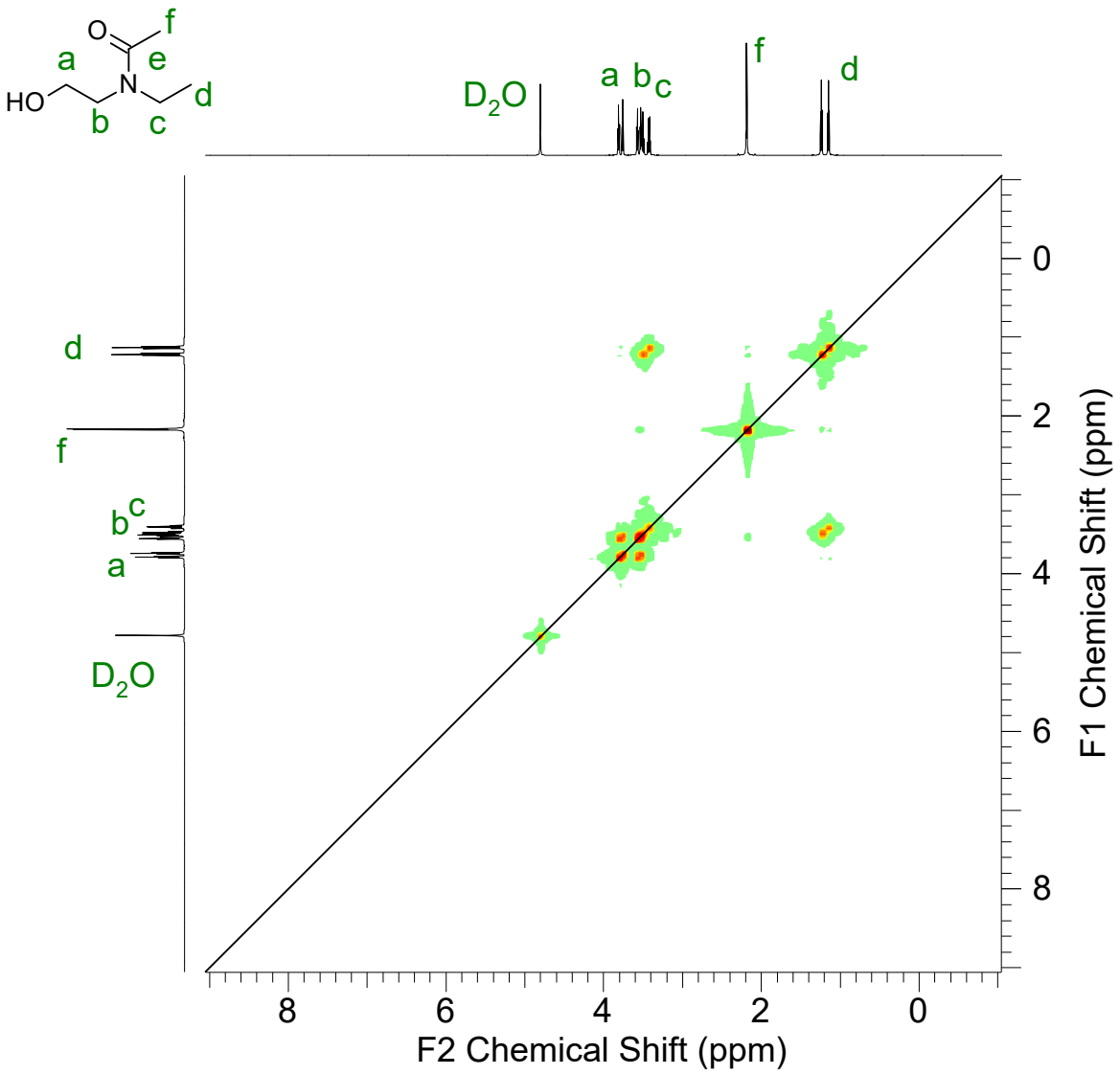

Figure 3.27. ^{1}H-^{1}H COSY spectrum of *N*-ethyl-*N*-(2-hydroxyethyl)acetamide (NEHEA, in D_2O, 600 MHz).

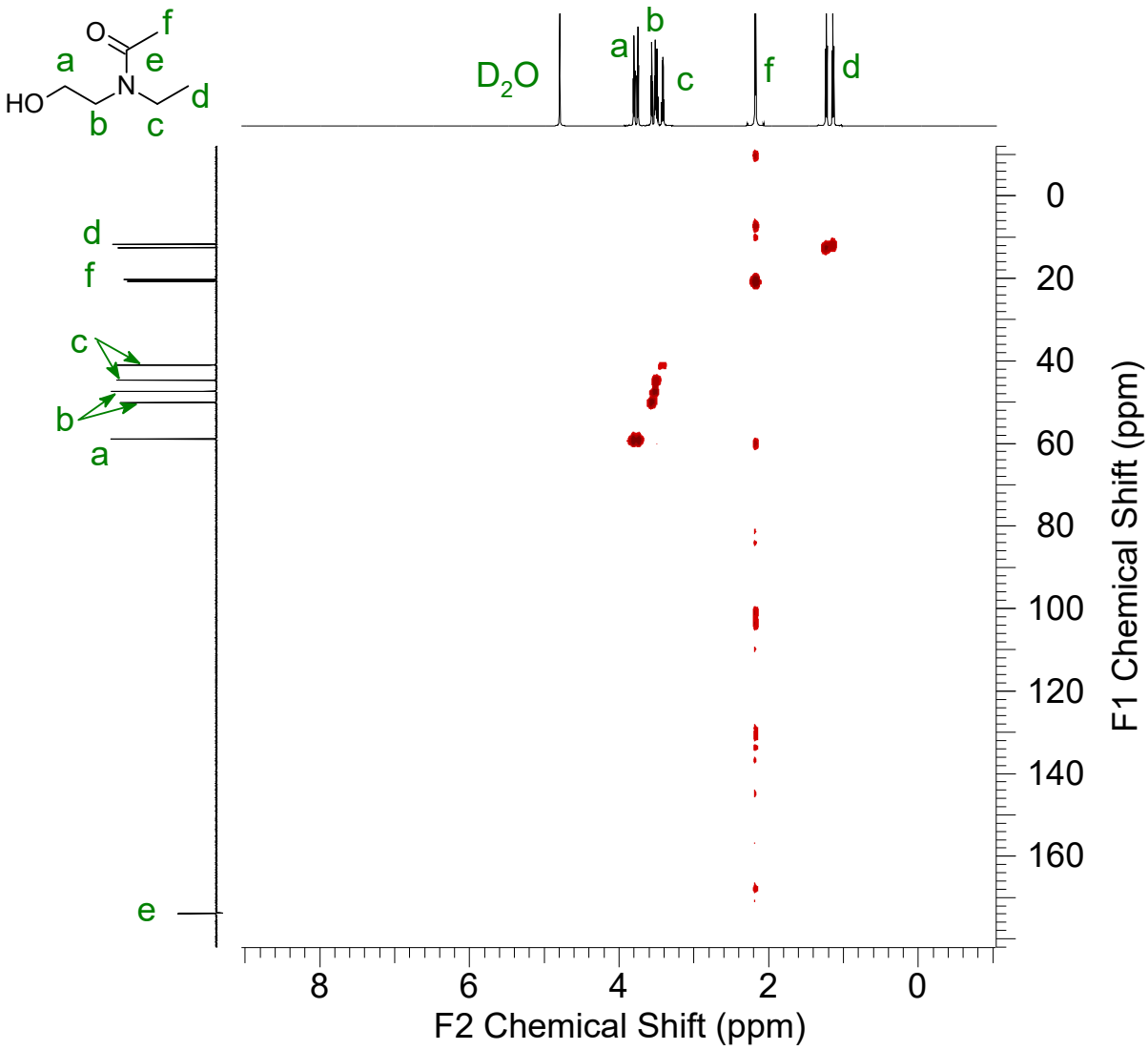

Figure 3.28. ^{1}H-^{13}C HMQC spectrum of *N*-ethyl-*N*-(2-hydroxyethyl)acetamide (NEHEA, in D_2O, 600 MHz for ^{1}H, 151 MHz for ^{13}C).

3.4.4.2 Preparation of NEAEA

To a mixture of NEHEA (12.49 g, 95.2 mmol, 1 equiv.), triethylamine (10.62 g, 105 mmol, 1.1 equiv.), and 130 mL of anhydrous DCM immersed in an ice-water bath, acryloyl chloride (9.50 g, 105 mmol, 1.1 equiv.) was added dropwise over 15 min. The esterification reaction was stirred overnight at rt. Then the white precipitate in the reaction mixture was filtered off by suction filtration and rinsed by diethyl ether. After filtering the solid and removing the DCM in the filtrate by rotary evaporator, the oily crude product was then purified by fractional vacuum distillation. The main fraction (bp = 65-67 °C at 0.08 Torr) was eluted by DCM through a short basic Al_2O_3 column to remove the residual acrylic acid. The NEAEA was finally obtained as a colorless liquid after the evaporation of DCM (16.31, yield: 93%).

HR-FAB-MS ($C_9H_{15}NO_3$): m/z^{exp} = 186.1131 (M + H), m/z^{theo} = 186.1130 (M + H).

^{1}H NMR (600 MHz, $CDCl_3$) δ_{ppm}: 1.13 & 1.20 (t, 3H, J = 7.0 Hz and 7.2 Hz, NCH_2CH_3), 2.11 & 2.12 (s, 3H, $COCH_3$), 3.39 & 3.42 (q, 2H, J = 7.3 Hz, NCH_2CH_3), 3.61 (overlapped, 2H, NCH_2CH_2), 4.31 (overlapped, 2H, NCH_2CH_2), 5.85 & 5.88 (dd, H, J = 10.5, 1.5 Hz and J = 10.5, 1.1 Hz, CH_2=CH), 6.13 (m, H, CH_2=CH), 6.39 & 6.42 (dd, H, J = 9, 1.4 Hz, CH_2=CH).

^{13}C NMR (600 MHz, $CDCl_3$) δ_{ppm}: 12.8 & 14.0 (NCH_2CH_3), 21.3 & 21.6 ($COCH_3$), 40.7 & 44.5 (NCH_2CH_3), 44.5 & 46.7 (NCH_2CH_2), 61.8 & 62.4 (NCH_2CH_2), 127.8 & 128.2 (CH_2=CH), 131.0 & 131.6 (CH_2=CH), 165.7 & 165.9 (COO), 170.2 & 170.5 (CON).

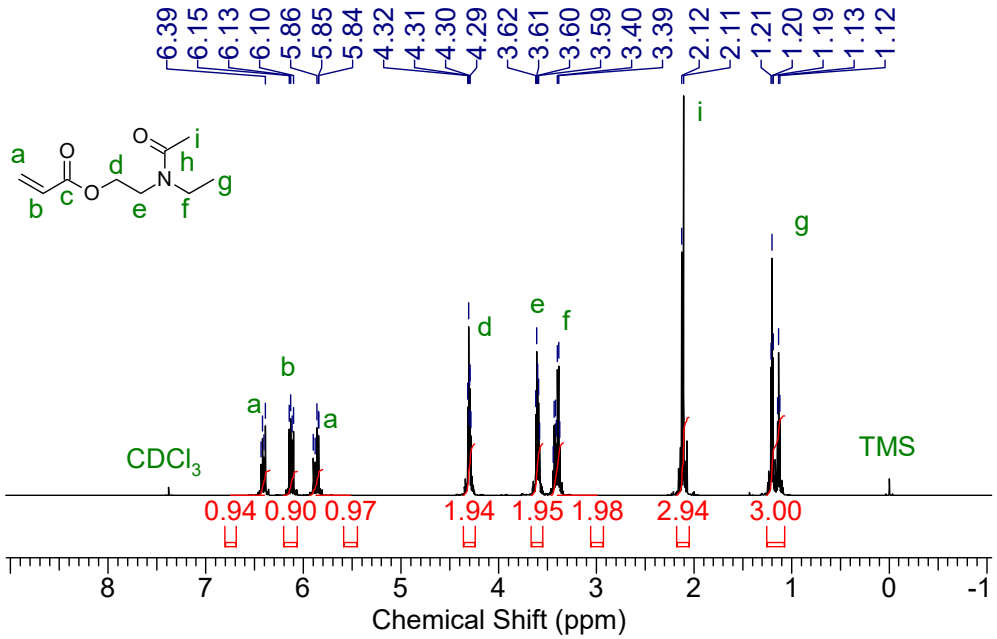

Figure 3.29. ^{1}H NMR spectrum of 2-(*N*-ethylacetamido)ethyl acrylate (NEAEA, in $CDCl_3$, 600 MHz).

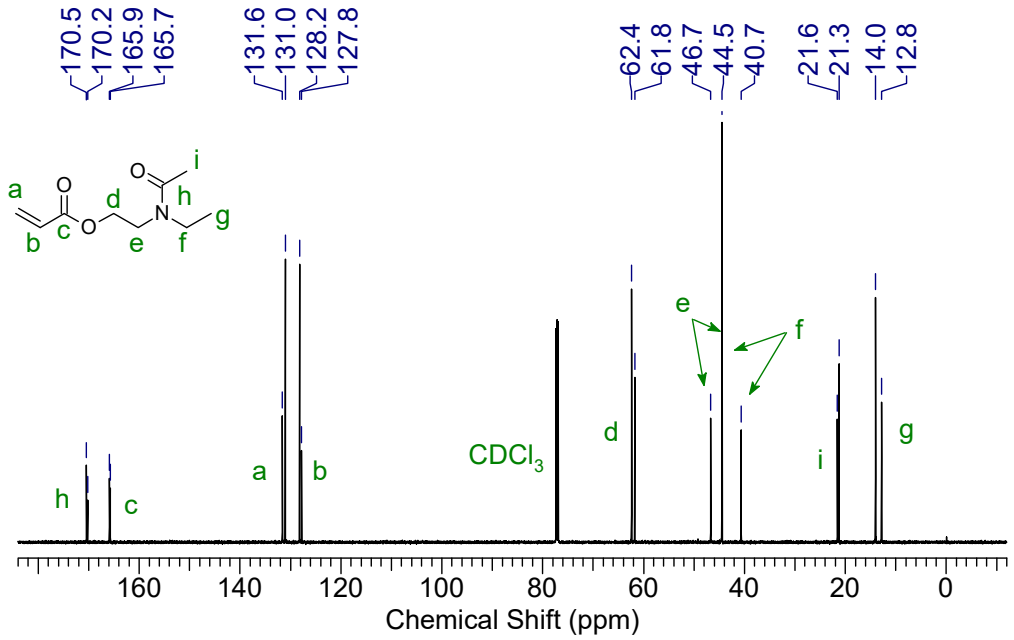

Figure 3.30. ^{13}C NMR spectrum of 2-(*N*-ethylacetamido)ethyl acrylate (NEAEA, in $CDCl_3$, 151 MHz).

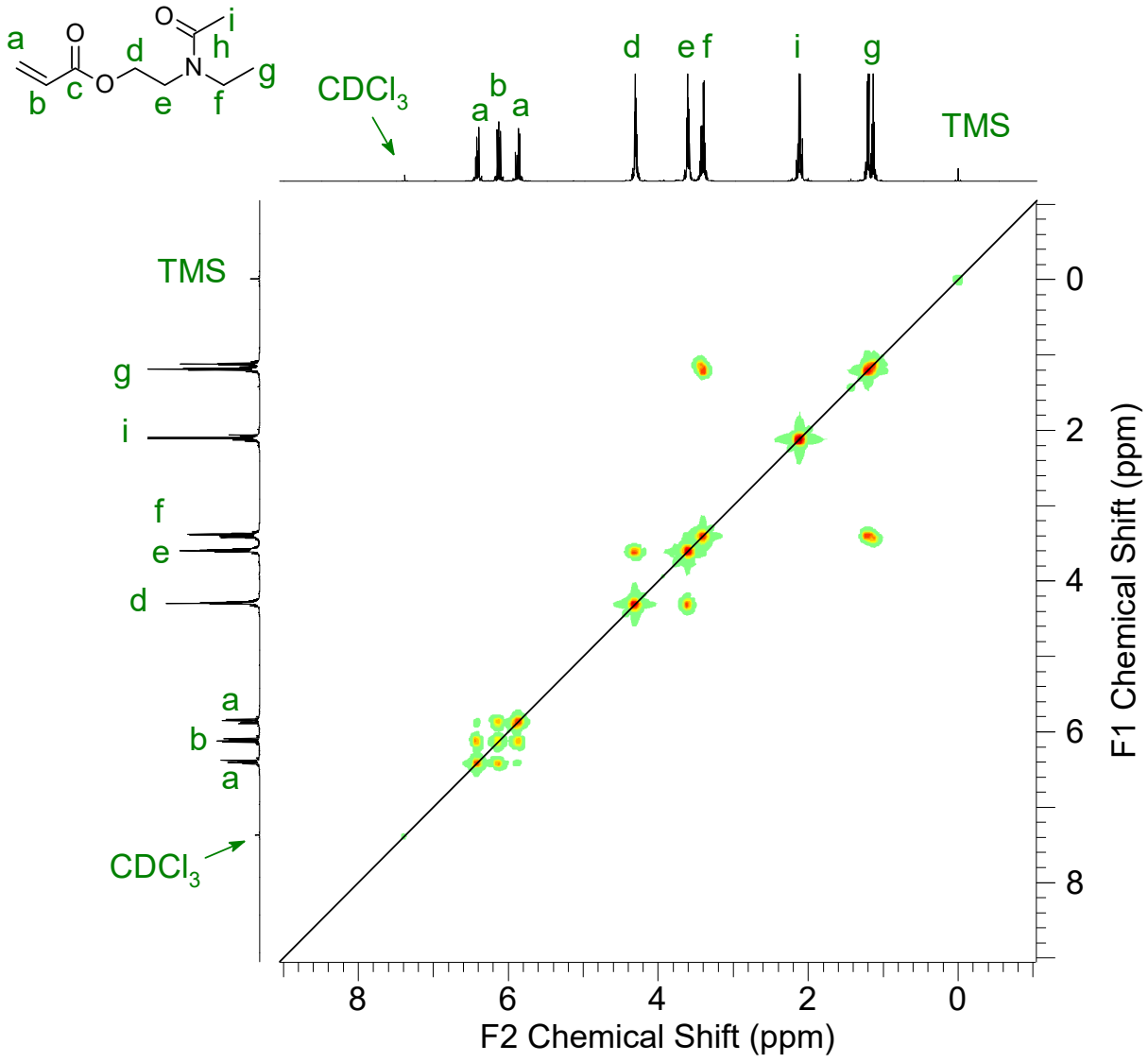

Figure 3.31. ^{1}H-^{1}H COSY spectrum of 2-(*N*-ethylacetamido)ethyl acrylate (NEAEA, in $CDCl_3$, 600 MHz).

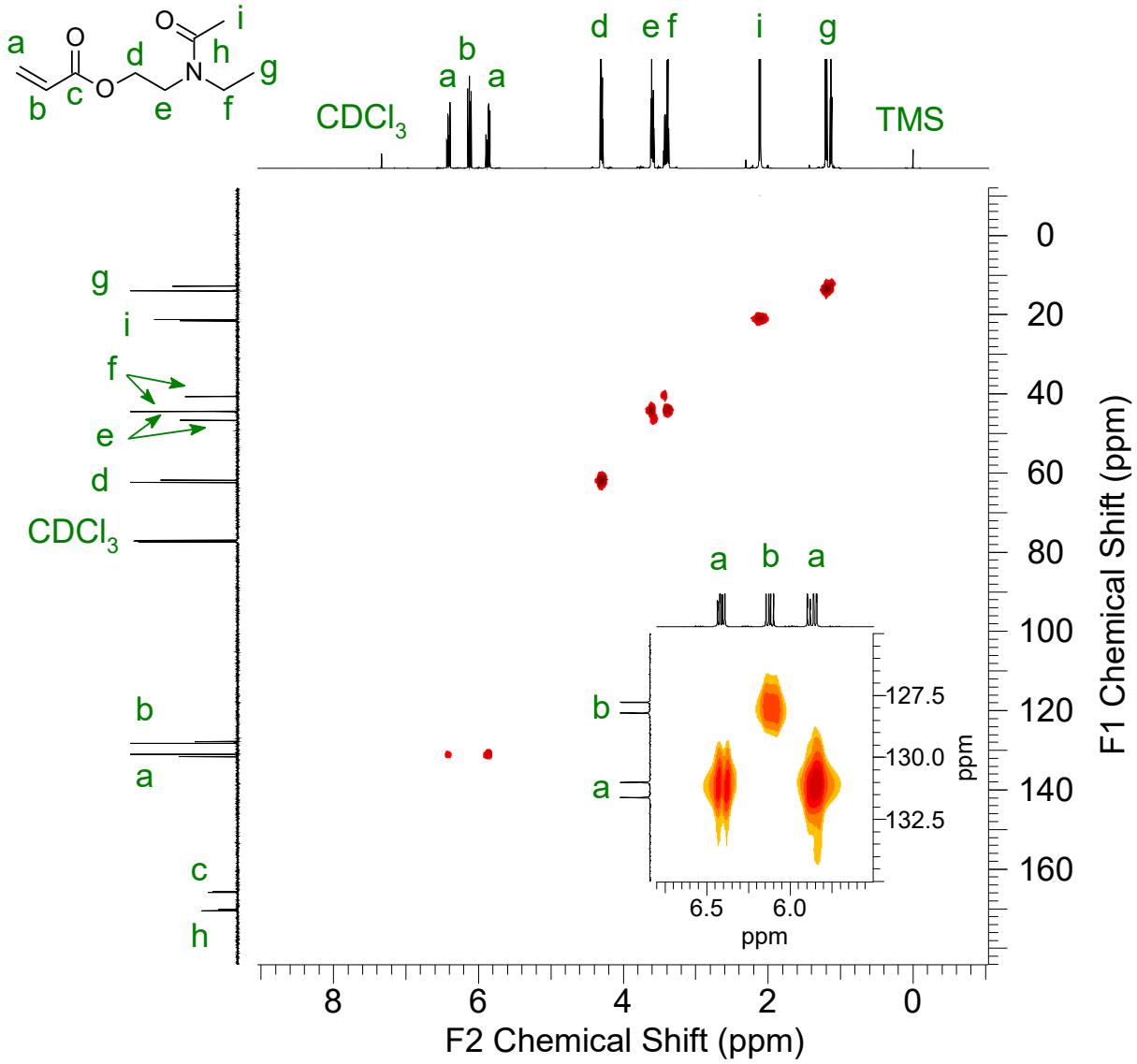

Figure 3.32. ^{1}H-^{13}C HMQC spectrum of 2-(*N*-ethylacetamido)ethyl acrylate (NEAEA, in $CDCl_3$, 600 MHz for ^{1}H, 151 MHz for ^{13}C).

3.5 Preparation of polymers

3.5.1 Preparation of homopolymers

The homopolymerization of tertiary amide monomers followed a similar procedure (illustrated in **Figure 3.2**). Hence, the preparation of PAEA is described as an example.

NMAEA (3.00 g, 17.52 mmol) and 2,2'-azobis(isobutyronitrile) (AIBN) (3.00 mg, 18.27 μmol) were stirred with 1,4-dioxane (12.0 g, 136.20 mmol) at rt. and the system was purged by N_2 continuously for half an hour. Then the reaction was heated up to 75 °C for 15.5 h until the mixture became visually viscous. After the 1,4-dioxane was removed by an evaporator, the crude polymer was dissolved in deionized water and dialyzed (MWCO = 6-8 kg mol^{-1}) against deionized water for 2 days. The PAEA was finally dried from lyophilization to yield a highly viscous solid (2.58 g, yield: 86%).

The conversion, reaction time, yield, M_n, and M_w/M_n of each homopolymer are summarized in **Table 3.1**. The GPC trace of each homopolymer is shown in **Figure 3.33**.

Table 3.1. Conversion, Reaction Time, Yield, M_n, and M_w/M_n of Synthesized Homopolymers

Polymer	Conv. [%][a]	Reaction time [h][b]	Yield [%]	M_n [kg mol^{-1}][c]	M_w/M_n[c]
PAEA	99	15.5	86	29	3.3
PAEM	94	6	39	12	1.9
PPEA	91	19.5	87	20	2.9
PEAE	96	24	77	18	3.0

[a]Determined by NMR. [b]The reaction was stopped when the polymerization solution became

visually viscous. [c]The molecular weight of homopolymers was determined by GPC using PMMA standards in DMF at 40 °C.

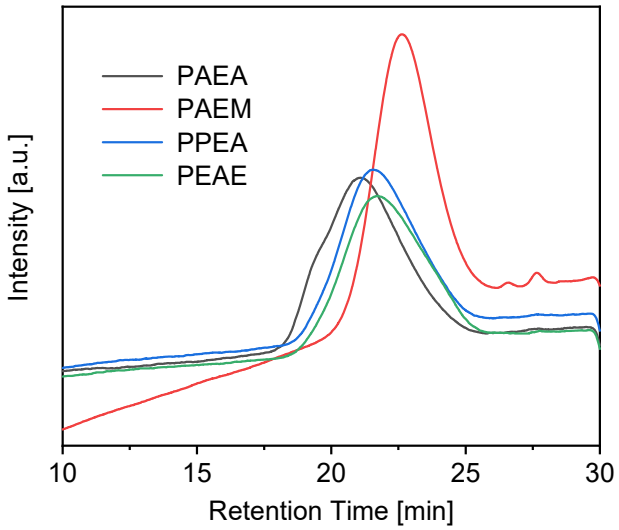

Figure 3.33. SEC traces of PAEA, PAEM, PPEA, and PEAE.

The chemical shift of NMR spectra and NMR spectra of all homopolymers are depicted as follows.

Poly[2-(*N*-methylacetamido)ethyl acrylate] (PAEA):

^{1}H NMR (600 MHz, D_2O) δ_{ppm}: 1.66-1.99 (m, 2H, C*H*$_2$CHCO), 2.18-2.22 (m, 3H, OCC*H*$_3$), 2.39 (br, H, CH$_2$C*H*CO), 2.99 & 3.17 (s, 3H, NC*H*$_3$), 3.69-3.78 (m, 2H, NC*H*$_2$CH$_2$), 4.27-4.32 (m, 2H, NCH$_2$C*H*$_2$).

^{13}C NMR (101 MHz, D_2O) δ_{ppm}: 20.7 & 21.1 (OC*C*H$_3$), 33.5-37.1 (N*C*H$_3$ and *C*H$_2$CHCO), 41.7 (CH$_2$*C*HCO), 46.4 & 49.1 (N*C*H$_2$CH$_2$), 62.6 (NCH$_2$*C*H$_2$), 173.7 & 174.1 (*C*ON), 175.6 (*C*OO).

Poly[2-(*N*-methylacetamido)ethyl methacrylate] (PAEM):

^{1}H NMR (600 MHz, D_2O) δ_{ppm}: 0.87-1.07 (m, 3H, CH_2CCH_3), 1.29-1.94 (m, 2H, CH_2CCH_3), 2.24 (s, 3H, $COCH_3$), 2.99-3.21 (m, 3H, NCH_3), 3.75-3.83 (m, 2H, NCH_2CH_2), 4.19 (m, 2H, NCH_2CH_2).

^{13}C NMR (101 MHz, D_2O) δ_{ppm}: 16.6 & 18.6 (CH_2CCH_3), 20.8 & 21.2 ($COCH_3$), 33.3 & 37.3 (NCH_3), 44.5 (CH_2CCH_3), 46.1 & 48.6 (NCH_2CH_2), 53.9 (CH_2CCH_3), 63.1 (NCH_2CH_2), 173.8 & 174.1 (CON), 178.0 & 179.0 (COO).

Poly[2-(*N*-methylpropionamido)ethyl acrylate] (PPEA):

^{1}H NMR (600 MHz, D_2O) δ_{ppm}: 1.14 (m, 3H, $COCH_2CH_3$), 1.64-1.97 (m, 2H, CH_2CHCO), 2.39-2.48 (m, 3H, CH_2CHCO and $COCH_2CH_3$), 3.00 & 3.18 (s, 3H, NCH_3), 3.71-3.78 (m, 2H, NCH_2CH_2), 4.27-4.31 (m, 2H, NCH_2CH_2).

^{13}C NMR (101 MHz, D_2O) δ_{ppm}: 8.9 & 9.4 ($COCH_2CH_3$), 26.1 & 26.6 ($COCH_2CH_3$), 33.6-36.4 (NCH_3 and CH_2CHCO), 41.5 (CH_2CHCO), 46.6 & 48.2 (NCH_2CH_2), 62.8 (NCH_2CH_2), 175.3 (CON), 176.8 (COO).

Poly[2-(*N*-ethylacetamido)ethyl acrylate] (PEAE):

^{1}H NMR (600 MHz, D_2O) δ_{ppm}: 1.16 & 1.27 (m, 3H, NCH_2CH_3), 1.65-1.99 (m, 2H, CH_2CHCO), 2.20 (s, 3H, $COCH_3$), 2.38 (m, H, CH_2CHCO), 3.43-3.51 (m, 2H, NCH_2CH_3), 3.66-3.75 (m, 2H, NCH_2CH_2), 4.25-4.30 (m, 2H, NCH_2CH_2).

^{13}C NMR (101 MHz, D_2O) δ_{ppm}: 12.2 & 13.2 (NCH_2CH_3), 20.6 & 21.1 ($COCH_3$), 34.4 (CH_2CHCO), 41.2-44.3 (NCH_2CH_3 and CH_2CHCO), 44.8 & 46.9 (NCH_2CH_2), 62.8 (NCH_2CH_2), 173.2 & 173.6 (*C*ON), 175.4 (*C*OO).

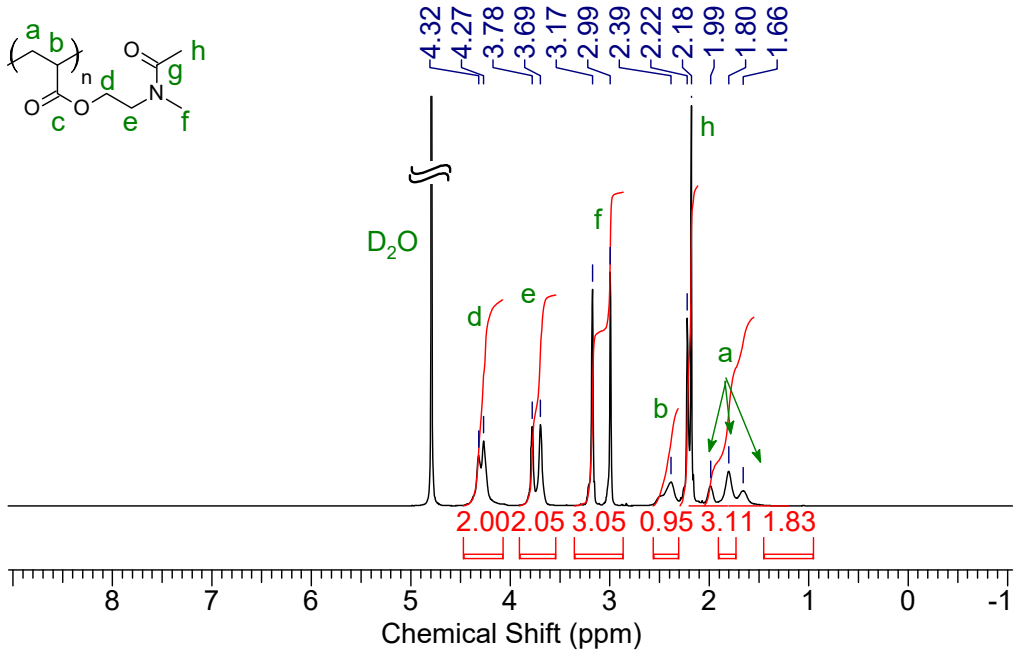

Figure 3.34. ^{1}H spectrum of poly[2-(*N*-methylacetamido)ethyl acrylate] (PAEA, in D_2O, 600 MHz).

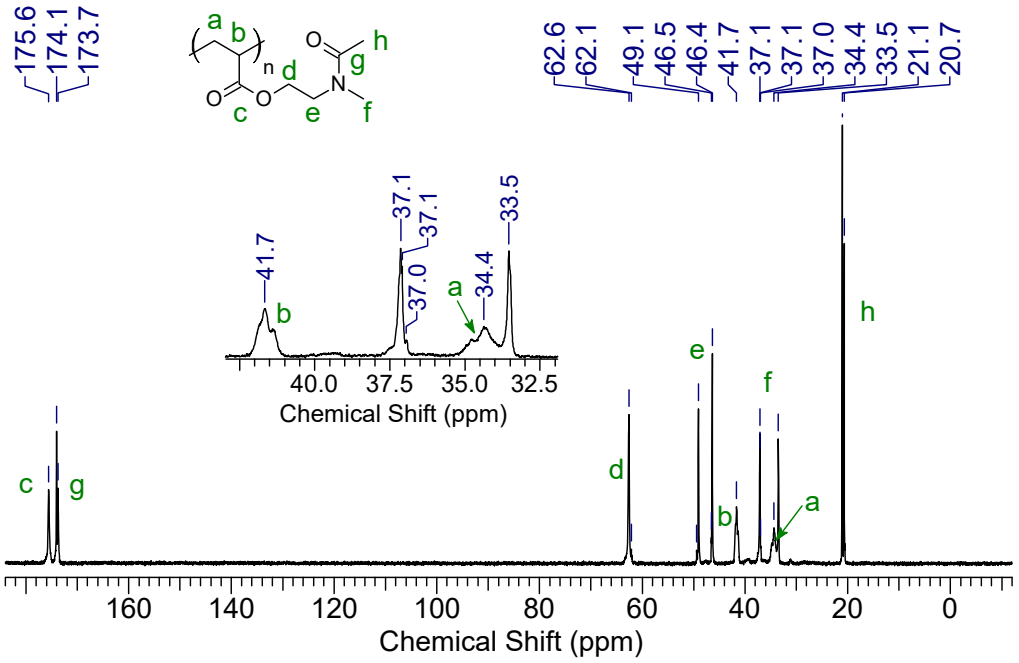

Figure 3.35. ^{13}C spectrum of poly[2-(*N*-methylacetamido)ethyl acrylate] (PAEA, in D_2O, 101 MHz).

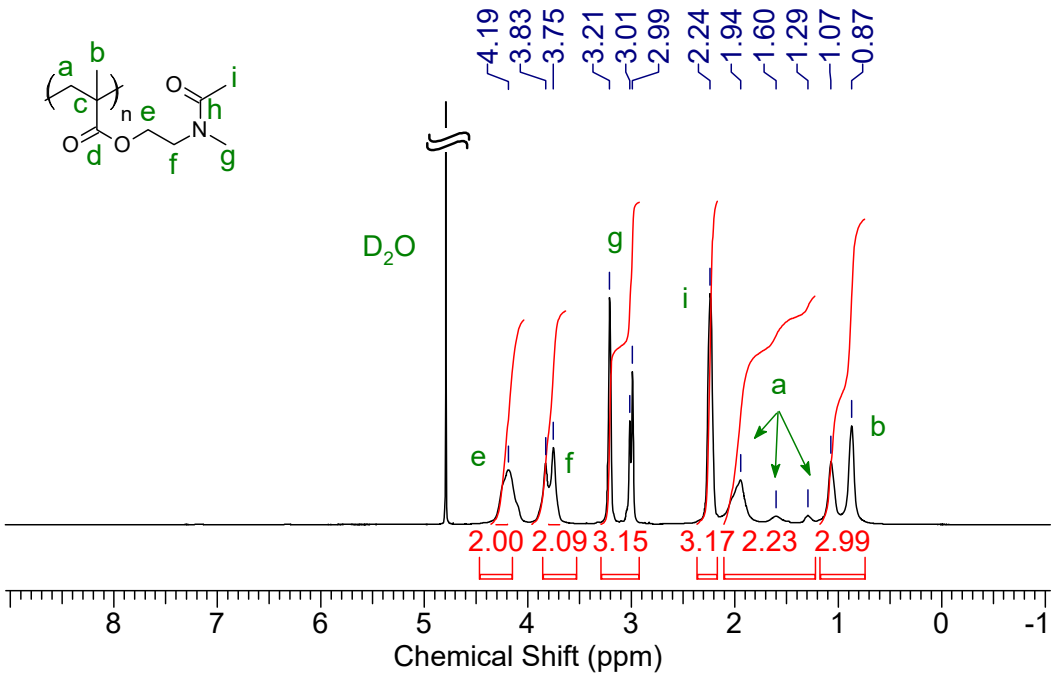

Figure 3.36. ^{1}H spectrum of poly[2-(*N*-methylacetamido)ethyl methacrylate] (PAEM, in D_2O,

600 MHz).

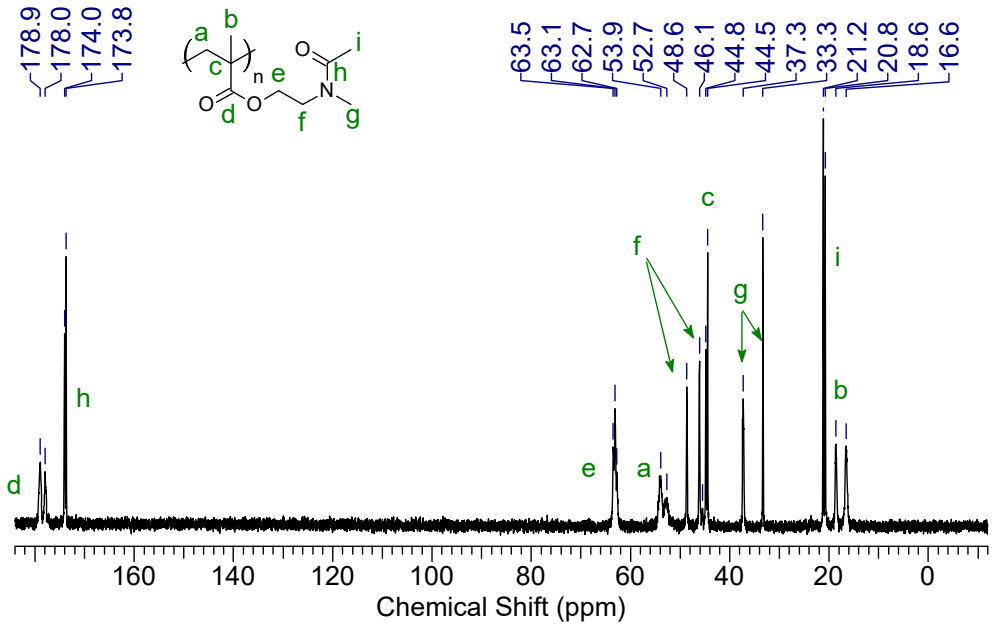

Figure 3.37. ^{13}C spectrum of poly[2-(*N*-methylacetamido)ethyl methacrylate] (PAEM, in D_2O, 101 MHz).

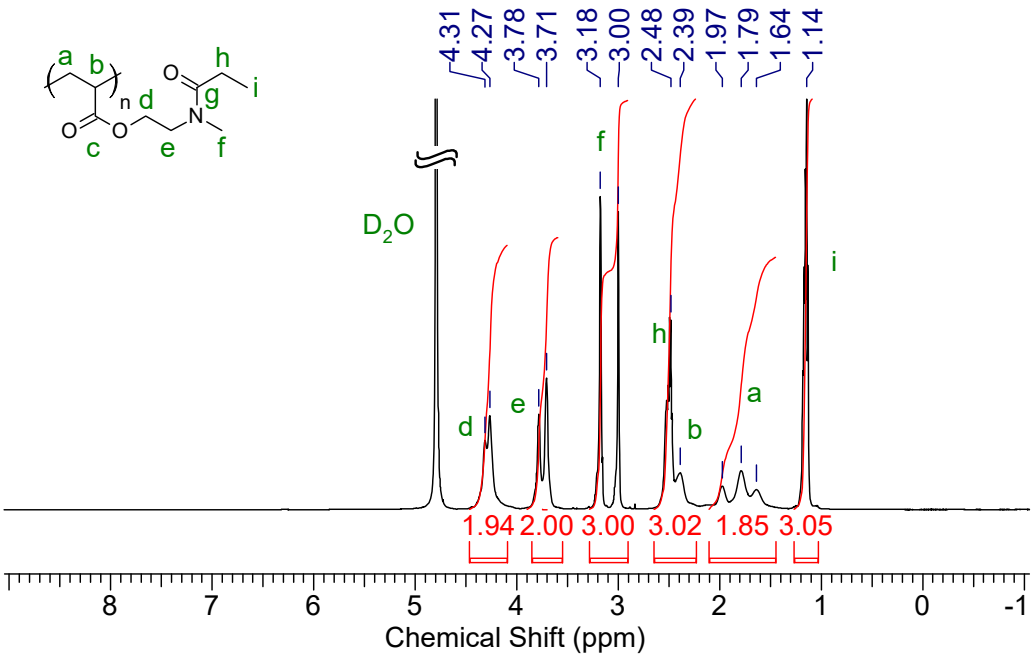

Figure 3.38. ^{1}H spectrum of poly[2-(*N*-methylpropionamido)ethyl acrylate] (PPEA, in D_2O,

600 MHz).

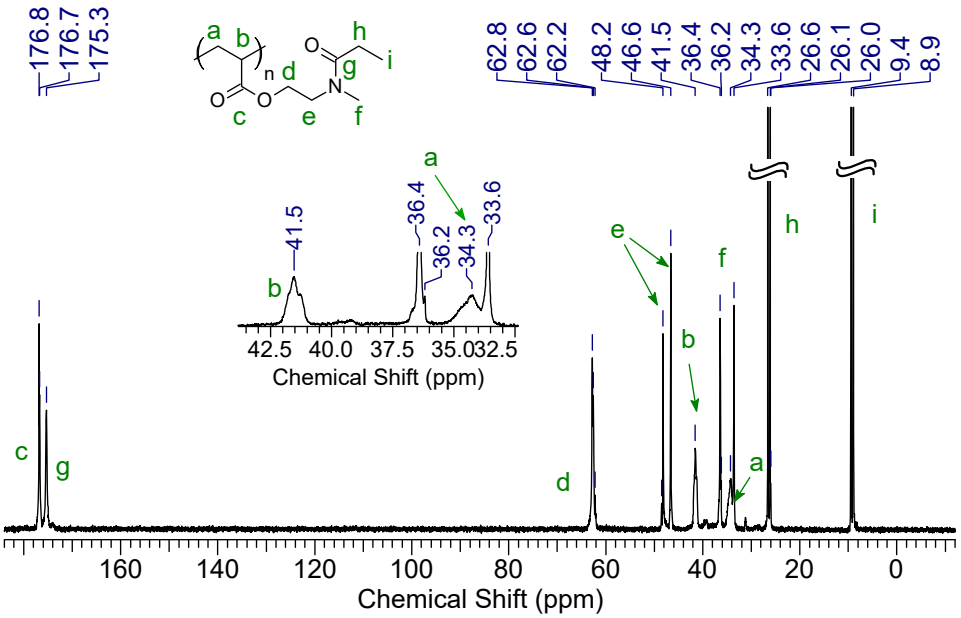

Figure 3.39. ^{13}C spectrum of poly[2-(*N*-methylpropionamido)ethyl acrylate] (PPEA, in D_2O, 101MHz).

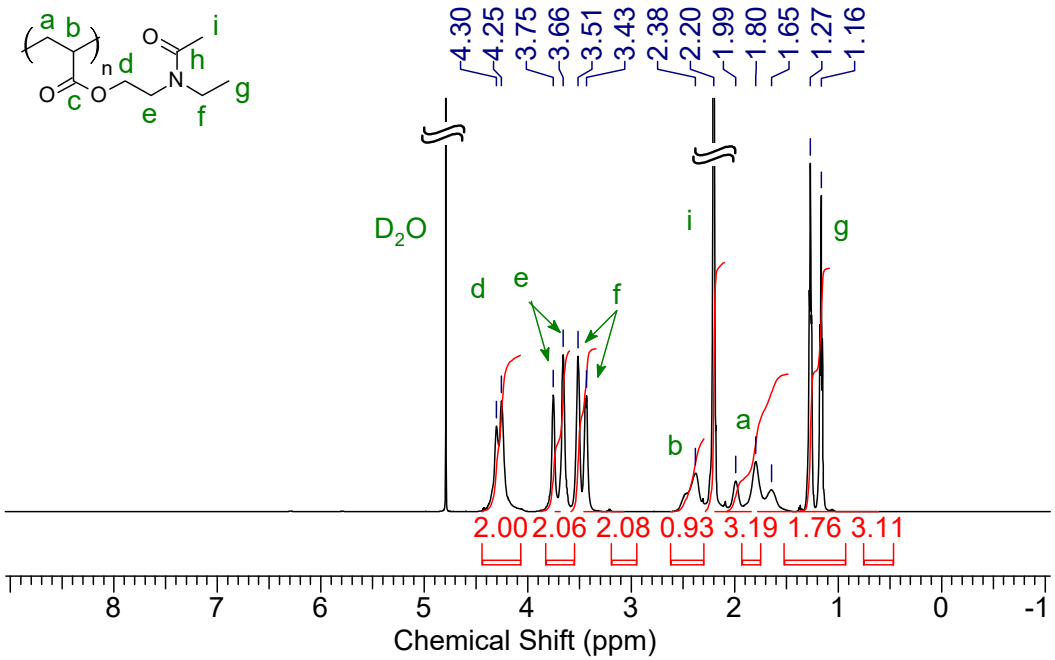

Figure 3.40. ^{1}H spectrum of poly[2-(*N*-ethylacetamido)ethyl acrylate] (PEAE, in D_2O, 600

MHz).

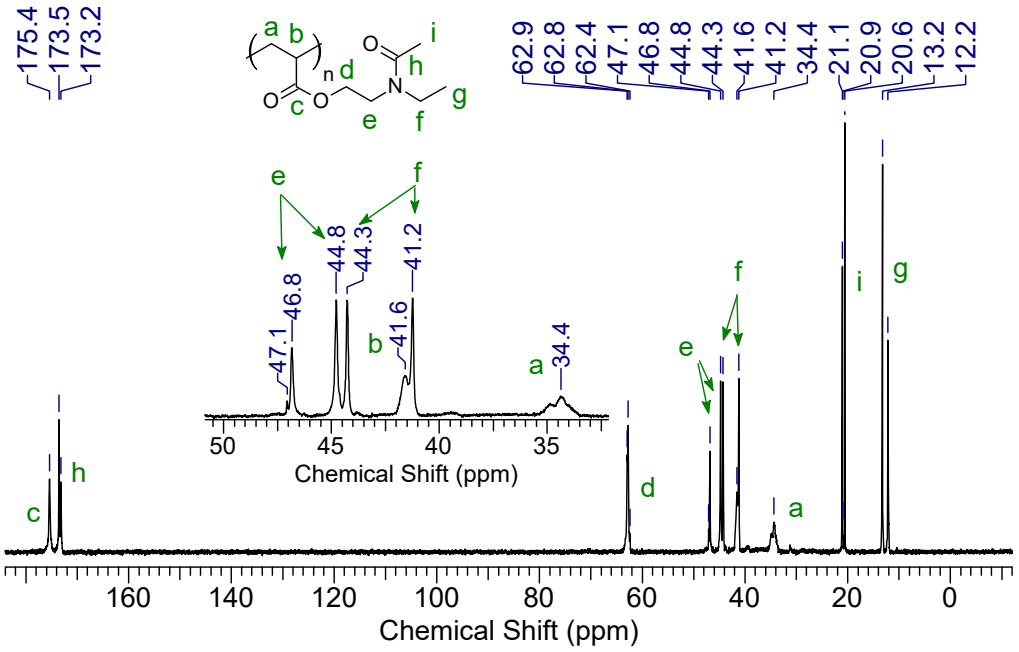

Figure 3.41. ^{13}C spectrum of poly[2-(*N*-ethylacetamido)ethyl acrylate) (PEAE, in D_2O, 101 MHz).

3.5.2 Preparation of copolymers

n-Butyl acrylate was chosen to copolymerize with tertiary amide acrylate, and *n*-butyl methacrylate was chosen to copolymerize with tertiary amide methacrylate (illustrated in **Figure 3.2**). The molar feed ratio of *n*-butyl (meth)acrylate to tertiary amide (meth)acrylate was tentatively set as 70:30, and the obtained copolymers were water-insoluble (see the photographs **Figure 3.42**). All the copolymerization followed a similar procedure. Hence, the preparation of poly[*n*-butyl acrylate$_{70}$-*co*-2-(*N*-methylacetamido)ethyl acrylate$_{30}$] (coPAEA) is described as an example.

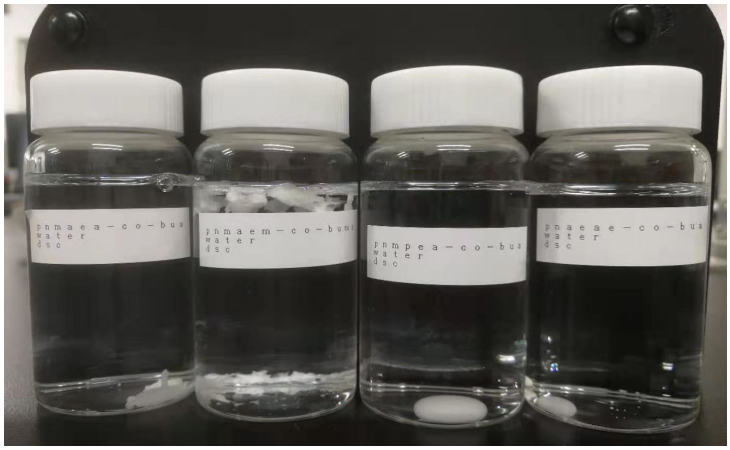

Figure 3.42 Photographs of prepared copolymers immersed in water for 2 weeks. They are PAEA, PAEM, PPEA, and PEAE from the left to right.

NMAEA (3.56 g, 210 mmol), *n*-butyl acrylate (6.28 g, 490 mmol), and AIBN (9.88 mg, 60.17μmol) were stirred with 1,4-dioxane (39.52 g, 448.56 mmol) at rt. and purged by N_2 continuously for half an hour. Then the reaction was heated up to 75 °C for 24 h until the mixture became visually viscous. The polymer solution was dissolved in a small amount of 1,4-dioxane and added dropwise into a large excess amount of hexane. Then the precipitate was dissolved in THF and precipitated in hexane again. Such dissolution/precipitation processes were repeated twice more. The precipitate was soaked in Milli Q water with stirring for 2 days to remove water-soluble impurities. To recollect the polymer, the precipitate was dissolved in THF again and concentrated by a rotary evaporator subsequently. The viscous coPAEA (7.6 g, yield: 77%) was finally obtained after drying in a vacuum oven at 60 °C for a couple of days.

The conversion, reaction time, composition, yield, M_n, and M_w/M_n of each copolymer are summarized in **Table 3.2**. The GPC trace of each homopolymer is shown in **Figure 3.43**.

Table 3.2. Conversion, Reaction Time, Composition, Yield, M_n, and M_w/M_n of Synthesized Copolymers

Polymer	Conv [%][a]		Reaction time [h][b]	Composition in copolymers [mol %][c]		Yield [%]	M_n [kg mol^{-1}][d]	M_w/M_n[d]
	Amide monomer	BuA or BMA		Amide monomer	BuA or BMA			
coPAEA	86	87	24	31	69	77	21	3.0
coPAEM	90	96	24	26	74	88	20	2.5
coPPEA	89	88	8	30	70	74	22	2.7
coPEAE	84	87	24	32	68	74	21	2.7

[a]Determined by NMR. [b]The reaction was stopped when the polymerization solution became visually viscous. [c]The molecular weight was determined by SEC using polystyrene standards in THF at 40 °C.

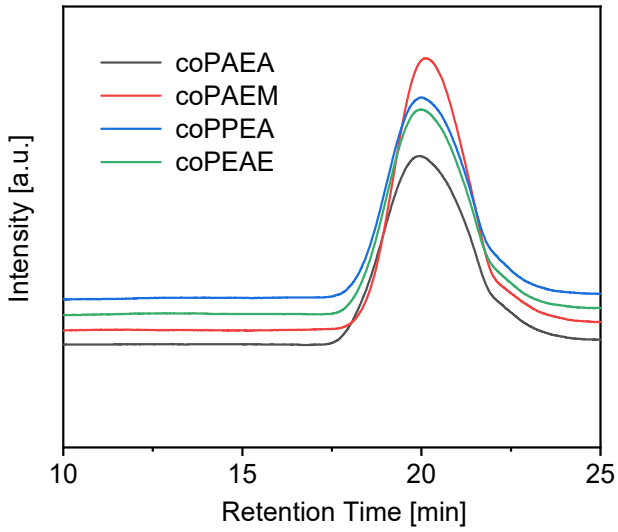

Figure 3.43. SEC traces of coPAEA, coPAEM, coPPEA, and coPEAE.

The molar composition of tertiary amide acrylate units in each copolymer is determined by the following equation,

Tertiary amide acrylate units (mol %) = ∑ δ(terminal methyl group substituted on carbonyl)/[∑ δ(terminal methyl group substituted on carbonyl) + ∑ δ(terminal methyl group of *n*-butyl (meth)acrylate)]

where ∑ δ(terminal methyl group substituted on carbonyl) is the integral of signal assigned to protons of the terminal methyl group substituted on carbonyl in the tertiary amide acrylate units in the ^{1}H NMR spectrum of the copolymer. In other words, it is the integral of f, f, g, and g signal marked in **Figure 3.44**, **Figure 3.45**, **Figure 3.46**, and **Figure 3.47**, respectively.

∑ δ(terminal methyl group of *n*-butyl (meth)acrylate) is the integral of signal assigned to protons of the terminal methyl terminal methyl group of *n*-butyl (meth)acrylate units in the ^{1}H NMR spectrum of the copolymer. In other words, it is the integral of j, k, and k signal marked in **Figure 3.44**, **Figure 3.46**, and **Figure 3.47**, respectively. In the case of **Figure 3.45**, because the methyl signal in the backbone (marked as b) overlaps with the terminal methyl in the *n*-butyl methacrylate (marked as j), the integral of the j signal is considered as half of the integral of b + j.

The chemical shift of NMR spectra and NMR spectra of copolymers are depicted as follow.

Poly[*n*-butyl acrylate$_{70}$-*co*-2-(*N*-methylacetamido)ethyl acrylate$_{30}$] (coPAEA):

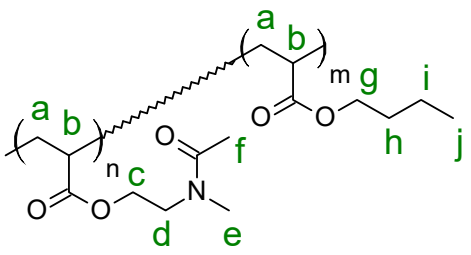

^{1}H NMR (600 MHz, $CDCl_3$) δ_{ppm}: 0.94 (s, C(j)H), 1.36-1.92 (m, C(a)H, C(h)H and C(i)H), 2.09 & 2.13 (s, C(e)H), 2.28 (s, C(b)H), 2.96 & 3.08 (s, C(f)H), 3.59 (m, C(d)H), 4.04 (m, C(c)H and C(g)H).

Poly[*n*-butyl methacrylate$_{70}$-*co*-2-(*N*-methylacetamido)ethyl methacrylate$_{30}$] (coPAEM):

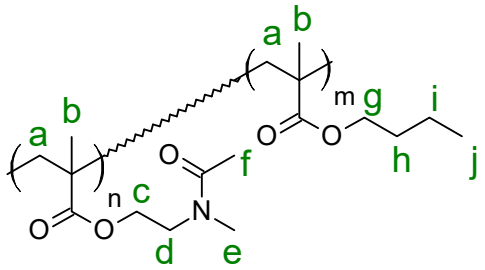

^{1}H NMR (600 MHz, $CDCl_3$) δ_{ppm}: 0.95 (m, C(b)H and C(j)H), 1.24-1.81 (m, C(i)H, C(h)H, and C(a)H), 2.13 (s, C(f)H), 2.95 & 3.12 (m, C(e)H), 3.61 (m, C(d)H), 3.94 (m, C(c)H and C(g)H).

Poly[*n*-butyl acrylate$_{70}$-*co*-2-(*N*-methylpropionamido)ethyl acrylate$_{30}$] (coPPEA):

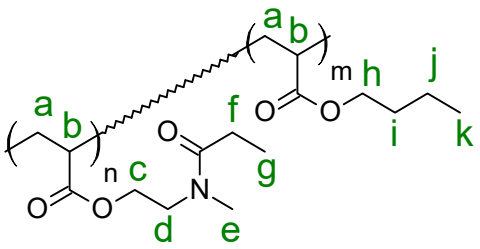

^{1}H NMR (600 MHz, $CDCl_3$) δ_{ppm}: 0.95 (m, C(k)H), 1.13 (m, C(g)H), 1.37-1.91 (m, C(a)H, C(i)H and C(j)H), 2.34 (m, C(f)H and C(b)H), 2.97 & 3.07 (s, C(e)H), 3.60 (m, C(d)H), 4.04 (m, C(c)H and C(g)H).

Poly[*n*-butyl acrylate$_{70}$-*co*-2-(*N*-ethylacetamido)ethyl acrylate$_{30}$] (coPEAE):

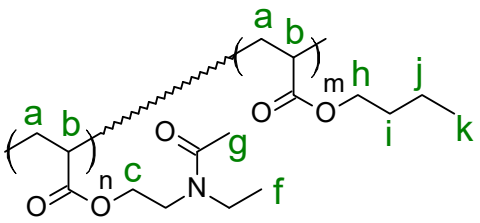

^{1}H NMR (600 MHz, $CDCl_3$) δ_{ppm}: 0.94 (m, C(k)H), 1.13 & 1.20 (m, C(f)H), 1.36-1.91 (m, C(a)H, C(i)H and C(j)H), 2.10 & 2.13 (s, C(g)H), 2.28 (m, C(b)H), 3.40 (m, C(e)H), 3.54 (m, C(d)H), 4.04 (m, C(c)H and C(g)H).

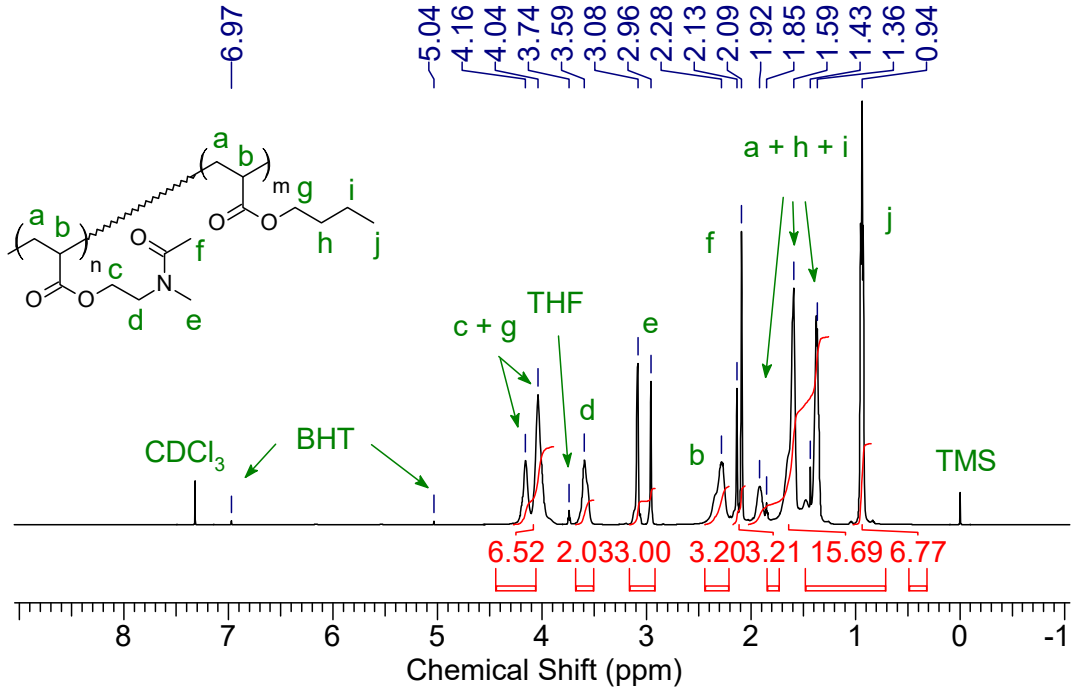

Figure 3.44. ^{1}H spectrum of poly[*n*-butyl acrylate$_{70}$-*co*-2-(*N*-methylacetamido)ethyl acrylate$_{30}$] (coPAEA, in $CDCl_3$, 600 MHz).

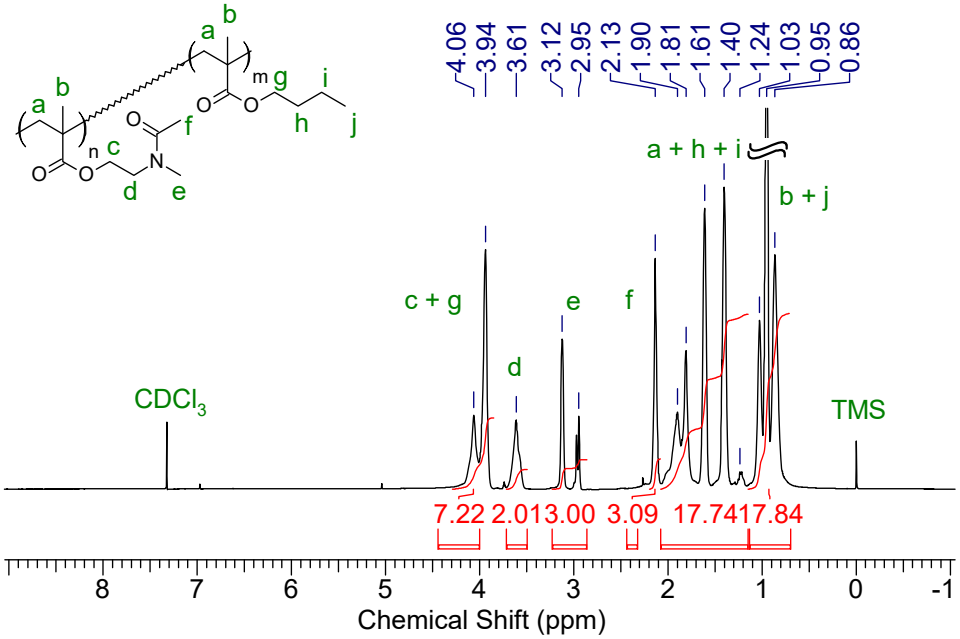

Figure 3.45. ^{1}H spectrum of poly[*n*-butyl methacrylate$_{70}$-*co*-2-(*N*-methylacetamido)ethyl

methacrylate$_{30}$) (coPAEM, in $CDCl_3$, 600 MHz).

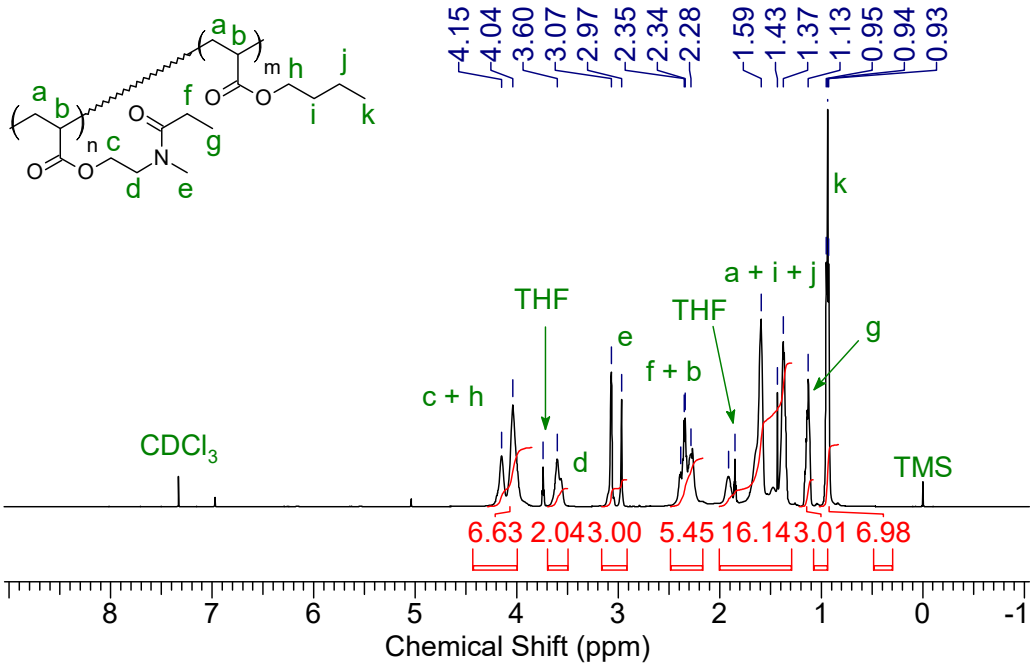

Figure 3.46. ^{1}H spectrum of poly[*n*-butyl acrylate$_{70}$-*co*-2-(*N*-methylpropionamido)ethyl acrylate$_{30}$] (coPPEA, in $CDCl_3$, 600 MHz).

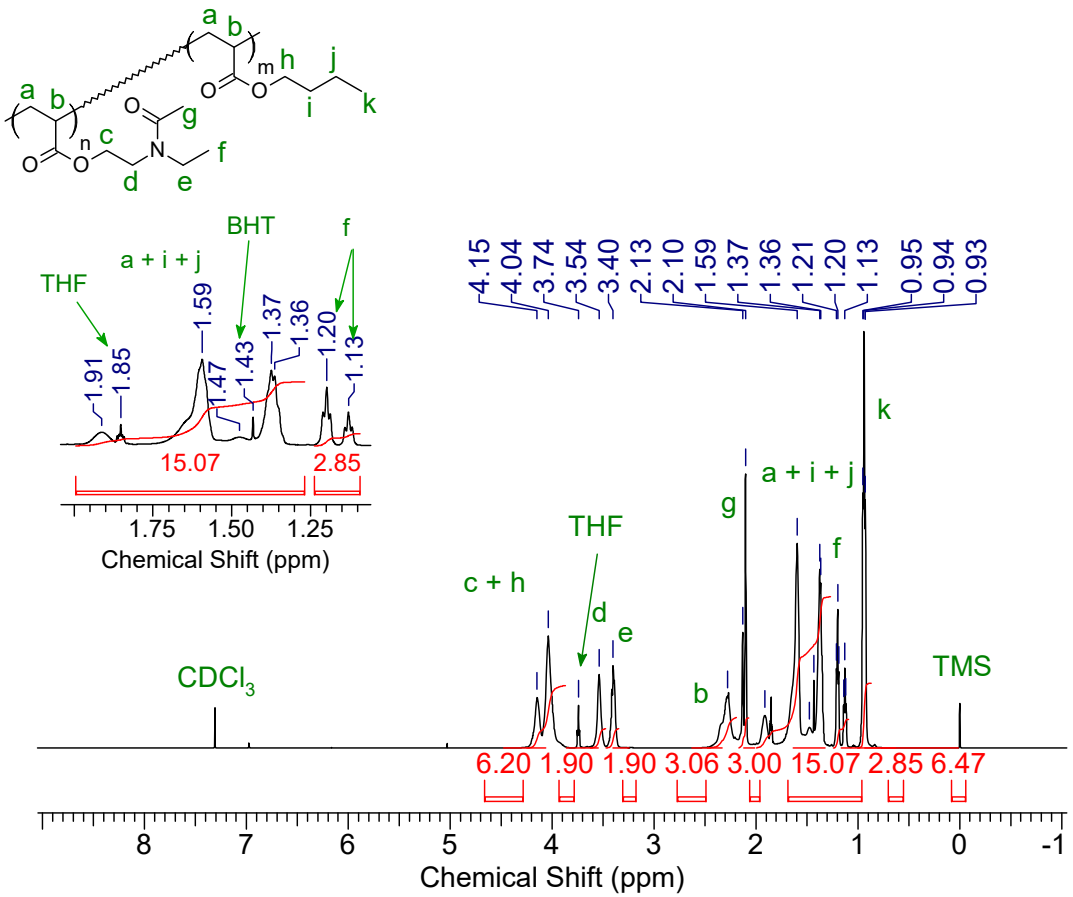

Figure 3.47. ^{1}H spectrum of poly[*n*-butyl acrylate$_{70}$-*co*-2-(*N*-ethylacetamido)ethyl acrylate$_{30}$] (coPEAE, in $CDCl_3$, 600 MHz).

3.6 Conclusion

In this chapter, combining the conclusions obtained in **Chapter 2**, as well as the construction strategy of PMPC and PMEA, four poly(tertiary amido acrylate) analogs, which contain tertiary amide frameworks in the side chains and can be regarded as POX derivatives, are designed. Through a two-step synthesis strategy, the steric hindrance around the tertiary amide in the (meth)acrylate monomer can be controlled. The monomers were easily polymerized by convenient

free radical polymerization. Since the prepared homopolymers are water-soluble, the water-insoluble copolymers were also synthesized by copolymerizing with their monomers with hydrophobic *n*-butyl (meth)acrylates to further coat on substrates directly.

3.7 Reference

(1) Monnery, B. D.; Jerca, V. V.; Sedlacek, O.; Verbraeken, B.; Cavill, R.; Hoogenboom, R. Defined High Molar Mass Poly(2-Oxazoline)s. *Angew. Chem. Int. Ed.* **2018**, *57* (47), 15400–15404.

(2) Sedlacek, O.; Monnery, B. D.; Filippov, S. K.; Hoogenboom, R.; Hruby, M. Poly(2-Oxazoline)s - Are They More Advantageous for Biomedical Applications Than Other Polymers? *Macromol. Rapid Commun.* **2012**, *33* (19), 1648–1662.

(3) Kadoma, Y.; Nakabayashi, N.; Masuhara, E.; Yamauchi, J. Synthesis and Hemolysis Test of the Polymer Containing Phosphorylcholine Groups. *Kobunshi Ronbunshu* **1978**, *35* (7), 423–427.

(4) Hayward, J. A.; Chapman, D. Biomembrane Surfaces as Models for Polymer Design: The Potential for Haemocompatibility. *Biomaterials* **1984**, *5* (3), 135–142.

(5) Tanaka, M.; Sato, K.; Kitakami, E.; Kobayashi, S.; Hoshiba, T.; Fukushima, K. Design of Biocompatible and Biodegradable Polymers Based on Intermediate Water Concept. *Polym. J.* **2015**, *47* (2), 114–121.

(6) Tanaka, M.; Hayashi, T.; Morita, S. The Roles of Water Molecules at the Biointerface of Medical Polymers. *Polym. J.* **2013**, *45*, 701–710.

(7) Yadav, V. K.; Babu, K. G. Reactions on a Solid Surface. A Simple, Economical, and Efficient Acylation of Alcohols, Amines over Al2O3. *J. Org. Chem.* **2004**, *69* (2), 577–580.

(8) Mahmoud, A. M.; Morrow, J. P.; Pizzi, D.; Nanayakkara, S.; Davis, T. P.; Saito, K.; Kempe, K. Nonionic Water-Soluble and Cytocompatible Poly(Amide Acrylate)s. *Macromolecules* **2020**, *53* (2), 693–701.

(9) Weber, C.; Becer, R. C.; Baumgaertel, A.; Hoogenboom, R.; Schubert, U. S. Preparation of Methacrylate End-Functionalized Poly(2-Ethyl-2-Oxazoline) Macromonomers. *Des. Monomers Polym.* **2009**, *12* (2), 149–165.

CHAPTER 4

Blood Compatibility and Hydration States of Poly(tertiary amido acrylate) Analogs and Their (Co)polymers

4.1 Introduction

The excellent water solubility of PMeOx and PEtOx enable them to apply as polymer therapeutics. Since the four poly(tertiary amido acrylate) analogs are water-soluble, to confirm whether they resemble the PMeOx and PEtOx in terms of biocompatibility and thus have similar application potential, their blood compatibility and cell viability, which are the two important aspects of biomaterials' screening, are investigated.[1] Thereinto, the blood compatibility is estimated by the hemolysis test which indicates the red blood cell damage in response to materials.[2] Furthermore, when the tertiary amide moiety in POXs is moderately sterically hindered, the POXs exhibit thermosensitivity. Similarly, for the prepared poly(tertiary amido acrylate) analogs, the tertiary amide moieties suffer different steric hindrances. Hence, the thermosensitivity of the poly(tertiary amido acrylate) analogs is also investigated in this chapter. For the water-insoluble copolymers, the blood compatibility is evaluated by the platelet adhesion test, plasma protein adsorption amounts, and conformational alterations of adsorbed fibrinogen on their spin-coated substrates. Finally, the hydration states of both homopolymers and copolymers were analyzed by DSC to understand the effect of the polymer chemical structure on blood compatibility from the perspective of IW.

4.2 Materials and methods

4.2.1 Materials

Triton X-100 and Tween 20 were purchased from MP Biomedicals, USA. Cell counting kit-8 for evaluating cell viability was acquired from Dojindo, Japan. Human serum albumin (HSA) was bought from Sigma-Aldrich, USA. A micro BCA protein assay kit for the quantification of adsorbed proteins was procured from Thermo Fisher Scientific, USA. Poly(ethylene terephthalate) (PET) film (Diafoil) was kindly donated by Mitsubishi Plastics, INC., Japan. Materials for the platelet adhesion test and ELISA, as well as the PMEA, PBuA, and PMPC are the same as using in **Chapter 2**. Other commercially available reagents were used as received unless otherwise specified.

4.2.2 Hemolysis of poly(tertiary amido acrylate) analogs

The homopolymer blood compatibility was evaluated by red blood cells (3.44×10^9 cells mL^{-1}) in human whole blood without dilution. Human whole blood was added to 96-well plates at a volume of 100 μL per well. Then, 100 μL, 70 μL, 50 μL, 30 μL, 10 μL, and 5 μL of homopolymer/PBS (−) (2 mg mL^{-1}) solutions were added together with 0 μL, 30 μL, 50 μL, 70 μL, 90 μL, and 95 μL PBS (−) separately to the test wells. In addition, 10 μL and 1 μL of homopolymer/PBS (−) (200 μg mL^{-1}) solutions were separately added with 90 μL and 99 μL PBS (−) to the test wells. Wells with 100 μL PBS (−), 100 μL Triton-X 100 [2 μg mL^{-1} to 2 mg mL^{-1} in PBS (−)] and 100 μL Tween 20 [2 μg mL^{-1} to 2 mg mL^{-1} in PBS (−)] mixed with 100 μL blood

were set as blank, positive and negative controls separately. The mixtures were well-mixed by pipetting. The 96-well plates were incubated at 37 °C for 2 h and centrifuged (2000 rpm, 5 min) afterward. 50 μL aliquots of supernatants were transferred into 96-well plates and mixed with 150 μL PBS (−). The lysed red blood cells were analyzed by a Tecan Infinite M Plex microtiter plate reader at a wavelength of 540 nm. Hemolysis was calculated using the following equation:

$$\text{Hemolysis (\%)} = (A_{\text{polymer}} - A_{\text{blank}})/(A_{\text{positive}} - A_{\text{blank}}) \times 100\%$$

where A_{polymer} = absorbance of the polymer-treated supernatant, A_{blank} = absorbance of the blank control, A_{positive} = absorbance of Triton-X-treated supernatant when the added concentration was 2 mg mL^{-1}.

4.2.3 Cell viability of poly(tertiary amido acrylate) analogs

The cell viability of homopolymers was determined by the CCK-8 kit. The human cervical cancer cell line (HeLa) and normal human dermal fibroblasts (NHDFs) were provided by RIKEN BRC, Japan, and Ronza, Poland, respectively. HeLa cells were cultured in Dulbecco's modified Eagle's medium (DMEM) (Gibco) containing 10% v/v fetal bovine serum (Gibco), 100 units mL^{-1} penicillin (Gibco), and 100 μg mL^{-1} streptomycin (Gibco) at 37 °C in a humidified incubator with 5% atmospheric CO_2. NHDFs were cultured in Dulbecco's modified Eagle's medium containing F12 (DMEM/F12) (Gibco) containing 10% v/v fetal bovine serum (Gibco), 100 units mL^{-1} penicillin (Gibco), and 100 μg mL^{-1} streptomycin (Gibco) at 37 °C in a humidified incubator with 5% atmospheric CO_2.

The cells were seeded in 96-well plates 24 h before the addition of polymer solutions. The seeding density of the HeLa cells was 1×10^4 cells per well and 5×10^3 cells per well for the NHDFs. After 24 h of incubation, the old media were removed, and 90 μL of fresh media together with 10 μL of homopolymer solutions were added where the concentration varied from 1 μg mL^{-1} to 10 mg mL^{-1} in PBS (−). The homopolymer solutions were filtered beforehand and prepared from the serial dilution of solutions with a concentration of 10 mg mL^{-1}. The cells were cultivated for 24 h. Then, the media were removed and replaced with 100 μL fresh media and 10% v/v CCK-8. The cells were incubated for an additional 1 h at 37 °C. Cell viability was determined by the absorbance at a wavelength of 450 nm under a microtiter plate reader. Wells incubated with only media, and CCK-8 were set as blank. Cells cultivated with 10 μL PBS (−) and 90 μL media instead were used as the positive control. The viability was calculated using the following equation:

$$\text{Cell viability (\%)} = (A_{\text{polymer}} - A_{\text{blank}})/(A_{\text{positive}} - A_{\text{blank}}) \times 100\%$$

where A_{polymer} = absorbance of the polymer-cultivated cells, A_{blank} = absorbance of the blank, A_{positive} = absorbance of the positive control.

4.2.4 Turbidity measurement

The turbidity measurement was carried out on a JASCO V-630 BIO spectrophotometer connected with a temperature controller and a water chiller. Homopolymers were dissolved in water and PBS (−) separately and measured under the following conditions: 500 nm wavelength, 1 °C min^{-1} temperature slope, 30 s stabilization time before measurement, and 0.1 °C data pitch.

4.2.5 Preparation of polymer coating substrates and contact angle measurement

The polymer substrates for the contact angle measurement and platelet adhesion test were prepared by a spin-coating method, basically according to our group's previous report.[3] Prepared copolymers: poly[*n*-butyl acrylate$_{70}$-*co*-2-(*N*-methylacetamido)ethyl acrylate$_{30}$] (coPAEA), poly[*n*-butyl methacrylate$_{70}$-*co*-2-(*N*-methylacetamido)ethyl methacrylate$_{30}$] (coPAEM), poly[*n*-butyl acrylate$_{70}$-*co*-2-(*N*-methylpropionamido)ethyl acrylate$_{30}$] (coPPEA), and poly[*n*-butyl acrylate$_{70}$-*co*-2-(*N*-ethylacetamido)ethyl acrylate$_{30}$] (coPEAE), as well as PMEA and PMPC, were dissolved in methanol. PBuA was dissolved in THF. All the polymers were dissolved in the solvent at a concentration of 10 mg mL^{-1}. Two kinds of bare PET substrates were cut from commercially available PET film (thickness = 125 μm) by a GCC C180II laser engraving machine. One was the disk with a diameter of 14 mm, and the other was a square with a side length of 8 mm. The bare PET substrates were cleaned by toluene and dried in a vacuum oven at rt overnight. 40 μL or 25 μL polymer solution was spin-coated onto the rounded or square PET substrate by a Mikasa Spin Coater MS-A100 with a protocol of 500 rpm for 1 s, 0 rpm for 5 s, ramp up for 2 s, 3000 rpm for 30 s, and ramp down for 2 s.

The polymer-coated surface's hydrophilicity was assessed by the sessile water drop contact angle and captive bubble contact angle through a KYOWA DMo-501 DropMaster on polymer-coated PET disks. For the sessile water drop contact angle measurement, a water droplet of 2 μL was rapidly placed on the substrate. Before measuring the captive bubble contact angle, the substrates were immersed in water for 24 h. The air bubble was injected beneath the hydrated

surface immersed in water.

4.2.6 Human platelet adhesion test

The human platelet adhesion tests were performed on the square polymer spin-coated substrates mentioned above. The procedures of the human platelet adhesion test are the same as described in **Chapter 2**, except that the volume of plasma solution initially placed was 200 μL instead of 480 μL.

4.2.7 Evaluation of adsorbed protein amount

The amount of adsorbed proteins on polymer surfaces was evaluated by micro BCA assay. All copolymer/methanol solutions (2 mg mL^{-1}, 25 μL) were cast into tissue culture-treated polystyrene (TCPS) 96-well plates. The plates were slowly air-dried over 3 days at room temperature. Then, 100 μL PBS (−) was added to each well to infiltrate the polymer surface at 37 °C for 1 h before the protein solution addition. After outwelling the PBS (−), 50 μL PPP or HSA solution [1 mg mL^{-1} in PBS (−)] was added to each well and incubated at 37 °C for 1 h, separately. Subsequently, each well was rinsed five times with PBS (−). The adsorbed proteins on each well were extracted by 30 μL freshly prepared sodium dodecyl sulfate (SDS) solution (5% w/v in 0.1 M NaOH) at 37 °C for 2 h's incubation. The extracted proteins were mixed with 70 μL PBS (−). After pipetting sufficiently, half of the protein mixture was transferred into another 96-well plate and mixed with 50 μL BCA solution. The protein standard curve was plotted against the absorbances of wells

containing 0.7, 1.75, 3.5, 7, and 17.5 μg mL^{-1} bovine serum albumin. For each copolymer, wells incubated with 50 μL PBS (−) instead of PPP or HSA were set as blank controls. The absorbance of extracted proteins that came from each copolymer cast well should be deducted from the blank control absorbance to exclude the possible reduction of Cu^{2+} from the copolymer.

4.2.8 Denaturation degree evaluation of fibrinogen

The conformational alteration of fibrinogen adsorbed on the copolymer surface was evaluated on the rounded spin-coated PET substrates. The procedures of the ELISA are the same as described in **Chapter 2**, except that the coloring time of the ABTS solution was 20 min instead of 30 min.

4.2.9 Evaluation of hydration states by DSC

The procedures of this section are the same as described in **Chapter 2**.

4.3 Results and discussion

4.3.1 Blood compatibility and cell viability of poly(tertiary amido acrylate) analogs

In the hemolysis test, PMeOx and PEtOx were involved to compare. As shown in **Figure 4.1a** and **b**, in contrast to the positive control Triton X-100, which showed increasing hemolytic activity with increasing concentration, all the prepared homopolymers were capable of maintaining the intactness of the red cell membranes even up to a high concentration of 1000 μg mL^{-1} as the negative control Tween-20 and established blood-compatible PMeOx and PEtOx.

Moreover, cell viability tests with HeLa cells and NHDFs were performed to observe the homopolymer cytocompatibility for other bio-related applications. After incubation with cells for 24 h, all the polymers demonstrated high cell viability from 0.1 μg mL^{-1} to 1000 μg mL^{-1} (**Figure 4.1c** and **d**). Given all the above, a conclusion can be preliminarily made: all homopolymers with tertiary amide "scions" on the poly(meth)acrylate "rootstocks" maintained the blood compatibility and cytocompatibility of the PMeOx and PEtOx. These results laid a foundation for the discussion of the hydration states of homopolymers in this work.

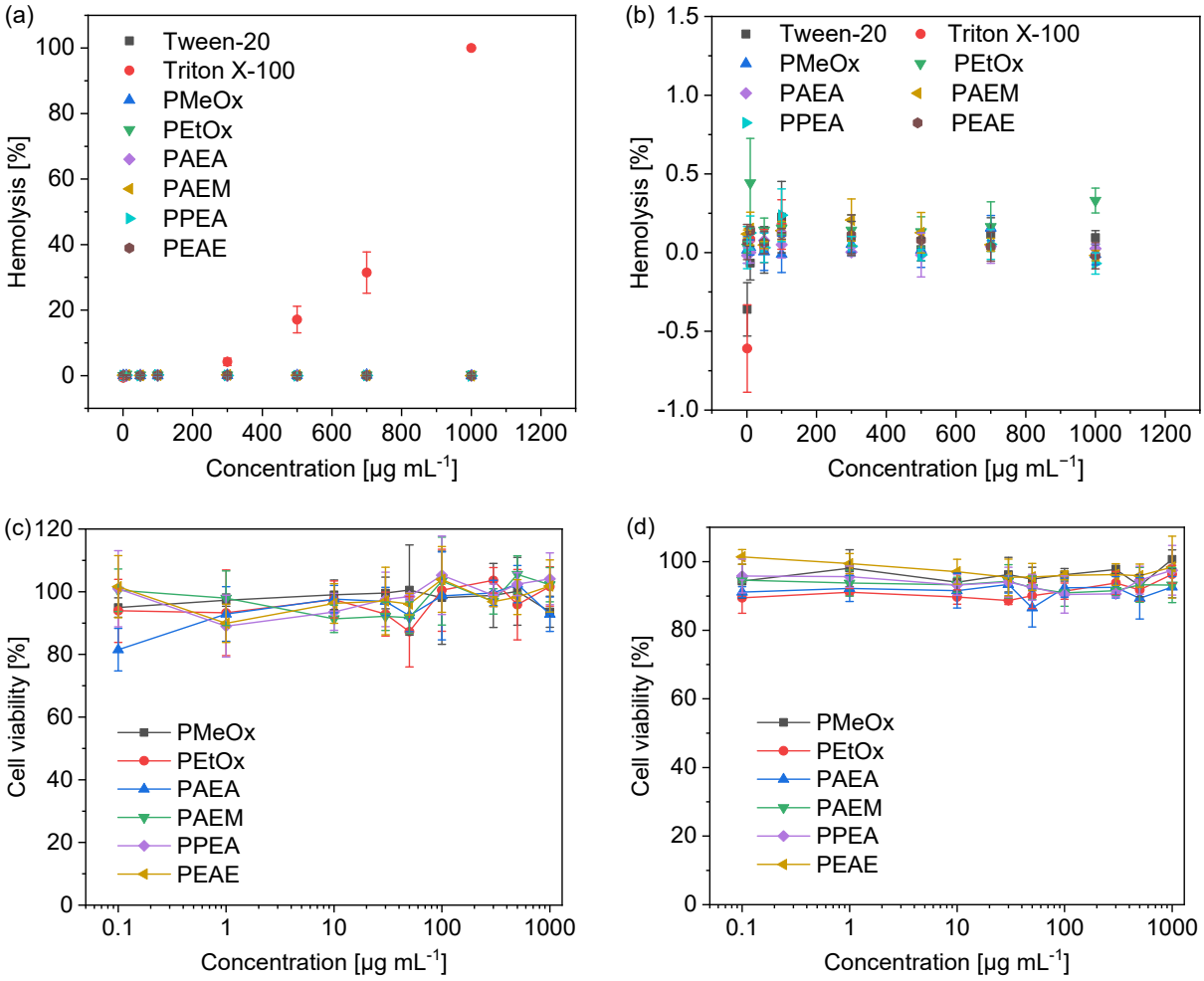

Figure 4.1. The in vitro test results of PMeOx, PEtOx, and homopolymers. (a) For the

hemolysis results, each data point represents the mean ± SD (n = 4). (b) The enlarged figure for hemolysis of approximately 0% in (a). (c) Cell viability of HeLa cells. Each data point represents the mean ± SD (n = 3) and (d) cell viability of NHDFs. Each data point represents the mean ± SD (n = 4).

4.3.2 Thermosensitivity of poly(tertiary amido acrylate) analogs

As shown in **Figure 4.2a**, PAEA and PAEM were dissolved in water at the tested concentration (10 mg mL^{-1}) and temperature range without transition, demonstrating good hydrophilicity. PPEA and PEAE showed cloud point temperatures (T_{cp}) of 37.0 °C and 65.0 °C in the heating process, respectively. The phase transition was reversible and showed no or slight hysteresis during the heating-cooling cycle, as 0 °C for PPEA and 3 °C for PEAE. In studies of the LCST of poly(*N*-isopropylacrylamide) (PNIPAM),[4] intrachain or interchain hydrogen bonds via C=O and NH were formed in collapsed PNIPAM when the temperature was higher than LCST, postponing the dissociation process of polymer chains in the globule state and leading to the hysteresis. This can explain the absence of hysteresis in PPEA because such hydrogen bonds were not available for tertiary amides. The absence of hysteresis was also observed in some polymers bearing tertiary amides such as poly(*N*,*N*-dimethylacrylamide) and poly(2-*n*-propyl-2-oxazoline).[5,6] However, Lai et al.[7] reported that poly(3-ethyl-*N*-vinyl-2-pyrrolidone) (C_2PVP), incorporating no secondary amide but tertiary amide in the sidechain, still exhibited slight hysteresis (1 °C) between the cooling and heating process as PEAE in this work, which was caused by a weak ‘‘crosslinking’’

interaction of a water molecule between two carbonyl groups. A similar situation was also found in the polymer/PBS (−) system (**Figure 4.2b**), except the T_{cp} of PPEA and PEAE decreased to 35 °C and 56 °C in the heating process due to the salting-out effect. A T_{cp} close to human body temperature and no hysteresis during the cooling-heating cycle found in PPEA might make it a promising alternative to PNIPAM and deserves more study in the future. The higher T_{cp} of PEAE than PPEA implied that the ethyl group linked to the carbonyl of amide was more effective in shielding water to form hydrogen bonds. The hysteresis observed in PEAE verified this conclusion to some extent. This further inspires us to find water-insoluble polymers by designing a more hydrophobic moiety to the carbonyl end.

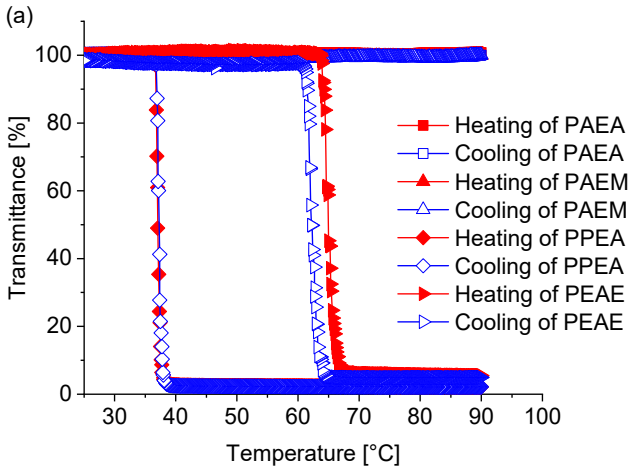

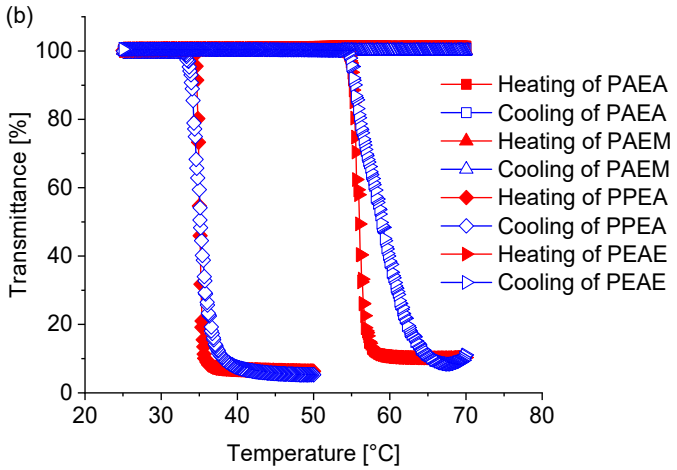

Figure 4.1. Turbidity measurements of (a) homopolymer aqueous solutions (10 mg mL^{-1}) and (b) homopolymer/PBS (−) solutions (10 mg mL^{-1}), in the heating and cooling process.

4.3.3 Hydrophilicity of copolymers coated surfaces

The hydrophilicity of the copolymer spin-coated PET substrates was evaluated by the in-air sessile water drop contact angle and in-water captive air bubble contact angle. The results are listed in **Table 4.1**. An apparent difference between the PET and copolymer surfaces confirmed the adequate coating of the polymer layer on PET. For coPAEA, coPPEA, and coPEAE, the water, and captive air bubble contact angle values were similar. In addition, the time-dependent water contact angle of these three copolymers had a similar trend (**Figure 4.3**). The water contact angles dropped rapidly from approximately 90°, close to the value of PBuA, and then slowed down to approximately 60°. Such a trend indicated rapid surface reconstruction. A segment in a copolymer adsorbs or orients selectively on the surface to minimize the system's interfacial free energy to respond to the environment.[8] In the air/polymer interface, the hydrophobic PBuA segment might

predominate on the surface, and the situation reversed when the polymer was in the water environment. Interestingly, the coPAEM surface remained hydrophobic during the water contact angle measurement but became even more hydrophilic than the other three counterparts after immersion in water for 24 h. It suggests that the segment reorientation could happen on the water/coPAEM interface but at a rate slower than that of coPAEA, coPPEA, and coPEAE. The reason for such difference is chain flexibility. Compared with the three polyacrylates, PAEA, PPEA, and PEAE, the methyl group on the backbone of PAEM decreases the chain flexibility which is reflected from its higher T_g (51.8 °C) in **Table 4.1**. What is more, complete reconstruction was available on the surface when the temperature was at or above T_g, whereas limited reconstruction could occur at a temperature below T_g.[9] Thus, during the sessile water drop contact angle measurement, the PBMA segments contributed to the higher hydrophobicity. With water penetrating the polymer chains, T_g decreased as water plasticization and reconstruction finally occurred on the coPAEM surface.

Table 4.1. Contact Angle on Copolymer Spin-coated PET Substrates[a]

Polymer	Contact angle [deg]	
	Sessile water drop	Captive air bubble
	30 s	24 h
PET	79.2 ± 0.8	121.1 ± 3.0
PBuA	84.9 ± 0.7	125.8 ± 0.8[b]
coPAEA	61.5 ± 1.1	137.7 ± 4.8
coPAEM	85.8 ± 2.2	146.9 ± 5.6
coPPEA	61.5 ± 2.7	135.6 ± 3.4
coPEAE	60.8 ± 3.0	140.3 ± 2.9

[a]Water in the air (sessile water drop) and an air bubble in water (captive air bubble). The data represent the means ± SD (n = 9 for sessile water drop, 3 substrates × 3 points, and n = 15 for the captive air bubble, 5 substrates × 3 points). [b]The value is referred to the literature.[10]

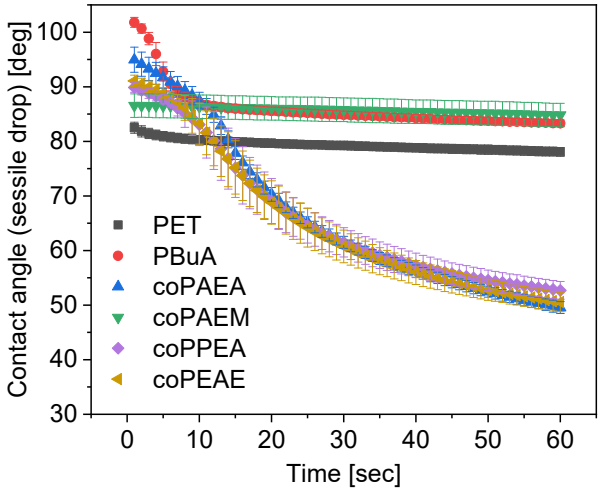

Figure 4.3. Time dependence of WCA on the surface of PET, PBuA and copolymers. The data represent the means ± SD (n = 9).

4.3.4 Platelet adhesion, protein adsorption and denaturation behavior on the surface

The number of adhered platelets, amount of adsorbed plasma proteins, and conformational change of adsorbed fibrinogen on the copolymer surfaces were measured to evaluate the copolymer coating's blood compatibility. The results are shown in **Figure 4.4**. The PBuA surfaces were set as positive controls, and PMPC or PMEA surfaces were set as negative controls to verify the reliability of the experimental results.

The high reliability of the platelet adhesion results (**Figure 4.4a**) is established from the

validity of the positive controls and negative controls. The coPAEM surface showed significant inhibition of platelet adhesion compared with its counterparts which performed similarly to each other. This discrepancy exactly coincided with the water contact angle results hinting that the surface properties played a role. Although coPAEA, coPPEA, and coPEAE did not perform ideally in antiplatelet adhesion, they reduced platelet adhesion compared with PBuA, especially in advanced activated platelets. Given that hydrophobic poly(*n*-butyl methacrylate) (PBMA) also showed low antiplatelet adhesion,[11,12] it can be ascertained that the PAEA, PAEM, PPEA, and PEAE segments improved blood compatibility. A micro BCA assay was conducted on copolymer cast 96-well TCPS plates to quantitively analyze the adsorbed plasma proteins, and ELISA was performed on copolymer spin-coated PET to investigate the exposure degree of the γ′ chains on the adsorbed fibrinogen. The PMEA control was not involved in the micro BCA assay because the film-forming stability on the TCPS plate was doubted. The reliability can be judged from the relatively low adsorption amount of HSA and PPP on PMPC and PBuA (**Figure 4.4b**). Overall, the adsorption trend of HSA was in line with that of PPP. Although the HSA concentration in plasma (40 mg mL^{-1}) was substantially higher than the tested concentration,[13] the adsorbed amount was almost reversed. This is probably due to the competitive adsorption of the plasma proteins and Vroman effects. The coPAEM surface exhibited a lower protein adsorption amount than coPAEA, coPPEA, and coPEAE. It seems that we can divide the four copolymers into two sets: one is the better-performing coPAEM, and the other is coPAEA, coPPEA, and coPEAE regarding the antifouling properties. However, the γ′ chains on the fibrinogen exposed a similar degree on the

four copolymer surfaces (**Figure 4.4c**). One possible reason for this inconsistent trend with the platelet adhesion results can be the PBS (−) priming during ELISA.[14] Another reason might be the binding sites on the fibrinogen to the platelet. Sivaraman and Latour reported that RGD-binding and non-RGD-binding platelet receptors mediated platelet adhesion on conformationally changed fibrinogen; namely, there are two different types of platelet binding sites on fibrinogen.[15] More specifically, RGD Aα 572-574 and possibly Aα 95-97 on the Aα chains also participated in addition to the binding sites on the γ chains.[16] Further complicating the matter is that the adsorption-induced conformational-changed albumin also promoted platelet adhesion via the binding between RGD-specific receptors on the platelet and arginine residues in the adsorbed albumin when the unfolding of the albumin exceeded a critical level.[13] Therefore, the binding sites of the γ chains in the conformationally changed fibrinogen may dominate the platelet adhesion on coPAEM, while a more complex platelet adhesion mechanism worked for the surfaces coated by coPAEA, coPPEA, and coPEAE. However, a clear conclusion can be made that the PAEA, PAEM, PPEA, and PEAE segments improved the blood compatibility in the respective copolymer, and the coPAEM surface performed best. To clarify the reason for this performance, we investigated the hydration states of the homopolymers and copolymers.

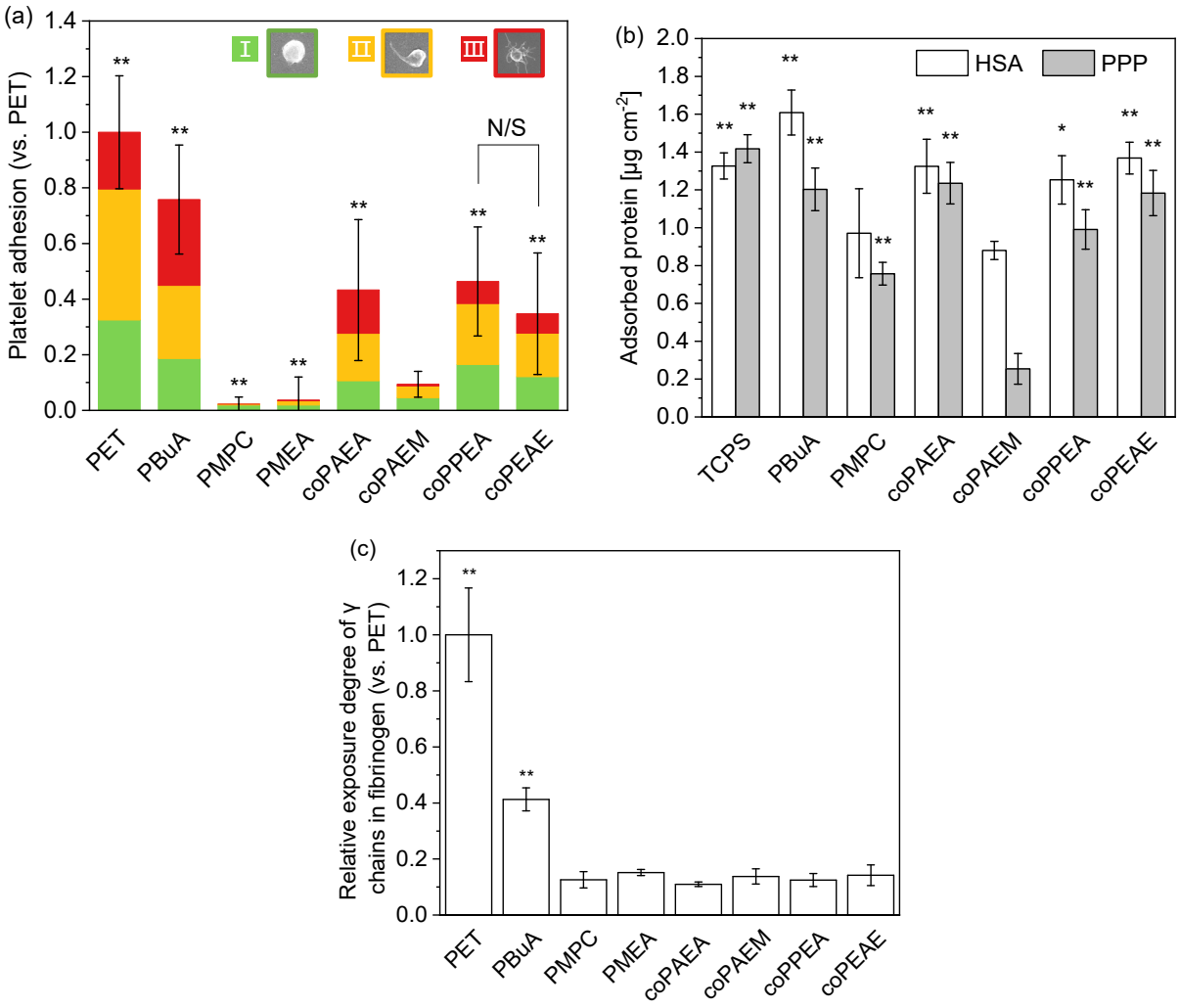

Figure 4.4 (a) Number of adhered platelets on copolymer spin-coated PET substrates. The number was normalized relative to that of PET. The data represent the mean ± SD (n = 9, 3 donors × 3 substrates). The green, yellow, and red bars in each column indicate the percentages of resting, moderately activated, and advanced activated platelets, respectively. A representative illustration of each activation state of the platelet is listed on the top of the columns and marked with the same color corresponding to that in the column. (b) The adsorbed amount of HSA and whole plasma proteins in the PPP by Micro BCA. The data represent the mean ± SD (n = 4). (c) Exposure degree

of the γ′ chains in fibrinogen on copolymer spin-coated PET substrates by ELISA. The degree was relative to that of PET. The data represent the mean ± SD (n = 5). In all figures, **: $P < 0.01$ versus coPAEM and *: $P < 0.05$ versus coPAEM.

4.3.5 Hydration states of homopolymers and copolymers

In the previous in vitro test, the homopolymer blood compatibility was demonstrated by the hemolysis and platelet adhesion test. The IW existing in hydrated homopolymers was measured to verify the universal homopolymer blood compatibility since low hemolysis and platelet adhesion were representative. The DSC thermograms for each homopolymer are shown in the **Figure 4.5-4.8**, and IW peaks were found, confirming that the polymers have sufficient blood compatibility potential. The content of IW, NFW, and FW of each homopolymer was calculated (**Figure 4.9**) and discussed to clarify whether hydration water resulted in the different performances of copolymers. The IW content in the homopolymers might be correlated to the blood compatibility of the copolymers, as the hydrophilic segments in the copolymer films reoriented toward the water and the proportion of hydrophilic units was similar in each copolymer. As shown in the DSC thermograms, with water content increasing, the exothermic peak appeared on the heating scan and gradually shifted onto the cooling scan. This peak shifting trend is the same as observed in the DSC thermograms of PMeOx and PEtOx. By using the same calculation method as theirs, the maximum molar content of IW before its peak merged with FW on the DSC thermogram of each homopolymer was calculated, as well as the corresponding NFW, FW, and T_g. The results were

summarized in **Table 4.2**. In the dry state, the T_g decreased as the sidechain became longer, either on the carbonyl end or on the nitrogen end. The T_g of the hydrated homopolymer was dramatically decreased compared with that of the dry state due to the plasticization of water. There were two carbonyl groups in each homopolymer unit, and a carbonyl can averagely interact with 0.5 to 2 water molecules directly.[17,18] The NFW content in the table for each homopolymer was more than 3 mol per molar unit, indicating that most carbonyl groups were adequately hydrated. The chain structure impacted the hydration degree and caused a slight difference in the NFW content. The IW content of PAEA, PPEA, or PEAE was higher than that of PAEM.

In addition, we also evaluated the hydrated water content in copolymers hydrated by water or PBS (−) (DSC thermograms see **Figure 4.10-4.11**), and the results are shown in **Table 4.3**. When the copolymers were hydrated in water, the IW content was comparable except for coPPEA. In our previous work,[19] we proposed that the IW content in hydrated water-insoluble polymer by PBS (−) showed a closer relationship to blood compatibility than that by water because of reducing the effect from confined water. Compared to that in water, the IW content in PBS (−) decreased by half or more for all copolymers. For coPAEA, coPPEA, and coPEAE, the IW in PBS (−) was comparable, and coPAEM held significantly less content. The trend was similar to the IW content in homopolymers. However, these results contradicted our recognition that the IW content is negatively correlated with the amount of adhered platelets. It is noteworthy that the relationship we obtained on IW content and the blood compatibility of water-insoluble polymers was under the premise that the polymer can fully and stably cover the substrate. However, dewetting-like surface

morphology changes were found on coPAEA, coPPEA, and coPEAE as PBuA during the platelet adhesion test, whereas the coPAEM remained a smooth film on PET substrate (**Figure 4.12**). That surface morphology changes probably caused by the higher chain mobility of the PBuA segments, increased the surface area exposed to the platelets and might lead to more platelets adhered. Considering the higher IW content in PAEA, PPEA, and PEAE, they are promising to contribute blood compatibility as hydrophilic components in copolymers if the hydrophobic components can form stable films. Moreover, the existence of IW in all homopolymers demonstrated that the tertiary amide moiety linked to poly(meth)acrylate is an effective moiety to afford IW if compared with poly(2-hydroxyethyl methacrylate).[20,21]

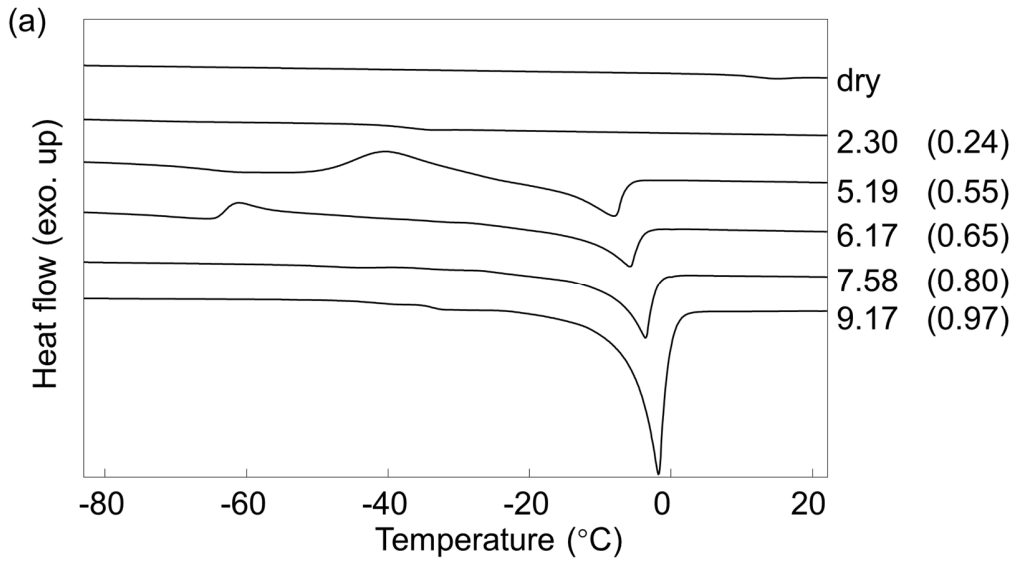

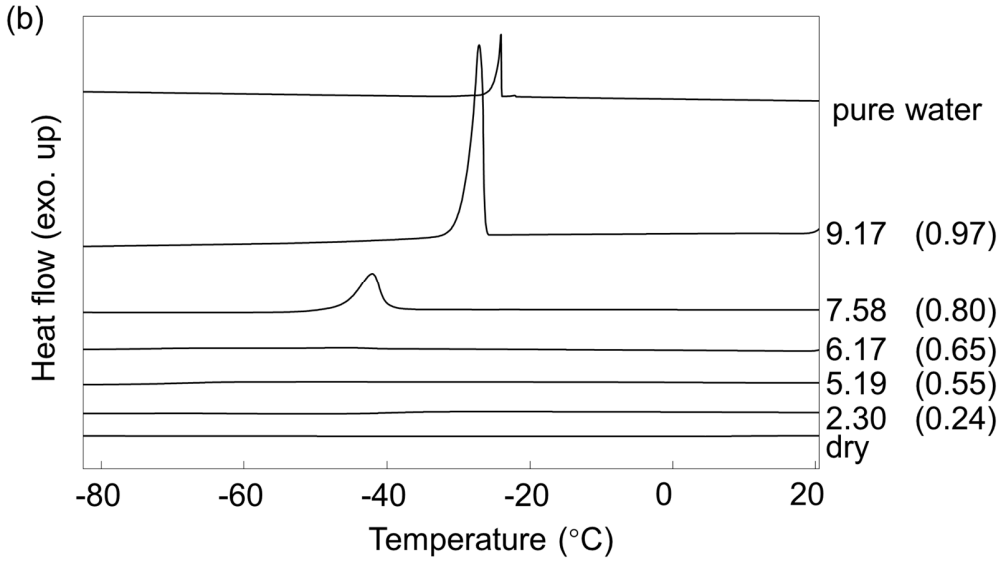

Figure 4.5. DSC thermograms of PAEA on the heating (a) and cooling scan (b). The figures marked on the right side of each curve represent N_{total}, and the figures in the brackets represent the corresponding total water contents in the form of weight ratios (W_{total}).

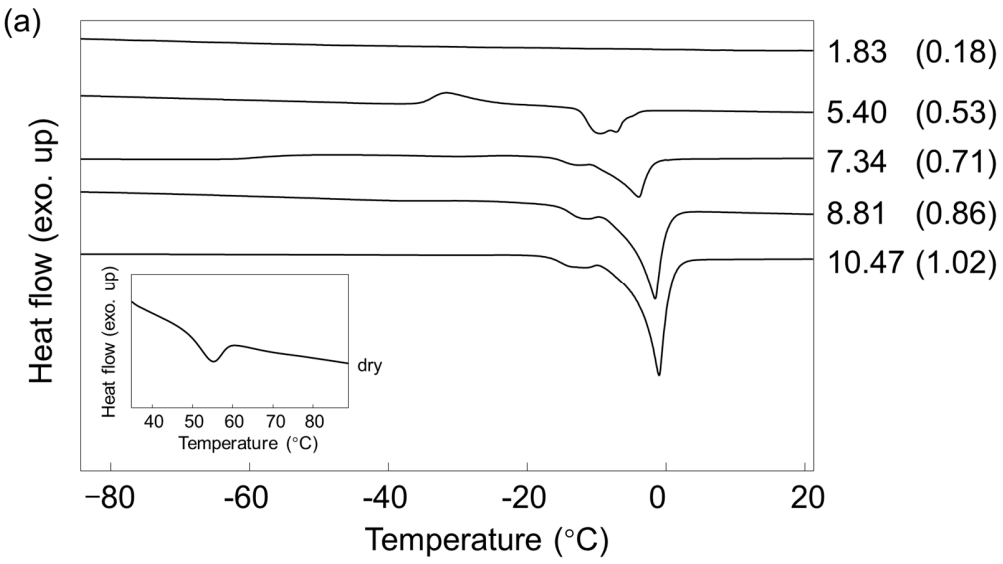

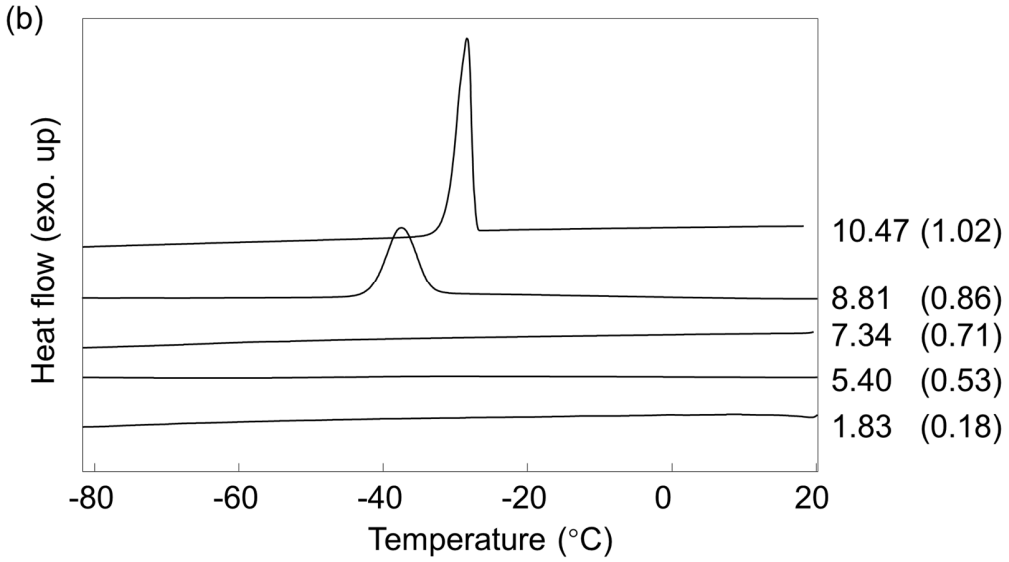

Figure 4.6. DSC thermograms of PAEM on the heating (a) and cooling scan (b). The figures marked on the right side of each curve represent N_{total}, and the figures in the brackets represent the corresponding W_{total}.

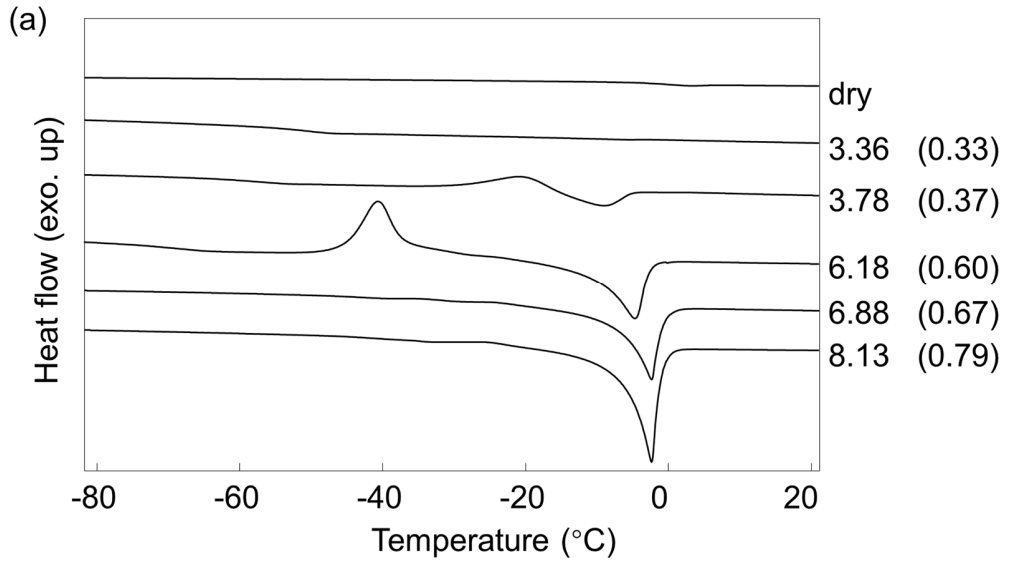

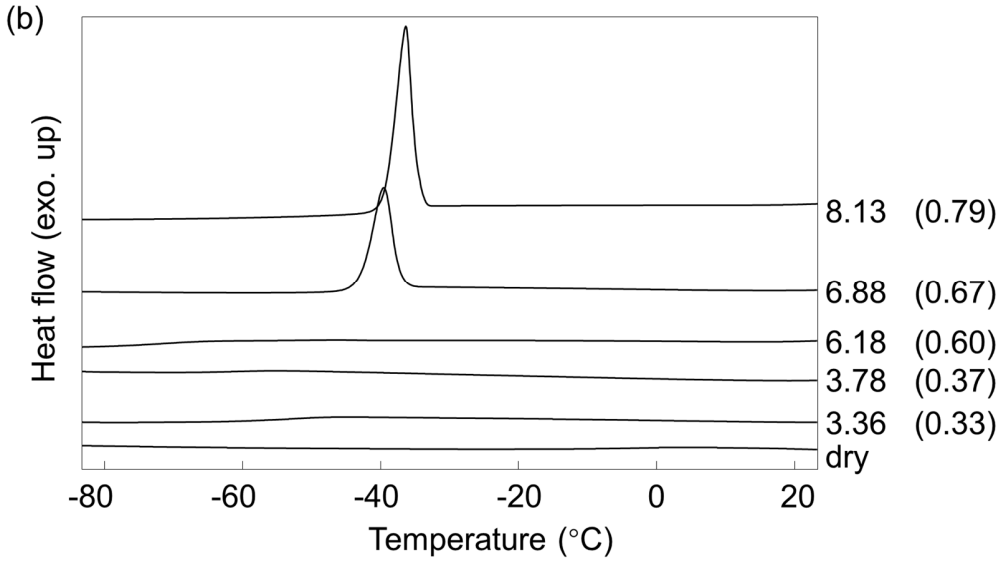

Figure 4.7. DSC thermograms of PPEA on the heating (a) and cooling scan (b). The figures marked on the right side of each curve represent N_{total}, and the figures in the brackets represent the corresponding W_{total}.

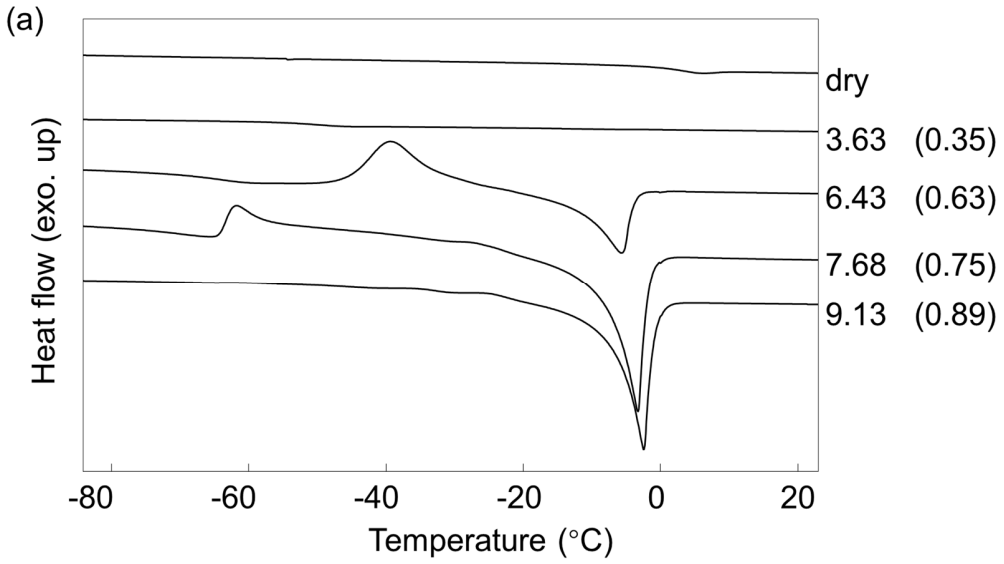

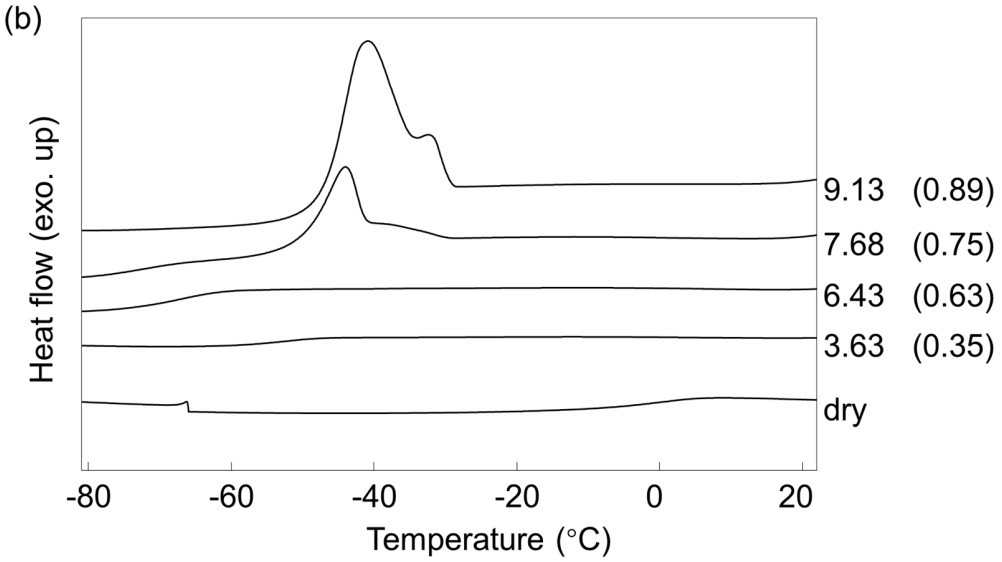

Figure 4.8. DSC thermograms of PEAE on the heating (a) and cooling scan (b). The figures marked on the right side of each curve represent N_{total}, and the figures in the brackets represent the corresponding W_{total}.

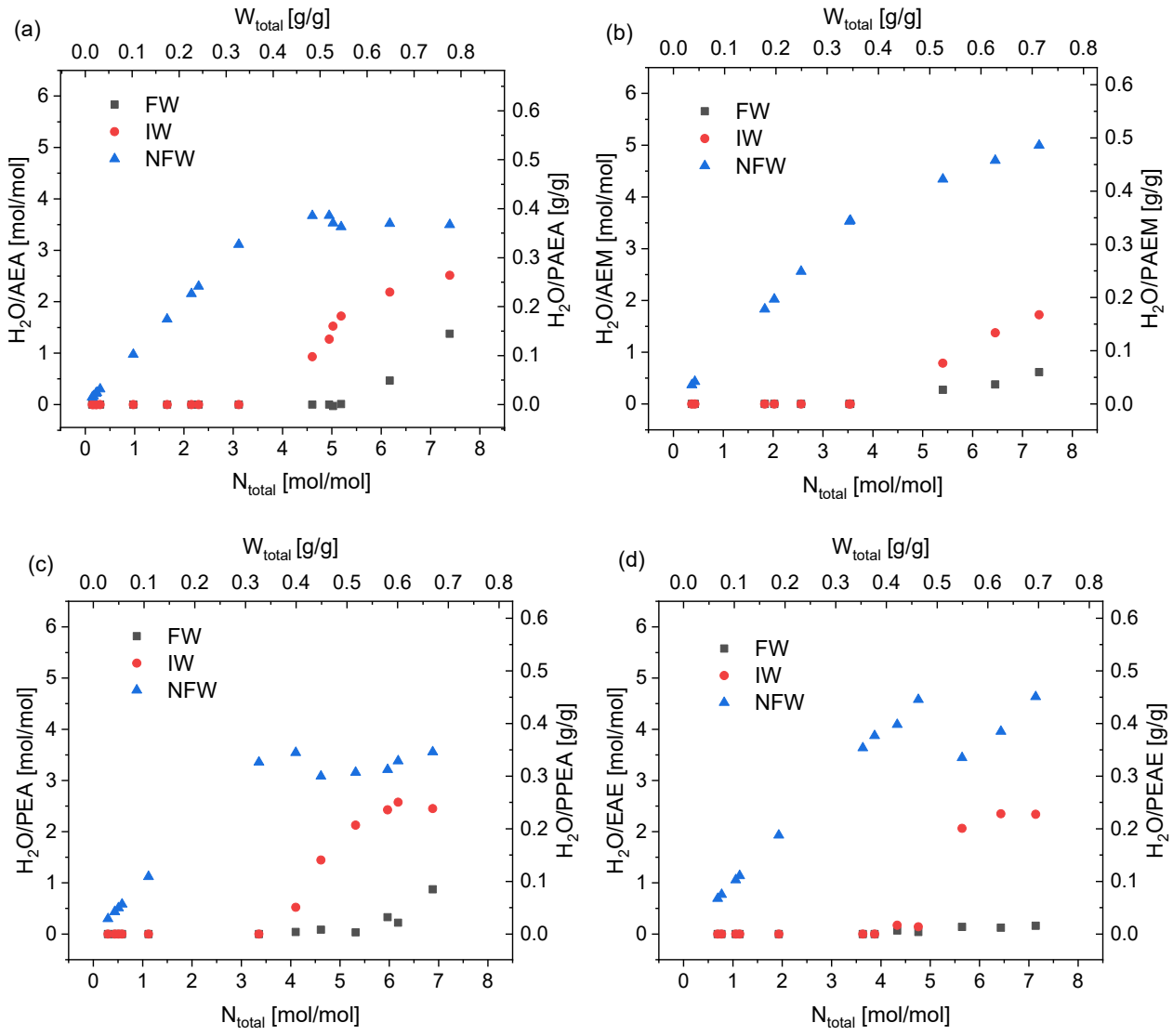

Figure 4.9. The contents of different hydrated water at different total water contents for PAEA (a), PAEM (b), PPEA (c), and PEAE (d).

Table 4.2. T_g and Hydrated Water Contents of Homopolymers

Polymer	T_g[a]		Hydrated water content [mol mol^{-1}]			
	Dry	Wet	NFW[c]	IW[c]	FW[c]	Total[d]
PAEA	10.8	−48.8	3.50	2.51	1.38	7.39
PAEM	51.8	ND[b]	5.00	1.72	0.62	7.34
PPEA	0.86	−42.0	3.56	2.45	0.87	6.88
PEAE	2.86	ND[b]	4.64	2.34	0.16	7.14

[a]Determined by DSC measurement performed at a rate of 5 °C min^{-1}. [b]Not detected. [c]The molar content of each hydrated water. [d]The total water contents of the NFW, IW, and FW in the table.

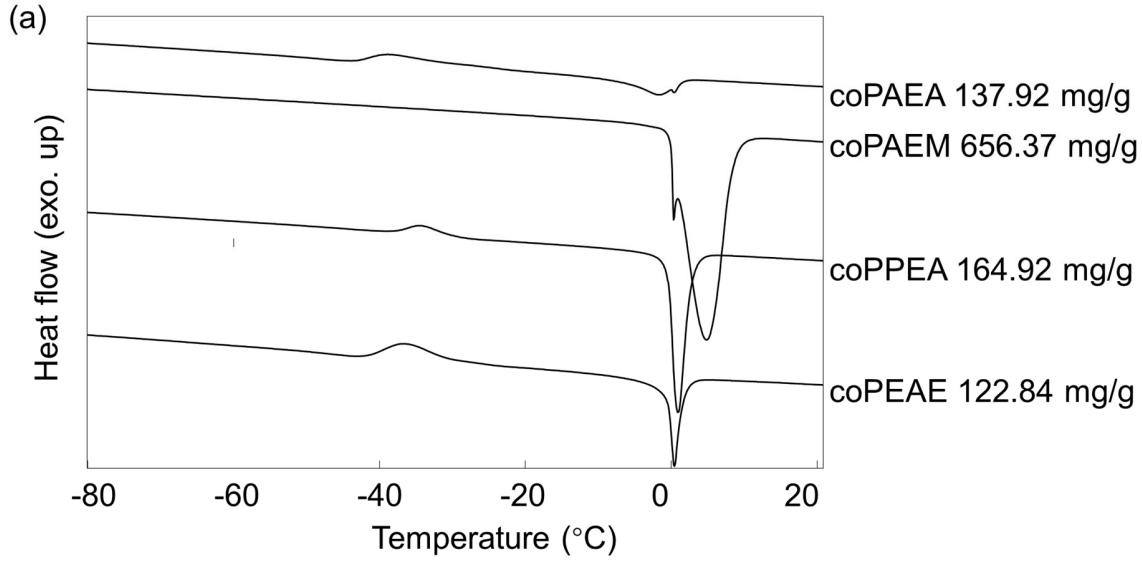

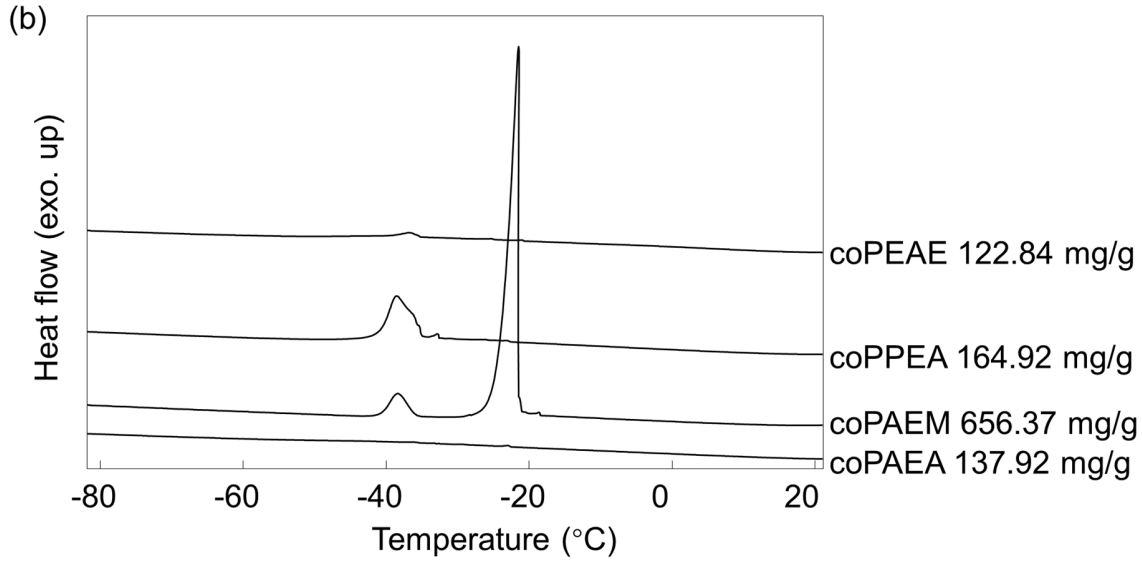

Figure 4.10. DSC thermograms of copolymers hydrated in water. (a) Heating scan and (b) cooling scan. The figure marked on the right side of each copolymer represents the W_{total} (mg/g) when the copolymer was just taken out from the water and the extra surface bulk water was wiped off.

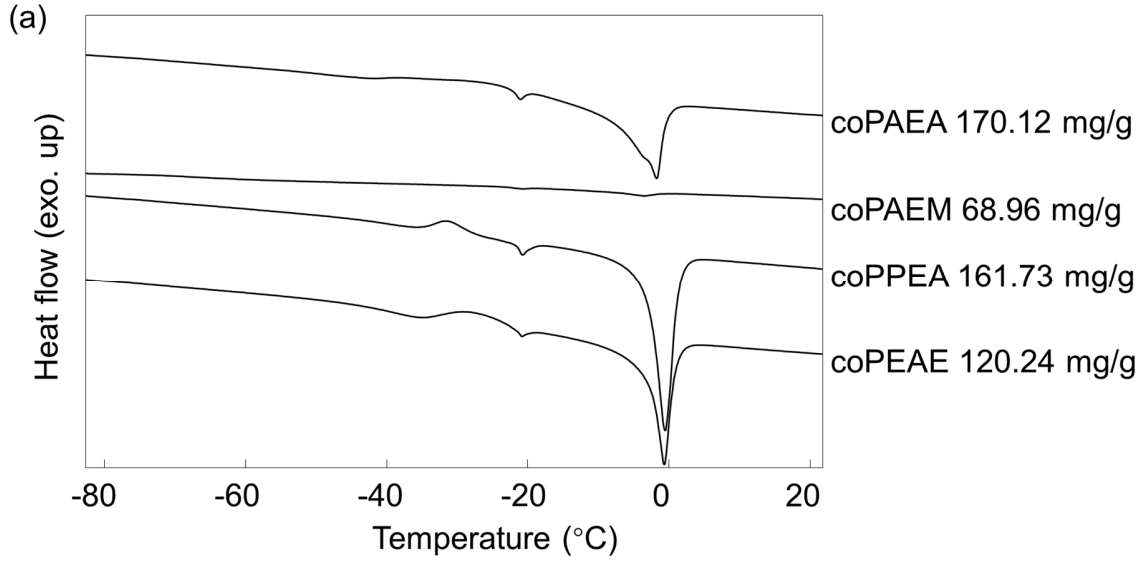

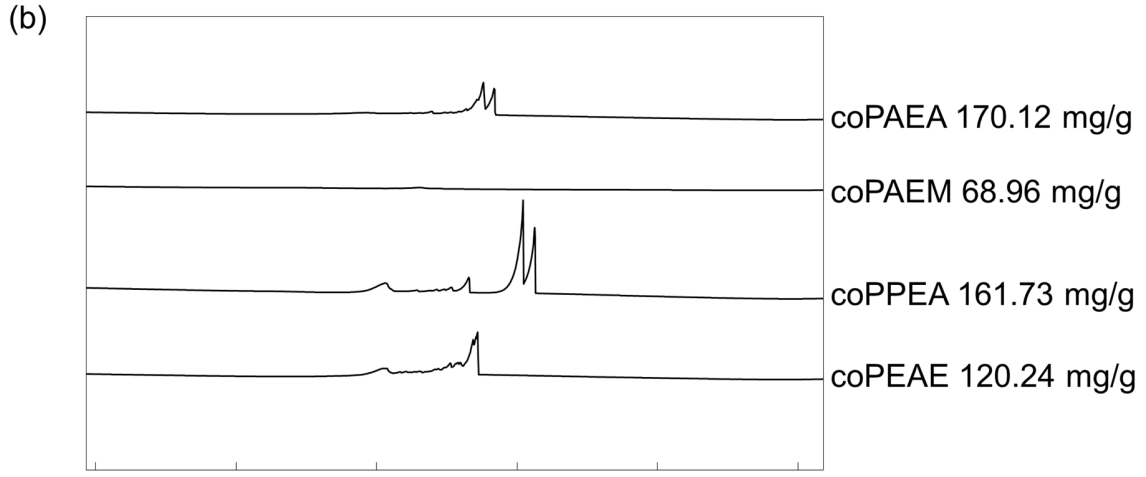

Figure 4.11. DSC thermograms of copolymers hydrated in PBS (−) solutions. (a) Heating scan and (b) cooling scan. The figure marked on the right side of each copolymer represents the W_{total} (mg/g) when the copolymer was just taken out from the PBS (−) solution and the extra surface bulk water was wiped off.

Table 4.3. T_g and Hydrated Water Contents of Copolymers in Water and PBS (−) Solution

Polymer	T_g[a]		Hydrated in water [mg/g]				Hydrated in PBS (−) [mg/g]			
	Dry	Wet	NFW[c]	IW[c]	FW[c]	Total[d]	NFW[e]	IW[e]	FW[e]	Total[d]
coPAEA	−26.1	ND[b]	79.2	44.9	13.9	138	82.7	22.8	64.6	170
coPAEM	ND	ND	46.0	38.8	571	656	62.9	3.96	2.08	69.0
coPPEA	−31.3	ND	26.1	79.6	59.2	165	45.4	17.5	98.8	162
coPEAE	−30.1	ND	65.1	37.7	20.1	123	57.6	15.2	47.4	120

[a]Determined by DSC measurement performed at a rate of 5 °C min^{-1}. [b]Not detected. [c]The weight content of each hydrated water in water hydrated copolymers. [d]The total water contents of the NFW, IW, and FW in the table. [e]The weight content of each hydrated water in PBS (−) hydrated copolymers.

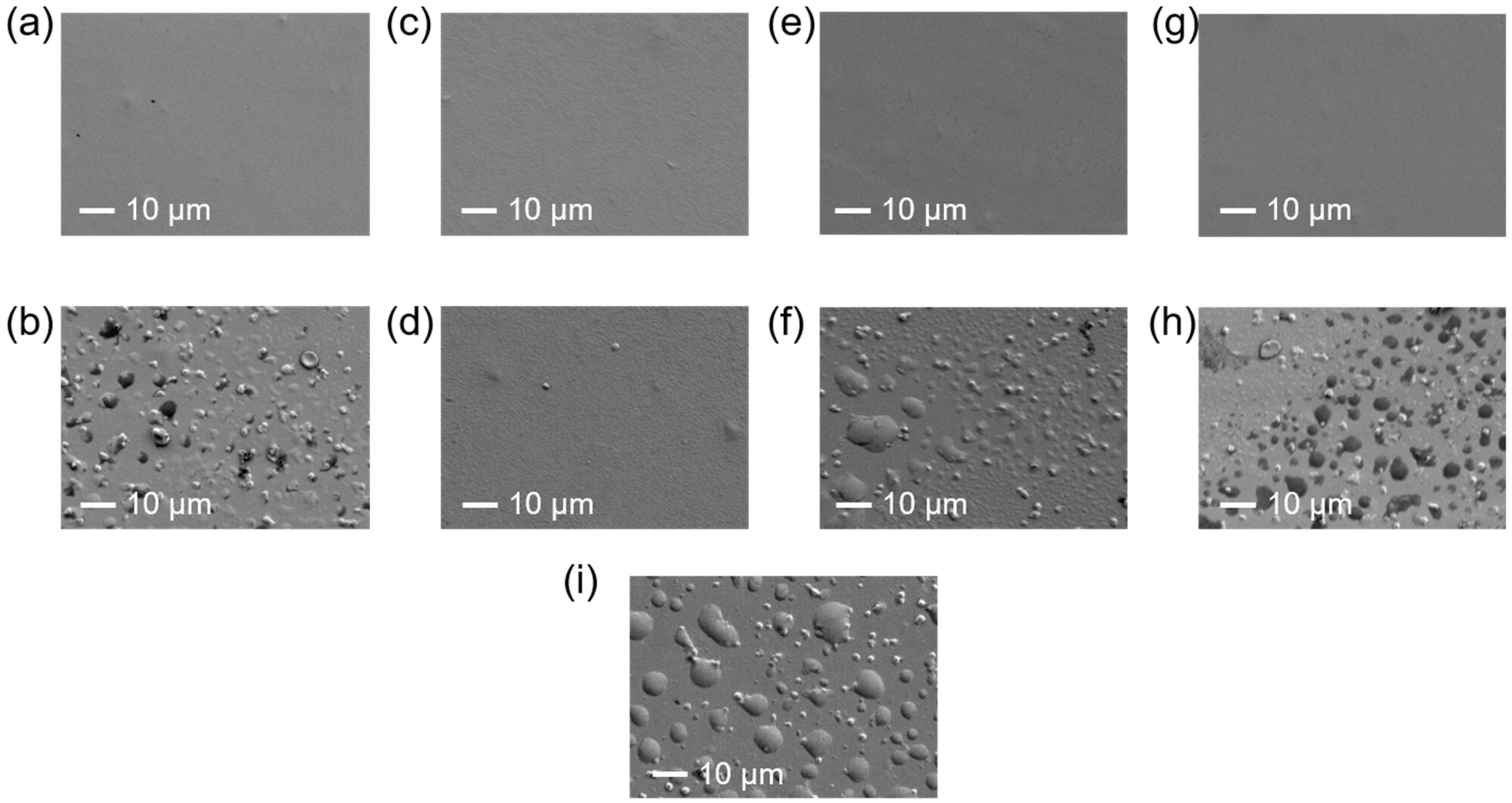

Figure 4.12. SEM images of dry copolymer spin-coated PET substrate, (a) coPAEA, (c) coPAEM, (e) coPPEA, (g) coPEAE; platelet adhesion on copolymer spin-coated PET substrates, (b) coPAEA, (d) coPAEM, (f) coPPEA, (h) coPEAE, and (i) PBuA.

4.4 Conclusion

In this chapter, the blood compatibility and hydration states of poly(tertiary amido acylate) and corresponding copolymers were investigated. All the poly(tertiary amido acylate) analogs showed compatibility with red blood cells and cytocompatibility against HeLa and NHDF cell lines as PMeOx or PEtOx. PPEA and PEAE were thermosensitive in water solutions, and the T_{cp} of the PPEA solution (10 mg mL^{-1}) was 37 °C. Among the four copolymers, coPAEM showed best blood compatibility to suppress the adsorption of plasma proteins, denaturation of adsorbed fibrinogen, and platelet adhesion. IW which can be seen as the "index" of blood compatibility was found in all homopolymers and copolymers by DSC. The present work demonstrated that the tertiary amide moiety in the sidechain of poly(meth)acrylate was an effective contributor to blood compatibility and IW. Furthermore, changing the vicinal groups linked to the tertiary amide moiety may widen the scope of blood-compatible polymers with different physicochemical properties.

4.5 Reference

(1) Wang, Y. X.; Robertson, J. L.; Spillman, W. B.; Claus, R. O. Effects of the Chemical Structure and the Surface Properties of Polymeric Biomaterials on Their Biocompatibility. *Pharm. Res.* **2004**, *21* (8), 1362–1373.

(2) Ratner, B. D.; Hoffman, A. S.; Schoen, F. J.; Lemons, J. E. *Biomaterials Science*, 3rd ed.; Academic Press, 2013.

(3) Kobayashi, S.; Wakui, M.; Iwata, Y.; Tanaka, M. Poly(ω-Methoxyalkyl Acrylate)s:

Nonthrombogenic Polymer Family with Tunable Protein Adsorption. *Biomacromolecules* **2017**, *18* (12), 4214–4223.

(4) Cheng, H.; Shen, L.; Wu, C. LLS and FTIR Studies on the Hysteresis in Association and Dissociation of Poly(N-Isopropylacrylamide) Chains in Water. *Macromolecules* **2006**, *39* (6), 2325–2329.

(5) Maeda, Y.; Nakamura, T.; Ikeda, I. Change in Solvation of Poly(N,N-Diethylacrylamide) during Phase Transition in Aqueous Solutions as Observed by IR Spectroscopy. *Macromolecules* **2002**, *35* (27), 10172–10177.

(6) Hoogenboom, R.; Thijs, H. M. L.; Jochems, M. J. H. C.; Van Lankvelt, B. M.; Fijten, M. W. M.; Schubert, U. S. Tuning the LCST of Poly(2-Oxazoline)s by Varying Composition and Molecular Weight: Alternatives to Poly(N-Isopropylacrylamide)? *Chem. Commun.* **2008**, 5758–5760.

(7) Lai, H.; Chen, G.; Wu, P.; Li, Z. Thermoresponsive Behavior of an LCST-Type Polymer Based on a Pyrrolidone Structure in Aqueous Solution. *Soft Matter.* **2012**, *8* (9), 2662–2670.

(8) Kasemura, T.; Takahashi, S.; Okada, T.; Maegawa, T.; Oshibe, T.; Nakamura, T. Surface Molecular Mobility for Copolymers Having Both Hydrophobic and Hydrophilic Side Chains via Dynamic Contact Angle Measurement. *J. Adhes.* **1996**, *59* (1–4), 61–74.

(9) Rouse, J. H.; Twaddle, P. L.; Ferguson, G. S. Frustrated Reconstruction at the Surface of a Glassy Polymer. *Macromolecules* **1999**, *32* (5), 1665–1671.

(10) Murakami, D.; Segami, Y.; Ueda, T.; Tanaka, M. Control of Interfacial Structures and

Anti-Platelet Adhesion Property of Blood-Compatible Random Copolymers. *J. Biomater. Sci. Polym. Ed.* **2020**, *31* (2), 207–218.

(11) Kitano, H.; Tada, S.; Mori, T.; Takaha, K.; Gemmei-Ide, M.; Tanaka, M.; Fukuda, M.; Yokoyama, Y. Correlation between the Structure of Water in the Vicinity of Carboxybetaine Polymers and Their Blood-Compatibility. *Langmuir* **2005**, *21* (25), 11932–11940.

(12) Mochizuki, A.; Kimura, M.; Ina, A.; Tomono, Y.; Tanaka, M. Study on the Water Structure and Blood Compatibility of Poly(Acryloylmorpholine-r-Butyl Methacrylate). *J. Biomater. Sci. Polym. Ed.* **2010**, *21* (14), 1895–1910.

(13) Sivaraman, B.; Latour, R. A. The Adherence of Platelets to Adsorbed Albumin by Receptor-Mediated Recognition of Binding Sites Exposed by Adsorption-Induced Unfolding. *Biomaterials* **2010**, *31* (6), 1036–1044.

(14) Koguchi, R.; Jankova, K.; Tanabe, N.; Amino, Y.; Hayasaka, Y.; Kobayashi, D.; Miyajima, T.; Yamamoto, K.; Tanaka, M. Controlling the Hydration Structure with a Small Amount of Fluorine to Produce Blood Compatible Fluorinated Poly(2-Methoxyethyl Acrylate). *Biomacromolecules* **2019**, *20* (6), 2265–2275.

(15) Sivaraman, B.; Latour, R. A. The Relationship between Platelet Adhesion on Surfaces and the Structure versus the Amount of Adsorbed Fibrinogen. *Biomaterials* **2010**, *31* (5), 832–839.

(16) Zhang, L.; Casey, B.; Galanakis, D. K.; Marmorat, C.; Skoog, S.; Vorvolakos, K.; Simon, M.; Rafailovich, M. H. The Influence of Surface Chemistry on Adsorbed Fibrinogen

Conformation, Orientation, Fiber Formation and Platelet Adhesion. *Acta Biomater.* **2017**, *54*, 164–174.

(17) Li, T.; Tang, H.; Wu, P. Molecular Evolution of Poly(2-Isopropyl-2-Oxazoline) Aqueous Solution during the Liquid–Liquid Phase Separation and Phase Transition Process. *Langmuir* **2015**, *31* (24), 6870–6878.

(18) Ping, Z. H.; Nguyen, Q. T.; Chen, S. M.; Zhou, J. Q.; Ding, Y. D. States of Water in Different Hydrophilic Polymers - DSC and FTIR Studies. *Polymer* **2001**, *42* (20), 8461–8467.

(19) Sonoda, T.; Kobayashi, S.; Herai, K.; Tanaka, M. Side-Chain Spacing Control of Derivatives of Poly(2-Methoxyethyl Acrylate): Impact on Hydration States and Antithrombogenicity. *Macromolecules* **2020**, *53* (19), 8570–8580.

(20) Tsuruta, T. On the Role of Water Molecules in the Interface between Biological Systems and Polymers. *J. Biomater. Sci. Polym. Ed.* **2010**, *21* (14), 1831–1848.

(21) Tanaka, M.; Mochizuki, A.; Ishii, N.; Motomura, T.; Hatakeyama, T. Study of Blood Compatibility with Poly(2-Methoxyethyl Acrylate). Relationship between Water Structure and Platelet Compatibility in Poly(2-Methoxyethylacrylate-Co-2-Hydroxyethylmethacrylate). *Biomacromolecules* **2002**, *3* (1), 36–41.

CHAPTER 5

Conclusions

Blood compatibility is the prerequisite for blood-contacting medical devices to serve patients. Once foreign materials contact with blood, a series of blood responses such as hemostasis, inflammation, and thrombus formation are evoked, which may further lead to serious complications as well. These adverse reactions not only impair patients' health but also increase their financial burden. With the extensive application of various blood-contacting medical devices in clinical practice nowadays, it is instant to improve the blood compatibility of the devices. The most widely adopted method is to modify the devices' surfaces with blood-compatible polymers. Understanding the blood compatibility mechanism of these polymers can effectively guide the advance of blood-compatible polymers. Among existing mechanisms, the hydration theory has aroused the wide interest of researchers. Based on the studies on various well-known biopolymers, our lab proposed the IW concept. It is believed the IW formed on polymers can prevent cells and proteins from directly contacting polymers, thus avoiding subsequent blood reactions. Furthermore, the content of IW is related to the polymer structure and blood compatibility, so it can also work as a guiding principle for the development of novel blood-compatible polymers. Based on these two points, this thesis focuses on the blood compatibility mechanism of POXs and the development of corresponding derivatives.

In **Chapter 1**, the research background of this thesis is overviewed, including the problems of

blood-contacting medical devices, the blood reactions on blood-contacting medical devices, and surface modification strategy. Additionally, the mechanism of blood-compatible polymers, especially the IW concept is highlighted. The characteristics of POXs are introduced as well.

Although the physicochemical properties, chemical modification, and biomedical application of POXs have been widely studied, their blood compatibility mechanism is few reported. In **Chapter 2**, PMeOx, PEtOx, PBuOx, and PPhOx were selected as POX models for the comparative study of their blood compatibility and hydration states. The four POXs were grafted onto glass substrates through photo-grafting, and their blood compatibility was estimated via platelet adhesion and the degree of denaturation of the adsorbed fibrinogen. The hydration states of the POXs were investigated using DSC and ATR-IR. The IW was present in the hydrated PMeOx and PEtOx but was scarce in the hydrated PBuOx and PPhOx. This could be the reason for the blood compatibility of PMeOx and PEtOx. The carbonyl groups in PMeOx and PEtOx could be fully hydrated. However, in PBuOx and PPhOx, water mainly existed as bulk water. The hydration of the carbonyl groups is hindered by the bulky side chains, and IW cannot be generated. This knowledge provides a perspective for understanding the biocompatibility of PMeOx and PEtOx from the water–polymer interactions and may inspire the development of novel blood-compatible POX derivatives.

According to **Chapter 2**, for PMeOx and PEtOx, the tertiary amide frameworks can be fully hydrated to generate IW. While in PBuOx and PPhOx, the tertiary amide frameworks are sterically hindered to form IW. Combining these conclusions and the construction of PMPC and PMEA, in

Chapter 3, four poly(tertiary amido acrylate) analogs, which are composed of (meth)acrylate backbones and tertiary amide moieties in the side chains, are designed. The monomers are synthesized through a two-step strategy, by which the steric hindrance around the tertiary amide in the monomers can be controlled. The monomers can be easily polymerized by convenient free radical polymerization. Since the prepared homopolymers are water-soluble, the water-insoluble copolymers were also synthesized by copolymerizing with their monomers with hydrophobic *n*-butyl (meth)acrylates to further coat on substrates directly.

In **Chapter 4**, the blood compatibility and hydration states of poly(tertiary amido acylate) and corresponding copolymers were investigated. All the poly(tertiary amido acylate) analogs showed compatibility with red blood cells and cytocompatibility against HeLa and NHDF cell lines as PMeOx or PEtOx. PPEA and PEAE were thermosensitive in water solutions, and the T_{cp} of the PPEA solution (10 mg mL^{-1}) was 37 °C. Among the four copolymers, coPAEM showed the best blood compatibility to suppress the adsorption of plasma proteins, denaturation of adsorbed fibrinogen, and platelet adhesion, which may be attribute to the stable polymer coating on the substrates. IW, which we proposed as the "index" of blood compatibility, was found in all homopolymers and copolymers by DSC. The present work demonstrated that the tertiary amide moiety in the sidechain of poly(meth)acrylate was an effective contributor to blood compatibility and IW. Furthermore, altering the vicinal groups linked to the tertiary amide moiety may inspire the development of "smart" blood-compatible polymers with thermosensitivity.

At last, it should be noted that, in this thesis, the generation mechanism of IW was analyzed

through the interaction between water molecules and tertiary amide moieties either in POXs or poly(tertiary amido acylate) analogs. However, it is believed that the mobility of polymer chains is also an important factor to generate the IW. Therefore, in addition to the DSC and ATR-IR used in this thesis, more characterization methods such as solid-state NMR, neutron scattering, terahertz time-domain spectroscopy, frequency modulation AFM, soft X-ray adsorption and emission spectroscopy are promising to evaluate the behaviors or states of IW, which would complete our understanding of IW and make a contribution to the biomaterials field.

Acknowledgements

This thesis condenses my three years' doctoral life. In this period, I have experienced the happiness of learning new knowledge, the encouragement after experimental failure, and the joy of harvest. This period of studying abroad would undoubtedly become the most precious treasure in my life. All of these cannot be achieved without the selfless and enthusiastic help from every member of Masaru Tanaka Lab.

First of all, I would like to express my sincere gratitude to the Japanese government for supplying the MEXT scholarship to support me to complete the doctoral study.

I would also like to express my most sincere gratitude and respect to Prof. Masaru Tanaka and Prof. Shingo Kobayashi. I appreciate Prof. Masaru Tanaka for recommending me to study at Kyushu University and opens the door of the field of biochemistry to me. When I entered the biochemistry field three years ago, I was like a kindergarten student, curious about everything but very ignorant. I would like to thank Prof. Masaru Tanaka for his always kind, patient, and professional guidance throughout my study. I am also heartily grateful to Prof. Shingo Kobayashi for his patient, amiable, professional instruction. He teaches me how to conduct experiments scientifically and realize my ideas step by step. Without him, I would not be able to progress in my research. When I was a middle school student, I have read a text named *Fujino Sensei* written by the famous Chinese writer Lu Xun. His Fujino Sensei was diligent in studying, tireless in teaching, and genial for students. The image of Fujino Sensei had impressed me since then, and to

some extent represents the image that I think a teacher should be. I think Prof. Masaru Tanaka and Prof. Shingo Kobayashi are my Fujino Sensei in my mind.

Except for my supervisor, I also would like to express my depth of gratitude to Prof. Masahiro Goto and Prof. Yoshiki Katayama for being my thesis review commissioners. I am grateful for their kind and precise suggestion for my defense.

I extend my most sincere thanks to Prof. Takahisa Anada, Prof. Daiki Murakami, Dr. Aki Kashiwazaki, Dr. Shin-nosuke Nishimura, Dr. Kei Nishida, and Dr. Shohei Shiomoto for their continuous, kind, and patient help for my research.

I am thankful to secretary Ms. Kumiko Araki, Ms. Tomoko Matthews, and technical staff Ms. Yukiko Tanaka and Ms. Aki Yamamoto, for their always meticulous, thoughtful, and tender support for my study and daily life.

I am also appreciative to all the students in Tanaka Lab. I spent the majority of my time and shared joyfulness with them during these three years. My graduation should partially owe to them, who always provided a harmonious and pleasant environment for me to study. I express my heartfelt thanks to Dr. Toshiki Sonoda, Rubaiya Anjum, Yasuki Okazaki, Tomoya Ueda, Hiroki Uehara, Haque Md Azizul, Koki Baba, Daichi Hiramatsu, Yuri Kato, Yuki Fujita, Nami Mawatari, Yuto Segami, and Shogo Sekida, Katsuki Morita, Shunsuke Nakao, Haruka Matsumoto, Kento Yoshida, Chiaki Umakoshi, Tomoki Otsuka and Michiharu Kawahara. I would especially appreciate Dr. Toshiki Sonoda, Rubaiya Anjum, Yasuki Okazaki, and Tomoya Ueda. Except for knowledge, their friendship is the most precious thing I have gained. Dr. Sonoda would never be

fed up giving his most patient, kind, and professional help to me. His noble personality is worth learning for me. Yasuki Okazaki and Tomoya Ueda are always eager to help me deal with the difficulties in my experiments with their warmest smile. They deserve my deepest respect. Rubaiya Anjum is my best friend in the lab. We always comfort and encourage each other and release pressure together.

Furthermore, I appreciate my Chinese friends Wang Mengmeng, Meng Fanfei, Zhang Zhi, Dr. Guo Binling, and Dr. Tian Quanzhi in Kyushu University for their always company, help, and encouragement. Lastly, I extend my sincerest gratitude to my husband, Dr. Luo Wuhui, and my parents. They always bear my caprice and temper in silence but return me the strongest and warmest spiritual supports in the world at any moment.

July 2021

Shichen Liu